UNIVERSITY OF OKLAHOMA

GRADUATE COLLEGE

Naturalness and novel statistical methods on the string landscape

A DISSERTATION

SUBMITTED TO THE GRADUATE FACULTY

in partial fulfillment of the requirements for the

Degree of

DOCTOR OF PHILOSOPHY

By

DAKOTAH MARTINEZ
Norman, Oklahoma
2024

Naturalness and novel statistical methods
on the string landscape

A DISSERTATION APPROVED FOR THE
HOMER L. DODGE DEPARTMENT OF PHYSICS AND
ASTRONOMY

BY THE COMMITTEE CONSISTING OF

Dr. Howard Baer, Chair

Dr. Kuver Sinha

Dr. Braden Abbott

Dr. Doerte Blume

Dr. Nikola Petrov

This work is dedicated to my parents Dr. Denise Martinez and Abel Martinez, my sister Sierrah Martinez, my wife Emily Martinez, and my cats Rory and Charlie.

Your love and support are my guiding light to achieving my dreams.

Thank you for sharing this life with me.

Acknowledgements

I would like to thank my advisor, Howard Baer, for introducing me to the wonderfully intricate worlds of particle physics and supersymmetry. You allowed me a chance to prove myself in the field and recognized my capability, as well as helping me recognize it within myself. I would also like to send my deep thanks to Aaron Robison for believing in me and offering me the opportunities that began my career in multidisciplinary scientific research. My sincerest gratitude is extended towards Alexander Karabegov, my role model and former mentor, for being a true monolith of academic and personal integrity. You taking the initiative and time to train and guide me as you did is one of the most important and impactful factors that guided me to become the scientist I am today.

Finally, I would like to thank family and friends, particularly Dalton Gilstrap and Ronnie Laehn, for your patience and support in my journey to discover myself.

Table of Contents

List of Tables

List of Figures

Abstract

In this work, we formalize the concept of naturalness in supersymmetric effective field theories, as well as introduce novel methods for performing statistical analyses in the string landscape. We revisit the various measures of practical naturalness for models of weak-scale supersymmetry (SUSY) including: 1. electroweak (EW) naturalness; 2. naturalness via sensitivity to high-scale (HS) parameters [Ellis-Enquist-Nanopoulos-Zwirner/Barbieri-Giudice (EENZ/BG)]; 3. sensitivity of Higgs soft terms due to high-scale radiative corrections; and 4. stringy naturalness (SN) from the landscape. We debut a new numerical routine for calculating these measures from any SUSY Les Houches Accord file. A vast array of (metastable) vacuum solutions arise from string compactifications, each leading to different 4-d laws of physics. The space of these solutions, known as the string landscape, allows for an environmental solution to the cosmological constant problem. We argue that the landscape favors natural softly broken supersymmetric (SSB) models over particle physics models containing quadratic divergences, such as the Standard Model or unnatural SSB models by presenting a computable measure. An anthropic selection of the weak scale to within a factor of a few of our measured value — in order to produce complex nuclei as we know them (atomic principle) — provides statistical predictions for Higgs and sparticle masses in accord with LHC measurements. The predicted Higgs and superparticle spectra might be testable at HL-LHC or ILC via higgsino pair production but is certainly testable at higher energy hadron colliders with $\sqrt{s} \sim 30$–100 TeV.

Chapter 1

Particle physics and the string landscape

Modern physics can be mainly classified into two classes of theories. On one side, we are able to describe phenomena occurring at a small scale to an extreme precision – this is the essence of quantum field theory (QFT). On the other side, we can accurately describe phenomena occurring at large scales via Einstein's general relativity (GR). As physicists, we simultaneously seek a method to unify these concepts in addition to expanding our current understanding of these individual fields of research, as our current knowledge of each possesses certain gaps that must be remedied. At its core, physical processes can be described via specific interactions between matter and energy, mediated by the four fundamental forces at work within the universe. From weakest to strongest, these interaction forces are gravity (governing paths of motion through curved space and time), the weak force (governing radioactive beta decay of matter), the electromagnetic force (governing interactions of electrically charged particles), and the strong force (binding quarks together and stabilizing nuclei of atoms).

In this introduction, we conduct a brief literature reeview and briefly outline the details and issues underlying the Standard Model of particle physics, extensions to this Standard Model in supersymmetry to rectify these issues, and how gravity is incorporated into the mix with superstring theory on the string landscape. Then, with this background in place, we discuss concepts of naturalness as a guiding principle to new, undiscovered physics at the Large Hadron Collider

(LHC) and beyond. We will address how naturalness measures have typically played a role in the literature along with our new developments towards producing reliable numerical software to evaluate these measures, along with a new proposed measure for stringy naturalness and some preliminary results.

1.1 The Standard Model

The most experimentally verified quantum field theory is known as the Standard Model (SM) of particle physics, which incorporates three of these four forces – electromagnetism, the weak force, and the strong force. Algebraically, the SM is a non-Abelian Yang-Mills gauge theory and is described by the group $SU(3) \times SU(2) \times U(1)$, leading to the important particle physics lesson that dynamics of particles and interactions are described by symmetries [3]. Each of these forces has a corresponding "quantized" form in the SM, corresponding to a gauge boson, or integer-spin particle, that effectively communicates these forces between messengers and recipients of that interaction "message". The Standard Model also describes three generations of the fundamental matter fermions, or half-integer-spin particles, that constitutes the matter that then forms structure within the universe. Lastly, the SM also describes the spin-0 scalar boson, the Higgs boson, that plays a vital role in generating the fermion masses.

This mass generation is achieved by the spontaneous breakdown of the $SU(2) \times U(1)$ subgroup to the electromagnetic gauge group $U(1)_{\text{em}}$ – this breakdown is termed *spontaneous electroweak symmetry breaking* (EWSB). Briefly, this

breakdown is achieved by the spin-0 doublet ϕ, containing the Higgs of the SM, obtaining a non-zero vacuum expectation value (VEV). This VEV is then invariant under specific combinations of the generators for the $SU(2)$ and $U(1)$ gauge groups, generating a distinct $U(1)_{\text{em}}$ gauge group. Without this special breakdown, the matter fermions would fail to obtain masses due to gauge invariance under the electroweak $SU(2) \times U(1)$ group, but *with* this breakdown, masses for these fermions are generated through Yukawa-type interactions between quarks and the ϕ field's VEV.

Despite the tremendous success of this model, there are still features of our universe that fail to be satisfactorily explained by the SM alone. Some of the biggest issues herein are:

- A quantum description of the fourth fundamental force, gravity, is not present.

- In addition to failing to incorporate gravity, the Standard Model fails to describe the relative strengths of the fundamental forces, leading to the gauge hierarchy problem (GHP) [4, 5]. In particular, with the SM alone, the Higgs mass is expected to be significantly more massive than its measured value of $m_h \sim 125$ GeV. This value seems to only be attainable within the SM given an extreme degree of finetuning of parameters due to quadratically divergent contributions to the Higgs mass from scalar boson, gauge vector boson, and fermion loops, when these interactions are described via Feynman diagrams.

- A SM dark matter and dark energy candidate is missing from the SM, which is crucial, as dark matter and energy is predicted to constitute $\sim 85\%$ of the matter and energy content of the universe in order to describe its observed expanding nature.

Supersymmetry (SUSY) offers an elegant solution to many of these issues. Many supersymmetric constructions exist in the literature, with varying degrees of complexity, but the simplest and potentially most phenomenologically viable version of SUSY is present in the Minimal Supersymmetric Standard Model (MSSM) [3].

1.2 Supersymmetry

1.2.1 A brief introduction to SUSY

SUSY is an extension of the Standard Model that posits a symmetry between fermions (spin-half-integer particles) and bosons (spin-integer particles), the two fundamental classes of particles. In the Standard Model, fermions (e.g., quarks and leptons), are the constituents of matter, while bosons are the carriers of fundamental forces, as mentioned before. SUSY suggests that for every fermion, there is a bosonic superpartner, and for every boson, a corresponding fermionic superpartner.

In unbroken supersymmetry, it is predicted that these supersymmetric particles (sparticles) will have similar masses to their "twin" non-supersymmetric counterpart. However, we have not yet observed these superpartners experimentally,

suggesting the idea that if supersymmetry exists, it must be *broken* at some high scale, leading to a mechanism that generates masses at a scale much larger than the Standard Model slew of particles. The concept of a "broken" symmetry is fine, as we understand that the breaking of the electroweak symmetry $SU(2) \times U(1)$ down to the electromagnetic gauge group serves a vital role in generating fermion masses. So, even with this requirement of broken supersymmetry (which will be expanded upon shortly), SUSY offers a compelling framework for addressing several theoretical challenges faced by the Standard Model, some of which are given in the preceding section.

1.2.2 Motivation for SUSY

One of the primary motivations behind SUSY is the gauge hierarchy problem as mentioned in the previous section, concerning the stability of the Higgs boson mass against large, quadratically divergent radiative corrections. In the Standard Model, we saw that these corrections "should" drive the Higgs mass to extremely large values, unless an extreme degree of fine-tuning is present in the theory to maintain the observed value. Supersymmetry helps mitigate this issue through the introduction of superpartners that offer terms in the loop-corrected theory that *cancel* against these large corrections, stabilizing the Higgs mass. Once these quadratic divergences cancel, the only remaining divergences are merely logarithmic.

Another very compelling motivation is the concept of gauge unification, or unification of (three of) the fundamental forces. Such a unification would indicate

a high-energy origin of these forces as a singular concept, instead of requiring three separate constructions. In particular, the coupling constants of the strong, weak, and electromagnetic forces do not naturally unify at high energies within the Standard Model. However, when we incorporate SUSY and perform a Quantum Field Theory technique called renormalization to reparameterize the theory in such a way that naïvely divergent integrals can be shown to *not* diverge, we introduce a new parameter called the renormalization scale that carries the information of this reparameterization through the theory. In doing so, other parameters of the theory (such as gauge couplings) vary with the renormalization scale, producing a set of differential equations called the renormalization group equations (RGEs), stemming from the concept that physical observables should not depend on this mathematical artifact of the renormalization scale. These RGEs evolve the coupling constants, for example, with energy in a way that suggests they could converge or unify at a common high-energy scale (typically of the order $M_G \sim 2 \times 10^{16}$ GeV), hinting at a grand unified theory (GUT).

Furthermore, SUSY provides us a natural candidate for dark matter through the lightest supersymmetric particle (LSP). This is often assumed to be the SUSY particle termed the *neutralino*, which is generally stable under certain conditions and could constitute the dark matter we expect to make up a significant portion of the universe's mass-energy content. If R-parity is conserved, then this LSP is stable and could account for the dark matter observed.

1.2.3 The supersymmetry algebra

Mathematically, early constructions with the Wess-Zumino model[3] demonstrated the possibility of constructing a relativistic quantum field theory that is invariant under supersymmetric transformations. At its core, supersymmetry contains the SUSY algebra, which extends the standard Poincaré algebra known through relativity to be required for spacetime symmetries. This new SUSY algebra introduces spinorial generators (charges) $Q, \bar{Q}$ that serve to transform fermions into bosons and vice versa. These generators must satisfy certain anti-commutation relations[3]:

$$\{Q_a, \bar{Q}_b\} = 2\,(\gamma^\mu)_{ab}\,P_\mu,$$

$$\{Q_a, Q_b\} = -2(\gamma^\mu C)_{ab} P_\mu,$$

$$\{\bar{Q}_a, \bar{Q}_b\} = 2(C^{-1}\gamma^\mu)_{ab} P_\mu,$$

where P_μ is the standard 4-vector momentum. Through these relations, the SUSY generators close on the Poincaré algebra, such that supersymmetry is effectively a spacetime symmetry.

1.2.4 SUSY QFT and superfield formalism

In constructing a relativistic quantum field theory (QFT) that is invariant under SUSY transformations, we must extend the field content of the Standard Model to include superfields. Superfields are representations of the SUSY algebra combining both fermionic and bosonic degrees of freedom. As a simple example, consider the

chiral superfield Φ expressed in terms of a fermionic component field ψ, a scalar field ϕ, and an auxiliary field F (introduced to balance the degrees of freedom and ensure off-shell SUSY invariance). These fields transform into each other under some SUSY transformation. To combine these into a superfield, we introduce a Majorana spinor θ with four components who are Grassmann numbers, satisfying the relation

$$\{\theta_a, \theta_b\} = 0.$$

A general superfield is then expressed as (generally complex)

$$\begin{aligned}\Phi(x,\theta) =& \phi - i\sqrt{2}\bar{\theta}\gamma_5\psi - \frac{i}{2}\left(\bar{\theta}\gamma_5\theta\right)\mathcal{M} + \frac{1}{2}(\bar{\theta}\theta)\mathcal{N} + \frac{1}{2}(\bar{\theta}\gamma_5\gamma_\mu\theta)V^\mu \\ &+ i\left(\bar{\theta}\gamma_5\theta\right)\left[\bar{\theta}\left(\lambda + \frac{i}{\sqrt{2}}\not{\partial}\psi\right)\right] - \frac{1}{4}\left(\bar{\theta}\gamma_5\theta\right)^2\left[\mathcal{D} - \frac{1}{2}\Box\phi\right].\end{aligned} \tag{1.1}$$

This expansion is in terms of the sixteen component fields $\mathcal{M}, \mathcal{N}, V^\mu, \lambda$, and $\mathcal{D}$.

The action S for a SUSY theory is then constructed to be invariant under SUSY transformations, requiring careful consideration of the interactions between component fields within the superfields. In the Minimal Supersymmetric Standard Model (MSSM) to be introduced shortly, the Lagrangian contains terms such as kinetic terms, Yukawa interactions, and potential terms. The key is that the entire action S respects the supersymmetry, while the Lagrangian transforms under this symmetry as a total derivative.

1.2.5 Soft SUSY breaking

While SUSY does elegantly address several theoretical issues, since we have not observed superpartner masses with the same masses as their SM counterparts, we must be consistent with this experimental evidence of the observed particle spectrum and realize that SUSY is a broken symmetry. However, we do not want to break SUSY in such a way that the cancellations of quadratic divergences mentioned earlier are lost (termed *hard* SUSY breaking). Soft SUSY breaking introduces explicit SUSY-breaking terms into the Lagrangian, which then ensures that SUSY breaking occurs at a "low" energy scale without reintroducing the GHP.

Soft SUSY-breaking terms typically include mass terms for the superpartners (to generate their experimentally-expected large masses, relative to their SM counterparts), trilinear scalar couplings, and bilinear scalar couplings [6]. These terms will break SUSY while maintaining the desirable features of SUSY, such as the stabilization of the Higgs mass and the unification of gauge coupling constants.

1.2.6 The Minimal Supersymmetric Standard Model (MSSM)

Among the various possible SUSY theories, the MSSM stands out due to its parsimony and its potential for phenomenological viability. The MSSM extends the SM by introducing the minimal set of new particles required to implement supersymmetry. This includes superpartners for each Standard Model Particle, as well as additional Higgs bosons to accommodate anomaly cancellation. The MSSM is built on the assumption of $\mathcal{N} = 1$ SUSY, meaning there is a single

SUSY generator. This is the simplest form of supersymmetry and implies there is one superpartner for each SM particle.

In $\mathcal{N} = 1$ SUSY, the SUSY algebra includes a single set of SUSY generators Q and $\bar{Q}$, as mentioned above, serving to transform fermions into bosons and vice versa. Higher $\mathcal{N}$ SUSY does not allow chiral matter as required in the Standard Model. The presence of a single SUSY charge simplifies our theoretical framework, while still addressing the key issues underlying the SM we want to resolve. This minimal approach also makes the MSSM more accessible and testable in phenomenological studies and collider experiments. Additionally, the MSSM predicts the lightest Higgs boson (which coincides with the experimentally found Higgs boson) mass to lie within a narrow range that explicitly contains the measured value of 125 GeV.

The MSSM extends the SM by introducing superpartners for each of the existing particles, as suggested. Specifically:

- **Quarks and leptons:** Each quark and lepton has a scalar superpartner known as a squark and a slepton, respectively.

- **Gauge bosons:** Each gauge boson has a fermionic superpartner known as a gaugino. For example, the gluon's superpartner is the gluino, the W and B bosons' superpartners are the winos and bino, and the photon's superpartner is the photino.

- **Higgs bosons:** The Higgs sector is expanded to include two Higgs doublets, introducing five physical Higgs bosons. Out of these five, two are CP-

even, one is CP-odd, and two are electrically charged Higgs bosons. Their fermionic superpartners are then called higgsinos.

The MSSM's action is constructed to be invariant under $\mathcal{N} = 1$ SUSY transformations. The terms in the Lagrangian include:

- **Kinetic terms:** This ensures proper dynamics for all fields and generates gauge interactions.
- **Superpotential:** This is a function of the chiral superfields that dictates the interactions between the fields. It includes Yukawa interactions similar to those in the Standard Model, but extended to include interactions between Higgs fields and their superpartners.
- **Soft SUSY breaking terms:** These terms explicitly break SUSY at low energies without reintroducing the hierarchy problem. Included here are mass terms for the scalar and gaugino sparticles, trilinear scalar couplings (also called A-terms), and bilinear scalar couplings (also called B-terms).

Despite its theoretical appeal, the MSSM's predictions must be tested experimentally. The search for superpartners is a major focus of experiments at particle colliders such as the Large Hadron Collider (LHC), a proton-proton collider at CERN which operates at $\sqrt{s} = 13.6$ TeV. To date, no direct experimental evidence of superpartners has been found, leading to constraints on the parameter space of the MSSM. However, some experiments have shown a few-σ deviations from the expectations of the SM, indicating that SUSY or some other extension of the

SM may be required. These ongoing searches are crucial for either validating the MSSM or guiding physicists towards alternative theories. In the following chapters, we will delve deeper into the structure, particle content, and phenomenological implications of the MSSM, highlighting its role as a cornerstone in the quest for a more comprehensive understanding of fundamental physics. Next, we will introduce some specific, common realizations of the MSSM in the literature through the CMSSM and NUHMi models, where $i = 1, 2, 3, 4$, along with the concept of the string landscape to implement gravity into the theory, and how some universes within a broader "multiverse", or landscape of universes, could support the idea of the MSSM emerging from this landscape. In later chapters, we will present our new results that compare finetuning measures within these models and more, both within the context of our universe and within multiple possible universes in a broader "landscape" of universes that may lead to large-scale structure formation, the capability of chemistry to exist, and the possibility of observers within these universes. Many of our results for traditional naturalness measures are presented as a numerical refinement of older calculations that used assumptions leading to inaccuracies in the results. Some of the most common MSSM models used in the literature for phenomenological analyses are introduced briefly now.

1.2.7 Minimal supergravity model (mSUGRA) and the Constrained MSSM (CMSSM)

The Constrained Minimal Supersymmetric Standard Model (CMSSM) is a specific version of the Minimal Supersymmetric Standard Model (MSSM), characterized

by its simplicity and predictive power. It assumes:

1. **Universality of SSB parameters:** At the Grand Unification Theory (GUT) scale $\sim 2 \cdot 10^{16}$ GeV where the $SU(2)$ and $U(1)$ gauge couplings unify under renormalization group evolution, the soft SUSY-breaking parameters are taken to be universal, meaning [7]:

   - A common scalar mass (m_0);
   - A common gaugino mass ($m_{1/2}$);
   - A common trilinear coupling A_0.

2. **Radiative electroweak symmetry breaking:** The Higgs sector parameters are fixed by the requirement of electroweak symmetry breaking driven by radiative corrections. In the CMSSM, this may come at the expense of extreme finetuning amongst parameters, as we will delve into later in this work. For example, the μ parameter of the MSSM, or the Higgsino mass parameter, may be tuned such that the experimentally-observed value of the Z-boson mass, $m_Z^2 = 91.2^2$ GeV^2 is obtained from Higgs scalar potential minimization conditions. This scenario may be obtained within the framework of gravity-mediated SUSY breaking through a "minimal" choice of the Kähler potential [3]. In the CMSSM, the $B\mu$ parameter can be swapped for a specification of the value of the ratio of the Higgs VEVs, $\tan(\beta) = v_u/v_d$.

Generally, these assumptions significantly reduce the number of free parameters within the MSSM, making the CMSSM a highly constrained and testable framework for SUSY phenomenology. The CMSSM is often linked with the concept of

minimal supergravity (mSUGRA) GUTs, a theoretical framework that provides a mechanism for breaking supersymmetry in a hidden sector and transmitting this breaking to the observable sector via gravitational interactions [8, 9]. Key features of mSUGRA include:

1. Supersymmetry is broken in a hidden sector [10].

2. The breaking is communicated to the observable sector through gravitational interactions [11].

3. At the GUT scale, the soft SUSY-breaking terms are universal, leading to the CMSSM parameter structure.

mSUGRA provides a strong theoretical foundation for the universality assumptions of the CMSSM.

1.2.8 Non-universal Higgs models (NUHMi)

Non-universal Higgs models (NUHM) extend the CMSSM by relaxing the universality condition(s) for the Higgs sector and scalar mass parameters. This allows for more flexibility in the Higgs, squark, and slepton sectors (for higher values of i) while keeping the universality for other gaugino and trilinear coupling parameters [12]. There are four "flavors" of NUHM models, which are characterized below and expanded upon later in this work. The extra non-universality granted by these models may allow for a better fit to experimental data [13, 14]. The extra degrees of freedom afforded also permit much lower levels of finetuning, compared to the CMSSM, for example. Explicit comparisons on the grounds of finetuning

and naturalness will be made in later chapters, but we present a review of the four main types of NUHM models below.

NUHM1

This model is characterized by having one additional parameter to those set forth in the CMSSM, allowing the Higgs masses $m_{H_u}^2$ and $m_{H_d}^2$ to still be unified with *each other* at the GUT scale, but perhaps at a value separate from the other scalar masses, which are set at m_0 [15]. The parameter set for this model is then:

$$m_{H_{u,d}}^2, m_0, m_{1/2}, A_0, \tan(\beta).$$

NUHM2

This model introduces two additional parameters to the CMSSM parameter set by allowing both Higgs mass parameters to be non-universal. This causes the parameter space for this model to consist of:

$$m_{H_u}^2, m_{H_d}^2, m_0, m_{1/2}, A_0, \tan(\beta).$$

In practice for phenomenology, it is common for the GUT-scale values of $m_{H_{u,d}}^2$ to be swapped for the weak-scale values of μ and m_A, the pseudoscalar mass, to be specified.

NUHM3

This model introduces three additional parameters to the CMSSM parameter set by allowing both Higgs mass parameters to be non-universal, as well as allowing the third generation squark and slepton masses to unify at a value separate from the first two generations [14]. This causes the parameter space for this model to consist of:

$$m_{H_u}^2, m_{H_d}^2, m_0(3), m_0(1,2), m_{1/2}, A_0, \tan(\beta).$$

Here, $m_0(i)$ denotes the unified scalar mass at the GUT scale for the squarks and sleptons of the i'th generation.

NUHM4

Finally, this model has the most non-universality of the NUHM models by introducing *four* additional parameters to the CMSSM parameter set. The Higgs masses are allowed to be non-universal, and the first, second, and third generations of squarks and sleptons are each allowed to unify at distinct values from other generations [15, 16]. This causes the parameter space for this model to consist of:

$$m_{H_u}^2, m_{H_d}^2, m_0(3), m_0(2), m_0(1)m_{1/2}, A_0, \tan(\beta).$$

1.3 The string landscape

String theory is a theoretical framework that attempts to reconcile quantum mechanics and general relativity by positing that the fundamental building blocks

of the universe are not point-like particles but rather one-dimensional objects known as strings. These strings can vibrate at different frequencies, with each vibration mode corresponding to a different particle. One of the remarkable aspects of string theory is that it naturally incorporates gravity, making it a strong candidate for a theory of everything.

However, string theory is not a single theory but a framework that encompasses a multitude of possible solutions. These solutions are characterized by different ways of compactifying the extra dimensions required by string theory. In most string theories, our familiar four-dimensional spacetime is supplemented by six or seven additional spatial dimensions which are compactified into a Calabi-Yau space. The manner in which these extra dimensions are compactified leads to different low-energy physical laws, effectively creating a vast "landscape" of possible universes[17].

1.3.1 The landscape of vacua

The concept of the string landscape refers to the multitude of possible vacuum states or solutions in string theory. Each vacuum state corresponds to a different set of 4-d physical laws, particle spectra, and constants of nature. It is estimated that the number of possible vacua in the string landscape is on the order of 10^{500} or even larger[17]. This vast number of solutions implies a rich diversity of possible universes, each with its own distinct physical properties. However, a key note is that only a subset of these may be able to support observers, due to factors such as the cosmological constant[18] and the predicted value of the weak scale and its

correlation with chemistry, or the "atomic principle"[19].

In the context of the string landscape, our universe is just one of many possible "pocket universes" (PU) that exist within a broader multiverse [20]. Each pocket universe corresponds to a different point in the string landscape, characterized by a specific vacuum state with its own unique physical laws and parameters. The idea of a multiverse composed of pocket universes raises many profound questions about the nature of physical reality and the origin of the specific properties observed in our universe. One intriguing possibility is that the properties of our universe, such as the values of fundamental constants and the presence of the SM, are the result of a selection process within the multiverse. This selection process may be influenced by anthropic considerations, where only universes with properties conducive to the development of large-scale structure and life are observed.

The MSSM may be seen as one possible low-energy effective field theory (EFT) emerging from the string landscape. In some pocket universes, the vacuum state of string theory may break supersymmetry in such a way that the low-energy physics resembles the MSSM, at least within some "neighborhood" of the landscape[19, 21, 22]. This provides a natural context for the MSSM and its phenomenological viability within the broader framework of string theory. Some relevant key notes from the theory are summarized below:

1. **Compactification and SUSY breaking:** Different ways of compactifying the extra dimensions in string theory can lead to different mechanisms of SUSY breaking. In some compactifications, SUSY may be broken at a low

scale $F_X \sim (10^{11}\text{ GeV})^2 \ll m_P^2$, resulting in the MSSM with TeV-scale soft terms as the EFT at lower energies.

2. **Vacuum selection and anthropic principle:** The string landscape allows for the possibility that the MSSM is realized in a universe (such as ours) due to anthropic selection. Universes with the MSSM might be more conducive to the formation of complex- and large-scale structures, as well as observers, leading to their preferential observation. As an example of vacuum selection and anthropic principles, the immense number of vacuum states that are viable within the string landscape framework provided a setting for Weinberg's anthropic solution to the cosmological constant (CC) problem by realizing that pocket universes with too high of a CC will expand too rapidly and result in a universe devoid of large-scale structure such as galaxies [18].

3. **Predictive power and experimental tests:** While the string landscape presents a challenge for making precise predictions, it also provides a framework for understanding the diversity of possible low-energy theories. Experimental tests at particle colliders and observations of cosmological phenomena can provide indirect evidence for or against specific compactifications and the presence of supersymmetry. However, it may yet be possible to offer *statistical* predictions of the theory from the large set of possible vacua. This is what is addressed in Chapters 4 and 5, where we offer a novel way of analyzing the density of vacua resulting from some supersymmetric

EFT in the string landscape as a means of statistically comparing different vacuum possibilities on the landscape.

To finalize our introduction, the string landscape offers a rich tapestry of possible universes, each with its own unique physical laws and particle content. Within this landscape, the MSSM emerges as a compelling candidate for the low-energy effective theory in some pocket universes. This connection between the MSSM and the string landscape provides a broader context for understanding the origins and implications of supersymmetry and offers intriguing possibilities for future theoretical and experimental exploration.

In the following chapters, we will explore specific models and mechanisms within the string landscape that lead to the MSSM, examine the implications of these models for our understanding of fundamental physics, and discuss how ongoing and future experiments might provide insights into the structure of the multiverse and the nature of our universe. To begin, we will address the concepts of finetuning and naturalness, in regards to resolving the Little Hierarchy Problem that has arisen in the research field, since we have not yet experimentally observed superpartners. In doing so, we will present how traditional finetuning measures overestimate the degree of electroweak finetuning via a newly developed software that operates on the existing architecture for presenting supersymmetric particle spectra for phenomenological studies [23, 24]. Then we will present new analyses of the string landscape incorporating new probability measures for a vacuum supporting observers to emerge from the string landscape, along with their implementation into publicly available software.

Chapter 2

Practical naturalness as a guide to new physics

2.1 Naturalness

As mentioned in the Introduction, WSS provides us with a solution to the gauge hierarchy problem by stabilizing the Higgs boson mass under quantum corrections, while introducing a variety of new states of matter, the superpartners of the SM. Phenomenologically, SUSY theory is supported by the data from the following virtual effects.

1. The three gauge couplings unify at a high scale $M_{\rm GUT}$ to a remarkable precision due to the radiative effects of renormalization group running [25, 26, 27, 28].

2. The Higgs boson mass $m_h \sim 125$ GeV lies directly within the narrow window of possible values predicted in the Minimal Supersymmetric Standard Model (MSSM) [29].

3. The top quark was predicted to be heavy – $\sim 100 - 200$ GeV – by SUSY to facilitate radiative electroweak symmetry breaking (EWSB) prior to its experimental discovery [30, 31].

4. Electroweak precision corrections to observables favor heavy SUSY over the SM in the m_t vs. m_W plane [32].

Additionally, superstring theory provides the most promising avenue for unify-

ing the SM with gravity. This comes at the price of requiring 6 or 7 extra spatial dimensions[33, 34, 35, 36, 37]. The low energy limit of string theory, characterized by $E < m_P$, where m_P is the reduced Planck mass, is expected to be $10-d$ supergravity (SUGRA), after integrating out Kaluza-Klein modes. The $10-d$ SUGRA theory must then be compactified down to an extremely small $6-d$ space K tensored with our usual $4-d$ (approximately) Minkowski spacetime M_4: $M_{10} = M_4 \times K$. Originally, K was taken to be a $6-d$ compact Ricci-flat Kähler manifold with special holonomy[38]. This type of Calabi-Yau manifold admits a conserved Killing spinor, which in effect leads to a remnant $N = 1$ SUSY on M_4.

The cosmological constant (CC) problem remained a thorny issue until the early 2000s when it was realized that string flux compactifications could lead to an enormous number of vacuum states each with different $4-d$ laws of physics, and in particular, different Λ_{CC} values[39]. Such large numbers of vacuum states ($N_{vac} \sim 10^{500}$ is an oft-quoted number[40]) provided a setting for Weinberg's anthropic solution to the CC problem[18]. But if the landscape[41] of string vacua provides a solution to the CC problem, might it also enter into other naturalness problems, such as the m_{weak}/m_P (or related, m_{SUSY}/m_P) hierarchy problems (where $m_P \simeq 2.4 \times 10^{18}$ GeV)? We will return to this subject in later chapters. First, we must clarify the underlying concept of "naturalness" that continues to guide our expectations of new physics and the scales at which those new physics occur.

In spite of this impressive litany of successes, it is common nowadays to dismiss weak scale supersymmetry (WSS)[3] as a viable beyond-the-Standard Model (BSM)

theory due to the apparent lack of new physics signals at the CERN LHC[42]. The data from LHC, which is by-and-large in accord with SM expectations[43], is in contrast to early theoretical expectations for WSS based upon naturalness arguments that superpartners would emerge with mass values not far from the weak scale $m_{weak} \simeq m_{W,Z,h} \sim 100$ GeV[44, 45, 46, 47, 48, 49, 50, 51, 52]. At present, such arguments are being used to set policy and guide future facilities for the High Energy Physics (HEP) frontier[53, 54]. Given the stakes involved, it is essential to go back and review the naturalness-based arguments to assess when and where and if they present a reliable guide to the search for new physics.

2.1.1 The Little Hierarchy Problem and Practical Naturalness

Supersymmetry offers a 't Hooft technically natural solution[55] to the hierarchy of scales problem in that, as the hidden sector SUSY breaking scale m_{hidden} (which determines the magnitude of the soft terms via $m_{soft} \sim m_{3/2} \sim m_{hidden}^2/m_P$ in gravity-mediation and hence of the weak scale via the scalar potential minimization conditions in Appendix A) is taken to zero, the model becomes more (super)symmetric. The SUSY solution to this *big* hierarchy problem (BHP) – stabilizing the weak scale so that it doesn't blow up to the Planck or GUT scale – is *not* the naturalness issue which concerns many contemporary SUSY theorists. Indeed, 't Hooft naturalness remains a valid solution to the BHP even for very large gaps $m_{soft} \gg m_{weak}$. Instead, it is the so-called *little hierarchy problem* (LHP) which is of concern[56, 57]:

how can it be that $m_{weak} \sim m_{W,Z,h} \sim 100$ GeV is so much smaller than the soft SUSY breaking terms, which, according to LHC data, are $m_{soft} \gtrsim 1$ TeV (owing to LHC bounds $m_{\tilde{g}} \gtrsim 2.2$ TeV, $m_{\tilde{t}_1} \gtrsim 1.1$ TeV, $\cdots$)[58]?

In addressing the LHP, what is of concern is what we call the notion of **practical naturalness** (PN)[59][1]:

An observable $\mathcal{O} = o_1 + \cdots + o_n$ is practically natural if all *independent* contributions o_i to $\mathcal{O}$ are comparable to or less than $\mathcal{O}$.

(Here, *comparable to* means within a factor of several from the measured value.) Practical naturalness embodies the notion of naturalness that is most often used in successful applications of naturalness. For instance, by requiring the charm quark mass contribution

$$\Delta m_K(c) \simeq \frac{G_F}{\sqrt{2}} \frac{\alpha}{6\pi} \frac{f_K^2 m_K}{\sin^2\theta_W} \cos^2\theta_C \sin^2\theta_C \frac{m_c^2}{m_W^2} \tag{2.1}$$

to be comparable to or less than the measured $K_L - K_S$ mass difference $\Delta m_K \sim 3.5 \cdot 10^{-12}$ MeV, Gaillard and Lee[62] were able to predict $m_c \sim 1.5$ GeV several months before the charm quark was discovered[2].

Weak scale naturalness plays a key role in determining the viability of Beyond the Standard Model theories such as SUSY. For the case of the SM, where the

[1] This is in accord with Veltman's notion of naturalness as presented in Ref. [60]. See also Susskind[61].

[2] It is still a breathtaking exercise to plug in the numbers and see the charm quark mass emerge.

Higgs potential is given by

$$V = -\mu_{SM}^2 \phi^\dagger \phi + \lambda (\phi^\dagger \phi)^2, \tag{2.2}$$

a vacuum expectation value $v = \sqrt{\mu_{SM}^2/\lambda}$ develops and the tree-level Higgs boson mass is given by $m_h^2 = 2\mu_{SM}^2$. The loop-corrected Higgs mass is quadratically divergent up to some cutoff scale Λ_{SM} where

$$m_h^2 = 2\mu_{SM}^2 + \delta m_h^2 \tag{2.3}$$

where at one loop

$$\delta m_h^2 \simeq \frac{3}{4\pi^2}\left(-\sum_i \lambda_i^2 + \frac{g^2}{4} + \frac{g^2}{8\cos^2\theta_W} + \lambda\right)\Lambda_{SM}^2 \tag{2.4}$$

where the λ_i are Yukawa couplings for the ith fermion, g is the $SU(2)_L$ gauge coupling and λ is the Higgs quartic coupling[63]. Requiring practical naturalness then leads to $\Lambda_{SM} \lesssim 1$ TeV whilst finetuning is required for much higher values of $\Lambda_{SM} \gg 1$ TeV.

In SUSY models with the MSSM as the LE-EFT, then the weak scale is actually predicted in terms of the weak scale soft SUSY breaking terms and superpotential μ parameter. Minimization of the Higgs potential in the MSSM leads to Eq. 2.9, which will be described briefly.

An essential element of practical naturalness is that the contributions o_i should be independent of one another in the sense that if one of the o_i is varied, then

the others don't necessarily vary. For instance, Dirac was bothered by various divergent contributions to perturbative QED observables. However, these were *dependent* contributions in that if the regulator was varied, the different divergent terms would also vary. One should always first *combine dependent terms* before evaluating naturalness. Once dependent terms are combined, then a measure of naturalness emerges:

$$\Delta \equiv \max_i |o_i|/|\mathcal{O}|. \tag{2.5}$$

Using PN, we see that QED perturbation theory is practically natural in that the leading terms are comparable to the measured observables whilst higher order terms (once dependent terms are combined) are typically much smaller.

One must properly address the evaluation of electroweak finetuning in an attempt to address the LHP. In the next section, we revisit several proposed naturalness measures which have been applied to various supersymmetric models. As opposed to 't Hooft naturalness, these measures determine the degree of *practical naturalness*. Historically, the first of these is the EENZ/BG[44, 45] measure (labeled here as $\Delta_{\rm BG}$) which determines the sensitivity of the measured value of the weak scale to variation in model parameters p_i (i labels the various parameters under consideration). Typically the p_i have been taken to be the various soft SUSY breaking terms starting at a high effective field theory (EFT) cutoff scale $\Lambda = m_{GUT} \simeq 2 \times 10^{16}$ GeV:

$$\Delta_{\rm BG} \equiv \max_i |\frac{\partial \log m_Z^2}{\partial \log p_i}| = max_i |\frac{p_i}{m_Z^2}\frac{\partial m_Z^2}{\partial p_i}|. \tag{2.6}$$

For small $\Delta_{\rm BG} \lesssim 30$, then sparticle masses are expected below the several hundred GeV range although in some special regions of model parameter space, such as the focus point region[64, 65] of the minimal supergravity[66] (mSUGRA) or constrained MSSM[7] (CMSSM) model, multi-TeV scale top squarks can be allowed. Despite its popularity, this measure has been argued to *overestimate* finetuning in SUSY models by large factors and to give ambiguous answers depending on exactly which parameters are chosen to be the fundamental p_i[67, 68].

A second measure, which we label here as $\Delta_{\rm HS}$ (for high scale sensitivity of the up-Higgs soft mass $m_{H_u}^2$), starts with the approximate SUSY Higgs mass relation $m_h^2 \sim \mu^2 + m_{H_u}^2(weak)$ where $m_{H_u}^2(weak) = m_{H_u}^2(\Lambda) + \delta m_{H_u}^2$. One then requires

$$\Delta_{\rm HS} = \delta m_{H_u}^2 / m_h^2 \tag{2.7}$$

to be small. (It is the large top-quark Yukawa coupling f_t which radiatively drives $m_{H_u}^2$ from its large SUGRA value at the high scale to small, usually negative values at the weak scale so that EW symmetry is spontaneously broken.) This measure, which is inconsistent with $\Delta_{\rm BG}$ in that it doesn't allow for multi-TeV top squarks even in the FP region, has lead to intense scrutiny of LHC top squark searches since it is expected that $\delta m_{H_u}^2 \sim \frac{6f_t^2}{(4\pi)^2} m_{\tilde{t}}^2 \log \frac{\Lambda^2}{m_{\tilde{t}}^2}$[69, 70, 71, 72, 73, 74, 75]. $\Delta_{\rm HS}$ was found to lead to violations of the finetuning rule[67]: that it is not allowed to claim finetuning amongst *dependent* terms which contribute to some observable $\mathcal{O}$. In this case, $\delta m_{H_u}^2$ and $m_{H_u}^2(\Lambda)$ are dependent due to renormalization group running, leading to overestimates in finetuning. To see this, we see that the

one-loop renormalization group equation (RGE) for the $m^2_{H_u}$ parameter is given below. The more complete two-loop expression is presented in Appendix B, Eqs. (B.14, B.37).

$$\beta^{(1\ell)}_{m^2_{H_u}} = 6\mathrm{Tr}\left[(m^2_{H_u} + \mathcal{M}^2_{\widetilde{Q}} + \mathcal{M}^2_{\widetilde{U}})\mathcal{Y}^2_U + \mathbf{a}^2_U\right] - \frac{3}{5}g_1^2\left(2M_1^2 - \widetilde{S}\right) - 6g_2^2M_2^2 \quad (2.8)$$

Here, $M_{1,2}$ represent the $U(1)$ and $SU(2)$ gaugino masses, $g_{1,2}$ their respective gauge group couplings, $\widetilde{S}$ is a function of $m^2_{H_u}$ and the other scalar masses (presented in Eq. (B.13)), $\mathcal{M}_{\tilde{i}}$ are squark mass squared matrices in generation space, $\mathbf{a}_U$ is the up-type soft trilinear coupling matrix in generation space, and $\mathcal{Y}_U$ is the up-type Yukawa coupling matrix in generation space. Clearly, the evolution of $m^2_{H_u}$ directly depends on its own value.

A third measure is the *electroweak* measure $\Delta_{\rm EW}$[76, 77] which is touted to be more conservative and model independent than the others, and also unavoidable (within the context of the MSSM). It is based on the SUSY Higgs potential minimization condition

$$m_Z^2/2 = \frac{m^2_{H_d} + \Sigma^d_d - (m^2_{H_u} + \Sigma^u_u)\tan^2\beta}{\tan^2\beta - 1} - \mu^2 \simeq -m^2_{H_u} - \mu^2 - \Sigma^u_u(\tilde{t}_{1,2}) \quad (2.9)$$

where all right-hand-side (RHS) entries are taken as their weak scale values in the renormalization group running and

$$\Delta_{\rm EW} \equiv \max_i |C_i|/(m_Z^2/2). \quad (2.10)$$

C_i are the independent entries on the RHS of Eq. 2.9. As an aside, the approximation on the far RHS of Eq. 2.9 tends to hold for moderate to large values of $\tan(\beta)$, but neglects some potentially important terms arising from the higher-order Σ contributions, or from large $m_{H_d}^2$ values, especially in certain cases of non-universal Higgs masses at the GUT scale. For these reasons, the approximation here should be used cautiously, depending on the application – the full expressions, presented in Appendix A, lead to more numerically stable and complete analyses. This measure was preceded by Chan *et al.*[78] who suggested that the magnitude of the SUSY conserving μ parameter could serve as a finetuning measure all by itself. This measure is sometimes criticized in that it apparently lacks sensitivity to high scale parameters (more on this later).

A fourth entry has been formerly known to not be a quantifiable measure, but known nonetheless as *stringy naturalness* (SN), which arises from Douglas' consideration of the string landscape picture[79]:

> **Stringy naturalness:** An observable $\mathcal{O}_1$ is more (stringy) natural than observable $\mathcal{O}_2$ if more *phenomenologically viable* string vacua lead to $\mathcal{O}_1$ than to $\mathcal{O}_2$.

In this work, we present a method by which stringy naturalness may be quantified within regions of the string landscape. To quantify stringy naturalness, at least two ingredients are needed: 1. the expected distribution of some quantity within the landscape of vacua possibilities and 2. an anthropic selection ansatz for which many choices would lead to universes that are unable to support observers. For the

case of SUSY models, the first of these is usually how soft terms are distributed in the landscape while the second of these is the magnitude of the weak scale itself: if the predicted value of m_{weak} within each pocket universe is too far displaced from its measured value in our universe, then nuclear physics goes astray, and atoms as we know them fail to appear– leading to no complex chemistry as seems to be needed for life as we know it (atomic principle)[80]. An attempt to compute and display stringy naturalness via density of dots in model parameter space has been made in Ref. [81].

In the present work, we reexamine these several measures of naturalness, filling in some of the many gaps of understanding that exist in the literature. Part of our work is based on a new computation of $\Delta_{\rm BG}$ naturalness based on evaluating numerically the derivatives in Eq. 2.6. This new computation is embedded in the publicly available code DEW4SLHA[77] so that the updated code can provide values of each of the measures $\Delta_{\rm BG}$, $\Delta_{\rm HS}$ and $\Delta_{\rm EW}$ given an input SUSY Les Houches Accord (SLHA) file[82].[3] We also compute ratios of naturalness measures to determine the extent of which some measures can overestimate finetuning in SUSY models. For instance, in the SUSY theory review contained in the Particle Data Book[83], it is suggested that the overestimates may range up to a factor 10; in contrast, we find overestimates ranging up to factors of over 1000.

[3]The code DEW4SLHA, written by D. Martinez, is available at *https://www.dew4slha.com.*

2.2 On the evaluation of electroweak finetuning

2.2.1 Sensitivity to high scale parameters: EENZ/BG naturalness

Historically, the first measure of SUSY model naturalness was proposed by Ellis *et al.* in Ref. [44] and subsequently used by Barbieri and Giudice[45] to compute sparticle mass upper bounds in the mSUGRA/CMSSM model: Eq. 2.6. The measure purports to compute sensitivity of the measured value of the weak scale to variation in high scale parameters p_i. The $\Delta_{\rm BG}$ measure is actually a measure of practical naturalness of the weak scale in the case where $m_Z^2 = a_1 p_1 + \cdots + a_n p_n$. Let's suppose the jth contribution to m_Z^2 is largest. Then $\Delta_{\rm BG} = \max_i |(p_i/m_Z^2)\partial m_Z^2/\partial p_i| = |a_j p_j/m_Z^2|$ in accord with Eq. 2.5. The various $|a_i p_i/m_Z^2| \equiv c_i$ terms are labeled sensitivity coefficients[84]. The rub here is what choice to take as to the free parameters p_i. [4]

The starting point is to express m_Z^2 in terms of weak scale SUSY parameters as in Eq. 2.9:

$$m_Z^2 \simeq -2m_{H_u}^2 - 2\mu^2 \tag{2.11}$$

where the partial equality is obtained for moderate-to-large $\tan(\beta)$ values and where we assume for now that the radiative corrections are small. To evaluate Δ_{BG}, one needs to know the explicit dependence of $m_{H_u}^2$ and μ^2 on the fundamental parameters. Semi-analytic solutions to the one-loop renormalization group

[4] Giudice remarks in Ref. [63]: "It may well be that, in some cases, Eq. 2.6 overestimates the amount of tuning. Indeed, Eq. 2.6 measures the sensitivity of the prediction of m_Z as we vary parameters in *theory space*. However, we have no idea how this *theory space* looks like, and the procedure of independently varying all parameters may be too simple-minded" . See also discussion in Ref. [50].

equations for $m_{H_u}^2$ and μ^2 can be found for instance in Refs. [85, 86]. For the case of $\tan\beta = 10$, then[52, 87, 84]

$$\begin{aligned} m_Z^2 \simeq & -2.18\mu^2 + 3.84M_3^2 + 0.32M_3M_2 + 0.047M_1M_3 \\ & -0.42M_2^2 + 0.011M_2M_1 - 0.012M_1^2 - 0.65M_3A_t \\ & -0.15M_2A_t - 0.025M_1A_t + 0.22A_t^2 + 0.004M_3A_b \\ & -1.27m_{H_u}^2 - 0.053m_{H_d}^2 \\ & +0.73m_{Q_3}^2 + 0.57m_{U_3}^2 + 0.049m_{D_3}^2 - 0.052m_{L_3}^2 + 0.053m_{E_3}^2 \\ & +0.051m_{Q_2}^2 - 0.11m_{U_2}^2 + 0.051m_{D_2}^2 - 0.052m_{L_2}^2 + 0.053m_{E_2}^2 \\ & +0.051m_{Q_1}^2 - 0.11m_{U_1}^2 + 0.051m_{D_1}^2 - 0.052m_{L_1}^2 + 0.053m_{E_1}^2, \end{aligned} \tag{2.12}$$

where all terms on the right-hand-side are understood to be GUT scale parameters. As an example, if we adopt $m_{Q_3}^2$ as a fundamental parameter, then the sensitivity coefficient $c_{m_{Q_3}^2} = 0.73m_{Q_3}^2/m_Z^2$ and for $m_{Q_3} = 3$ TeV, then one finds $c_{m_{Q_3}^2} \simeq 800$ so that $\Delta_{\rm BG} > 800$ and the model is certainly finetuned. If instead we declare all scalar masses unified to m_0, then there are large cancellations and instead one finds $c_{m_0^2} = 0.013m_0^2/m_Z^2 \sim 14.2$: a reduction in finetuning by over a factor 50! Clearly, whether or not soft terms are correlated or not makes a big difference in the evaluation of $\Delta_{\rm BG}$!

Numerical routine to compute $\Delta_{\rm BG}$

The evaluation of Δ_{BG} can be done by approximating the partial derivatives with the method of finite difference quotients (particularly, central differences

here). That is, for finding the partial derivative with respect to a parameter p_1 of $m_Z^2(p_1, p_2, \ldots, p_n)$, where p_i are the fundamental parameters of the model chosen for evaluating Δ_{BG}, then

$$\frac{\partial m_Z^2\,(p_1, p_2, \ldots, p_n)}{\partial p_1} \approx \frac{m_Z^2(p_1 + h_1, p_2, \ldots, p_n) - m_Z^2(p_1 - h_1, p_2, \ldots, p_n)}{2h_1}. \quad (2.13)$$

h_1 is the size of the variation of the differentiation parameter p_1, which is then used to determine the resulting change in m_Z^2. Since this is a partial derivative, all other input parameters are left fixed at their original values prior to differentiation.

To compute this derivative, m_Z^2 must be evaluated in the right-hand side of Eq. 2.13 as an *output* of the m_Z^2 Higgs minimization condition, Eq. 2.9, at the weak renormalization scale $Q_{\rm SUSY} = \sqrt{m_{\tilde{t}_1} m_{\tilde{t}_2}}$ to minimize radiative corrections in the Higgs minimization condition. For the partial derivative of m_Z^2 with respect to p_i, the GUT-scale parameter p_i defined at the renormalization scale $Q_{\rm GUT}$ is varied to $p_i + h_i$, with $h_i \ll p_i$. Then the *new* set of GUT-scale parameters $\{p_1, p_2, \ldots, p_i + h_i, \ldots, p_{n-1}, p_n\}$ are evolved from $Q_{\rm GUT}$ down to $Q_{\rm SUSY}$ using the full two-loop MSSM renormalization group equations (RGEs). Lastly, the varied value $m_Z^2(p_1, p_2, \ldots, p_i + h_i, \ldots, p_{n-1}, p_n)$ is computed from the tree-level Higgs minimization condition for m_Z^2, giving a value slightly deviated from 91.2^2. This value is then used in Eq. 2.13 and the process is repeated for the other direction of variation.

In this numerical derivative approach, two sources of error can enter and skew

the results: truncation error and roundoff error. Below are some descriptions of these errors and how we minimize them.

- Truncation error is the error of approximating the true, analytical derivative of m_Z^2, a tangent line to the m_Z^2 curve, with our numerical two-point method, producing a secant line to the m_Z^2 curve. For a given derivative variation size of h, the truncation error for this two-point method is suppressed by a term of $\mathcal{O}(h^2)$. This error remains relatively small so long as the step size $h < 1$ and the higher-order derivatives of m_Z^2 are reasonably bounded.

- Roundoff error comes from representing the values $p_1, p_2, \ldots, p_n$, and h_1 in Eq. 2.13 as floating point numbers, where the computer must "round off" most decimal values after a certain number of digits due to storage limitations in binary. Because of this, there is a non-zero spacing between two consecutive floating point numbers x and y, and this spacing is called the unit of least precision (denoted ULP(x)). Careful error analysis reveals that the roundoff error is proportional to the step size used in the evaluation. This roundoff error is then minimized when, for a two-point central difference, the step size h_i for the derivative with respect to some p_i is chosen as $h_i \approx [\text{ULP}\,(p_i)]^{1/3}$. In order for $h_i < 1$ to occur, the ULP(p_i) must then also be less than unity.

Numerical error may also enter through the numerical solution of the RGEs, though similar numerical considerations can help control these errors as well. With these sources of error in mind, the error in evaluating this derivative will

remain small, i.e., $\mathcal{O}(< 1)$, so long as $|p_i| \lesssim 10^{15}$ in magnitude for all i. This leads to $h_i < 1$ for double-precision floating point numbers. DEW4SLHA offers the option of performing this calculation with even higher accuracy derivative approximations, such as a four-point or eight-point central difference quotient to further minimize truncation error.

The numerical evaluation of $\Delta_{\rm BG}$ has several advantages over the semi-analytic formulae using expansions such as Eq. 2.12.

- The numeric routine uses full two-loop RGEs including all third generation Yukawa couplings[88] and one- and partial two-loop radiative corrections, while semi-analytic expansions use one-loop RGEs without loop-corrected weak-scale contributions.

- The semi-analytic expansions were formulated to compute the Higgs potential at a scale $Q \sim m_Z$ whilst the numeric routine uses an optimized scale choice $Q^2 = m_{\tilde{t}_1} m_{\tilde{t}_2}$ which matches the higher scales for MSSM/SM decoupling that are expected from LHC data.

- Usually the semi-analytic expansions are computed for a particular $\tan\beta$ value while the numeric evaluation is valid for all $\tan\beta$.

To illustrate the comparison between the two methods, in Fig. 2.1*a*) we compute the ratio Δ_{BG}(numerical)/$\Delta_{\rm BG}$(semianalytic) in the m_0 vs. $m_{1/2}$ plane of the mSUGRA/CMSSM plane for $A_0 = 0$ and $\tan\beta = 10$ with $\mu > 0$. The blue region corresponds to a ratio ~ 0.5 while for small m_0 we find Δ_{BG}(numerical)/$\Delta_{\rm BG}$(semianalytic) $\lesssim$

1 and for large m_0 then we find Δ_{BG}(numerical)/$\Delta_{\rm BG}$(semianalytic) $\gtrsim 1$ with the ratio reaching as high as ~ 2 near the lower focus point region.

In Fig. 2.1*b*) we again compute the ratio $\Delta_{\rm BG}$(numerical)/$\Delta_{\rm BG}$(semianalytic) in the m_0 vs $m_{1/2}$ plane of the mSUGRA/CMSSM, but now for $A_0 = -2m_0$ and $\tan\beta = 10$ with $\mu > 0$. The large value of A_0 here permits the Higgs mass to be within the allowed range of 125 ± 2 GeV. The broad orange and red regions throughout the RHS of the plane correspond to where $\Delta_{\rm BG}$(numerical) $\sim$ $\Delta_{\rm BG}$(semianalytic). The largest discrepancy between the evaluation methods occurs on the LHS of the plane near the stau LSP region, where $\Delta_{\rm BG}$(numerical) $\sim$ $0.6\Delta_{\rm BG}$(semianalytic). Fig. 2.1*c*) instead shows the ratio comparing the numerical method to the semianalytic method in the m_0 vs $m_{1/2}$ plane of the *NUHM2* model with $\mu = 200$ GeV, $m_A = 2$ TeV and $A_0 = -1.6m_0$. Again, the broad orange and red region on the RHS of this plane shows very good agreement between the two methods: $\Delta_{\rm BG}$(numerical) $\sim \Delta_{\rm BG}$(semianalytic). On the LHS above the CCB minima region, where $m_{1/2} > m_0$, then the semianalytic method result becomes somewhat larger than the numerical method result, leading to a minimal ratio $\Delta_{\rm BG}$(numerical) $\sim 0.57\Delta_{\rm BG}$(semianalytic).

Numerical results for $\Delta_{\rm BG}$

In Fig. 2.2, we compute contours and color-coded regions of $\Delta_{\rm BG}$ in the mSUGRA/CMSSM model using a numerical routine to evaluate the sensitivity coefficients. This routine is embedded in the publicly available computer code DEW4SLHA which computes the three measures of naturalness $\Delta_{\rm BG}$, $\Delta_{\rm HS}$ and

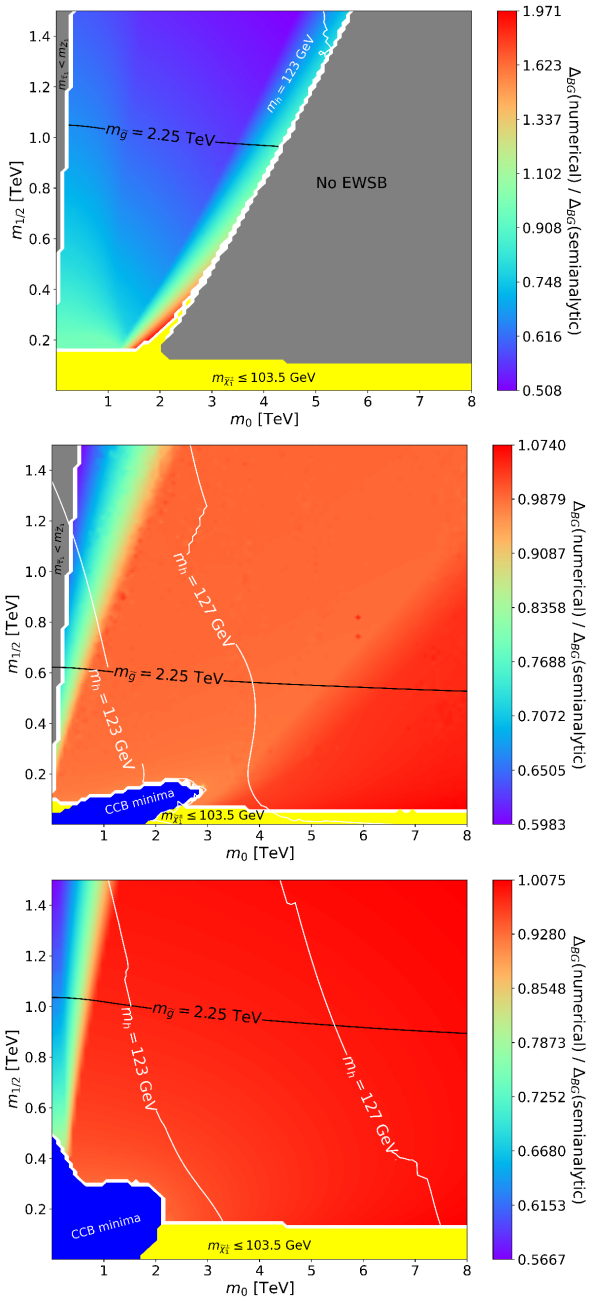

Figure 2.1: Plot of Δ_{BG}(numerical)/$\Delta_{\rm BG}$(semianalytic) in the m_0 vs. $m_{1/2}$ plane of *a*) the CMSSM/mSUGRA model with $A_0 = 0$, $\tan\beta = 10$ and $\mu > 0$, *b*) the CMSSM/mSUGRA model with $A_0 = -2m_0$ and *c*) the NUHM2 model with $\mu = 200$ GeV and $A_0 = -1.6m_0$ with $m_A = 2$ TeV. We use the code DEW4SLHA to compute Δ_{BG}(numerical) using a numerical algorithm for the sensitivity coefficients and SoftSUSY v4.1.17 for the spectrum.

$\Delta_{\rm EW}$ for any model based on its Les Houches Accord spectrum generator output file. The results in Fig. 2.2 agree well with those presented by Allanach *et al.* in Ref. [89].

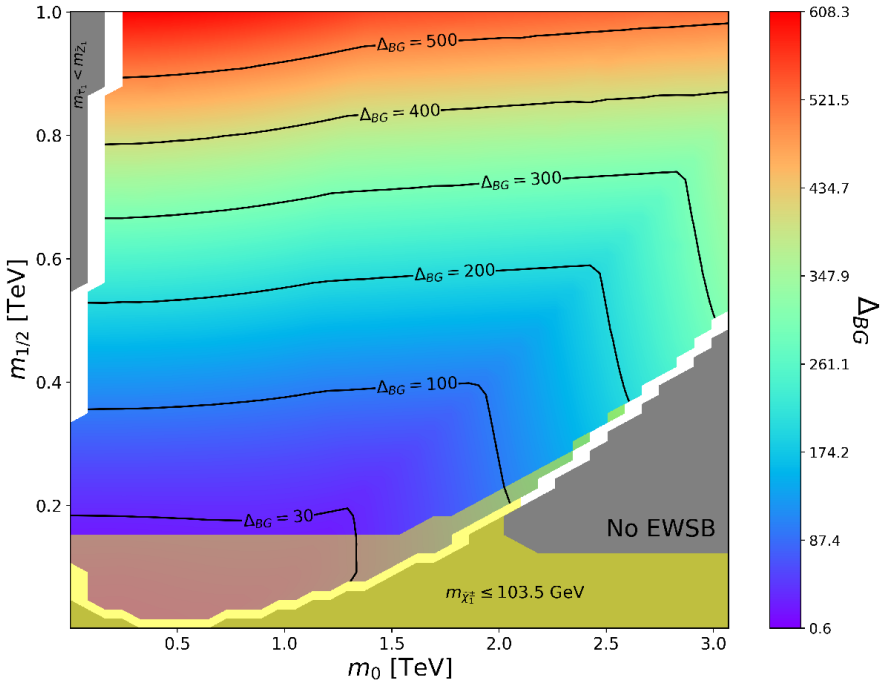

Figure 2.2: Plot of naturalness contours Δ_{BG} in the m_0 vs. $m_{1/2}$ plane of the CMSSM/mSUGRA model with $A_0 = 0$, $\tan\beta = 10$ and $\mu > 0$. We use the code DEW4SLHA to compute Δ_{BG} using a numerical algorithm for the sensitivity coefficients and SoftSUSY for the spectrum.

In truth, the various supposedly independent high scale soft terms are introduced by hand in the mSUGRA/CMSSM model as a *parametrization of our ignorance* as to the SUSY breaking mechanism. Indeed, in the case of gravity-mediation, if we specify a specific SUSY breaking mechanism, then all soft terms are calculable in terms of the gravitino mass $m_{3/2}$. An example is the famous

dilaton-dominated SUSY breaking model[90]: in this case

$$m_0 = m_{3/2} \quad \text{with} \quad m_{1/2} = -A_0 = \sqrt{3} m_{3/2}. \tag{2.14}$$

In such a case, then it doesn't make sense that the soft terms are independent: invoking PN, we should combine dependent terms in Eq. 2.12. Then $m_Z^2 \simeq -2.18\mu^2 + 14.494 m_{3/2}^2$. Adopting $m_{3/2} = 3$ TeV as in the previous example, then we find $\mu = 7735$ GeV and $\Delta_{\rm BG} = c_{m_{3/2}^2} = 15683$.

The SUSY μ parameter evolves very little from the GUT scale to the weak scale, due to the supersymmetric non-renormalization theorems[6]. The ratio of $\mu(m_{\rm weak})/\mu(m_{\rm GUT})$ is shown in Fig. 2.3 for the $\tan\beta$ vs. $\mu(m_{\rm weak})$ plane in the mSUGRA/CMSSM model. The deviation between $\mu(m_{\rm weak})/\mu(m_{\rm GUT})$ is typically a few percent, climbing to $\sim 10\%$ at very large $\tan\beta$.

Now, in the case where all soft terms are determined in terms of $m_{3/2}$ (such as gravity-mediation, anomaly-mediation and mirage-mediation), then we expect roughly that

$$m_Z^2 \simeq -2\mu^2 + a \cdot m_{3/2}^2 \tag{2.15}$$

and since μ hardly evolves, then $a \cdot m_{3/2}^2 \simeq -2m_{H_u}^2(weak)$. In this case – with all correlated soft terms (which we may dub as the SUGRA1 model) – then $\Delta_{\rm BG} \sim c_{m_{3/2}^2} = a m_{3/2}^2/m_Z^2 \simeq \max[2\mu^2, 2m_{H_u}^2(weak)]/m_Z^2$. This latter case we will find is nearly the same as $\Delta_{\rm EW}$ aside from the inclusion of the radiative corrections to the weak scale scalar potential.

In Fig. 2.4, we plot naturalness contours in the same parameter plane as in

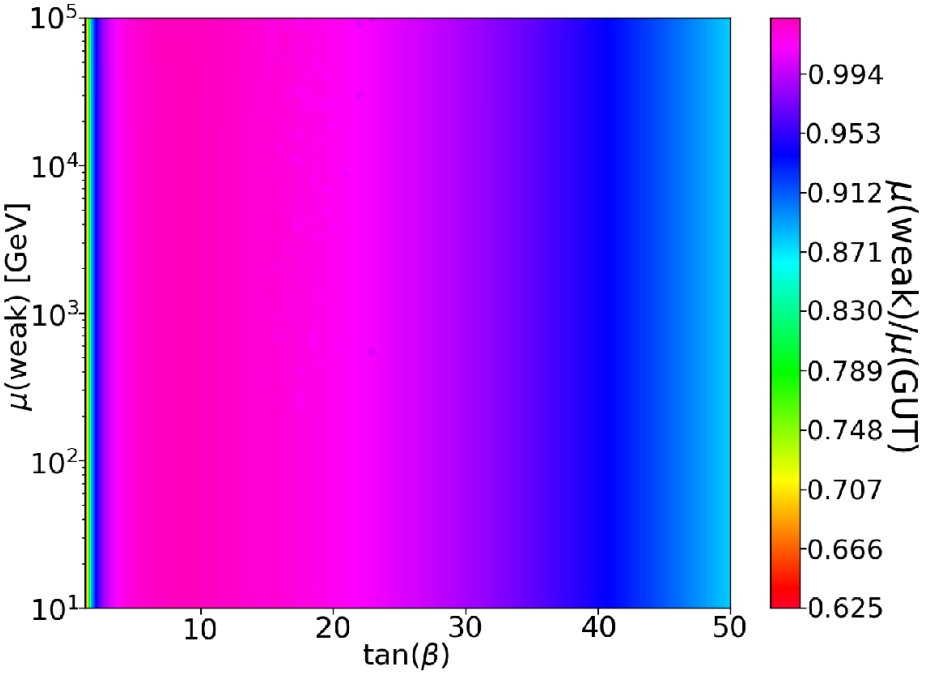

Figure 2.3: Ratio of μ/μ_0 in the $\tan\beta$ vs. μ(weak) plane, where μ_0 is the GUT-scale value of the μ parameter.

Fig. 2.2, but now assuming instead the one-soft-parameter SUGRA1 model. For SUGRA1, we have

$$m_Z^2 = -2.18\mu_0^2 + a \cdot m_0^2 \quad \text{(SUGRA1)} \tag{2.16}$$

where the constant a can be determined via $a = (m_Z^2 + 2.18\mu_0^2)/m_0^2$. In this case, the naturalness contours roughly follow the contours of constant μ value. (The μ term all by itself has been advocated as a measure of naturalness by Chan *et al.*[78].) For the case of SUGRA1, the naturalness contours are very different from the case of independent high scale soft terms assumed in the mSUGRA/CMSSM model.

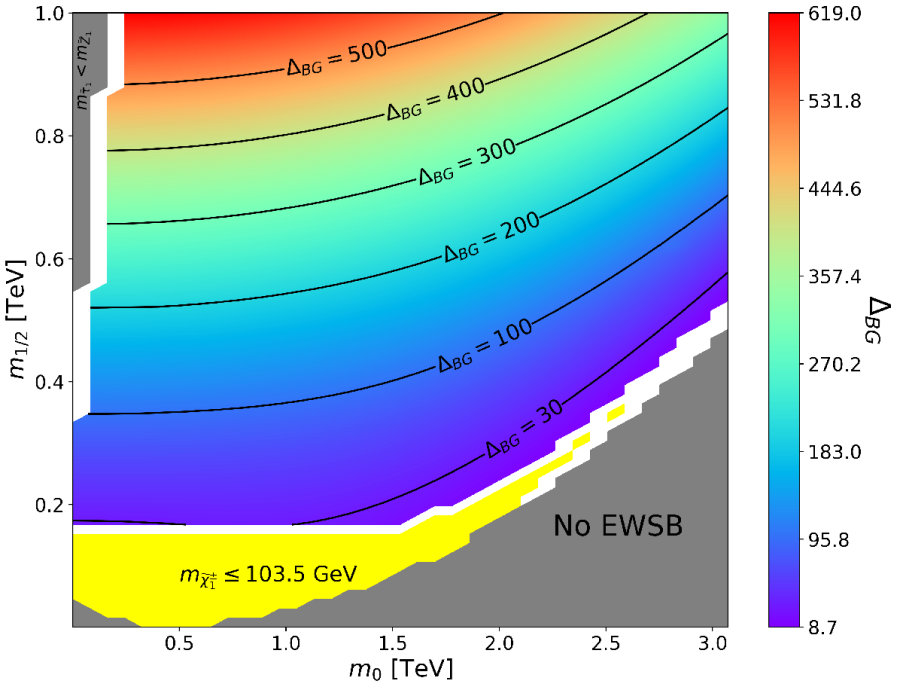

Figure 2.4: Plot of naturalness contours Δ_{BG} in the m_0 vs. $m_{1/2}$ plane of the one-soft-parameter SUGRA1 model with $A_0 = 0$, $\tan\beta = 10$ and $\mu > 0$. We use SoftSUSY to generate the spectra.

One may also define a SUGRA2 model. Here, we assume that since gaugino masses arise from the gauge kinetic function, this soft term is independent of the others which are determined instead by the Kähler function, but where A_0 is determined in terms of m_0 (such as $A_0 = -2m_0$) so that

$$m_Z^2 = -2.18\mu_0^2 + 3.786m_{1/2}^2 - 0.427m_0^2 + 1.642m_{1/2}m_0 \quad (SUGRA2). \qquad (2.17)$$

Finally, SUGRA3 allows that A_0 is somehow independent from m_0 (or $m_{3/2}$) so

that

$$m_Z^2 = -2.18\mu_0^2 + 3.786m_{1/2}^2 + 0.013m_0^2 + 1.642m_{1/2}m_0 + 0.22A_0^2 \quad (SUGRA3). \tag{2.18}$$

For the three cases, we find that the $\Delta_{\rm BG}$ values are very different in the SUGRA1, SUGRA2 or SUGRA3 models just depending on which parameters are assumed to be truly independent.

In Fig. 2.5, we show color coded regions of $\Delta_{\rm BG}$ as computed in the m_0 vs. $m_{1/2}$ plane of the NUHM2 model where $\tan\beta = 10$, $A_0 = -1.6m_0$ with $\mu = 200$ GeV and $m_A = 2$ TeV. In frame *a*), we assume all soft terms are correlated as in Eq. 2.16. In this case, since μ is fixed, there is a constant value of $\Delta_{\rm BG} = 21.2$ throughout the plane.

In frame *b*), we instead assume two independent soft parameters m_0 and $m_{1/2}$ (but with A_0 fixed in terms of m_0) so that we are in the SUGRA2 model, Eq. 2.17. Here, the value of $\Delta_{\rm BG}$ is vastly different from frame *a*), reaching up to values of ~ 3900 in the upper-right corner: a factor of ~ 180 times greater than the frame *a*) value. Here, the $\Delta_{\rm BG}$ finetuning is dominated by the $m_{1/2}$ value but not so much by m_0. In frame *c*), instead we show values of $\Delta_{\rm BG}$ assuming three independent soft parameters as in Eq. 2.18. In this case, with A_0 fixed as $A_0 = -1.6m_0$ but nonetheless declared as independent, we see a greater dependence on m_0, so $\Delta_{\rm BG}$ increases as m_0 increases, mainly because A_0 increases with increasing m_0. Here, $\Delta_{\rm BG}$ reaches maximal values of ~ 14500 in the upper-right corner, a factor ~ 680 larger than the frame *a*) value!

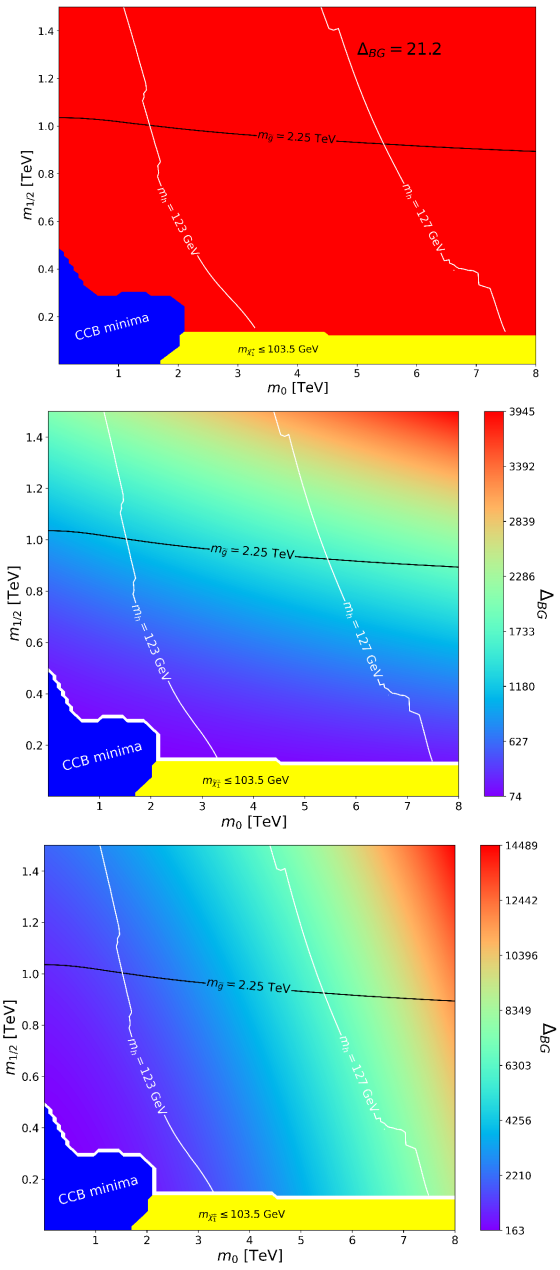

Figure 2.5: Plot of $\Delta_{\rm BG}$ values in the m_0 vs. $m_{1/2}$ plane for the NUHM2 model for $A_0 = -1.6m_0$, $\tan\beta = 10$ with $\mu = 200$ GeV and $m_A = 2$ TeV. In *a*), we plot $\Delta_{\rm BG}$ assuming a single independent soft parameter $m_{3/2}$ while in *b*) we plot $\Delta_{\rm BG}$ for assumed two independent soft parameters m_0 and $m_{1/2}$ while in *c*) we plot assuming all three of m_0, $m_{1/2}$ and A_0 are independent. The spectrum is calculated using SoftSUSY and the naturalness measures with DEW4SLHA.

In summary, from the discussion of this Section, we see that the measure $\Delta_{\rm BG}$ could be a legitimate finetuning measure if there could be consensus on what constitutes *independent parameters* of the model. The plots also illustrate the extreme model-dependence of $\Delta_{\rm BG}$, where $\Delta_{\rm BG}$ can obtain values differing by several orders of magnitude depending on which parameters p_i are assumed fundamental or independent.

2.2.2 High scale finetuning

An alternative to EENZ/BG naturalness which we label as high scale finetuning (HS) emerged early on in the 21st century. It may have been intended originally as a figurative bullet point indicator to argue for sparticle masses near the weak scale[69], but later was taken more seriously[70, 73, 74, 75]. This measure seeks to apply PN to the Higgs boson mass relation (see *e.g.* Eq. 10 of [91])

$$m_h^2 \simeq \mu^2 + m_{H_u}^2(weak) + \text{EW} + \text{mixing} \tag{2.19}$$

where the EW corrections and mixings are already $\lesssim m_h^2$. The idea then is to break $m_{H_u}^2(weak)$ into $m_{H_u}^2(m_{\rm GUT}) + \delta m_{H_u}^2$ and require $\delta m_{H_u}^2 \lesssim m_h^2$. The full one-loop expression for $\delta m_{H_u}^2$ may be obtained by integrating its one-loop RGE from $m_{\rm GUT}$ to $m_{\rm weak}$:

$$\frac{dm_{H_u}^2}{dt} = \frac{2}{16\pi^2}\left(-\frac{3}{5}g_1^2M_1^2 - 3g_2^2M_2^2 + \frac{3}{10}g_1^2S + 3f_t^2X_t\right) \tag{2.20}$$

where $t = \log Q$, $S = m_{H_u}^2 - m_{H_d}^2 + Tr\left[\mathbf{m}_Q^2 - \mathbf{m}_L^2 - 2\mathbf{m}_U^2 + \mathbf{m}_D^2 + \mathbf{m}_E^2\right]$ and $X_t = m_{Q_3}^2 + m_{D_3}^2 + m_{H_u}^2 + A_t^2$. In the literature[73, 74, 75], to gain a simple expression, the terms with gauge couplings are ignored and X_t is approximated as $X_t \sim m_{Q_3}^2 + m_{D_3}^2 + A_t^2$, where $m_{Q_3}^2, m_{D_3}^2$, and A_t^2 here are GUT-scale values. Then a single step integration leads to

$$\delta m_{H_u}^2 \sim -\frac{3}{8\pi^2} f_t^2 \left(m_{Q_3}^2 + m_{U_3}^2 + A_t^2\right) \log\left(\Lambda / m_{\text{weak}}\right) \tag{2.21}$$

where the high scale Λ is usually assumed $\sim m_{\text{GUT}}$. The Δ_{HS} measure famously promoted three light third generation squarks below the 500 GeV scale[74], and motivated intensive searches by the LHC collaborations to root out light top-squark signals.

In order to compare Δ_{HS} more appropriately with Δ_{BG} and Δ_{EW}, we slightly redefine Δ_{HS} in terms of $m_Z^2/2$[92] where in this case we take

$$m_Z^2/2 = \frac{(m_{H_d}^2(\Lambda) + \delta m_{H_d}^2 + \Sigma_d^d) - (m_{H_u}^2(\Lambda) + \delta m_{H_u}^2 + \Sigma_u^u)\tan^2\beta}{\tan^2\beta - 1} - (\mu^2(\Lambda) + \delta\mu^2) \tag{2.22}$$

and Λ is some input high scale, perhaps m_P or m_{GUT}. Then

$$\Delta_{\text{HS}} = \max\left|\text{largest term on RHS of Eq. (2.22)}\right|. \tag{2.23}$$

In this way, the three measures become equal in certain limiting cases.

The Δ_{HS} measure is problematic on several counts

1. It violates the PN precept in that, in simplifying $\delta m_{H_u}^2$, all dependence on $m_{H_u}^2(\Lambda)$ is lost, which hides the fact that $\delta m_{H_u}^2$ is actually dependent on $m_{H_u}^2(\Lambda)$. In fact, the bigger the assumed value for $m_{H_u}^2(\Lambda)$, then the bigger is the cancelling correction $\delta m_{H_u}^2$[93]. This is shown in Fig. 2.6 where we show the exact two-loop value of $\delta m_{H_u}^2$ vs. $m_{H_u}^2(GUT)$, where the clear dependence of $\delta m_{H_u}^2$ on $m_{H_u}^2(GUT)$ is shown. The plot also shows that the bigger $m_{H_u}(GUT)$ becomes, then the more EW-natural the model becomes in that $m_{H_u}^2(weak)$ becomes comparable to m_Z^2 on the right-hand-side shortly before EWSB is no longer broken. The splitting up of $m_{H_u}^2(weak)$ into $m_{H_u}^2(\Lambda) + \delta m_{H_u}^2$ turns $\Delta_{\rm HS}$ into contradiction with $\Delta_{\rm BG}$, where $m_{H_u}^2(weak)$ is expanded into high scale parameters in Eq. 2.12 but not split into $m_{H_u}^2(\Lambda) + \delta m_{H_u}^2$. This splitting of $m_{H_u}^2(weak)$ into dependent parts destroys the cancellations needed for focus point SUSY[64, 65] which is promoted as allowing for TeV-scale top-squarks.

2. Electroweak symmetry breaking in SUSY models is accomplished by driving $m_{H_u}^2$ to negative values owing to the large top-quark Yukawa coupling f_t. Indeed, the REWSB mechanism is touted as one of the triumphs of WSS since it required $m_t \sim 100 - 200$ GeV[94] at a time when experiments seemed to indicate $m_t \sim 40$ GeV. By requiring $\delta m_{H_u}^2$ to be small, then often $m_{H_u}^2(weak)$ will not be large-negative enough to cause EWSB. In the context of vacua selection in the string landscape, such models without EWSB would likely not lead to inhabitable universes and would be vetoed.

This can be viewed as a selection mechanism to favor models with large enough $\delta m_{H_u}^2$ such that EW symmetry is properly broken (see *e.g.* Fig. 3 of Ref. [95].)

3. There is also substantial ambiguity in evaluating $\Delta_{\rm HS}$. In Fig. 2.7 we show the value of $\delta m_{H_u} \equiv sign(\delta m_{H_u}^2)\sqrt{|\delta m_{H_u}^2|}$ vs. $m_{H_u}(m_{\rm GUT})$ for a NUHM2 benchmark point with $m_0 = 4.5$ TeV, $m_{1/2} = 1$ TeV, $A_0 = -7.2$ TeV with $\tan\beta = 10$ and $m_A = 2$ TeV. The approximate expression Eq. 2.21 is shown as the flat red-dashed line which of course doesn't depend on $m_{H_u}^2(m_{\rm GUT})$. The solid blue curve is the exact (numerical) two-loop RG expression for δm_{H_u} and is shown to deviate from the approximate result by well over a factor of 2 at low $m_{H_u}(m_{\rm GUT})$ and only agrees with the approximation far into the excluded region where the electroweak symmetry isn't properly broken. Alternatively, one may use the $m_h^2 \simeq \mu^2 + m_{H_u}^2 + \delta m_{H_u}^2$ equation for a particular set of input parameters including $m_{H_u}^2(m_{\rm GUT})$ (*e.g.* in the NUHM2 model) to compute the value of $\delta m_{H_u}^2$ and then try to finetune $m_{H_u}^2(m_{\rm GUT})$ to enforce $m_h = 125$ GeV. But as one tunes the value of $m_{H_u}^2(m_{\rm GUT})$, then the value of $\delta m_{H_u}^2$ changes accordingly (as indicated by the various dotted lines for different input μ values), so that instead of finetuning, one must adopt an iterative procedure to try and find a solution. Sometimes the solution will migrate into the noEWSB region while other times the iterations can find a viable solution.

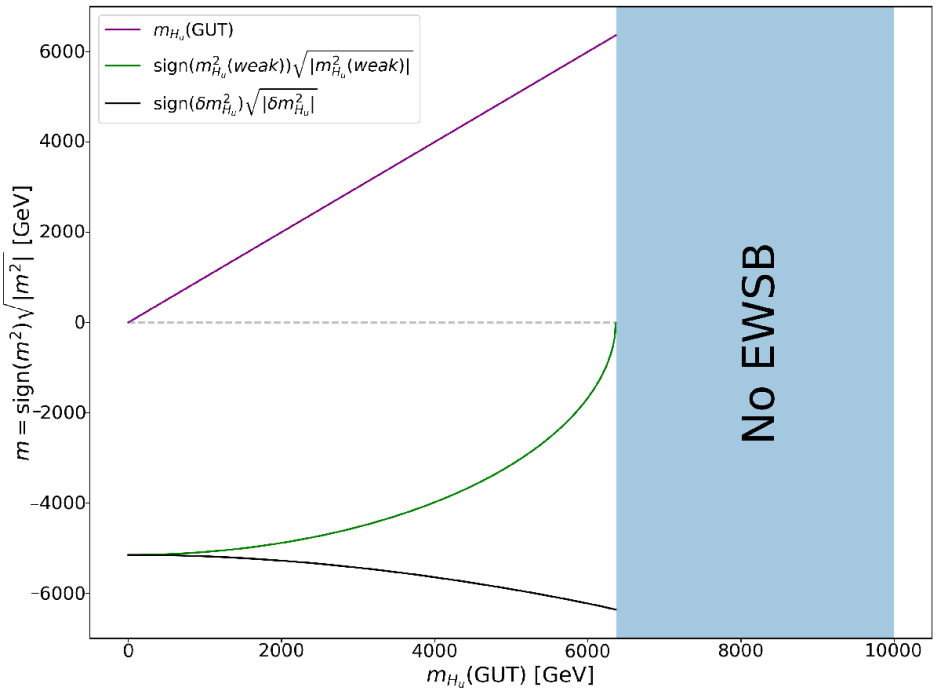

Figure 2.6: Plot of $sign(\delta m^2_{H_u}) \cdot \sqrt{|\delta m^2_{H_u}|}$ vs. $m_{H_u}(GUT)$ for the NUHM2 model with $m_0 = 5$ TeV, $m_{1/2} = 1.2$ TeV, $A_0 = -1.6 m_0$, $\tan\beta = 10$ and $m_{H_d} = 5$ TeV.

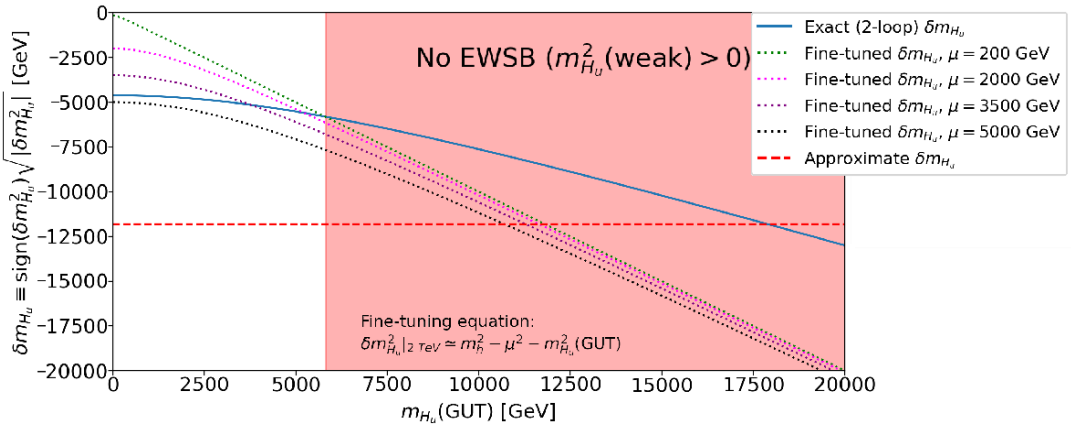

Figure 2.7: Plot of $sign(\delta m^2_{H_u}) \cdot \sqrt{|\delta m^2_{H_u}|}$ vs. $m_{H_u}(GUT)$ for the NUHM2 model with $m_0 = 4.5$ TeV, $m_{1/2} = 1$ TeV, $A_0 = -7.2$ TeV and $\tan\beta = 10$ with $m_A = 2$ TeV. We show the approximate expression Eq. 2.20 (red-dashed curve) along with exact 2-loop expression (blue solid) along with the value gleaned from finetuning for various values of μ.

2.2.3 Electroweak naturalness

As mentioned before, the electroweak naturalness measure $\Delta_{\rm EW}$ measures the largest contribution on the right-hand-side of Eq. (2.9) and compares that to $m_Z^2/2$. This is the most conservative, unavoidable measure of naturalness since it is independent of any high scale model. Even when high scale parameters are correlated in some way, those correlations are typically lost under RG running and subsequent computation of the physical sparticle mass eigenstates. The interpretation of $\Delta_{\rm EW}$ is clear: if any one of the RHS contributions to Eq. (2.9) is far larger than $m_Z^2/2$, then it is highly implausible (but not impossible) that some other contribution would accidentally be large, opposite-sign such that the two conspire to give an m_Z value of just 91.2 GeV. In this sense, natural models correspond to plausible models; models with large $\Delta_{\rm EW}$ are logically possible, but highly implausible. We'll see later that this manifests itself as a *probability*, or likelihood, to emerge from scans over the string landscape.

The tree-level contributions to $\Delta_{\rm EW}$ are instructive:

- the SUSY conserving μ parameter, which sets the mass scale for the W, Z, h and higgsinos enters the weak scale directly. We already know that $m_{W,Z,h} \sim 100$ GeV; the higgsinos should lie within a factor of several of the measured value of the weak scale. In light of LHC constraints, the SUSY LSP is likely a higgsino-like lightest neutralino, or at worst a gaugino-higgsino admixture.

- The value of $m_{H_u}^2$, where H_u acts as the SM Higgs doublet, should be driven

to small, usually negative values since it also sets the mass of the W, Z and h bosons.

- The value of m_{H_d} – which sets the mass scale for the heavier Higgs bosons A, H and $H^{\pm}$ – can be much larger since its contribution to the weak scale is suppressed by a factor of $\tan(\beta)$.

The loop-level contributions Σ_u^u and Σ_d^d are proportional to the individual particle/sparticle masses but since the Σ_d^d terms are suppressed by $\tan\beta$, the Σ_u^u terms are usually dominant. Of the Σ_u^u terms, usually $\Sigma_u^u(\tilde{t}_{1,2})$ are largest owing to the large top-quark Yukawa coupling. Since these terms are all suppressed by loop factors, the particle/sparticle masses which enter the Σ_u^u terms can be at the TeV or beyond scale before becoming comparable to the weak scale. Explicit expressions for the Σ_u^u and Σ_d^d are given in the Appendices to Ref's [96] and [77]. The dominant terms are given by

$$\Sigma_u^u(\tilde{t}_{1,2}) = \frac{3}{16\pi^2} F(m^2_{\tilde{t}_{1,2}}) \left[f_t^2 - g_Z^2 \mp \frac{f_t^2 A_t^2 - 8g_Z^2(\frac{1}{4} - \frac{2}{3}x_W)\Delta_t}{m^2_{\tilde{t}_2} - m^2_{\tilde{t}_1}} \right] \tag{2.24}$$

where $F(m^2) = m^2\left(\log\frac{m^2}{Q^2} - 1\right)$ and the optimized scale choice is taken as $Q^2 = m_{\tilde{t}_1} m_{\tilde{t}_2}$. Also, $\Delta_t = (m^2_{\tilde{t}_L} - m^2_{\tilde{t}_R})/2 + m_Z^2 \cos 2\beta(\frac{1}{4} - \frac{2}{3}x_W)$ with $g_Z^2 = (g^2 + g'^2)/8$ and $x_W = \sin^2\theta_W$; in the denominator of Eq. 2.24, the tree-level masses should be used.

Some highlights of the Σ_u^u terms include the following.

- For $\Delta_{\rm EW} \lesssim 30$, the top-squark contributions $\Sigma_u^u(\tilde{t}_{1,2})$ allow for top-squarks

up to $m_{\tilde{t}_1} \lesssim 3$ TeV and $m_{\tilde{t}_2} \lesssim 8$ TeV. The explicit expressions contain large cancellations for large A_t both for $\Sigma_u^u(\tilde{t}_1)$ and $\Sigma_u^u(\tilde{t}_2)$. The large A_t helps to lift m_h into the 125 GeV range since m_h is maximal for $x_t \sim \sqrt{6} m_{\tilde{t}}$[29]. This is in contrast to $\Delta_{\rm BG}$ and $\Delta_{\rm HS}$ which both prefer small trilinear soft terms. In Fig. 2.8 we show color-coded regions of $\Delta_{\rm BG}$ in the $m_{1/2}$ vs. A_0 plane of the mSUGRA/CMSSM model for $m_0 = 5$ TeV, $\tan\beta = 10$ and $\mu > 0$. We also show contours of Higgs mass $m_h = 123$ and 127 GeV, and contours of $\Delta_{\rm EW}$ and $\Delta_{\rm HS}$. The grey region around $A_0 \sim 0$ is the focus point region. From the plot, we see that $\Delta_{\rm HS}$ is always large, $\Delta_{\rm HS} \gtrsim 6000$, due to the large value of m_0. Meanwhile, $\Delta_{\rm BG}$ reaches as low as ~ 1000, also in the FP region. $\Delta_{\rm EW}$ can reach as low as 62 in between the two $\Delta_{\rm EW} = 125$ contours. As expected from the mSUGRA/CMSSM model, no points allow for both low finetuning and $m_h \sim 125$ GeV.

- Since first/second generation Yukawa couplings are tiny, then these sparticle masses can be much larger than the third generation, with first/second generation squarks and sleptons ranging up to $30 - 50$ TeV. In the context of the string landscape, this leads to a quasi-degeneracy/decoupling solution to the SUSY flavor and CP problems[97].

- Gluinos affect the Σ_u^u via RG running and directly at the two-loop level[98]. They can range up to $m_{\tilde{g}} \lesssim 6$ TeV for $\Delta_{\rm EW} \lesssim 30$, well beyond present LHC bounds[99].

A positive feature of $\Delta_{\rm EW}$ is its model independence (within the context of

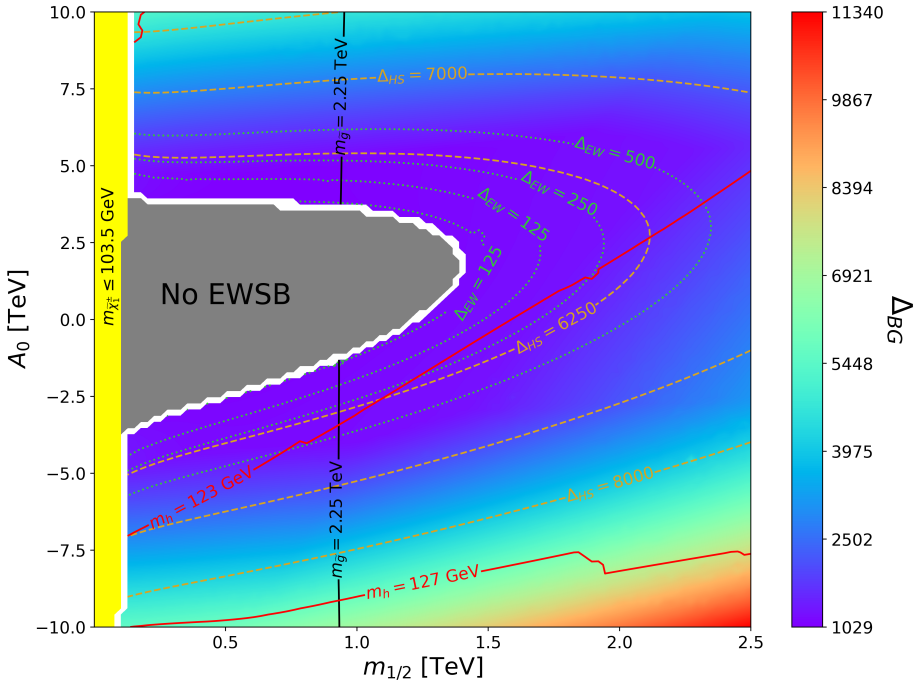

Figure 2.8: Plot of color-coded values of $\Delta_{\rm BG}$ in the $m_{1/2}$ vs. A_0 plane of the mSUGRA/CMSSM model for $m_0 = 5$ TeV, $\tan\beta = 10$ and $\mu > 0$. We also show contours of Higgs mass $m_h = 123$ and 127 GeV, and contours of $\Delta_{\rm EW}$ and $\Delta_{\rm HS}$.

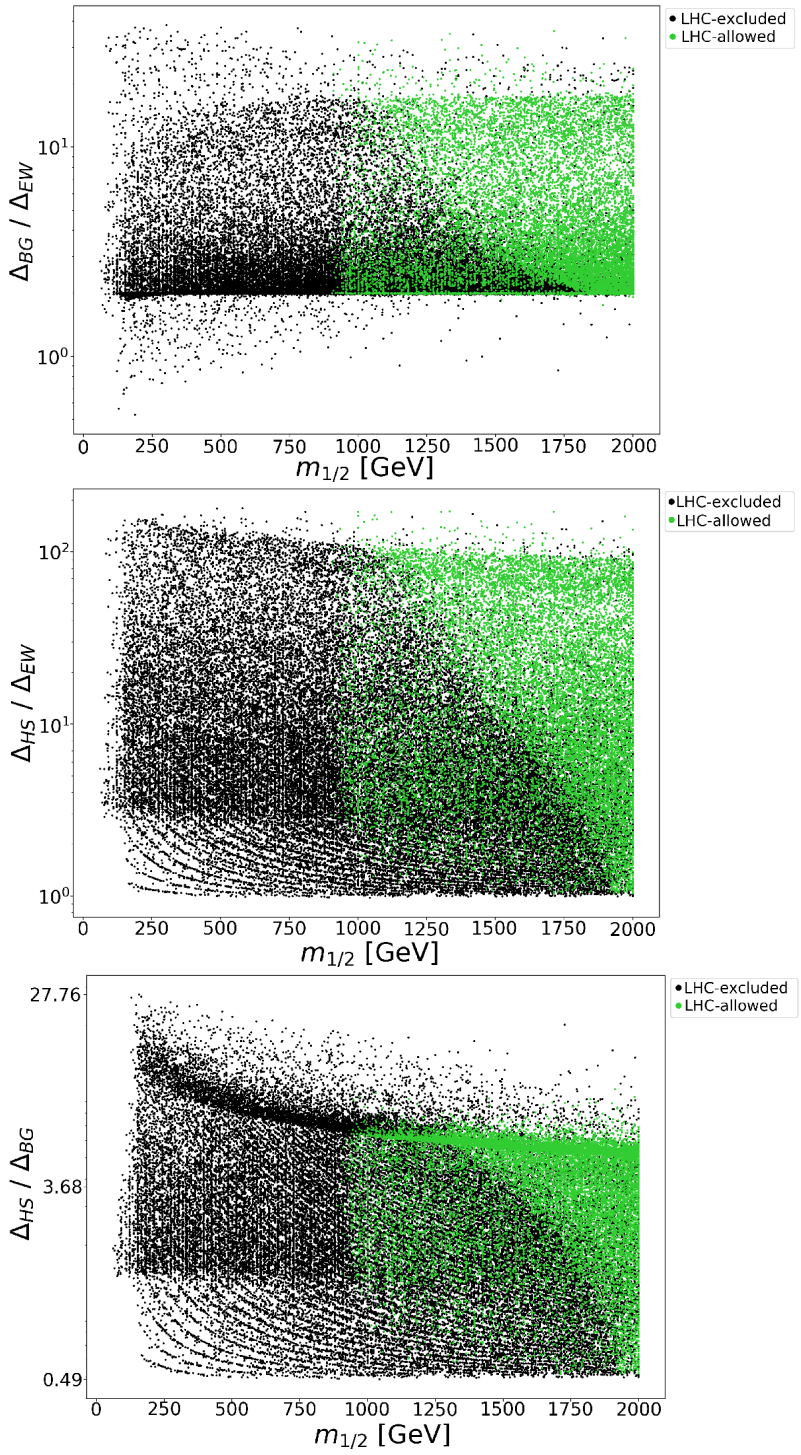

Figure 2.9: Scatter plots of ratios of three naturalness measures, $\Delta_{\rm BG}, \Delta_{\rm HS}, \Delta_{\rm EW}$ in a scan of the CMSSM. The results demonstrate that the traditional naturalness measures $\Delta_{\rm BG}, \Delta_{\rm HS}$ vastly overestimate the degree of electroweak finetuning. Panel (a) plots the ratio $\Delta_{\rm BG}/\Delta_{\rm EW}$, panel (b) plots the ratio $\Delta_{\rm HS}/\Delta_{\rm EW}$, and panel (c) plots the ratio $\Delta_{\rm HS}/\Delta_{\rm BG}$.

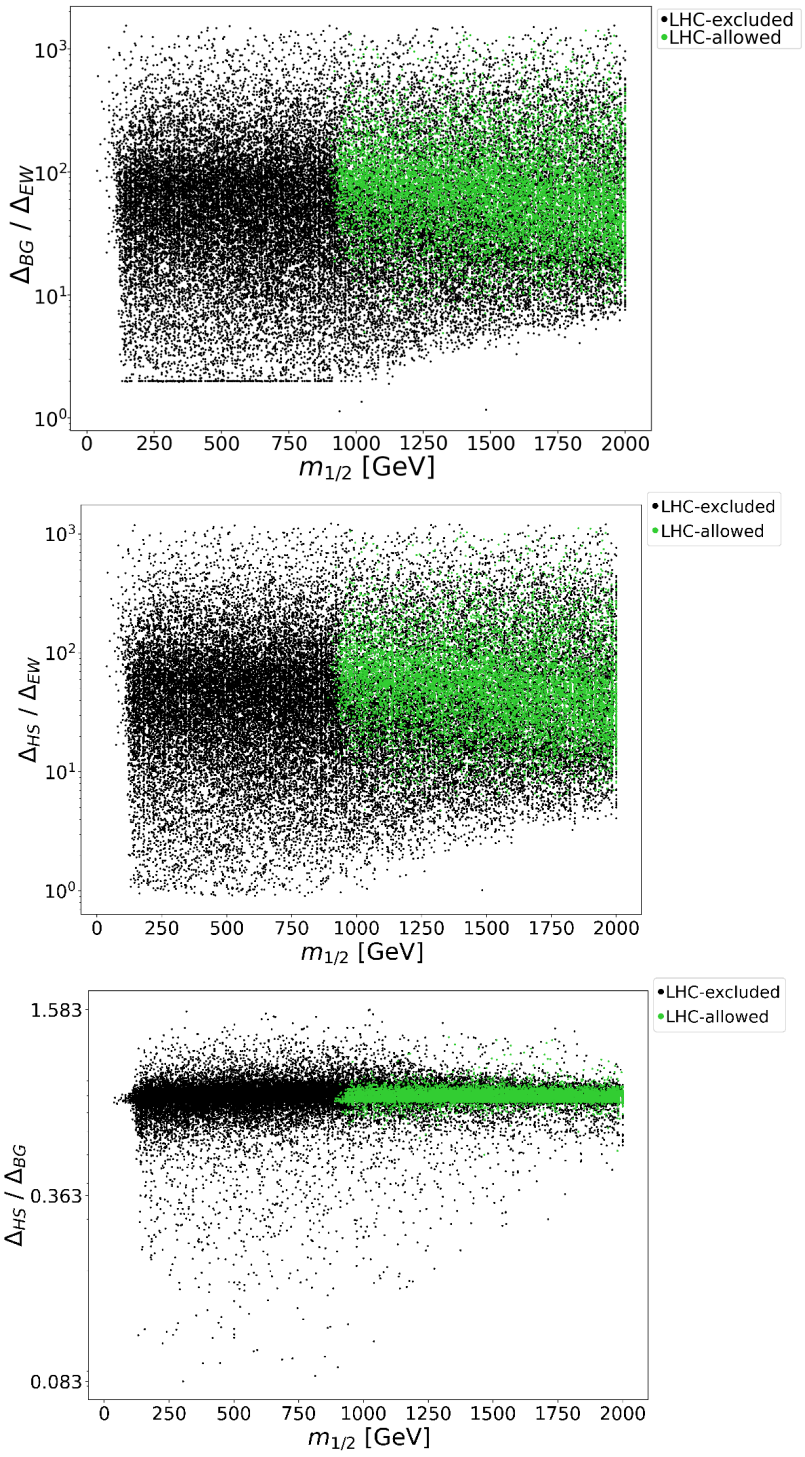

Figure 2.10: Scatter plots of ratios of three naturalness measures, $\Delta_{\rm BG}, \Delta_{\rm HS}, \Delta_{\rm EW}$ in a scan of the NUHM2 model. The results demonstrate that the traditional naturalness measures $\Delta_{\rm BG}, \Delta_{\rm HS}$ vastly overestimate the degree of electroweak finetuning. Panel (a) plots the ratio $\Delta_{\rm BG}/\Delta_{\rm EW}$, panel (b) plots the ratio $\Delta_{\rm HS}/\Delta_{\rm EW}$, and panel (c) plots the ratio $\Delta_{\rm HS}/\Delta_{\rm BG}$.

models for which the MSSM is the weak scale EFT). The amount of finetuning only depends on the weak scale spectrum which is generated, but not on how it is obtained. Thus, if one generates a certain weak scale spectrum via some high scale model, or just the pMSSM, then one gets the same value of $\Delta_{\rm EW}$. This of course isn't true for the measures $\Delta_{\rm HS}$ or $\Delta_{\rm BG}$. In these senses, $\Delta_{\rm EW}$ offers a "minimal" or conservative estimation of the degree of electroweak finetuning, leading to the conclusion that typically $\Delta_{\rm HS}$ and $\Delta_{\rm BG}$ overestimate the degree of finetuning by as much as a factor of 1000, as exemplified in Figs. 2.9 and 2.10.

A common criticism of $\Delta_{\rm EW}$ is that it doesn't account for high scale parameter choices and correlations. This is not exactly true as discussed earlier. The μ parameter evolves only slightly from $m_{\rm GUT}$ to $m_{\rm weak}$, as shown in Fig. 2.3. With $\mu(m_{\rm GUT}) \simeq \mu(m_{\rm weak})$, and in the context of all soft terms correlated (as should be the case in a well specified SUSY breaking model), then $\Delta_{\rm BG} \simeq \Delta_{\rm EW}$, sans the radiative corrections Σ_u^u and Σ_d^d. Also, if the dependent terms $m_{H_u}^2(\Lambda)$ and $\delta m_{H_u}^2$ are combined, as required by PN, then $\Delta_{\rm HS} \simeq \Delta_{\rm EW}$, sans radiative corrections. Furthermore, the specific choices of high scale parameters can lead to more or less finetuning via Eq. 2.9. In fact, a string landscape selection for larger soft terms often results in smaller values of $\Delta_{\rm EW}$ as compared to any selection for small or weak scale soft terms[100].

2.2.4 Stringy naturalness: anthropic origin of the weak scale

A fourth entry into the naturalness debate comes from Douglas with regards to the string landscape: stringy naturalness, as remarked above. An advantage of

stringy naturalness is that it actually provides an explanation for the magnitude of the weak scale, and not just naturalness of the weak scale. The distribution of vacua in the multiverse as a function of m_{soft} is expected to be

$$dN_{vac} \sim f_{SUSY}(m_{soft}) \cdot f_{EWSB}(m_{soft}) dm_{soft}. \tag{2.25}$$

Douglas[101] advocates for a power-law draw to large soft terms based on the supposition that there is no favored value for SUSY breaking fields on the landscape: $f_{SUSY} \sim m_{soft}^{2n_F+n_D-1}$ where n_F is the number of (complex-valued) F-breaking fields and n_D is the number of (real-valued) D-breaking fields giving rise to the ultimate SUSY breaking scale. The distribution f_{EWSB} is suggested as $f_{EWSB} = \Theta(30 - \Delta_{\rm EW})$[102] such that the value of the weak scale in each pocket universe lies within the ABDS window[80], the so-called atomic principle. Until now, SN has not admitted a clear numerical measure[81, 103]. A novel method for quantifying this concept will be presented in Chapter 5.

2.3 Radiative natural SUSY and its phenomenology

Radiative natural SUSY refers to a class of supersymmetric models designed to address the naturalness problem of the Higgs boson mass by ensuring that the finetuning of parameters is minimized. Radiative natural SUSY balances the need for naturalness with compliance to experimental constraints, maintaining the attractive features of supersymmetry while addressing the Little Hierarchy Problem. This is achieved through the mechanism of radiative electroweak symmetry breaking and the particular choice of superpartner masses. Key features of radiative natural SUSY include:

1. **Radiative electroweak symmetry breaking (REWSB):** This is a mechanism where the electroweak symmetry breaking occurs dynamically through radiative corrections. The running of the RGEs from the high-energy scale to the low-energy scale naturally induces a negative squared mass for the Higgs fields, leading to spontaneous electroweak symmetry breaking.

2. **Naturalness criteria:** To minimize finetuning, the superpartner masses are chosen such that the loop corrections to the Higgs mass are small. This typically requires:

    - Light stops (top squarks): The masses of the top squarks ($\widetilde{t}_1$ and $\widetilde{t}_2$) are kept relatively low, usually below 1 TeV. This reduces the quantum corrections to the Higgs mass parameter.

- Light higgsinos: The higgsino mass parameter (typically denoted by μ) is also kept close to the electroweak scale, as large values of μ would require finetuning to achieve the correct value of the Z boson mass, m_Z^2, and thus correct electroweak symmetry breaking.

3. **Heavy first and second generation squarks and sleptons:** To evade the stringent constraints from flavor physics and CP-violating processes, the masses of the first and second generation squarks and sleptons are typically much heavier [3]. This hierarchy helps in maintaining naturalness while complying with experimental limits.

4. **Gluino mass:** The gluino, which is the supersymmetric partner of the gluon, can be relatively heavy (up to a few TeV) without introducing significant finetuning issues, due to these terms appearing in two-loop terms in the radiative corrections to the minimization conditions, which are suppressed by a factor of $\sim 1/(16\pi^2)^2$. This allows radiative natural SUSY models to satisfy the bounds from LHC searches for colored superparticles.

Given that radiative natural SUSY (RNS) satisfactorily addresses the Little Hierarchy Problem, it is important to determine whether the spectra predicted by RNS are phenomenologically viable with our current understanding of experimental data in SUSY searches. In fact, some rather strict bounds on masses have been produced from this data, though we will demonstrate how natural SUSY is expected to be revealed at future LHC upgrades. Early expectations from naturalness predicted superpartners at or around the weak scale[44, 45, 48, 47].

For instance, the naturalness upper bound for the gluino was predicted (under the naturalness measure $\Delta_{BG} \lesssim 30$) to be $m_{\tilde{g}} \lesssim 400$ GeV. In contrast, the current mass limits from LHC Run 2 searches with 139 fb^{-1} claim $m_{\tilde{g}} \gtrsim 2.25$ TeV[104, 105]. The yawning gap between the weak scale and the superpartner mass scale – the Little Hierarchy Problem (LHP)[56] – has lead many authors to conclude[106, 107, 108] that the weak scale supersymmetry[3] hypothesis is under intense pressure, and possibly even excluded.

However, it has been pointed out in Chapter 2 that the resolution to the LHP lies instead in that conventional early measures of naturalness over-estimated the finetuning[67, 109, 68, 103], and that the appropriate measure of practical weak-scale naturalness is Δ_{EW} as in Eq. (2.10). One can quickly read off the consequences for a low value of Δ_{EW}:

- $m_{H_u}^2$, which in the decoupling limit functions like the SM Higgs doublet and gives mass to the W, Z and h bosons, must be driven under radiative EWSB to *small*, typically negative values, a condition known as radiatively-driven naturalness (RNS). Thus, electroweak symmetry is *barely broken*.

- The μ parameter, which feeds mass to the W, Z and h bosons as well as to the higgsinos, must be within a factor of several of $m_{W,Z,h} \sim 100$ GeV.

- $m_A \sim m_{H_d}$ in the decoupling limit can live in the TeV regime since the contribution of $m_{H_d}^2$ is suppressed by a factor of $\tan^2(\beta)$.

- Top squark contributions to the weak scale are loop suppressed and so can live in the TeV range while maintaining naturalness.

- The gluino contributes at two-loops[98] and via RG running contributions to the stop soft masses[75, 74] and so also can live in the TeV range.

- First and second generation sfermion contributions to the weak scale are via Yukawa-suppressed 1-loop terms and via 2-loop RG contributions (which are dominant)[110]. Thus, they can live in the 10-50 TeV regime which helps solve the SUSY flavor and CP problems[97].

An advantage of Δ_{EW} is that it is model independent insofar as it only depends on the weak scale sparticle and Higgs mass spectrum and not on how they are arrived at. Thus, a given spectrum will generate the same value of Δ_{EW} whether it was computed from the pMSSM or some high scale model. Also, requiring the contributions to $m_Z^2/2$ to be comparable to or less than its measured value typically corresponds to an upper limit of $\Delta_{EW} \lesssim 30$. The turn-on of finetuning for $\Delta_{EW} \gtrsim 30$ is visually displayed in Fig. 1 of Ref. [59]. While WSS seems ruled out under the older naturalness measures[44, 45, 48, 47], there is still plenty of natural parameter space left unexplored by LHC under the Δ_{EW} measure[111]. However, the Δ_{EW} measure does predict the existence of light higgsino-like EWinos $\tilde{\chi}_1^{\pm}$ and $\tilde{\chi}_{1,2}^0$ with mass $\sim 100 - 350$ GeV. The light higgsinos can be produced at decent rates at LHC, but owing to their small mass gaps $m_{\tilde{\chi}_2^0} - m_{\tilde{\chi}_1^0} \sim 5 - 10$ GeV, there is only small visible energy released in their decays, making detection a difficult[112] (but not impossible[113, 114]) prospect. The higgsino-like LSP $\tilde{\chi}_1^0$ is thermally underproduced as dark matter, leaving room for axionic dark matter as well[115].

The Δ_{EW} naturalness measure is built in to the Isajet/Isasugra[116, 117] event/spectrum generator. Also, the crucial 1-loop corrections to the Higgs potential have been calculated within the (non-standard) notation of WSS[96]. As a result, of the spectrum generators available, Isasugra has been used the most for such studies. These include sparticle mass bounds from naturalness, and parameter space limits and lucrative collider signatures from natural SUSY. However, a variety of other SUSY/Higgs spectra generators are available, including SUSPECT[118], SoftSUSY[119] and SPHENO[120]. Some special Higgs spectrum calculators include FeynHIGGS[121] and SUSYHD[122] and others[29]. Thus, it would be useful to know how other spectrum generators compare to Isasugra in their natural SUSY spectra. For this reason, we have built a computer code DEW4SLHA which operates on a SUSY Les Houches Accord file (SLHA)[82] which is the standard output of spectrum generators. The program computes the associated value of Δ_{EW}, Δ_{BG}, and Δ_{HS} and all the various contributions.

2.3.1 Natural SUSY benchmark points

Using the code DEW4SLHA, we can now compare spectra generated from the various spectra calculators for a particular natural SUSY benchmark point. For the BM point, we adopt the two-extra-parameter non-universal Higgs model (NUHM2)[13, 15] with input parameters

$$m_0,\ m_{1/2},\ A_0,\ \tan\beta,\ \mu,\ m_A \tag{2.26}$$

where we have traded the high scale Higgs soft masses $m_{H_u}^2$ and $m_{H_d}^2$ for the more convenient weak scale parameters μ and m_A. Then we adopt the benchmark parameter values $m_0 = 5$ TeV, $m_{1/2} = 1.2$ TeV, $A_0 = -8$ TeV, $\tan\beta = 10$, $\mu = 200$ GeV and $m_A = 2$ TeV. A pictorial representation of the spectra using SoftSUSY is shown in Fig. 2.11 where we see that indeed the higgsinos and Higgs boson h lie in the $100 - 200$ GeV range whilst the top-squarks and gluino live in the several TeV regime.

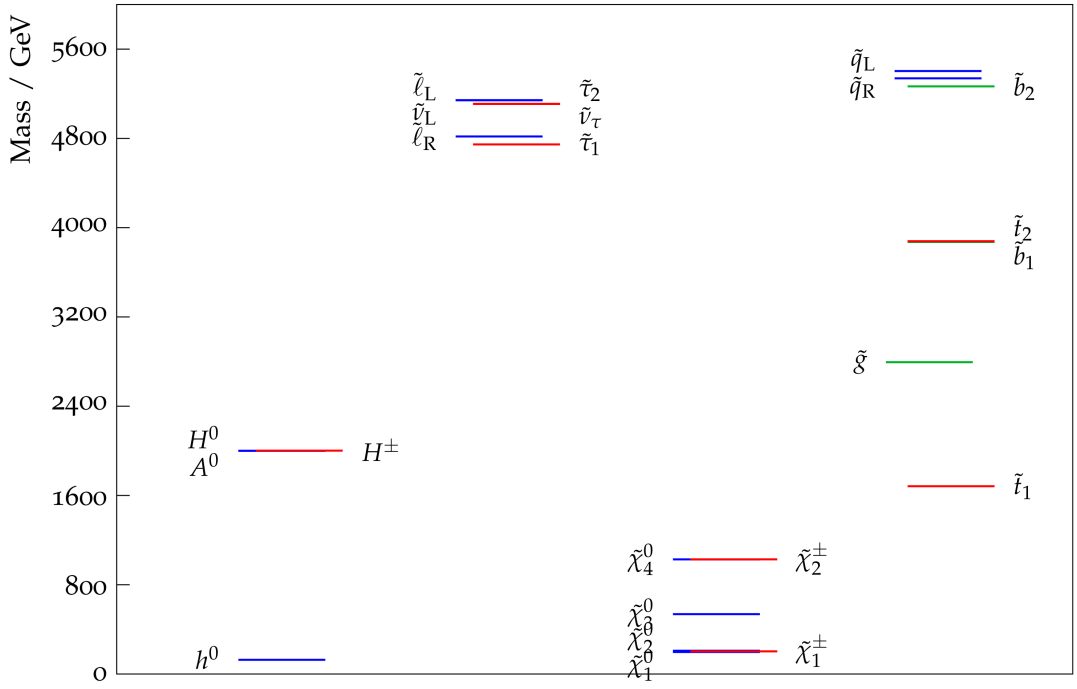

Figure 2.11: Sparticle and Higgs mass spectra for a natural SUSY benchmark point from SoftSUSY.

In Table 2.1, we list the mass spectra and Δ_{EW} values from each of four spectra generators. For ISAJET, we use version 7.88[116] while for SUSPECT we use version 2.51[118]. For SoftSUSY, we use version 4.1.10[119] including two-loop corrections to $m_{\tilde{g}}$ and the default two-loop corrections to m_h. We use SPHENO

version 4.0.4[120] with MSSM-to-SM matching at scale $Q = m_{SUSY} = \sqrt{m_{\tilde{t}_1} m_{\tilde{t}_2}}$. In contrast, SoftSUSY imposes EFT matching at $Q = m_Z$ while ISAJET uses multiple scales[16]. The gluino masses are all within 1.5% of each other. The naturalness parameters for three codes are all less than thirty; the outlier here is SPHENO where also the light top squark mass $m_{\tilde{t}_1}$ is somewhat higher than the other codes. Here, the top squark masses are highly sensitive to mixing which comes from the weak scale value of A_t and indeed the values of $A_t(Q)$ for Isasugra/SoftSUSY/SUSPECT/SPHENO are -4898/-4830/-4894/-5090 GeV, respectively. Thus, SPHENO has slightly more stop mixing than the other codes which increases Δ_{EW} somewhat. Another difference comes from the value of m_h generated: both SoftSUSY and SUSPECT generate $m_h \sim 127.4$ GeV whilst SPHENO generates $m_h = 125.2$ GeV and Isasugra generates $m_h = 124.7$ GeV. It can be remarked that Isasugra has the least sophisticated light Higgs mass calculation, and includes only third generation sparticle 1-loop contributions to m_h. Another feature is that the Isasugra value of $m_{\tilde{\chi}_1^\pm}$ is about six GeV higher than SoftSUSY and SUSPECT while the SPHENO is six GeV lower. These values depend sensitively on the scale choice at which each EWino mass is calculated. For instance, Isasugra uses the Pierce *et al.* (PBMZ)[123] recipe to calculate each mass separately at each mass scale.

In Table 2.2, we list the top 46 contributions to Δ_{EW} from each of the spectra codes. We see from line 1 that the largest contribution comes for each code from $\Sigma_u^u(\tilde{t}_2)$ which sets the value of Δ_{EW}, and where we see that SPHENO gives the largest value. The second largest contribution comes from $\Sigma_u^u(\tilde{t}_1)$ as might be

parameter	Isasugra	SoftSUSY	SUSPECT	SPHENO
$m_{\tilde{g}}$	2830.7	2794.3	2838.6	2827.6
$m_{\tilde{u}_L}$	5440.3	5403.2	5406.0	5412.8
$m_{\tilde{u}_R}$	5561.7	5521.3	5523.0	5521.8
$m_{\tilde{e}_R}$	4823.0	4817.3	4818.1	4825.8
$m_{\tilde{t}_1}$	1714.3	1682.8	1746.9	1942.1
$m_{\tilde{t}_2}$	3915.1	3879.0	3899.2	3947.0
$m_{\tilde{b}_1}$	3949.1	3871.6	3891.7	3939.1
$m_{\tilde{b}_2}$	5287.5	5266.4	5277.2	5281.7
$m_{\tilde{\tau}_1}$	4745.7	4746.1	4749.1	4757.4
$m_{\tilde{\tau}_2}$	5110.2	5109.7	5110.8	5107.2
$m_{\tilde{\nu}_\tau}$	5116.8	5108.7	5113.8	5106.2
$m_{\widetilde{\chi}_2^\pm}$	1020.2	1027.5	1030.6	1031.9
$m_{\widetilde{\chi}_1^\pm}$	209.7	203.1	203.0	197.3
$m_{\widetilde{\chi}_4^0}$	1033.5	1027.3	1031.1	1032.0
$m_{\widetilde{\chi}_3^0}$	540.1	536.4	537.2	538.1
$m_{\widetilde{\chi}_2^0}$	-208.3	-208.6	-208.7	-203.0
$m_{\widetilde{\chi}_1^0}$	197.9	197.2	197.1	191.9
m_h	124.7	127.3	127.5	125.2
$\Delta_{\rm EW}$	24.8	23.0	28.2	44.1

Table 2.1: Sparticle and Higgs mass spectra from four spectra generators for a natural SUSY benchmark point with $m_0 = 5$ TeV, $m_{1/2} = 1.2$ TeV, $A_0 = -8$ TeV, $\tan\beta = 10$ with $\mu = 200$ GeV and $m_A = 2$ TeV.

expected. The next several largest contributions come from H_d, μ and H_u and $\Sigma_u^u(\tilde{b}_{1,2})$ although the ordering of these differs among the codes. In general, the agreement for the remaining contributions is typically within expectations.

Order	Isajet	SoftSUSY	Suspect	Spheno
1	24.819, $\Sigma_u^u(\widetilde{t}_2)$	23.015, $\Sigma_u^u(\widetilde{t}_2)$	28.227, $\Sigma_u^u(\widetilde{t}_2)$	44.062, $\Sigma_u^u(\widetilde{t}_2)$
2	19.367, $\Sigma_u^u(\widetilde{t}_1)$	18.318, $\Sigma_u^u(\widetilde{t}_1)$	20.372, $\Sigma_u^u(\widetilde{t}_1)$	27.465, $\Sigma_u^u(\widetilde{t}_1)$
3	10.449, $\Sigma_u^u(\mathcal{O}(\alpha_s\alpha_t))$	10.074, H_d	10.294, H_d	11.205, H_u
4	10.424, H_d	9.618, μ	9.621, μ	10.298, H_d
5	9.625, μ	6.985, $\Sigma_u^u(\mathcal{O}(\alpha_s\alpha_t))$	7.405, $\Sigma_u^u(\mathcal{O}(\alpha_s\alpha_t))$	9.621, μ
6	5.861, H_u	4.557, $\Sigma_u^u(\widetilde{b}_2)$	4.044, $\Sigma_u^u(\widetilde{b}_2)$	8.321, $\Sigma_u^u(\mathcal{O}(\alpha_s\alpha_t))$
7	4.164, $\Sigma_u^u(\widetilde{\tau}_2)$	4.316, $\Sigma_u^u(\widetilde{\tau}_2)$	3.761, $\Sigma_u^u(\widetilde{\tau}_2)$	3.604, $\Sigma_u^u(\widetilde{b}_1)$
8	3.933, $\Sigma_u^u(\widetilde{b}_2)$	3.252, $\Sigma_u^u(\widetilde{\tau}_1)$	2.801, $\Sigma_u^u(\Sigma$ 2nd gen. $\widetilde{q})$	2.505, $\Sigma_u^u(\widetilde{\tau}_2)$
9	2.970, $\Sigma_u^u(\widetilde{\tau}_1)$	2.909, $\Sigma_u^u(\Sigma$ 2nd gen. $\widetilde{q})$	2.801, $\Sigma_u^u(\Sigma$ 1st gen. $\widetilde{q})$	2.486, $\Sigma_u^u(\widetilde{b}_2)$
10	2.912, $\Sigma_u^u(\Sigma$ 2nd gen. $\widetilde{q})$	2.909, $\Sigma_u^u(\Sigma$ 1st gen. $\widetilde{q})$	2.653, $\Sigma_u^u(\widetilde{\tau}_1)$	2.468, $\Sigma_u^u(\Sigma$ 2nd gen. $\widetilde{q})$
11	2.912, $\Sigma_u^u(\Sigma$ 1st gen. $\widetilde{q})$	2.761, H_u	2.507, $\Sigma_u^u(\widetilde{b}_1)$	2.468, $\Sigma_u^u(\Sigma$ 1st gen. $\widetilde{q})$
12	2.003, $\Sigma_u^u(\widetilde{b}_1)$	2.101, $\Sigma_u^u(\widetilde{b}_1)$	1.212, $\Sigma_u^u(\widetilde{\chi}_2^+)$	1.263, $\Sigma_u^u(\widetilde{\chi}_2^+)$
13	1.169, $\Sigma_u^u(\widetilde{\chi}_2^+)$	1.191, $\Sigma_u^u(\widetilde{\chi}_2^+)$	9.235e-1, $\Sigma_u^u(\widetilde{Z}_3^0)$	1.133, $\Sigma_u^u(\widetilde{\tau}_1)$
14	9.765e-1, $\Sigma_u^u(\widetilde{Z}_3^0)$	9.114e-1, $\Sigma_u^u(\widetilde{Z}_3^0)$	7.312e-1, H_u	9.538e-1, $\Sigma_u^u(\widetilde{Z}_3^0)$
15	6.987e-1, $\Sigma_u^u(\widetilde{Z}_4^0)$	6.924e-1, $\Sigma_u^u(\widetilde{Z}_4^0)$	7.076e-1, $\Sigma_u^u(\widetilde{Z}_4^0)$	7.381e-1, $\Sigma_u^u(\widetilde{Z}_4^0)$
16	5.98e-1, $\Sigma_u^u(H^\pm)$	6.083e-1, $\Sigma_u^u(H^\pm)$	6.264e-1, $\Sigma_u^u(H^\pm)$	6.755e-1, $\Sigma_u^u(H^\pm)$
17	1.532e-1, $\Sigma_u^u(t)$	1.438e-1, $\Sigma_u^u(t)$	1.440e-1, $\Sigma_u^u(t)$	2.064e-1, $\Sigma_u^u(\widetilde{Z}_1^0)$
18	5.924e-2, $\Sigma_u^u(\widetilde{Z}_1^0)$	7.522e-2, $\Sigma_u^u(\widetilde{Z}_1^0)$	7.687e-2, $\Sigma_u^u(\widetilde{Z}_1^0)$	1.361e-1, $\Sigma_u^u(t)$
19	5.543e-2, $\Sigma_d^d(H^0)$	5.305e-2, $\Sigma_d^d(H^0)$	5.564e-2, $\Sigma_d^d(H^0)$	5.831e-2, $\Sigma_d^d(H^0)$
20	4.758e-2, $\Sigma_d^d(\widetilde{Z}_3^0)$	4.397e-2, $\Sigma_d^d(\widetilde{Z}_3^0)$	4.507, $\Sigma_d^d(\widetilde{Z}_3^0)$	4.649e-2, $\Sigma_d^d(\widetilde{Z}_3^0)$
21	4.3e-2, $\Sigma_u^u(Z^0)$	4.175e-2, $\Sigma_d^d(\widetilde{b}_2)$	3.909e-2, $\Sigma_d^d(\widetilde{b}_2)$	4.341e-2, $\Sigma_d^d(\widetilde{t}_1)$
22	4.3e-2, $\Sigma_d^d(\widetilde{b}_2)$	3.783, $\Sigma_u^u(Z^0)$	3.825e-2, $\Sigma_u^u(Z^0)$	3.889e-2, $\Sigma_u^u(Z^0)$
23	3.748e-2, $\Sigma_d^d(\widetilde{t}_1)$	3.438, $\Sigma_d^d(\widetilde{t}_1)$	3.713e-2, $\Sigma_d^d(\widetilde{t}_1)$	2.793e-2, $\Sigma_d^d(\widetilde{b}_2)$
24	3.198e-2, $\Sigma_d^d(\Sigma$ 2nd gen. $\widetilde{q})$	3.128e-2, $\Sigma_d^d(\Sigma$ 2nd gen. $\widetilde{q})$	3.075e-2, $\Sigma_d^d(\Sigma$ 2nd gen. $\widetilde{q})$	2.706e-2, $\Sigma_d^d(\Sigma$ 2nd gen. $\widetilde{q})$
25	3.198e-2, $\Sigma_d^d(\Sigma$ 1st gen. $\widetilde{q})$	3.128e-2, $\Sigma_d^d(\Sigma$ 1st gen. $\widetilde{q})$	3.075e-2, $\Sigma_d^d(\Sigma$ 1st gen. $\widetilde{q})$	2.706e-2, $\Sigma_d^d(\Sigma$ 1st gen. $\widetilde{q})$
26	2.329e-2, $\Sigma_u^u(h^0)$	2.377e-2, $\Sigma_u^u(h^0)$	2.395e-2, $\Sigma_u^u(h^0)$	2.323e-2, $\Sigma_u^u(h^0)$
27	1.875e-2, $\Sigma_d^d(\widetilde{Z}_4^0)$	1.841e-2, $\Sigma_d^d(\widetilde{Z}_4^0)$	1.895e-2, $\Sigma_d^d(\widetilde{Z}_4^0)$	2.152e-2, $\Sigma_u^u(\widetilde{Z}_2^0)$
28	1.669e-2, $\Sigma_d^d(\widetilde{\tau}_1)$	1.787e-2, $\Sigma_d^d(\widetilde{\tau}_1)$	1.504e-2, $\Sigma_d^d(\widetilde{\tau}_1)$	1.974e-2, $\Sigma_d^d(\widetilde{Z}_4^0)$
29	1.279e-2, $\Sigma_d^d(\widetilde{\chi}_2^+)$	1.276e-2, $\Sigma_d^d(\widetilde{\chi}_2^+)$	1.326e-2, $\Sigma_d^d(\widetilde{\chi}_2^+)$	1.719e-2, $\Sigma_d^d(\widetilde{Z}_1^0)$
30	1.102e-2, $\Sigma_d^d(\widetilde{\tau}_2)$	1.107e-2, $\Sigma_u^u(H^0)$	1.079e-2, $\Sigma_u^u(H^0)$	1.553e-2, $\Sigma_d^d(\widetilde{b}_1)$
31	1.095e-2, $\Sigma_d^d(\mathcal{O}(\alpha_s\alpha_t))$	1.101e-2, $\Sigma_d^d(\widetilde{\tau}_2)$	1.034e-2, $\Sigma_d^d(\widetilde{b}_1)$	1.380e-2, $\Sigma_d^d(\widetilde{\chi}_2^+)$
32	9.869e-3, $\Sigma_u^u(\widetilde{Z}_2^0)$	8.412e-3, $\Sigma_d^d(\widetilde{b}_1)$	9.897e-3, $\Sigma_d^d(\widetilde{\tau}_2)$	8.754e-3, $\Sigma_u^u(H^0)$
33	8.366e-3, $\Sigma_d^d(\widetilde{b}_1)$	7.381e-3, $\Sigma_d^d(\mathcal{O}(\alpha_s\alpha_t))$	7.391e-3, $\Sigma_d^d(\mathcal{O}(\alpha_s\alpha_t))$	8.132e-3, $\Sigma_d^d(\mathcal{O}(\alpha_s\alpha_t))$
34	8.083e-3, $\Sigma_u^u(H^0)$	7.315e-3, $\Sigma_u^u(\widetilde{Z}_2^0)$	7.180e-3, $\Sigma_u^u(\widetilde{Z}_2^0)$	7.408e-3, $\Sigma_{d,u}^{d,u}(H^\pm)$
35	6.658e-3, $\Sigma_{d,u}^{d,u}(H^\pm)$	6.542e-3, $\Sigma_{d,u}^{d,u}(H^\pm)$	6.877e-3, $\Sigma_{d,u}^{d,u}(H^\pm)$	6.470e-3, $\Sigma_d^d(\widetilde{\tau}_2)$
36	5.469e-3, $\Sigma_u^u(W^\pm)$	5.400e-3, $\Sigma_u^u(W^\pm)$	5.467e-3, $\Sigma_u^u(W^\pm)$	6.324e-3, $\Sigma_d^d(\widetilde{\tau}_1)$
37	2.611e-3, $\Sigma_d^d(\widetilde{Z}_2^0)$	2.660e-3, $\Sigma_d^d(\widetilde{Z}_2^0)$	2.717e-3, $\Sigma_d^d(\widetilde{Z}_2^0)$	5.561e-3, $\Sigma_u^u(W^\pm)$
38	1.081e-3, $\Sigma_d^d(\widetilde{Z}_1^0)$	2.305e-3, $\Sigma_d^d(\widetilde{Z}_1^0)$	2.428e-3, $\Sigma_d^d(\widetilde{Z}_1^0)$	2.441e-3, $\Sigma_u^u(\widetilde{\chi}_1^+)$
39	7.420e-4, $\Sigma_d^d(h^0)$	2.044e-3, $\Sigma_u^u(\widetilde{\chi}_1^+)$	2.336, $\Sigma_u^u(\widetilde{\chi}_1^+)$	1.630e-3, $\Sigma_d^d(\widetilde{Z}_2^0)$
40	4.723e-4, $\Sigma_{d,u}^{d,u}(Z^0)$	7.568e-4, $\Sigma_d^d(h^0)$	7.776e-4, $\Sigma_d^d(h^0)$	7.394e-4, $\Sigma_d^d(h^0)$
41	4.205e-4, $\Sigma_u^u(\widetilde{\chi}_1^+)$	4.069e-4, $\Sigma_{d,u}^{d,u}(Z^0)$	4.199e-4, $\Sigma_{d,u}^{d,u}(Z^0)$	4.265e-4, $\Sigma_{d,u}^{d,u}(Z^0)$
42	1.000e-4, $\Sigma_d^d(\widetilde{t}_2)$	2.013e-4, $\Sigma_d^d(\widetilde{t}_2)$	2.673e-4, $\Sigma_d^d(\widetilde{t}_2)$	4.215e-4, $\Sigma_d^d(\widetilde{t}_2)$
43	6.007e-5, $\Sigma_{d,u}^{d,u}(W^\pm)$	5.808e-5, $\Sigma_{d,u}^{d,u}(W^\pm)$	6.002e-5, $\Sigma_{d,u}^{d,u}(W^\pm)$	6.098e-5, $\Sigma_{d,u}^{d,u}(W^\pm)$
44	9.197e-6, $\Sigma_d^d(\widetilde{\chi}_1^+)$	2.608e-5, $\Sigma_d^d(\widetilde{\chi}_1^+)$	2.986e-5, $\Sigma_d^d(\widetilde{\chi}_1^+)$	3.085e-5, $\Sigma_d^d(\widetilde{\chi}_1^+)$
45	2.315e-8, $\Sigma_d^d(b)$	2.302e-8, $\Sigma_d^d(b)$	2.282e-8, $\Sigma_d^d(b)$	1.895e-8, $\Sigma_d^d(b)$
46	9.579e-9, $\Sigma_d^d(\tau)$	7.904e-9, $\Sigma_d^d(\tau)$	7.812e-9, $\Sigma_d^d(\tau)$	7.783e-9, $\Sigma_d^d(\tau)$

Table 2.2: Top 46 contributions to Δ_{EW} for our natural SUSY benchmark point for four different spectra calculator codes.

In Fig. 2.12, we show the values of *a)* m_h, *b)* $m_{\tilde{t}_{1,2}}$, *c)* Δ_{EW} and *d)* A_t versus A_0/m_0 for the NUHM3 model with parameters as in the caption but with varying A_0. (NUHM3 splits first/second generation sfermion soft terms from third generation ones so that $m_0(1,2) \neq m_0(3)$.) These plots are obtained using SoftSUSY and can be compared to similar plots in Ref. [76] using Isasugra. We see from frame *a)* that the value of m_h is actually maximal at large negative A_t

values (which are shown in frame *d*)). The large mixing in the stop sector lifts the value of m_h to the 125 GeV regime, but in this case only for *negative* A_t values. The stop mass eigenstates are shown in frame *b*) where again, when there is large mixing, the eigenstates have the largest splittings and $m_{\tilde{t}_1}$ becomes lowest in value. In frame *c*), we show the corresponding value of Δ_{EW}. Here we see that for large trilinear A_t, then there can be large cancellations in $\Sigma_u^u(\tilde{t}_{1,2})$ which lead to decreased finetuning. The kinks in the curve occur due to transitions from one maximal contribution to Δ_{EW} to a different one. The dominant contributions to Δ_{EW} in the middle of the plot comes from top-squark contributions whilst the left and right edges come from tau-slepton contributions (as in Fig. 2 of Ref. [76]). The low value of Δ_{EW} coincides with the uplift in m_h to ~ 125 GeV for large negative values of A_t.

In Fig. 2.13, we show the third generation contributions to Δ_{EW} vs. $A_0/m_0(3)$ for the same parameters as in Fig. 2.12, but using SoftSUSY. These can be compared with the same plot using Isasugra in Fig. 2 of Ref. [76]. Here, we see that the contributions from staus and sbottoms are generally rather small, and the top-squark contributions typically dominate. But for large $|A_0/m_0(3)|$, then cancellations in both $\Sigma_u^u(\tilde{t}_1)$ and $\Sigma_u^u(\tilde{t}_2)$ occur, and the stop contributions become comparable to those of the other third generation sparticles, giving reduced finetuning and greater naturalness.

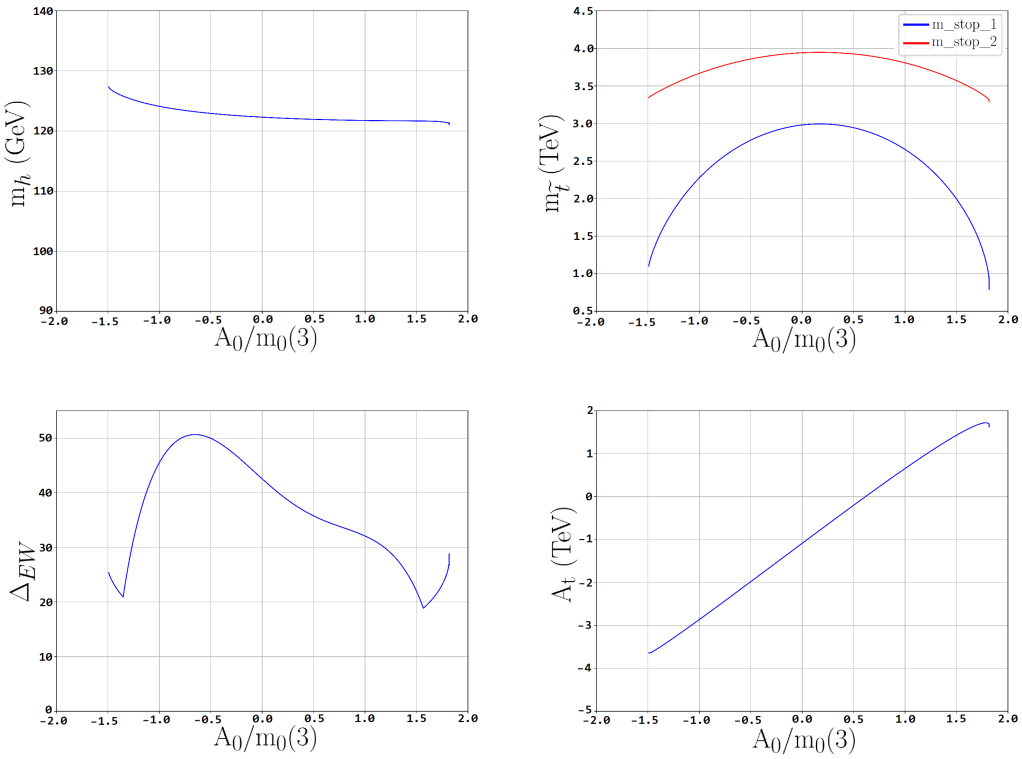

Figure 2.12: Values of *a*) m_h, *b*) $m_{\tilde{t}_{1,2}}$, *c*) Δ_{EW} and *d*) $A_t(Q)$ vs. $A_0/m_0(3)$ for the NUHM3 model with $m_0(1,2) = 10$ TeV, $m_0(3) = 5$ TeV, $m_{1/2} = 0.7$ TeV, $\tan\beta = 10$ with $\mu = 200$ GeV and $m_A = 2$ TeV.

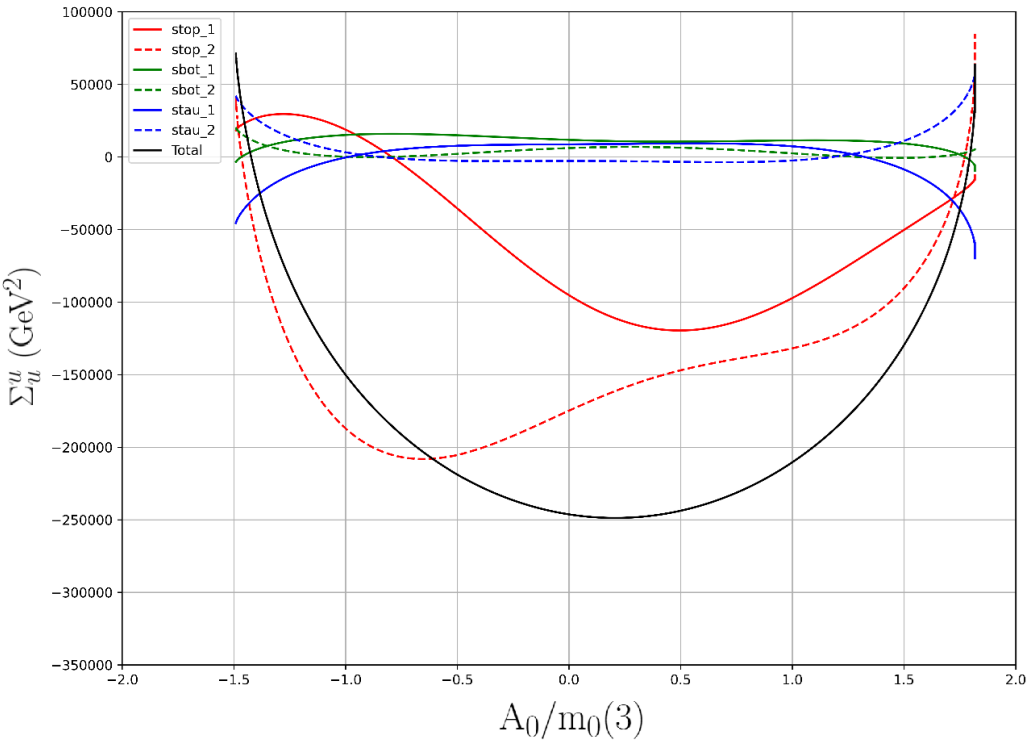

Figure 2.13: Third generation contributions to Δ_{EW} for the same model parameters as Fig. 2.12 vs. $A_0/m_0(3)$ in the m_0 vs. $m_{1/2}$ plane of the NUHM2 model with $\mu = 200$, $\tan\beta = 10$, $A_0 = -1.6m_0$ and $m_A = 2$ TeV.

2.3.2 Natural regions of m_0 vs. $m_{1/2}$ plane

In Fig. 2.14, we show the m_0 vs. $m_{1/2}$ parameter plane for the NUHM2 model with $A_0 = -1.6m_0$, $\mu = 200$ GeV and $m_A = 2$ TeV. The plot is generated using SoftSUSY but can be compared with similar results from Isasugra in Fig. $8b$ of Ref. [81]. From the plot, we see the lower-left corner is actually excluded due to charge-or-color-breaking (CCB) vacua which occur for too large A_0 values. Both SoftSUSY and Isasugra generate CCB regions there. We also show contours of Higgs mass $m_h = 123$ and 127 GeV. These are qualitatively similar to the Isasugra results but shifted to the right by a couple hundred GeV in m_0. Thus, much of the parameter space allows for the measured Higgs mass $m_h \sim 125$ GeV. We also show naturalness contours for $\Delta_{EW} = 15$ and 30. These can also be compared against the LHC Run 2 gluino mass limit $m_{\tilde{g}} \gtrsim 2.25$ TeV as shown by the light blue contour. The important point is that both SoftSUSY and Isasugra agree that the bulk of this parameter space plane is EW natural, in accord with LHC gluino mass limits, and in accord with the measured Higgs mass. This is in contrast to older naturalness measures which required much lower gluino masses[44, 45, 48, 47] and also Higgs boson masses[124].

2.4 Unnatural SUSY and its phenomenology

There also exist many renditions of supersymmetry that may yet still be potentially viable at the LHC, yet fail in addressing the LHP via practical naturalness due to a high degree of finetuning. Below, we address some of the most common versions of

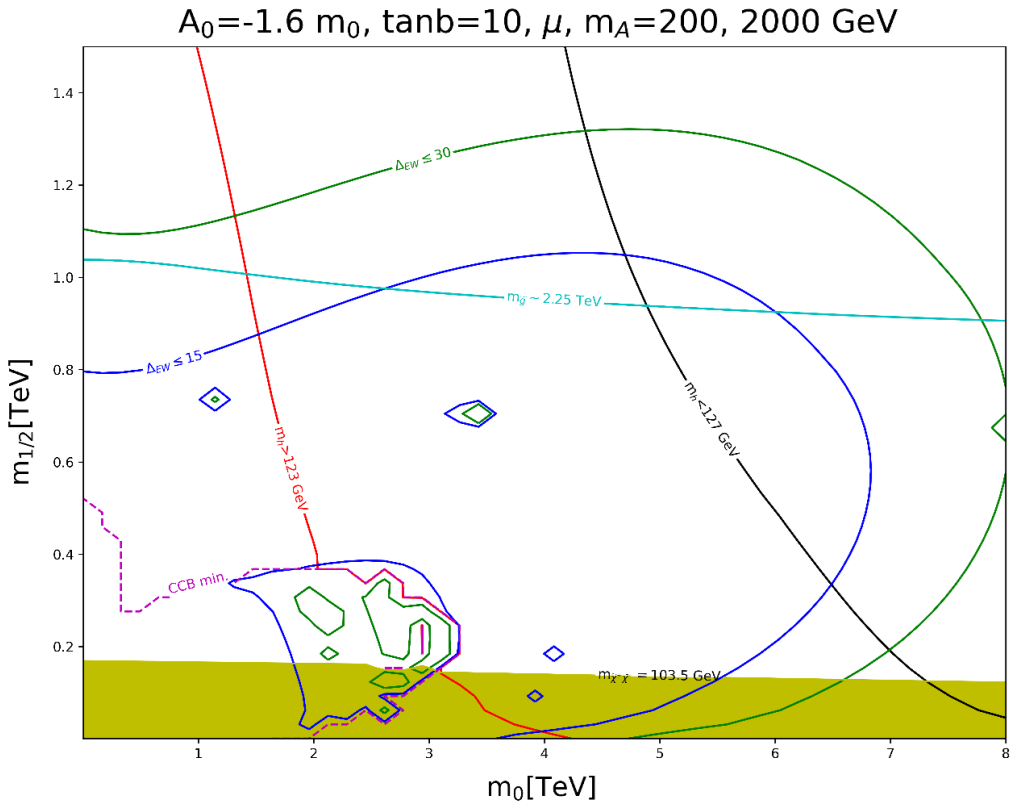

Figure 2.14: Contours of naturalness measure Δ_{EW} and m_h in the m_0 vs. $m_{1/2}$ plane of the NUHM2 model with $\mu = 200$, $\tan\beta = 10$, $A_0 = -1.6m_0$ and $m_A = 2$ TeV.

unnatural SUSY in the MSSM, with some brief descriptions of the phenomenology therein. Later, in Chapter 4, we devise a method on the string landscape that allows us to compare these unnatural models to RNS, which ultimately leads to the devised stringy naturalness calculation in Chapter 5.

2.4.1 CMSSM

For a long time, the mSUGRA[8] or CMSSM[7] model served as a sort of paradigm model for SUSY phenomenology. This model posits gravity-mediated SUSY breaking which induces a common scalar mass m_0, a common gaugino mass $m_{1/2}$ and a common trilinear soft term A_0 all prescribed at the GUT scale $m_G \simeq 2\times 10^{16}$ GeV. The weak scale soft terms are determined by RGE running to the weak scale, where electroweak symmetry is radiatively broken via a large top quark Yukawa coupling. The μ term is tuned via Eq. (2.9) to give the measured value of m_Z. In pre-LHC days, it was possible within the CMSSM model to gain accord with naturalness (low Δ_{EW}) and with an acceptable thermal relic abundance of the LSP. After LHC Run 2 – while respecting the LHC measured Higgs mass and also LHC sparticle search limits – natural CMSSM spectra are no longer possible[92, 68, 81].

For illustrative purposes, we compute the mSUGRA/CMSSM spectra using the Isasugra spectrum generator[116, 117] for a mSUGRA/CMSSM benchmark point with $(m_0,\ m_{1/2},\ A_0,\ \tan\beta = 5000\text{ GeV}, 1200\text{ GeV},\ -8000\text{ GeV}, 10)$ which yields a gluino mass $m_{\tilde{g}} = 2.8$ TeV (well above current LHC bounds) with $m_h = 124.3$ GeV and with $\Delta_{EW} = 2641$ (highly EW finetuned). The thermal

bino LSP abundance is $\Omega_\chi h^2 \simeq 249$ so non-thermal processes would need to be invoked to bring the relic density into alignment with the measured dark matter abundance[125].

2.4.2 PeV SUSY

PeV-scale supersymmetry[126, 127] is motivated by the possibility of SUSY breaking via "charged" SUSY breaking fields S. For charged SUSY breaking, scalar partners gain mass via Kähler potential terms $K \ni \frac{S^\dagger S}{m_P^2} Q^\dagger Q$ where the Q are visible sector fields and S are hidden sector fields which carry some charge, perhaps R charge. Thus, scalar fields gain a mass $m_Q^2 \sim F_S^\dagger F_S / m_P^2 \sim m_{3/2}^2$ whilst gaugino masses, which ordinarily gain mass via the gauge kinetic function $f \ni kS$ are forbidden. Hence, the leading contribution to gaugino masses (and also A-terms) are the loop-suppressed anomaly-mediated contributions $m_\lambda = \frac{\beta(g_\lambda)}{g_\lambda} m_{3/2}$ and we expect $M_1 \simeq m_{3/2}/120$, $M_2 \simeq m_{3/2}/360$ and $M_3 \simeq m_{3/2}/40$. The wino is then the LSP and can make up the dark matter. Thermally produced relic winos can make up all the missing dark matter for $m_{wino} \sim 3$ TeV. Then, with a 3 TeV wino, one expects scalar masses $\tilde{m} \sim 1000$ TeV, *i.e.* close to the PeV scale (1 PeV=1000 TeV). The PeV scale scalar masses provide a decoupling solution to the SUSY flavor and CP problems[128]. The μ parameter may range anywhere between m_{wino} and $\tilde{m}$. The resultant light Higgs mass is expected in the range $125 \text{ GeV} < m_h < 155 \text{ GeV}$[129].

2.4.3 Split SUSY

In split SUSY[130, 129, 131], the motivation is that the string landscape may provide a selection mechanism for the finetuning of the electroweak scale in that the weak scale must lie within the ABDS window in order to have a universe with complex atoms as we know them, which seem necessary for life. However, SUSY may still be needed for consistency with string theory, but the SUSY breaking scale may now be far higher than that which is usually required by naturalness. One may then allow masses of squarks and sleptons (which occur in multiplets of $SU(5)$) to be as high as $m_\phi \sim 10^9$ GeV while fermion masses, which are protected by chiral symmetry, can lie near the weak scale. This model then preserves the SUSY success stories of gauge coupling unification and WIMP dark matter while appealing to vacuum selection from the string landscape to "tune" the EW scale to its value as required by the atomic principle. Thus, in split SUSY, one expects both gauginos and higgsinos around the weak scale whilst squarks and sleptons decouple at some intermediate scale (*e.g.* 10^9 GeV). Such a split hierarchy of masses can arise from D-term SUSY breaking which maintains an approximate, accidental R-symmetry[131]. The very high scalar mass scale $\tilde{m}$ provides a decoupling solution to the SUSY flavor and CP problems and also alleviates the cosmological gravitino and moduli problems by making these particles sufficiently heavy and thus shortlived in the early universe. The striking signature of split SUSY models is long lived gluinos which may decay with displaced vertices or even outside of the collider detector. For scalar masses

as high as $\sim 10^9$ GeV, then the lightest Higgs scalar is expected to have mass $m_h \sim 130 - 145$ GeV[132].

2.4.4 High-scale SUSY

In high-scale SUSY (HS-SUSY)[133, 134, 135], it is assumed that the underlying 4-d theory is indeed SUSY, but with a much higher SUSY breaking scale than that which is usually assumed to solve the gauge hierarchy problem. Thus, in HS-SUSY, the superpartners are typically clustered at some very high mass scale $\tilde{m} \sim 10 - 10^{13}$ TeV. In HS-SUSY, the SM is the LE-EFT and only the light Higgs particle is expected to be produced at LHC. Indeed, by requiring the model to yield the measured Higgs mass $m_h \sim 125$ GeV, then $\tilde{m} \sim 10^1 - 10^7$ TeV[132, 136].

2.4.5 Mini-Split

Mini-Split[137] SUSY is a version of split SUSY wherein the scalar mass $\tilde{m}$ is lowered to the $\sim 10^{2-4}$ TeV range in order to accommodate the measured Higgs mass $m_h \simeq 125$ GeV while gauginos remain near the TeV scale. Several scenarios are envisaged in [137] including non-sequestered AMSB and $U(1)'$ mediation. These scenarios include a small A parameter while μ may be either at the gaugino scale (light) or at the scalar scale (heavy).

2.4.6 Simply unnatural SUSY

In simply unnatural SUSY[138] (SUN-SUSY), the scalar mass scale $\tilde{m}$ is determined by the measured value of the Higgs mass $m_h \simeq 125$ GeV to be $\tilde{m} \sim 10^2 - 10^3$

TeV where the trilinear soft terms A_i are assumed to be tiny (little mixing in the stop sector). The SUSY μ term is also expected to be $\mu \sim \tilde{m}$ while the gaugino masses, which require an R-symmetry breaking to gain mass, are expected to be at the TeV scale. Minimally, the gaugino masses are expected to obtain the AMSB form, but the presence of heavy vector-like states could alter those relations leading to a more compressed gaugino spectrum. Typically, the wino is expected to be the LSP, and the relic abundance may be produced either thermally or non-thermally due to late-decaying TeV-scale moduli fields.

2.4.7 Spread SUSY

In Ref. [139], it is emphasized that there may exist a forbidden region on the scale of SUSY breaking $\tilde{m}$ such that if $\tilde{m} \gtrsim \mathcal{O}(1)$ TeV, then LSP dark matter will be overproduced which can violate the anthropic bounds which disfavor/forbid DM overproduction in that the baryon-to-DM ratio may be insufficient for baryonic structure formation in the universe[140]. This forbidden region should persist up to $\tilde{m} \sim T_R$ where T_R is the reheat temperature of the universe at the end of inflation. Higher values of $\tilde{m} > T_R$ are allowed in that SUSY particles wouldn't be produced during the reheat process. Taking $\tilde{m} > T_R$ then leads to a very heavy SUSY spectrum (High Scale SUSY) whilst taking $\tilde{m} \sim 1$ TeV leads to Spread SUSY in the case of SUSY breaking via "charged" hidden sector fields (where scalars gain mass $\tilde{m}$ but gauginos and A terms do not) or via uncharged hidden sector fields (which leads to all sparticles at $\tilde{m} \sim 10$ TeV, dubbed the "environmental MSSM"). The spread SUSY spectrum divides into two possibilities:

1. scalar masses $\tilde{m} \sim 10^5$ TeV with gauginos at 10^2 TeV and higgsinos at ~ 1 TeV and 2. scalars around 10^3 TeV with higgsinos and gravitinos $\sim 10^2$ TeV and gauginos ~ 1 TeV. Thus, the spread SUSY models typically have SUSY mass spectra spread across *three* mass scales.

2.4.8 G_2MSSM

The G_2MSSM labels the sort of SUSY spectra expected to emerge from 11-dimensional M-theory compactified on a manifold of G_2 holonomy[141, 142] which preserves $N = 1$ SUSY in the low energy 4-d effective field theory (LE-EFT). The LE-EFT then consists of the usual MSSM fields plus an assortment of moduli fields which are string remnants from the compactification. Scalar masses $\tilde{m}$ and the lightest modulus field are expected to gain masses of order the gravitino mass $m_{3/2}$ and in order to solve the cosmological moduli/gravitino problems then $\tilde{m} \sim 30 - 100$ TeV. Gaugino masses are suppressed relative to scalars by a factor $\log(m_P/m_{3/2}) \sim 30$ so gauginos (and higgsinos) are expected at the 1-3 TeV range and may have comparable moduli/anomaly-mediated contributions. The LSP may be bino or wino-like but the relic density is seriously affected by non-thermal production via the late-decaying lightest modulus field[143]. In later renditions, the possibility of a hidden sector LSP is entertained[144].

Chapter 3

Scalar sequestering: an alternate solution to the LHP

Other methods exist for addressing the Little Hierarchy Problem and must be addressed in turn. Recall from the previous chapter that the non-appearance of supersymmetric matter at the CERN Large Hadron Collider[58] (LHC) has potentially opened up a different naturalness problem[107]: the little hierarchy problem (LHP) concerning the burgeoning mass gap between the weak scale $m_{weak} \sim m_{W,Z,h} \sim 100$ GeV and the so-called soft SUSY breaking scale $m_{soft} \sim m_{sparticles}$, *i.e.*, why is $m_{weak} \ll m_{soft} \gtrsim 1 - 10$ TeV?

Unnatural SUSY with large $|\mu| \gg m_{weak}$, while possible, seems at first glance highly implausible. However, model builders have proposed a way to remain natural even with $|\mu| \gg m_{weak}$ by discovering models where the *combinations* $m_{H_{u,d}}^2 + \mu^2$ are driven to be tiny, while $\sqrt{|m_{H_{u,d}}^2|}$ and μ individually can each be large at the weak scale. This method is called *scalar sequestering* (SS)[145, 146, 147, 148].

The method of hidden sector sequestering (HSS) of visible sector operators arises from postulating the existence of a strongly interacting nearly superconformal hidden sector (HS) which is operative between the messenger scale M_* (taken to be of order the reduced Planck mass $\sim m_P$ in the case of gravity mediation) and a much lower intermediate scale M_{int} where the superconformal symmetry is broken and SUSY is also broken. This method of sequestering was

originally proposed[149] as a means to obtain anomaly-mediated SUSY breaking (AMSB) models[150, 151] when geometric sequestering was shown to be difficult to realize[152].

Under HSS, the various soft SUSY breaking terms get squeezed to tiny values via RG running between m_* and M_{int} by a power-law behavior:

$$m_{soft}(M_{int}) \sim (M_{int}/m_*)^{\Gamma} m_{soft}(m_*) \tag{3.1}$$

where the exponent Γ includes combinations of classical and anomalous dimensions of HS fields S. Γ is not directly calculable due to the strong dynamics in the HS but is instead assumed to be ~ 1. For $M_{int} \sim 10^{11}$ GeV and $\Gamma \sim 1$, then the suppression of gravity-mediated soft terms can be $\sim 10^{-7}$ in which case the AMSB soft terms would be dominant. Additional symmetries seemed to be required in order for HSS to be viable; nonetheless, the lesson was that (model dependent) hidden sector effects could potentially modify the assumed running of SUSY model parameters as expected under the MSSM only[153, 154]. HSS was then found to offer a solution to the needed suppression of various problematic operators. For instance, in gauge mediation[155] the $B\mu$ soft term is expected with $B\mu \gg \mu^2$, leading to the famous $B\mu/\mu$ problem. HSS could be used to suppress $B\mu(M_{int}) \sim 0$ thus solving the problem[156, 145]. Also, in gravity mediation, scalar masses arise via hidden sector-visible sector couplings such as

$$\int d^4\theta \frac{c_{ij}}{m_P^2} S^\dagger S Q_i^\dagger Q_j \tag{3.2}$$

where the Q_i are visible sector fields and the S are hidden sector fields which acquire an auxiliary field SUSY breaking vev $F_S \sim (10^{11}\ \text{GeV})^2$. In gravity-mediation, such operators are unsuppressed by any known symmetry (leading to the SUSY flavor problem), but could be squeezed to tiny values via scalar sequestering. A third application of (scalar) sequestering is to ameliorate the LHP while maintaining large μ values: $|\mu| \gg m_{weak}$. This case, which is the subject of this dissertation chapter, makes use of Eq. 3.2 to suppress via hidden sector running all scalar masses to ~ 0. However, in the case where the Giudice-Masiero mechanism[157] is assumed[1] to generate a weak scale value of μ, then the scalar sequestering actually applies to m_Q^2 for matter scalars, but to the combinations $m_{H_{u,d}}^2 + \mu^2$ for Higgs scalars. In this case, at the intermediate scale M_{int}, then one expects $m_Q^2 \sim 0$ but with $m_{H_{u,d}}^2 \sim -\mu^2$ so that μ can be large whilst the combination $m_{H_{u,d}}^2 + \mu^2$ is small: this has the potential to fulfill the naturalness requirement in Eq. 2.9 while maintaining large $|\mu| \gg m_{weak}$ since μ^2 and $m_{H_{u,d}}^2$ are no longer independent.

In this dissertation, we examine the phenomenology of SUSY models with scalar sequestering. In Sec. 3.1, we present a brief review of the theory underlying scalar sequestering. Two different theory approaches have emerged: strong scalar sequestering where hidden sector running overwhelms MSSM running[145, 146], and moderate scalar sequestering[148], wherein hidden sector running and MSSM running are comparable, leading to quasi-fixed point behavior for the intermediate scale soft term boundary conditions. In Sec. 3.2, we examine strong SS, dubbed

[1]Twenty solutions to the SUSY μ problem are reviewed in Ref. [158]

here as the PRS (Perez, Roy and Schmaltz) scheme[146]. Here, the intermediate scale boundary conditions are so determinative that only one (or a few) parameters completely determine the SUSY phenomenology. In this case, problems emerge for appropriate electroweak symmetry breaking, vacuum stability, and dark matter physics (with typically a charged LSP and sometimes a left-sneutrino LSP). The latter case with a charged LSP can be dispensed with via either an assumed R-parity violation[159, 160] or assumed LSP decays to non-MSSM DM particles such as an axino $\widetilde{a}$[161]. In Sec. 3.3, we verify these results with parameter space scans in the PRS scheme with and without unified gaugino masses. In Sec. 3.4, we instead adopt the scheme in [148] – we refer to this scheme as SPM (Stephen P. Martin)– with more limited HS running which is comparable to MSSM running. In this scheme, for the case of unified gaugino masses (UGM), we find that although SS reduces the amount of EW finetuning, significant weak scale finetuning arising from large top-squark masses remains, so that the finetuning problem cannot be said to be eliminated for large μ. However, in the case of non-universal gaugino masses (NUHM) which lead to large stop mixing and $m_h \simeq 125$ GeV, then evidently low finetuning along with appropriate EWSB can be achieved for more moderate values of $\mu \sim 1$ TeV.

3.1 Brief review of scalar sequestering

Let us assume a gravity-mediated generation of soft SUSY breaking terms since gauge-mediation gives rise to trilinear soft terms $A \sim 0$ and hence requires large,

unnatural values of top squarks[68] to generate $m_h \sim 125$ GeV[162]. At some scale $m_* < m_P$, the (superconformal) hidden sector becomes strongly interacting. Its coupling to visible sector fields leads to suppression of scalar soft breaking masses and also the bilinear soft term $b \equiv B\mu$. At some intermediate scale M_{int}, the conformal symmetry is broken and the hidden sector is integrated out of the low energy EFT. Also around this scale, SUSY is broken at a scale $Q^2_{SUSY} \sim F_S$.

Under gravity-mediation, the following operators give rise to the usual soft terms:

$$\int d^2\theta c_\lambda \frac{S}{m_P} WW + h.c. \Rightarrow m_\lambda \sim c_\lambda (F_S/m_P), \tag{3.3}$$

$$\int d^2\theta c_A \frac{S}{m_P} \phi_i \phi_j \phi_k + h.c. \Rightarrow A_{ijk} \sim c_A (F_s/m_P), \tag{3.4}$$

$$\int d^4\theta c_{ij} \frac{R}{m_P^2} \phi_i^\dagger \phi_j \Rightarrow m^2_{\phi_{ij}} \sim c_{ij} (F_S/m_P)^2, \tag{3.5}$$

and

$$\int d^4\theta c_b \frac{R}{m_P^2} H_u H_d + h.c. \Rightarrow B\mu \sim c_b (F_S/m_P)^2, \tag{3.6}$$

where S is a HS chiral superfield and R is a real product of hidden sector fields with $R \sim S^\dagger S + \cdots$. In addition, for the scalar sequestering model, one assumes the μ term is initially suppressed (by some symmetry?) but then arises via the Giudice-Masiero[157] mechanism at the scale m_{soft} via

$$\int d^4\theta c_\mu \frac{S^\dagger}{m_P} H_u H_d \Rightarrow \mu_{GM} \sim c_\mu (F_S/m_P). \tag{3.7}$$

The holomorphic terms ($\int d^2\theta$) are protected against renormalization effects by

non-renormalization theorems but the non-holomorphic terms are not. The latter terms give rise to scalar masses $m^2_{\phi_{ij}}$ and the bilinear soft term $B\mu$, and will scale between m_* and M_{int} as $(M_{int}/m_*)^\Gamma$ where the exponent Γ is related to the anomalous dimension of the S field.

While Γ is not directly calculable since the HS is strongly interacting, under the assumption that Γ is large and positive, *e.g.* ~ 1, then the factor $(M_{int}/m_*)^\Gamma$ can lead to large suppression of scalar masses and $B\mu$ as compared to gaugino masses, A-terms and μ. However, while μ can remain large under scalar sequestering, the combination $\hat{m}^2_{H_{u,d}} \equiv m^2_{H_{u,d}} + \mu^2$ gets driven to tiny values by the $(M_{int}/m_*)^\Gamma$ factor.

3.2 Scalar sequestered SUSY: PRS boundary conditions

In the PRS scheme[145, 146], the SS is assumed to dominate any MSSM running of soft terms. In this case, one expects the usual MSSM running for gaugino masses, A-terms and μ between the high scale m_* and the intermediate scale M_{int}, whilst HS effects suppress matter scalar masses $m^2_{\phi_{ij}}$, $B\mu$ and Higgs combinations $m^2_{H_{u,d}} + \mu^2$. Thus, (under the assumption of unified gaugino masses) the parameter space of the model is given by

$$m_{1/2},\ A_0,\ \mu \quad \text{and} \quad M_{int} \tag{3.8}$$

where the first three of these are given at the high scale m_*. Motivated by gauge coupling unification, we take $m_* = m_{GUT}$, the scale where g_1 and g_2 unify under

MSSM running, and where $m_{GUT} \simeq 2 \times 10^{16}$ GeV. Meanwhile, the matter scalar masses, $B\mu$ and $m_{H_{u,d}}^2 + \mu^2$ are taken to be ~ 0 at the scale $Q \sim M_{int}$.

3.2.1 Results for $M_{int} = 10^{11}$ GeV and $A_0 < 0$

As an illustration, we show in Fig. 3.1 the running of soft terms and μ for the case where $m_{1/2} = -A_0 = 1.5$ TeV with $\mu = 500$ GeV (the reason for $\mu \sim 500$ GeV is to be explained shortly). The pink shaded region shows the superconformal regime, whilst the soft terms run according to MSSM-only RGEs in the left-side unshaded region. We see from frame *a*) that the matter scalars start running at $Q = 10^{11}$ GeV where the squark masses are pulled to large values $\gtrsim 2$ TeV due to the influence of the $SU(3)$ gaugino mass M_3. Left-slepton masses are pulled up by a large $SU(2)_L$ gaugino mass M_2 to the vicinity of ~ 650 GeV at m_{weak} whilst the right slepton masses are pulled up by the $U(1)_Y$ gaugino mass M_1 to ~ 300 GeV. The running of the bilinear b-term is given by

$$\frac{db}{dt} = \frac{\beta_b}{16\pi^2} \tag{3.9}$$

where the beta function is given at one-loop by

$$\beta_b^{(1)} = b(3f_t^2 + 3f_b^2 + f_\tau^2 - 3g_2^2 - \frac{3}{5}g_1^2) + \mu(6a_t f_t + 6a_b f_b + 2a_\tau f_\tau + 6g2^2 M_2 + \frac{6}{5}g_1^2 M_1) \tag{3.10}$$

where the f_i are Yukawa couplings, the g_i are gauge couplings, the $a_i = A_i f_i$ are the reduced trilinear couplings, and the M_i are gaugino masses (further RGEs are

given in, *e.g.*, Ref. [3]). The $\sqrt{b} = \sqrt{B\mu}$ term is pulled from zero at $Q = M_{int}$ to ~ 550 GeV at $Q = m_{weak}$ mainly by the second term of Eq. 3.10. Meanwhile, with $\mu = 500$ GeV, the $\text{sign}(m^2_{H_{u,d}}) * \sqrt{|m_{H_{u,d}}|}$ soft terms begin at -500 GeV and $m^2_{H_u}$ is driven to large negative values at m_{weak} due to the large top-quark Yukawa coupling f_t. Also, m_{H_d} is driven dominantly by the gaugino mass M_2 to small negative values ~ -100 GeV at m_{weak}. Frame *b*) shows the running of trilinear soft terms starting from $Q = m_{GUT}$. These terms are pushed to large negative values by the respective gauge interactions. In the case of A_t, this may help drive stop masses towards tachyonic values (i.e., negative squared mass values, where $m^2_{\tilde{t}} < 0$, implying the running mass is not a real value, which can affect minima of the scalar potential) and consequently to charge and/or color breaking (CCB) minima in the scalar potential. The importance of avoiding CCB minima is emphasized in the following phenomenological features. Since the Standard Model and its supersymmetric extensions assume a stable or metastable vacuum corresponding to the observed universe, then if the scalar potential develops CCB minima, it implies that there are alternate vacua where either charge, color, or both are broken. This would mean that the universe could transition to these undesired vacua, leading to a state where the fundamental symmetries of electromagnetism and QCD are broken. Such a transition would likely result in a universe very different from the one we observe, as well as leading to other exotic phenomena and proton destabilization that would need to be explained. In particular, if it were allowed for squark and slepton (squared) masses to run negative, then these fields may be able to acquire non-zero vacuum expectation values (VEVs),

leading to the aforementioned undesirable observable consequences, which would be inconsistent with our current observations.

A major check on this very constrained PRS scheme is if the EW symmetry is properly broken. Let us recall the (tree-level) conditions for proper EWSB. First, one must check whether the scalar potential indeed *does not develop a minimum* at $h_u^0 = h_d^0 = 0$, the origin of neutral scalar field space. The stability of the critical point satisfying

$$\left.\frac{\partial V}{\partial h_u^0}\right|_{h_u^0=h_d^0=0} = \left.\frac{\partial V}{\partial h_d^0}\right|_{h_u^0=h_d^0=0} = 0$$

are determined by the nature of the eigenvalues of the matrix of second derivatives of the scalar potential, V, evaluated at the origin of field space. We refer to this matrix of second derivatives as the Hessian. Here, the neutral scalar fields are denoted $h_{u,d}^0$.

The goal is to have a vacuum whose origin of field space is destabilized, else EWSB fails to occur properly. There are two cases in which this can happen:

1. the origin is a maximum in field space, or perhaps

2. the origin is a saddle point.

To determine the stability of the critical points we find, the type of critical point can be identified using the second variable partial derivative test. Case 1 occurs when the determinant of this Hessian is positive, but $m_{H_u}^2 + \mu^2 < 0$ at the SUSY scale; then, the origin of field space will be a maximum. This secondary condition is crucial, meaning the positive determinant *alone* is insufficient here to determine the nature of the critical point at the origin. When the determinant is positive,

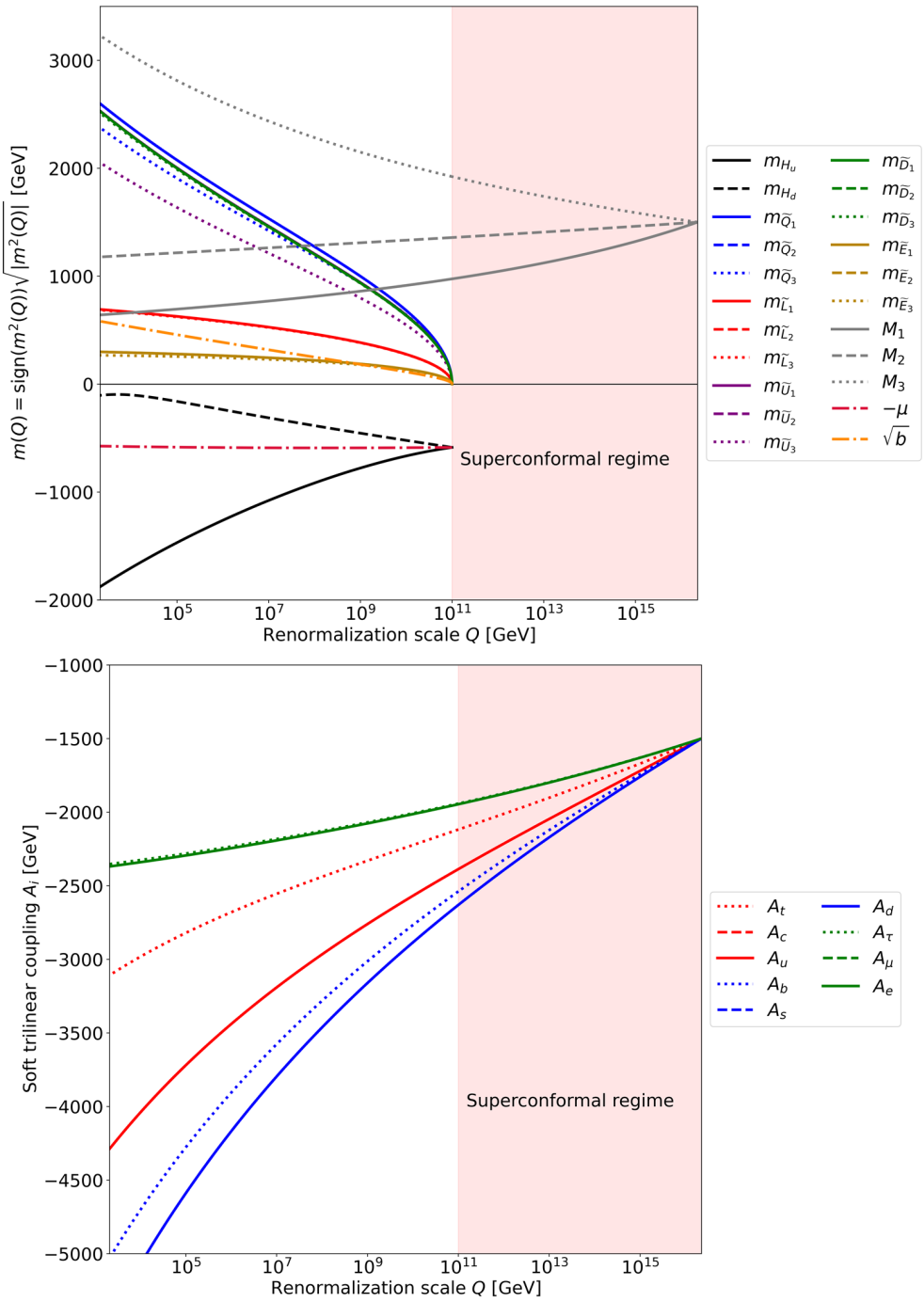

Figure 3.1: Running of soft terms and $-\mu$ in the PRS scalar sequestering scheme for $m_{1/2} = 1.5$ TeV, $A_0 = -m_{1/2}$, and $\mu = 500$ GeV. We also take the intermediate scale $M_{int} = 10^{11}$ GeV. In frame *a*) we show running scalar masses and the μ term, while in frame *b*) we show the running trilinear soft terms.

but $m_{H_u}^2 + \mu^2 > 0$, then the origin of field space will be a *minimum*, hence the scalar fields fail to acquire nonzero VEVs and EWSB fails to occur.

Case 2 occurs when the determinant of the Hessian of the scalar potential at the origin with respect to the neutral Higgs scalars is negative, as this implies its eigenvalues have opposite signs, leading to

$$(B\mu)^2 > (m_{H_u}^2 + \mu^2)(m_{H_d}^2 + \mu^2). \tag{3.11}$$

This is often referred to in the literature as the condition for having a maximum at the origin of field space, but is more accurately described as a saddle point. In either case of a maximum or a saddle point, the origin is destabilized, so proper EWSB may yet be achievable, barring failure in the conditions below. In particular, given that $m_{H_u}^2$ is driven large negative and $B\mu$ is driven small positive, this saddle point condition may not always occur, but maxima sometimes occur instead as in case 1!

Secondly, one must check that the scalar potential is bounded from below (vacuum stability) in the D-flat direction $h_u^0 = h_d^0$ leading to the requirement that

$$m_{H_u}^2 + m_{H_d}^2 + 2\mu^2 > 2|B\mu|. \tag{3.12}$$

Given that $m_{H_u}^2$ is large negative, this condition also may be subject to failure, in which case the scalar potential is unbounded from below (UFB).

If an appropriate EWSB occurs, then minimization of the Higgs potential

allows one to determine the Higgs vevs v_u and v_d, with $\tan\beta = v_u/v_d$ as usual. The minimization conditions can be recast at tree-level as

$$B\mu = \frac{\left(m_{H_u}^2 + m_{H_d}^2 + 2\mu^2\right)\sin(2\beta)}{2} \tag{3.13}$$

and

$$m_Z^2/2 = \frac{m_{H_d}^2 - m_{H_u}^2\tan^2\beta}{\tan^2\beta - 1} - \mu^2. \tag{3.14}$$

Usually, in models like mSUGRA, the first of these is used to trade $B\mu$ for $\tan\beta$ and the second is used to determine the magnitude of μ. In the present case, since the boundary condition for $B\mu$ is ~ 0 at $Q = M_{int}$, it is not available to determine a unique value of $\tan\beta$, since the running of the soft parameters depends on the Yukawa couplings which in turn depend on v_u and v_d, whose values then define $\tan\beta$. Furthermore, from Eq. 3.14 we see that μ is not freely available to be determined by the measured value of $m_Z = 91.2$ GeV. Thus, the equations 3.13 and 3.14 must be used to map out the derived values of m_Z in the μ vs. $\tan\beta$ plane.

This is shown in Fig. 3.2 for the case at hand. Here, we see that for large μ values, then m_Z^2 is computed to be negative. For smaller μ, then typically m_Z is of order the TeV scale. For a given value of $\tan\beta$, one can choose μ near the edge of the gray excluded region where $m_Z \sim 100$ GeV. For Fig. 3.1, we have chosen $\tan\beta = 10$ which then fixes $\mu \sim 500$ GeV. Unfortunately, for all choices of μ and $\tan\beta$ shown in the plane, we find the scalar potential to be UFB in the D-flat direction.

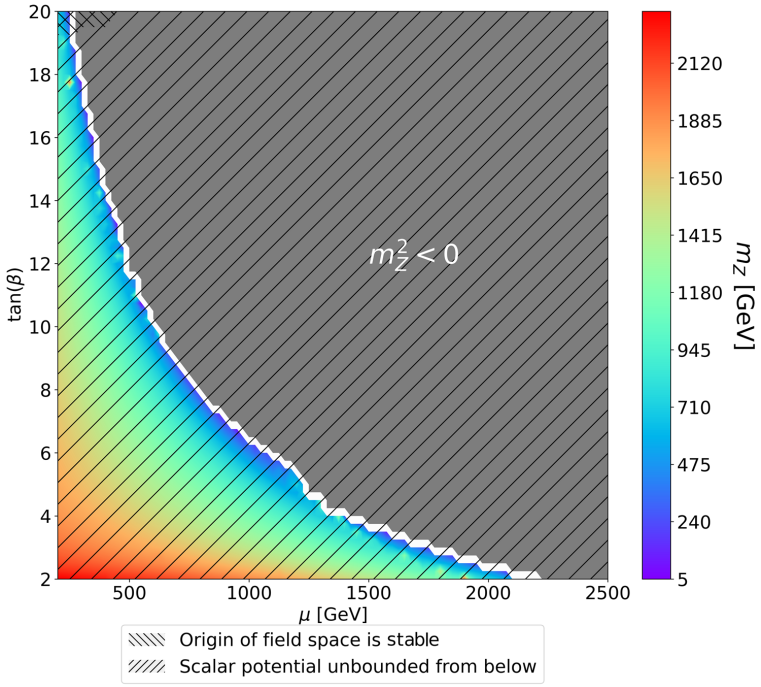

Figure 3.2: Computed value of m_Z in the μ_{GUT} vs. $\tan\beta$ plane for the PRS BM point with $m_{1/2} = -A_0 = 1.5$ TeV, and $M_{\rm int} = 10^{11}$ GeV.

3.2.2 Results for $A_0 > 0$

In Fig. 3.3, we show a PRS point that does develop appropriate EWSB where $M_{int} = 4 \times 10^{11}$ GeV and $m_{1/2} = A_0 = 1$ TeV. For $\tan\beta = 21.25$, we find $\mu \simeq 1.8$ TeV. In this case, with $A_0 = 1$ TeV, we see from frame *b*) that the A_i parameters are all positive for large Q, with A_t and A_b becoming small and then negative around $Q \lesssim 10^{10}$ GeV. This feeds into the b parameter evolution causing b to run at $Q < M_{int}$ to negative values until the large negative A_i terms cause it to turn up and become positive around $Q \sim m_{weak}$, aiding in appropriate EWSB. While this model does develop a viable EW vacuum, the slepton masses evolve only to $m_{E_i} \sim 250$ GeV at $Q \sim m_{weak}$ so that slepton masses are well below both the μ and M_1 terms. Thus, for this point we have a charged slepton as the lightest SUSY particle. The derived sparticle mass spectra for this case are shown in Fig. 3.4.

In the case shown, with the MSSM-only as the low energy EFT, then one would expect a charged stable relic, and dark matter wouldn't be dark. One can circumvent this situation by adding extra particles or interactions to the low energy EFT. An example of the former would be to add a Peccei-Quinn (PQ) sector with an axino $\widetilde{a}$ as the LSP so that $\tilde{e}_R \to e\widetilde{a}$. In this case, one would get a potentially long-lived but unstable slepton and one must avoid collider and other constraints on such objects. The slepton lifetime would depend on the assumed value of the PQ scale f_a. An example of added interactions would be to postulate broken R-parity so that the slepton LSP decays to SM particles. Then one must

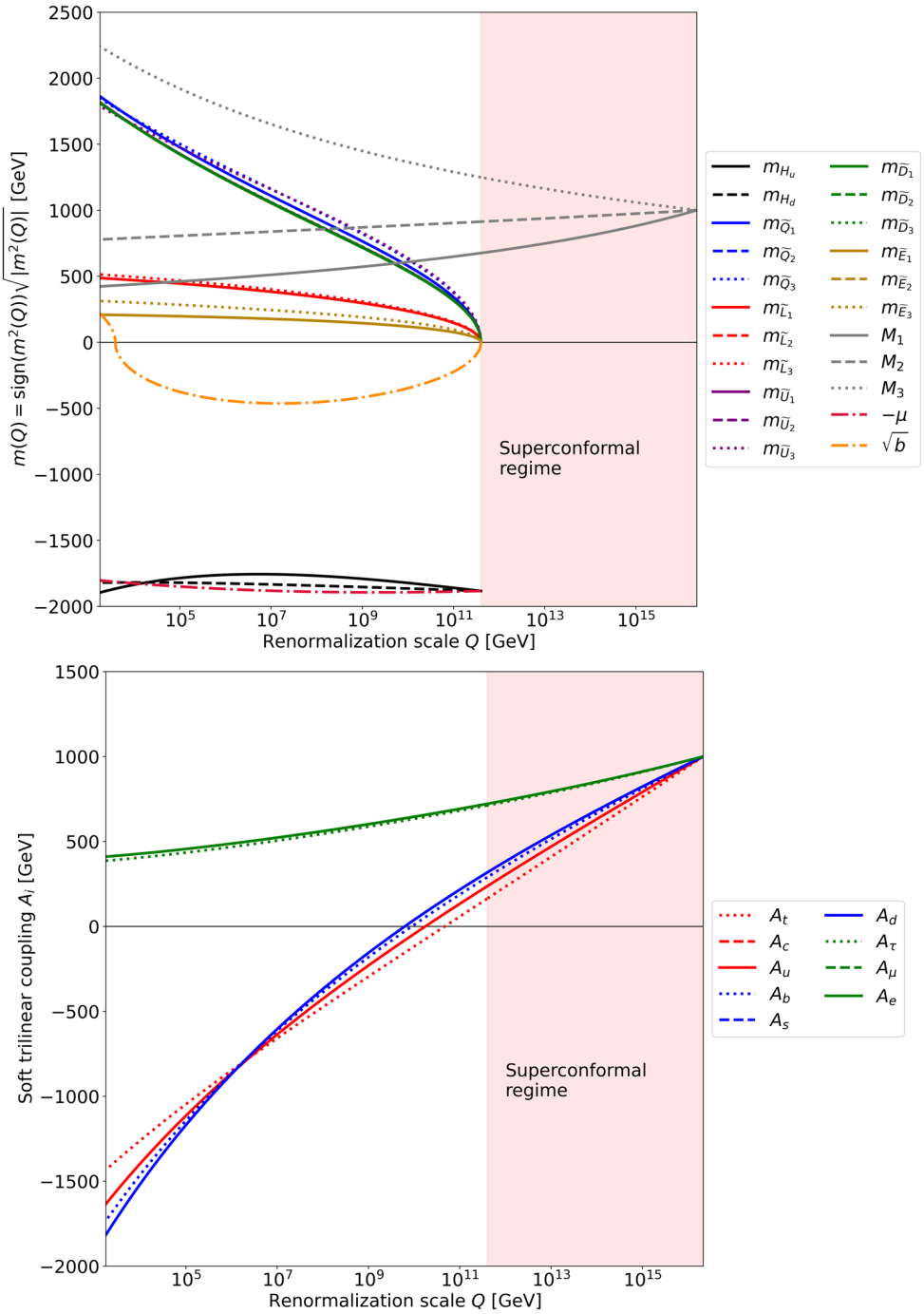

Figure 3.3: Running of soft terms and μ in the PRS scalar sequestering scheme for $m_{1/2} = 1$ TeV, $A_0 = m_{1/2}$, and $\mu = 1.8$ TeV. We take the intermediate scale $M_{int} = 4 \times 10^{11}$ GeV. In frame a) we show running scalar masses and μ term while in frame b) we show the running trilinear soft terms.

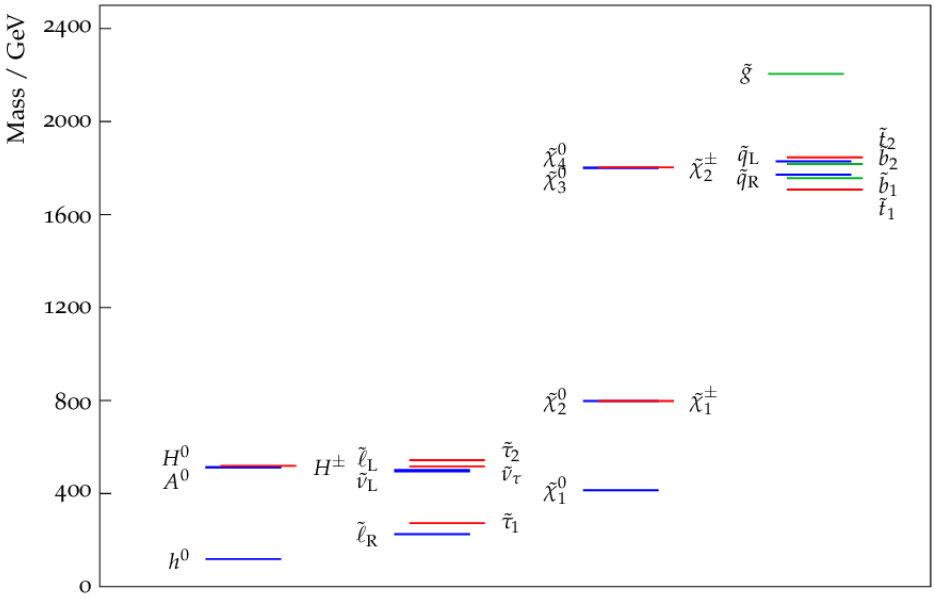

Figure 3.4: The resulting mass spectrum with a characteristic slepton as the LSP for the PRS scheme with $m_{1/2} = 1$ TeV, $A_0 = m_{1/2}$, and $\mu = 1.8$ TeV. The spectrum was produced using SoftSUSY v4.1.17 [1] and slhaplot [2].

explain why some RPV couplings are substantial whilst others are very small, as required by proton stability bounds[159, 160].

3.3 Parameter space scans: PRS scheme

3.3.1 Universal gaugino masses

In order to search for viable weak scale SUSY spectra in the PRS scheme, we implement a scan over the PRS parameter space:

- $m_{1/2}$: $0.2 \rightarrow 5$ TeV
- A_0 : $-5 \rightarrow +5$ TeV
- M_{int} : $10^6 \rightarrow 10^{14}$ GeV.

Our code then scans over values of $(\mu, \tan\beta)$ leading to $m_Z \sim 91.2$ GeV. We then check for CCB minima, points that are UFB, and appropriate EWSB. For points that pass all criteria with appropriate EWSB, we then check for a neutral or a charged LSP.

Our first results are shown in Fig. 3.5 where we show scan points *a*) in the A_0 vs. M_{int} plane and *b*) in the A_0 vs. $m_{1/2}$ plane. From frame *a*), we see that only the yellow points satisfy all EWSB constraints, although all the surviving points have a slepton as the LSP. In particular, the $A_0 < 0$ points almost all have either CCB minima (for large negative A_0) or else an UFB potential. For $A_0 > 0$, then the scalar potential is better behaved but frequently does not have appropriate EWSB. The scan points with appropriate EWSB are much more prominent at large M_{int} and large $m_{1/2}$.

In Fig. 3.6, we show our scan points in the $m_{1/2}$ vs. μ plane. Here, we see some structure where $\mu \sim 2m_{1/2}$ is favored. These qualitative features were also found by Perez, *et al.* in Ref. [146] where most of their parameter space was excluded by EWSB constraints except for large M_{int} where they also found $\mu \sim 2m_{1/2}$ and for their lone sample point, they also obtained a slepton as the LSP.

Given our overall scan results in the PRS scheme, we find the strong scalar sequestering scenario (with unified gaugino masses) rather difficult (but not impossible) to accept: the bulk of p-space points have problematic EWSB and any surviving points have a charged LSP thus requiring new particles and/or new interactions to evade cosmological constraints on charged relics from the Big Bang.

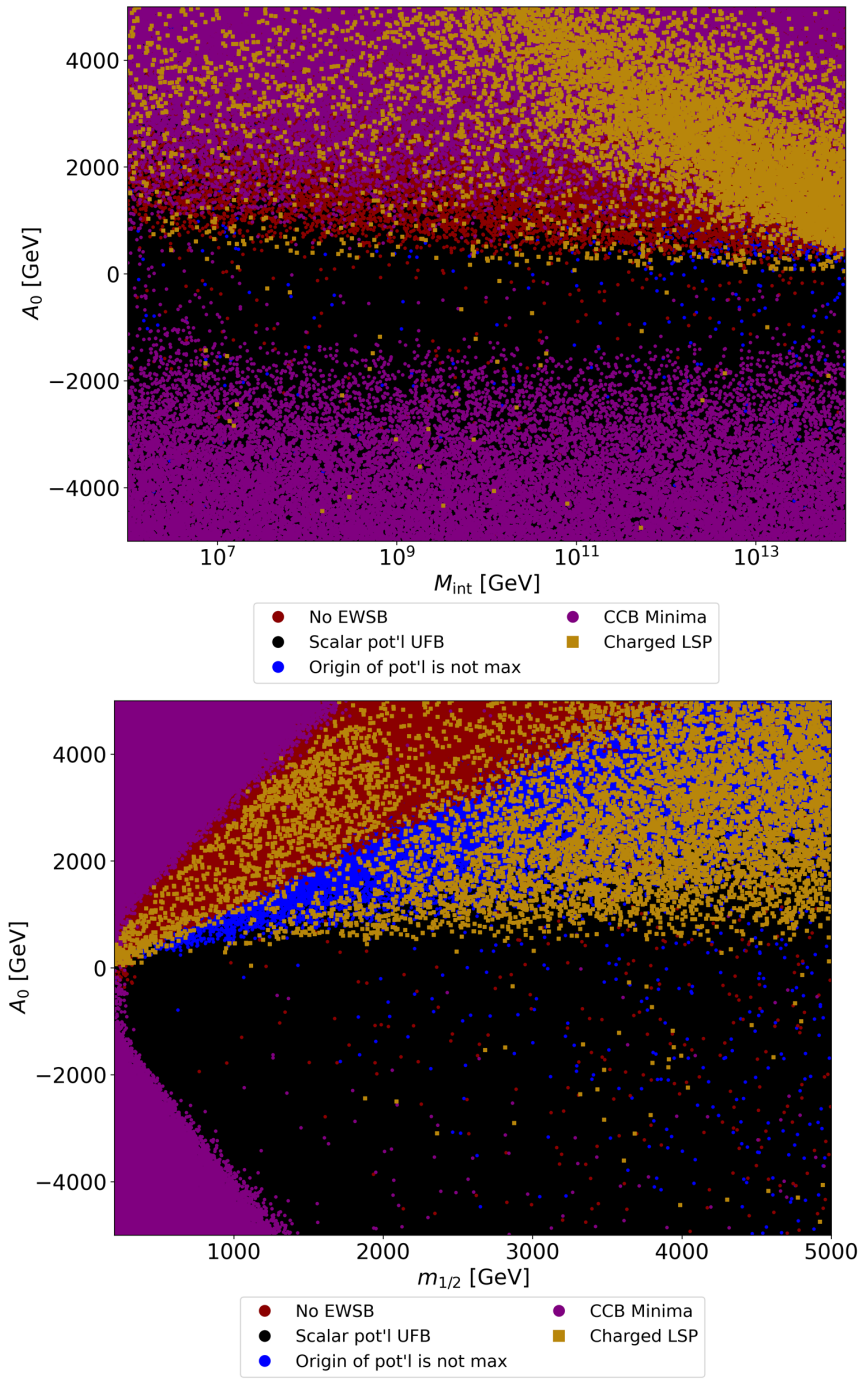

Figure 3.5: Scan over the PRS parameter space with UGMs in the *a*) A_0 vs. M_{int} plane and *b*) the A_0 vs. $m_{1/2}$ plane.

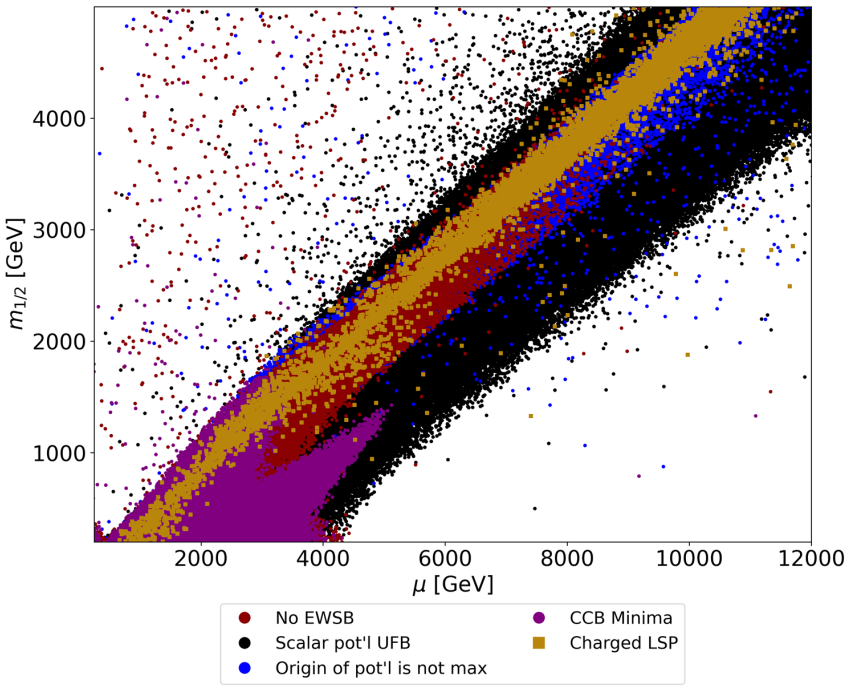

Figure 3.6: Scan over the PRS parameter space with UGMs in the $m_{1/2}$ vs. μ plane.

3.3.2 Non-universal gaugino masses

Varying M_1 and M_2

One possibility to try to circumvent the slepton-LSP problem in the PRS scheme is to appeal to NUGMs, by dialing down either M_1 or M_2 from their unifed values until either the bino or the wino becomes the LSP. The computed sparticle mass spectra are shown in Fig. 3.7 in frame *a*) for varying M_1 and in frame *b*) for varying M_2. From frame *a*), we see that as M_1 diminishes, the lightest neutralino mass $m_{\tilde{\chi}_1^0}$ does indeed decrease (moving from unified gaugino masses on the right to small M_1 on the left as shown by the lavender dashed curve). However, as M_1 decreases, then upward RGE pull on m_{Ei} (right-slepton soft mass of generation i) from the $U(1)_Y$ gaugino also diminishes, and ultimately $m^2_{E_{1,2}}$ go tachyonic (i.e.,

$m^2_{E_{1,2}} < 0$, indicating charge breaking minima within the scalar potential) around $M_1 \sim 0.23 m_{1/2}$. Note in this case that the stau soft mass remains larger due to a large negative X_τ term in the $m^2_{E_3}$ RGE owing to large negative $m^2_{H_d}$. This is shown in Fig. 3.8 which shows the soft mass running for a case with small M_1 compared to $m_{1/2}$. This behavior where the bino fails to become LSP in the PRS scheme with small M_1 appears rather general when we scan over all M_1 values (to be shown shortly).

Likewise, in frame *b*), we take M_2 to be its unified value on the right-side of the plot, and then dial its value down to try to gain a wino as LSP. Around $M_2 \sim 0.58 m_{1/2}$, the $m_{\widetilde{\chi}^\pm_1}$ and $m_{\widetilde{\chi}^0_1}$ mass curves coincide, showing that the lightest neutralino has gone from bino to wino. However, in this case, the right-sleptons remain LSP until $M_2 \sim 0.35 m_{1/2}$ whence the left sleptons, and particularly here the left-sneutrino, becomes LSP. Left-sneutrinos have direct detection cross sections for scattering on Xe nuclei of $\sigma(\tilde{\nu}_{eL} Xe \to \tilde{\nu}_{eL} Xe)$ of $\sim 4.5 \times 10^{-23}$ cm^2[163], about 23 orders of magnitude larger than current LZ limits[164], and so are excluded as dark matter. For somewhat lower values of M_2, then $B\mu$ runs to very small values, leading to a UFB scalar potential. This behavior also seems rather general from our PRS scan with NUGMs.

Scan over PRS scheme with NUGMs

For completeness in our search for viable weak scale SUSY spectra in the PRS scheme, we can adopt the case of non-universal gaugino masses and scan over this expanded parameter space:

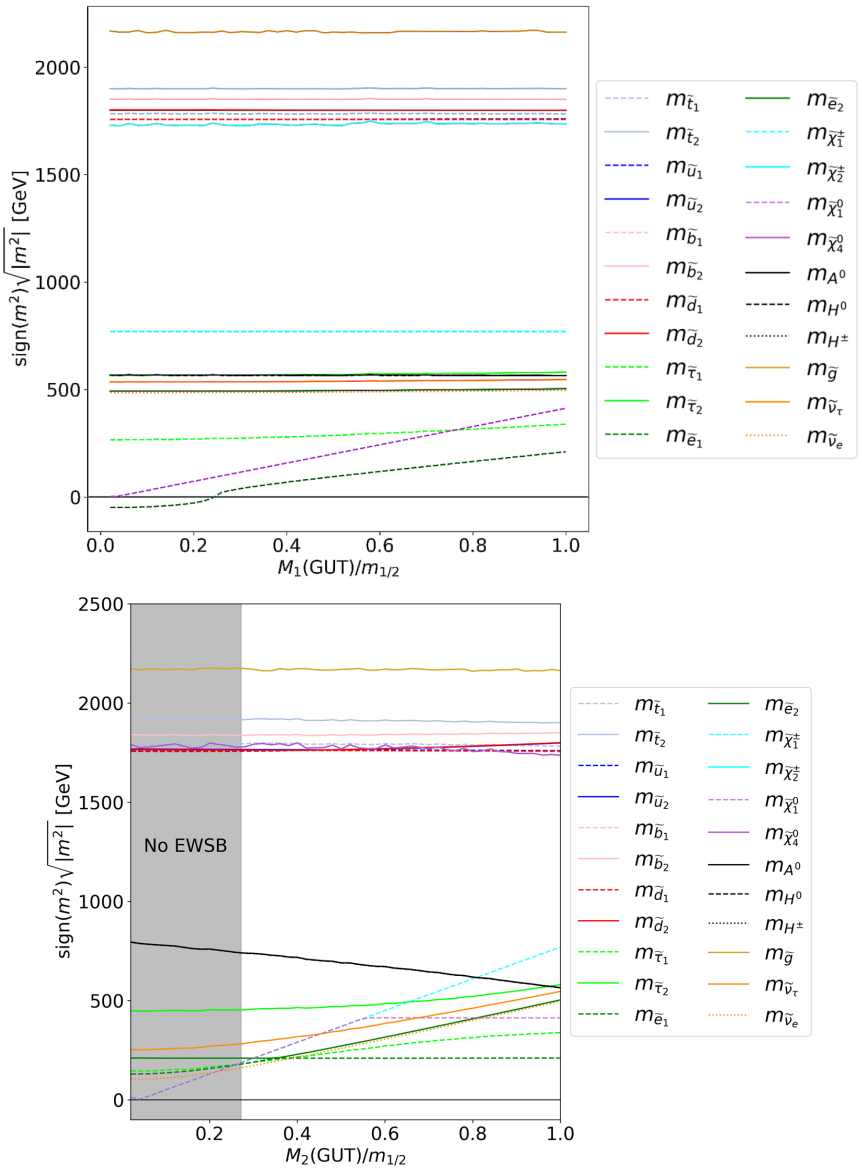

Figure 3.7: The SUSY mass spectrum vs. GUT-scale gaugino mass parameters M_1, M_2 in the PRS model varied below $m_{1/2}$. In both frames, the spectrum at the far right is similar to the spectrum seen in Fig. 3.4. In frame *a*) the mass spectrum as $M_1(\mathrm{GUT})$ is varied below $m_{1/2}$ to zero is plotted. The neutralino never becomes the LSP, as the selectron and smuon remain lighter until CCB minima are realized. In frame *b*) we display the mass spectrum as $M_2(\mathrm{GUT})$ is varied below $m_{1/2}$ to zero. Near $M_2 \sim 0.4 m_{1/2}$, the sneutrino briefly becomes the LSP before the Higgs potential becomes unbounded from below due to a lack of running in the $b = B\mu$ parameter. Thus, a neutralino LSP cannot be achieved here. In both frames, we take $m_{1/2} = M_3(\mathrm{GUT}) = A_0 = 1$ TeV, $M_{\mathrm{int}} = 4 \cdot 10^{11}$ GeV, and $\tan(\beta) = 21.25$.

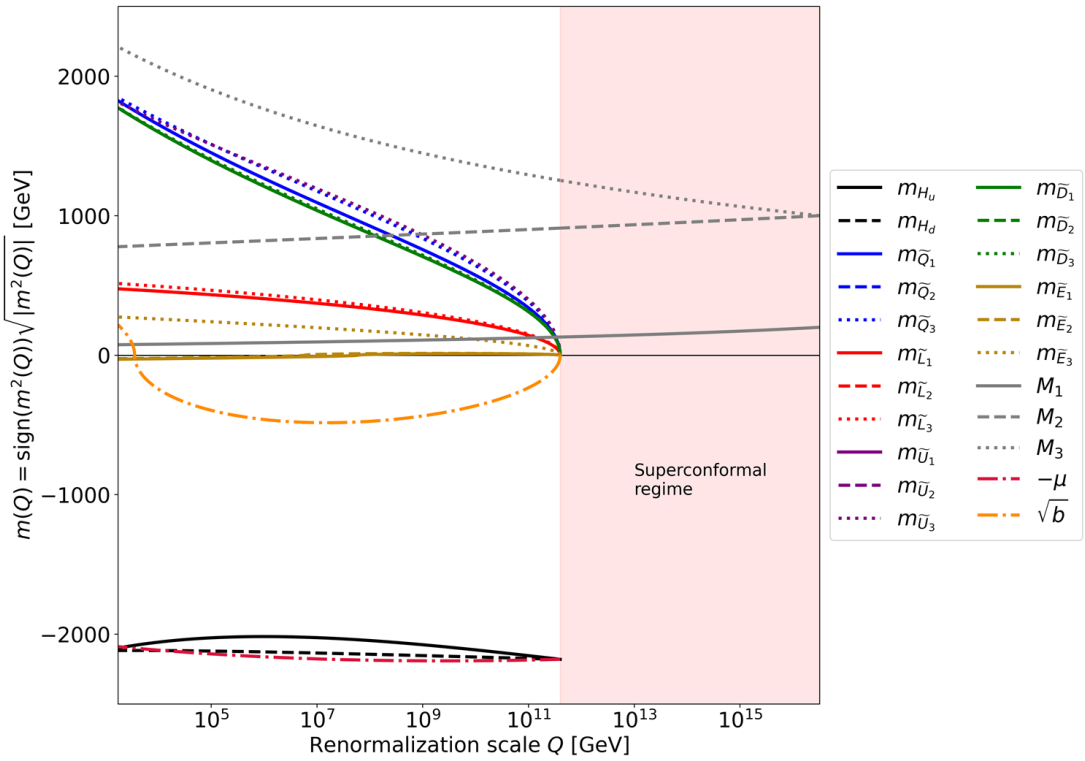

Figure 3.8: Example RGE running of the soft masses from Fig. 3.7*a*) demonstrating the CCB nature of a point with $m^2_{\widetilde{e}_R} < 0$ with $M_1(\mathrm{GUT}) \sim 0.15 m_{1/2}$. Though the left-handed slepton states (red) evolve to moderate values, the right-handed slepton states of the first two generations evolve to be negative at the SUSY scale due to the small value of M_1.

- $M_1(\text{GUT}):\ 0.2 \to 5$ TeV
- $M_2(\text{GUT}):\ 0.2 \to 5$ TeV
- $M_3(\text{GUT}):\ 0.2 \to 5$ TeV
- $A_0:\ -5 \to +5$ TeV
- $M_{int}:\ 10^6 \to 10^{14}$ GeV.

Similar to above, our code then finds pairs of $(\mu, \tan\beta)$ leading to $m_Z \sim 91.2$ GeV. We then check for CCB minima, points that are UFB, and appropriate EWSB. For points that pass all criteria with appropriate EWSB, we then check for a neutral or a charged LSP along with LHC constraints on the gluino mass and lightest stop mass. As discussed above, one may try to dial down the $M_1(\text{GUT})$ parameter to obtain a neutralino LSP, this leads to both CCB and EWSB issues in this model. The issue of a charged LSP persists as in the UGM case, though it is possible to accommodate a sneutrino LSP in some cases, when $M_2(\text{GUT}) < M_1(\text{GUT})$. However, this scenario is severely ruled out due to direct dark matter detection constraints.

Our non-universal gaugino mass scan results are demonstrated in Fig. 3.9 where we show scan points *a*) in the A_0 vs. M_{int} plane and *b*) in the $M_1(\text{GUT})/M_2(\text{GUT})$ vs. $M_3(\text{GUT})$ plane. Even with NUGMs, we do not find any points where EWSB is appropriately broken but without a charged slepton or left-sneutrino LSP.

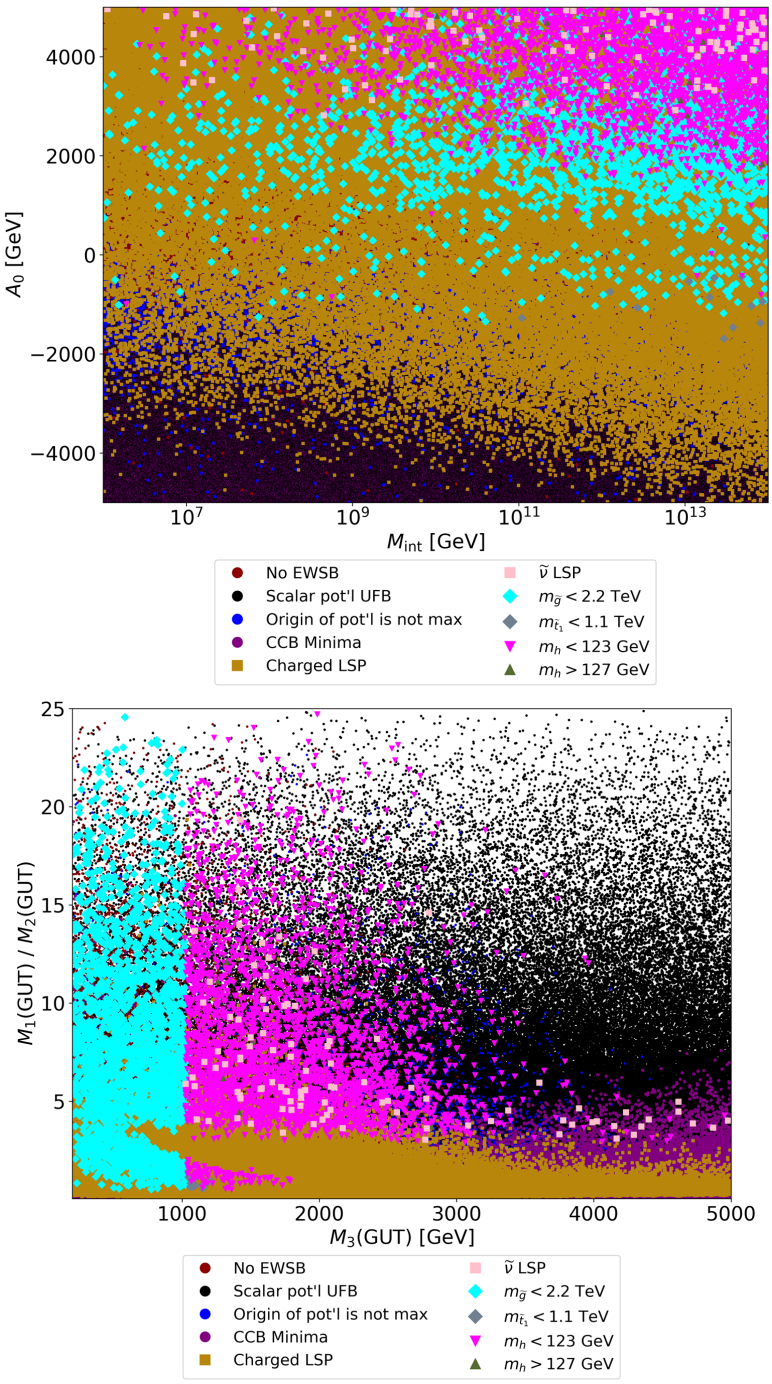

Figure 3.9: Scan over the PRS parameter space with NUGMs in the *a*) A_0 vs. M_{int} plane and *b*) the M_1(GUT)/M_2(GUT) vs. M_3(GUT) plane.

3.4 Scalar sequestered SUSY: SPM approach

In the SPM approach[148], it is noticed that there exist bounds on the scaling dimension Γ such that Γ is positive but not too large, with $\Gamma \sim 0.3$ maximally[165, 166, 167]. In this case, the superconformal running may be much less, and comparable to the MSSM running. Let us denote the dimension 1 soft breaking terms as m_1 and dimension 2 soft terms as m_2. Then, after several field rescalings, the dimension-1 terms (the M_i, a_{ijk} and μ) run according to

$$\frac{dm_1}{dt} = \beta_{m_1}^{MSSM} \tag{3.15}$$

while dimension-2 terms (matter scalars $m_{\phi_{ij}}^2$, $\hat{m}_{H_{U,d}}$ and b) run as

$$\frac{dm_2}{dt} = \Gamma m_2^2 + \beta_{m_2}^{MSSM} \tag{3.16}$$

where the β^{MSSM} are the usual MSSM beta functions and $t = \log(Q/Q_0)$ where Q is the energy scale and Q_0 is a reference scale. For the superconformal regime with $M_{int} < Q < m_*$, then $\Gamma \neq 0$ but for $Q < M_{int}$, then the superconformal symmetry is broken and integrated out, and $\Gamma \to 0$.

An intriguing effect in this case is that the m_2^2 terms can run until the $\Gamma m_2^2 \simeq \beta_{m_2}^{MSSM}$ which defines a *quasifixed point* for the m_2^2 running at $m_2^2 \simeq -\beta_{m_2}^{MSSM}/\Gamma$. Approximate expressions for the fixed point values are given by SPM[148], but will not be repeated here. Thus, the m_2^2 terms tend to approach their quasifixed point values as $Q \to M_{int}$ instead of zero, as in the PRS scheme. This behavior

helps to ameliorate the problems of the PRS scheme with respect to EWSB. The approach to the quasifixed point values are shown in Figs. 3.10 and 3.11 for five m_2^2 cases.

In the SPM scheme, the m_2^2 values approach (but do not exactly meet) their quasifixed point values at $Q = M_{int}$, so that the boundary conditions at $Q = M_{int}$ are no longer fixed. Thus, to generate a workable model, we must expand the parameter space from the PRS scheme. For SPM, therefore, one must reintroduce the various m_2^2 boundary conditions at $Q = m_*$, and we will take

$$m_0,\ m_{1/2},\ A_0,\ \mu,\ b = B\mu. \tag{3.17}$$

After checking for appropriate EWSB, and then employing the EWSB minimization conditions, one can again solve for the derived value of m_Z. This is shown in Fig. 3.12 where we show color-coded regions of m_Z in the A_0 vs. $\mu(GUT)$ plane for $m_0 = 10$ TeV, $m_{1/2} = 4.5$ TeV and $\tan\beta = 15$. From the plot, one sees that there is no unique solution for $m_Z \simeq 91.2$ GeV but rather two disconnected regions depending on the sign of μ, with a different μ value being obtained for each choice of A_0.

3.4.1 Case with UGMs

In the SPM paper, Martin has plotted out sample spectra for two cases, one with unified gaugino masses (UGM) and one with non-unified gaugino masses (NUGM). For the case of UGM, he shows sparticle mass spectra vs. $m_{1/2}$ for $m_0 = m_{1/2}$

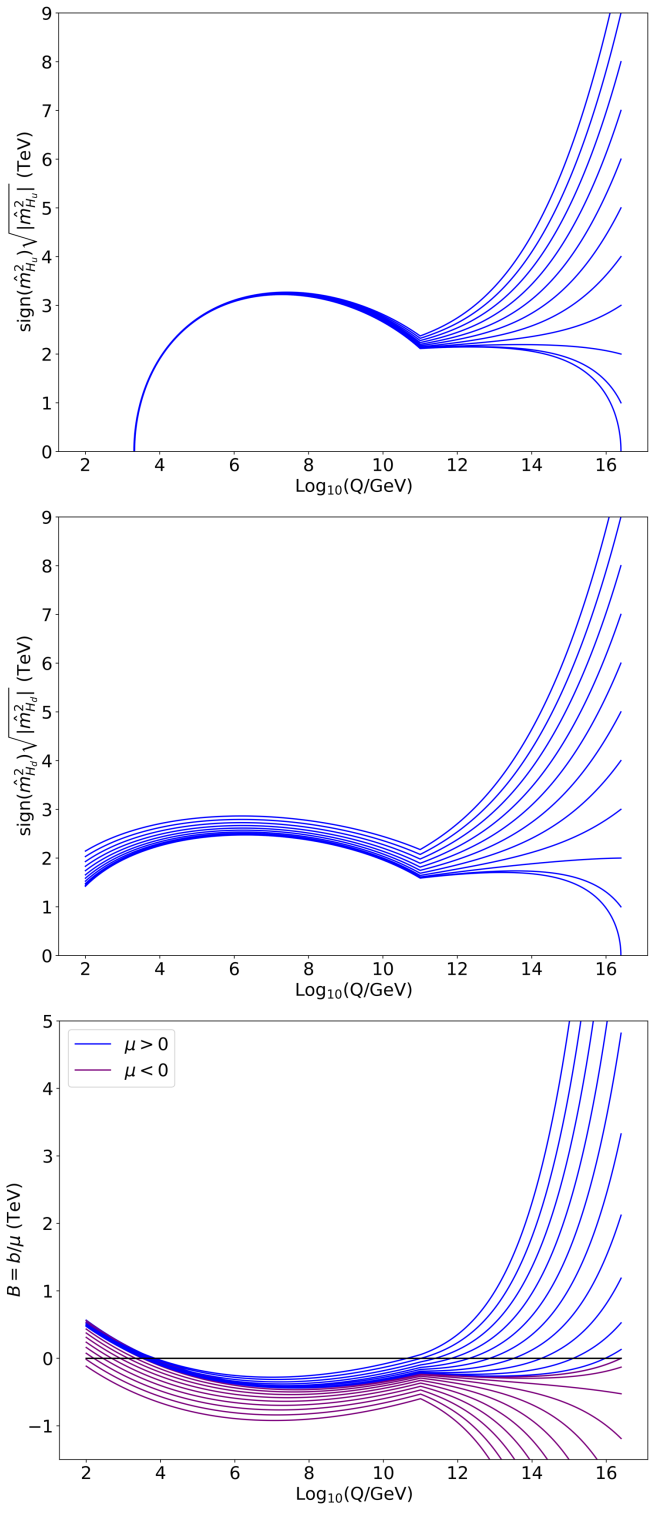

Figure 3.10: Running of various m_2^2 parameters from $Q = m_{GUT}$ to $Q = m_{weak}$ under the SPM scheme with $\Gamma = 0.3$

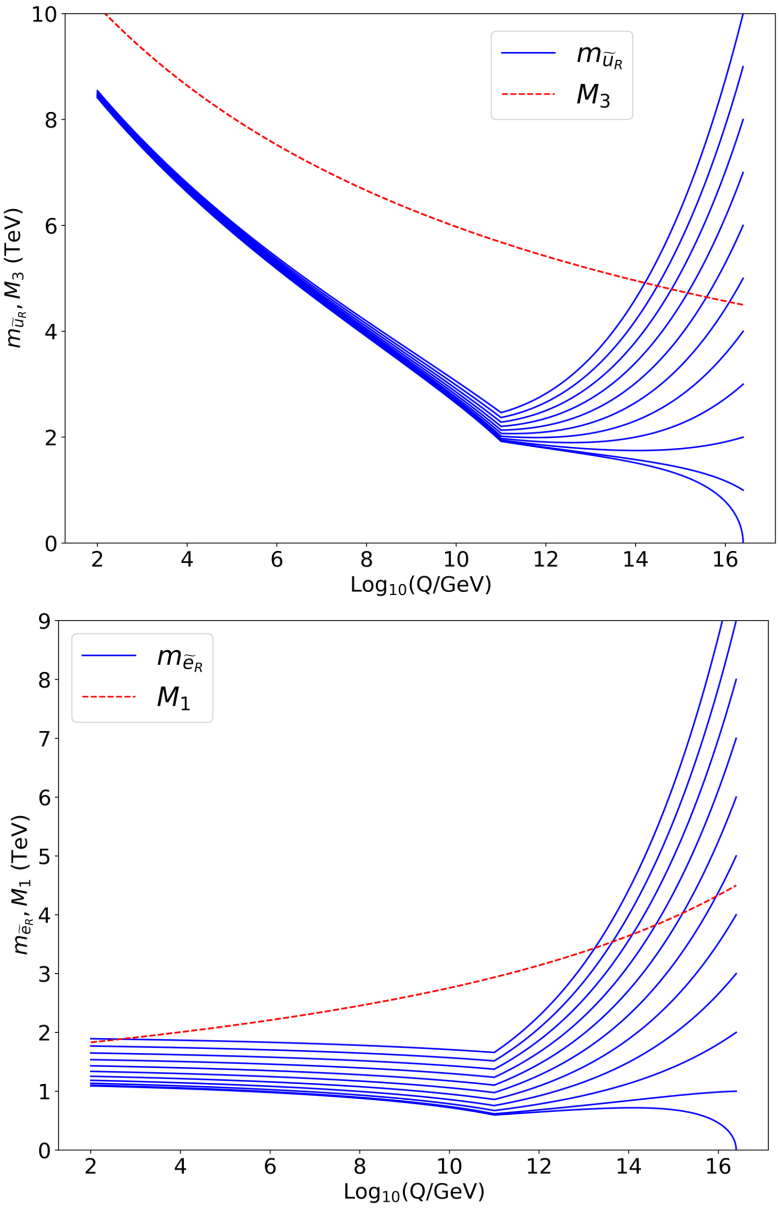

Figure 3.11: Running of various mass dimension 2 and dimension 1 parameters from $Q = m_{GUT}$ to $Q = m_{weak}$ under the SPM scheme with $\Gamma = 0.3$.

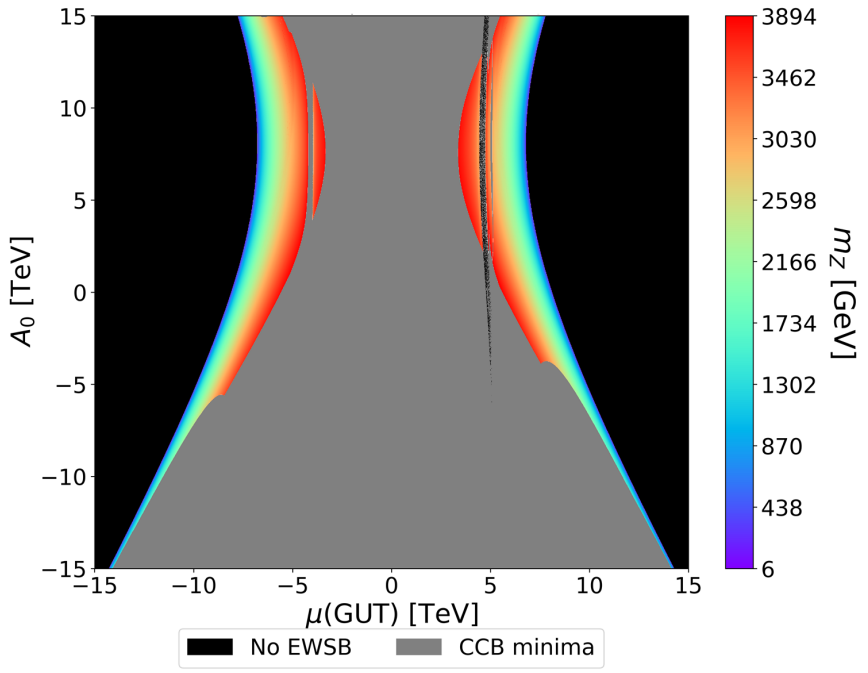

Figure 3.12: Color-coded regions of the derived value of m_Z in the μ vs. A_0 plane for $\tan\beta = 15$ with $m_0 = 10$ TeV and $m_{1/2} = 4.5$ TeV.

and also for $m_0 = 2.5m_{1/2}$, with $\tan\beta = 15$ and with $b = m_{1/2}^2$, where A_0 and μ are solved for. For the $m_0 = m_{1/2}$ case, he always finds a right selectron as the LSP (as do we), so that either additional R-parity violating interactions or lighter DM particles (such as axino) are needed to avoid charged stable relics from the early universe. In the case of $m_0 \gtrsim 2.5m_{1/2}$, then the bino can become LSP. In Fig. 3.13, we reproduce these results for the case of $m_0 = 2.5m_{1/2}$. The region between the pink shaded boundaries has 123 GeV $< m_h <$ 127 GeV (as computed here using FeynHiggs[168]). Typically, in such cases with heavy sparticles in the multi-TeV range and a bino as the LSP, the thermally-produced neutralino relic density $\Omega_\chi h^2 \gg 0.12$. However, from Fig. 3.13 we do see that since slepton masses are very nearly equal to $m(bino)$, then coannihilation is available to reproduce the measured DM relic density. We also see that the higgsino mass $\simeq \mu$ is very large, varying from $\sim 5-10$ TeV over the range of $m_{1/2}$ shown. This would make the model very unnatural under the conservative Δ_{EW} measure. However, the point here is that a mechanism is now present to drive the combination $m_{H_u}^2 + \mu^2$ to small values, thus potentially ameliorating the LHP.

Since we have now arrived at acceptable spectra for the case of scalar sequestering in the SPM scheme, we next want to check whether it really solves the LHP. In Fig. 3.14, we compute in frame *a*) the top five signed contributions to the naturalness measure Δ_{EW}. The largest contributions come from μ and $m_{H_u}(weak)$, which are seen here as the blue and red curves. These lie in the $\sim 10^4$ range, making the model highly finetuned under Δ_{EW}. In frame *b*), we define a revised finetuning measure Δ'_{EW}, which is the same as Δ_{EW} except that

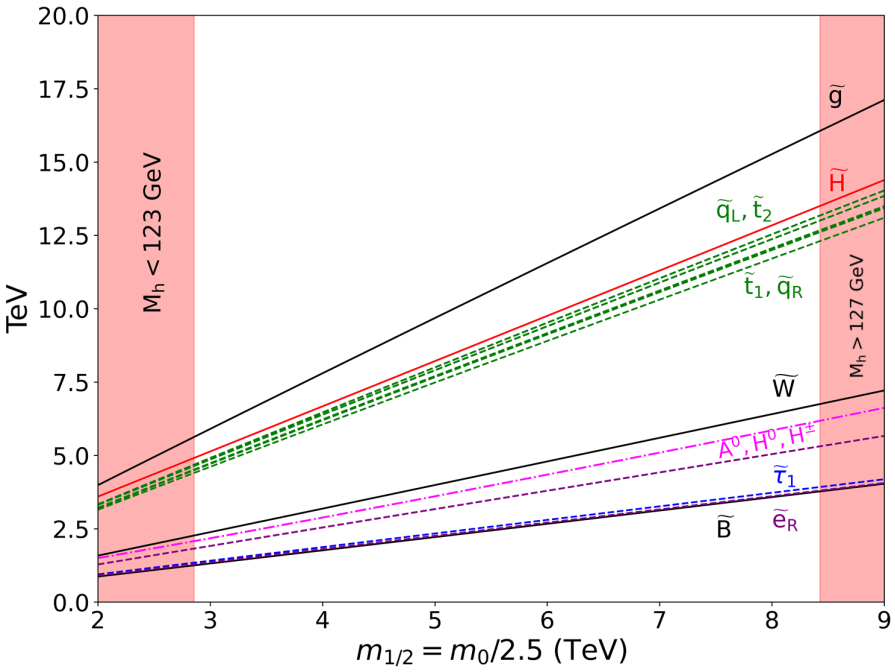

Figure 3.13: Sparticle masses vs. $m_{1/2}$ in the SPM UGM case with $m_{1/2} = m_0/2.5$.

now $m_{H_u}^2 + \mu^2$ and $m_{H_d}^2 + \mu^2$ are combined into single entities since they are now *dependent* (due to the CFT running above $Q = M_{int}$). In frame b), we see the top five contributions to Δ'_{EW}. In this case, the $\Sigma_u^u(\tilde{t}_{1,2})$ terms and $\hat{m}_{H_u}^2$ terms are largest, typically of order $\sim 10^3$. Thus, we find that although the SPM scheme in the UGM case has reduced finetuning, it is still found to be highly finetuned, mainly due to the large lightly-mixed top-squark masses contributing to the radiative corrections $\Sigma_u^u(\tilde{t}_{1,2})$.

3.4.2 Case with NUGM

Along with the UGM case, SPM also considers the case with NUGMs. This case is motivated by obtaining a large stop mixing element A_t which can enhance $m_h \to 125$ GeV via maximal stop mixing rather than too large of stop masses.

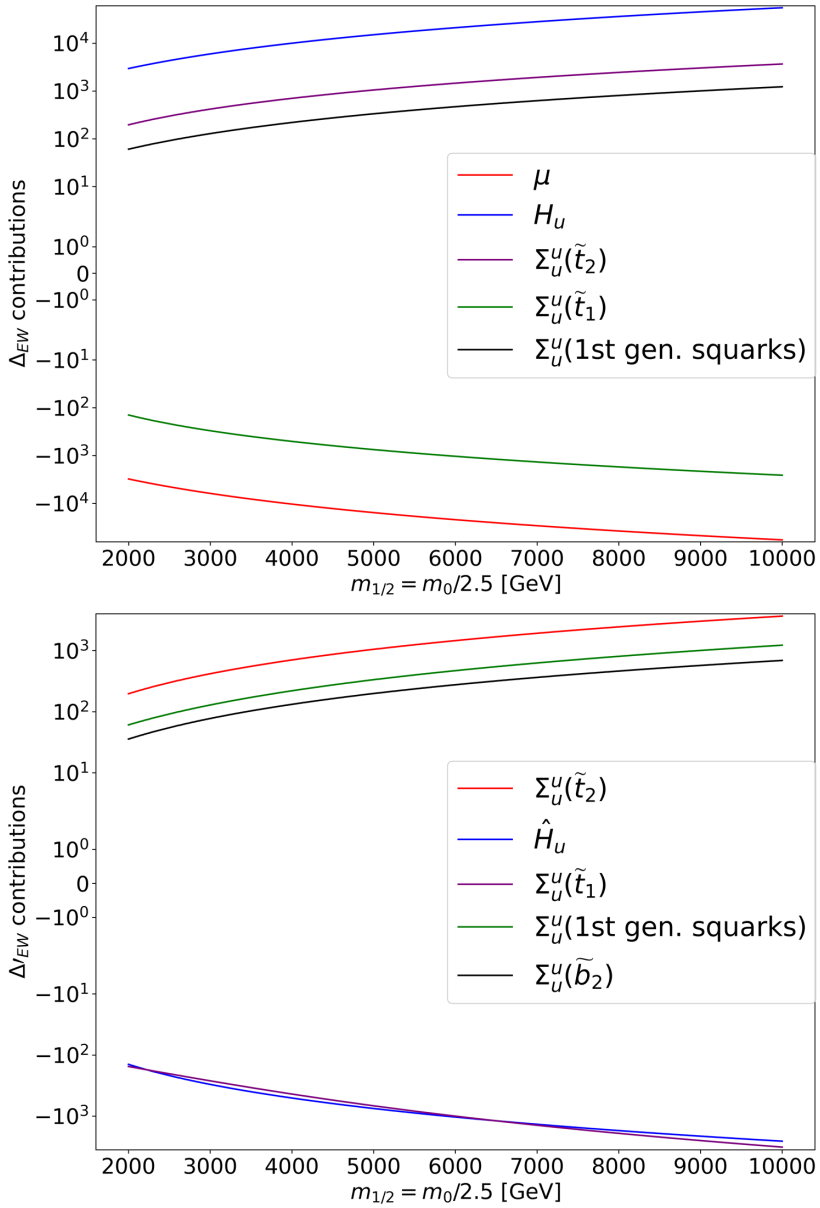

Figure 3.14: Top five signed contributions to *a*) Δ_{EW} and *b*) Δ'_{EW} for the UGM spectra with $m_0 = 2.5m_{1/2}$.

This can be achieved with $M_3 \ll M_2$ while adjusting M_1 so that the bino remains as the LSP. In Fig. 3.15, we show the weak scale sparticle mass spectra in the SPM scheme with NUGMs. We plot vs. m_0 where $M_3 = 1.2$ TeV, $M_2 = 4$ TeV, and $M_1 = 2$ TeV (all M_i defined at $Q = m_{GUT}$). Our calculations match well with the results of SPM. From the plot, we see that for low m_0 we still get a slepton as the LSP (this time, it is the τ-slepton $\tilde{\tau}_1$). For higher values of m_0, then sfermion masses increase as expected and for $m_0 \gtrsim 6$ TeV one obtains $m_{\tilde{\ell}} \gtrsim m(bino)$ and so we get a bino as the LSP. Also, with $M_3(m_{GUT})$ only 1.2 TeV, then squarks and sleptons are much lighter than in Fig. 3.13. With large stop mixing, then $m_h \sim 125$ GeV with not-too-heavy of stops and a chance for naturalness. The higgsinos are heavy and lie near $m_{\tilde{H}} \sim 2.3$ TeV.

In Fig. 3.16 we compute the top five signed contributions to the finetuning measures *a*) Δ_{EW} and *b*) Δ'_{EW} for the same parameters as in Fig. 3.15. From frame *a*), we see that the m_{H_u} and μ contributions to Δ_{EW} are opposite sign but with absolute values $\sim 10^3$ so that the spectra are finetuned under Δ_{EW}. However, the SS of $m^2_{H_{u,d}} + \mu^2$ means these quantities are no longer independent and instead Δ'_{EW} should be used. From frame *b*), we see the top five contributions to Δ'_{EW} are typically of order ~ 10: thus, this case of the SPM scheme with NUGMs seems natural even with higgsino masses of ~ 2.3 TeV. (The breaks in the curves of frame *b*) occur due to different contributions to Eq. 2.9 vying to be within the top five.)

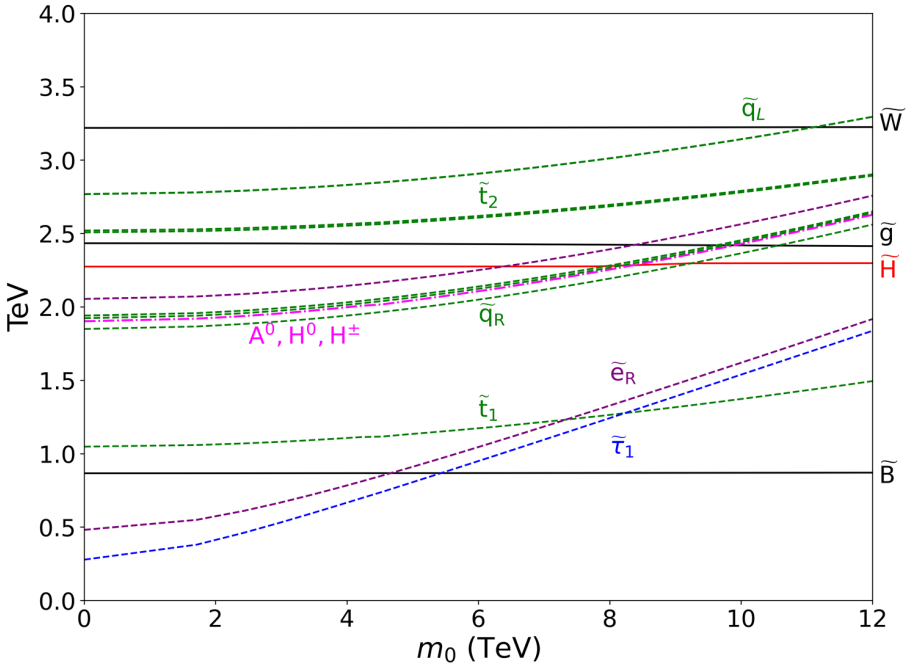

Figure 3.15: Sparticle and Higgs masses vs. m_0 in the SPM scheme with NUGM where $M_1 = 2$ TeV, $M_2 = 4$ TeV, and $M_3 = 1.2$ TeV, with $b = (2 \text{ TeV})^2$, $\tan\beta = 15$ and $\mu > 0$.

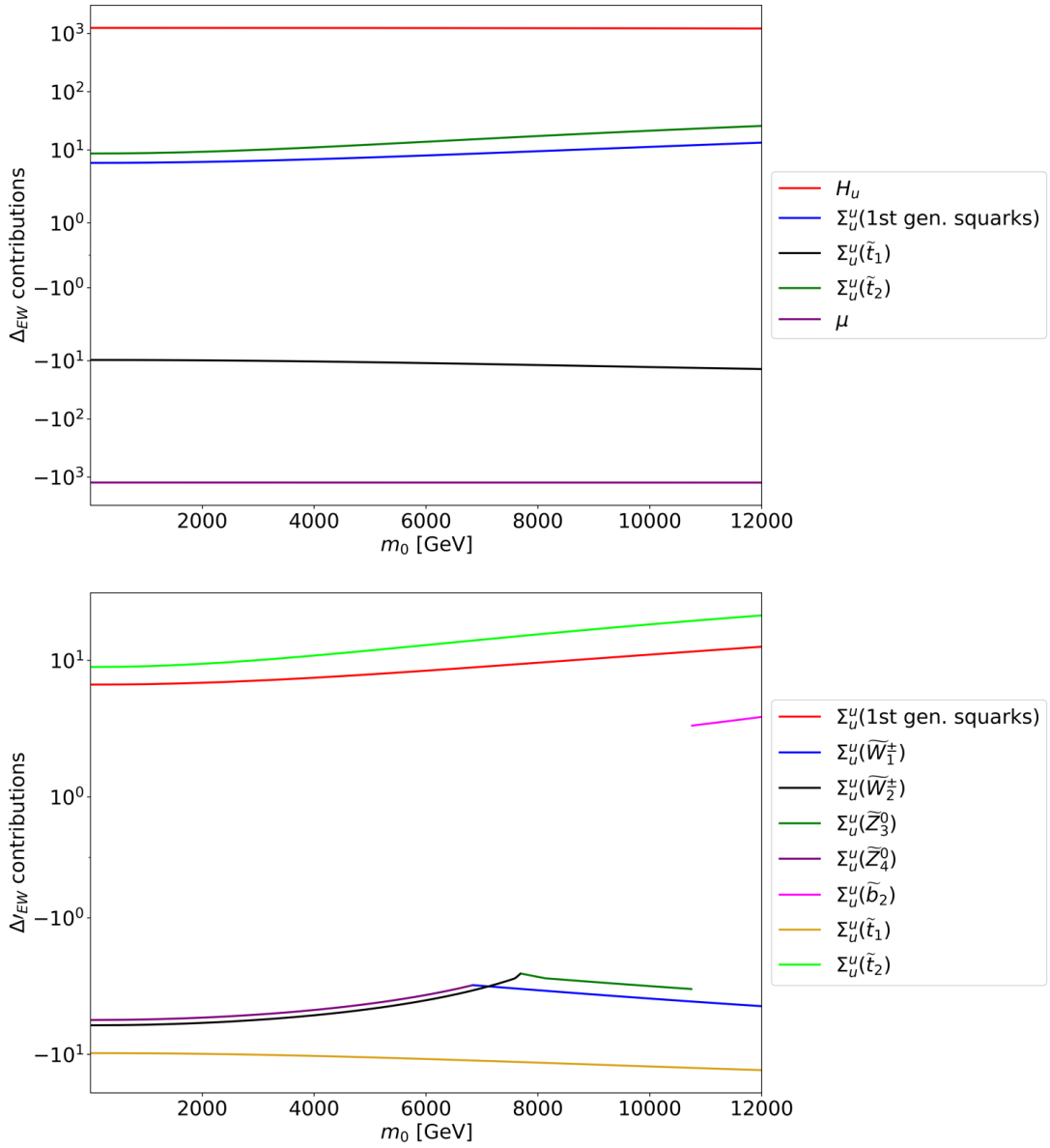

Figure 3.16: Top five signed contributions to *a)* Δ_{EW} and *b)* Δ'_{EW} vs. m_0 for the SPM scheme with NUGM where $M_1 = 2$ TeV, $M_2 = 4$ TeV, and $M_3 = 1.2$ TeV, with $b = (2 \text{ TeV})^2$ and $\tan\beta = 15$.

Chapter 4

The string landscape: a statistical approach

4.1 Distributions on the string landscape

Supersymmetry is a key ingredient in superstring theory constructs. An advantage of compactification of 10-d string theory on a Calabi-Yau manifold[38] is that it preserves some remnant spacetime supersymmetry in the 4-d theory. Likewise, compactification of 11-d M-theory on a manifold of G_2 holonomy preserves some remnant spacetime supersymmetry[169]. Acharya[170] argues for the proposal that the landscape of all geometric, stable, string/M theory compactifications to Minkowski spacetime at leading order are supersymmetric. Non-SUSY preserving compactifications would lead to bubble of nothing instabilities and presumably lie within the swampland[171].

Making contact with 4-d physics at the TeV scale (which is currently being explored at the CERN LHC), it is apparent that $N = 1$ spacetime SUSY must be broken.[1] But the question is: broken at which scale? The gauge hierarchy problem (GHP) suggests SUSY which is broken at or around the weak scale, thus providing a "natural" solution to the GHP wherein all quadratically divergent contributions to the Higgs boson mass cancel. Weak scale supersymmetry is also supported experimentally via the measured value of gauge couplings, whose values unify at a scale $m_{GUT} \simeq 2 \times 10^{16}$ GeV[26] under renormalization group evolution[172] within the Minimal Supersymmetric Standard Model[173] (MSSM)

[1]For a recent review of the status of SUSY after LHC Run 2, see [111].

while they do not within the context of the Standard Model (SM). In addition, the measured value of the Higgs boson mass falls directly within the narrow range of values allowed by the MSSM[29]. Unfortunately, superpartners have so far failed to appear at LHC leading to an apparent naturalness crisis[107].

An apparent alternative to naturalness has emerged from the string landscape[41]. Under flux compactifications[174], an enormous number of different compactification possibilities are available[39, 40], each leading to different 4-d laws of physics. Each of these possibilities can be accessed within the context of an eternally-inflating multiverse[175]. This scenario provides the proper setting to realize Weinberg's anthropic solution to the cosmological constant problem[18]: we find ourselves in a (pocket) universe with a tiny cosmological constant $\Lambda_{cc} \sim 10^{-123} m_P^2$ because if Λ_{cc} was much larger, the universe would expand so fast that structure (galaxies, stars, etc.) would not be able to form and life as we know it would not arise. Such a solution to the CC problem is known as an *environmental* (or *anthropic*) solution: environmental selection of a tiny cosmological constant within the plenitude of pocket universes within the greater multiverse can select a highly fine-tuned value for one (or more) of our fundamental physical constants. Such a solution may stand in apparent opposition to a natural solution to the CC problem.

Can the GHP also be explained via environmental/anthropic reasoning rather than naturalness? Maybe. In the seminal papers by Agrawal, Barr, Donoghue and Seckel (ABDS)[80, 176], the scenario of the Standard Model emerging from the multiverse via an anthropic solution to the hierarchy problem is investigated.

The authors consider the SM as the low energy effective field theory (LE-EFT), but with a variable magnitude for the weak scale. If the weak scale were a factor of $\sim 2-5$ times larger than its actual value, then up-down quark mass differences would increase, leading to nuclear instability: one enters a domain of the universe where only protons exist, with no complex nuclei. For the weak scale reduced by a factor of two from its measured value, then protons become unstable and beta decay to neutrons: there would be no Hydrogen, just neutron rich matter. In terms of the Higgs vacuum expectation value v, one finds $0.5 \lesssim v/v_0 \lesssim (2-5)$ (where v_0 is the Higgs vev in our universe). This narrow range of values for the weak scale has been dubbed the *ABDS window* in that values of v outside this range would not lead to a universe with life as we know it. The anthropic requirement for v to lie within the ABDS window could allow for a tuning of the weak scale within the wider multiverse. It also selects out a narrow range of allowed values: namely $m_{weak} \simeq m_{W,Z,h} \sim 100$ GeV and can *explain* the magnitude of the weak scale rather than just accommodate it. The requirement for the magnitude to lie within the ABDS window is sometimes also referred to as the *atomic principle* in that it is required in order for any pocket universe to contain complex atoms which seem necessary for a rich chemistry and for life as we know it.

Building upon the SM and ABDS, Arkani-Hamed and Dimopoulos[130, 129, 131] proposed a model known as Split Supersymmetry wherein the natural SUSY solution to the GHP is eschewed in exchange for an environmental solution. This then allows the possibility of a highly fine-tuned supersymmetric model. The authors then investigate the consequences of scalar masses $\tilde{m}$ far beyond the

naturalness limit, taking $\tilde{m}$ as high as $\sim 10^9$ GeV. SUSY fermions, higgsinos and gauginos, may be protected by a chiral or R-symmetry and may still live around the EW scale. This set-up maintains the successful gauge coupling unification and WIMP dark matter of SUSY models, but enlists the vast number of landscape solutions to effectively tune the weak scale to lie within the ABDS window as required by the atomic principle. The advantage of very heavy scalars (especially first/second generation matter scalars), as noted much earlier by Dine *et al.*[128] and others[177, 178] is that they provide a decoupling solution to the SUSY flavor and CP problems and may also suppress proton decay. In addition, under gravity mediation wherein scalars get mass of order the gravitino mass, this provides a solution to the cosmological gravitino and moduli problems.[2]

Thus, Split SUSY and a variety of successor models[139, 137] have been considered as legitimate expressions of what sort of SUSY models are expected to emerge from the string landscape. In the literature, it is sometimes claimed that a rather heavy Higgs mass and no sign of SUSY scalars at LHC might be construed as evidence for finetuning within the multiverse as opposed to a natural solution to the GHP, wherein there is no finetuning. Split SUSY, and the other high-scale SUSY models considered here, are motivated by the expectation that the soft SUSY breaking terms are statistically favored to occur at large as opposed to small values on the landscape via a power law relation $P(m_{soft}) \sim m_{soft}^{2n_F+n_D-1}$ which obtains if the complex-valued SUSY breaking F-term fields and real-valued SUSY breaking D-term fields are distributed uniformly on the landscape[101, 180, 22].

[2]For a recent overview of the cosmological moduli problem, see *e.g.* [179].

(Here, n_F is the number of hidden sector F-term fields and n_D is the number of hidden sector D-term fields contributing to the overall SUSY breaking scale $m^4_{\rm hidden} = \sum_i F_i^\dagger F_i + \sum_\alpha D_\alpha D_\alpha$.) This landscape draw to large soft terms must be balanced by the anthropic/environmental condition that the derived value of the weak scale in each pocket universe lies within the ABDS window of allowed values[95, 102].

In this chapter we survey a variety of finetuned models (both the SM and SUSY), including those in Section 2.4, and compare these to natural SUSY models, all within the context of the string landscape. What we find is somewhat at odds with the literature: natural SUSY models are more likely to emerge from the string landscape than finetuned models. We advance a particular probability measure P_μ which quantifies these probabilities. By taking ratios, we are able to evaluate the relative probabilities for different models to emerge from the landscape.

In radiatively-driven natural SUSY (RNS)[76, 96], large high scale soft terms can be radiatively driven to small weak scale values. Then all weak scale contributions to the weak scale are of order the weak scale. This corresponds to $\Delta_{EW} \lesssim 30$. The RNS models can be generated from NUHM2 or NUHM3 models[76, 96], from generalized mirage mediation[181] and from natural anomaly-mediation[182]. As an example, we take a simple NUHM2 model with first/second/third generation GUT scale scalar masses $m_0(1,2) = m_0(3) = 4.5$ TeV, $m_{1/2} = 1$ TeV, $A_0 = -7.2$ TeV, $\tan\beta = 10$ with $\mu = 200$ GeV and $m_A = 2$ TeV. The model has $m_{\tilde{g}} \sim 2.4$ TeV (LHC safe) with $\Delta_{EW} = 12.8$ and $m_h = 124.3$ GeV. The higgsino-like LSP is $m_\chi = 195.3$ GeV with $\Omega_\chi h^2 = 0.011$ (so room for additional axion dark matter).

While RNS models are typically slightly more natural for lower m_0 and $m_{1/2}$ values, we expect from the string landscape, under spontaneous SUSY breaking via a single F-term field distributed uniformly as a complex number throughout the landscape, a *linear* statistical draw to large soft terms[95]. For more SUSY breaking fields, the statistical draw goes as $f_{SUSY} \sim m_{soft}^{2n_F+n_D-1}$ where n_F is the number of hidden sector F breaking fields and n_D is the number of hidden sector D-breaking fields (the latter distributed as real numbers)[101, 180, 22].[3] Convolution of the statistical draw to large soft terms with the anthropic requirement that the derived weak scale lies within the ABDS window then leads to a probability distribution for m_h that rises to a peak around $m_h \sim 125$ GeV[102] (in part because A_0 is also drawn to large (negative) values giving maximal stop mixing[185]) with sparticles typically beyond LHC reach. In this rendition, naturalness is replaced by what Douglas calls *stringy naturalness*[79], where a mode is more stringy natural if more landscape vacua lead to such a result. In stringy natural SUSY, a 3 TeV gluino is more (stringy) natural than a 300 GeV gluino[81]. The RNS benchmark given above is thus highly stringy natural. Thus, under stringy naturalness, RNS models with LHC-compatible sparticle masses most commonly emerge from the landscape[186].

[3] In [183], it is found that a linear $n = 1$ soft term draw is obtained for KKLT[184] moduli-stabilization models.

4.2 A scheme for computing relative probabilities from the landscape

The central question we wish to address is: how likely are various SUSY models (and the SM) to arise from the landscape? To answer this, we will restrict ourselves to string vacua containing the MSSM as the low energy EFT, and where SUSY breaking is mediated by gravity, *i.e.* spontaneous SUSY breaking in a $N = 1$ supergravity framework.[187] In such a SUGRA framework, scalar masses are generically *non-universal*[188, 189, 90, 190] unless protected by some symmetry: *e.g.* the matter scalars of each generation fill the 16-dimensional spinor rep of $SO(10)$ so one might expect these to have a common mass $m_0(i)$, $i = 1 - 3$ a generation index.[4] Since the Higgs scalars come in split multiplets, there is no reason to expect $m_0(i) = m_{H_{u,d}}$ and thus we expect the LE-EFT to be a non-universal Higgs model (NUHM). This framework accommodates all of the high-scale and natural SUSY models under consideration here.[5] While an absolute probability for any particular LE-EFT (including those not within the realm of the MSSM) is not possible to calculate (at least at this time), we can make estimates of *relative* probabilities amongst gravity-mediated MSSM models based on certain reasonable assumptions.

In Table 4.1, we list a variety of supersymmetric models, along with the SM, and the proposed range for various first/second $m_0(1, 2)$ and third generation

[4] We regard the AMSB soft terms as included in the gravity-mediated soft terms.

[5] For instance, in this framework, there is no known reason to favor the CMSSM model over any of the NUHM models.

model	$\tilde{m}(1,2)$	$\tilde{m}(3)$	gauginos	higgsinos	m_h	P_μ
SM	-	-	-	-	-	$7\cdot 10^{-27}$
CMSSM ($\Delta_{EW}=2641$)	~ 1	~ 1	~ 1	~ 1	$0.1-0.13$	$5\cdot 10^{-3}$
PeV SUSY	$\sim 10^3$	$\sim 10^3$	~ 1	$1-10^3$	$0.125-0.155$	$5\cdot 10^{-6}$
Split SUSY	$\sim 10^6$	$\sim 10^6$	~ 1	~ 1	$0.13-0.155$	$7\cdot 10^{-12}$
HS-SUSY	$\gtrsim 10^2$	$\gtrsim 10^2$	$\gtrsim 10^2$	$\gtrsim 10^2$	$0.125-0.16$	$6\cdot 10^{-4}$
Spread ($\tilde{h}$LSP)	10^5	10^5	10^2	~ 1	$0.125-0.15$	$9\cdot 10^{-10}$
Spread ($\tilde{w}$LSP)	10^3	10^3	~ 1	$\sim 10^2$	$0.125-0.14$	$5\cdot 10^{-6}$
Mini-Split ($\tilde{h}$LSP)	$\sim 10^4$	$\sim 10^4$	$\sim 10^2$	~ 1	$0.125-0.14$	$8\cdot 10^{-8}$
Mini-Split ($\tilde{w}$LSP)	$\sim 10^2$	$\sim 10^2$	~ 1	$\sim 10^2$	$0.11-0.13$	$4\cdot 10^{-4}$
SUN-SUSY	$\sim 10^2$	$\sim 10^2$	~ 1	$\sim 10^2$	0.125	$4\cdot 10^{-4}$
G_2MSSM	$30-100$	$30-100$	~ 1	~ 1	$0.11-0.13$	$2\cdot 10^{-3}$
RNS/landscape	$5-40$	$0.5-3$	~ 1	$0.1-0.35$	$0.123-0.126$	1.4

Table 4.1: A survey of some unnatural and natural SUSY models along with general expectations for sparticle and Higgs mass spectra in TeV units. We also show relative probability measure P_μ for the model to emerge from the landscape. For RNS, we take $\mu_{min}=10$ GeV.

$m_0(3)$ scalar masses, along with the expected range for gaugino and higgsino masses and the range of the light Higgs mass. In the last column we list the relative probability measure P_μ to be explained below. For the two SUSY models CMSSM and RNS, we have approximate supersymmetry extending all the way down to the weak scale. For the remainder of SUSY models, which include rather high mass scales $\tilde{m}$, we assume the heavy SUSY states are integrated out at scale $Q\simeq\tilde{m}$ which then destroys softly broken SUSY below the $\tilde{m}$ scale, so that quadratic divergences arise which are proportional to $\Lambda=\tilde{m}$ as in Eq. 2.4. A pictorial comparison of the spectra from the various models is given in Fig. 4.1.

For the two SUSY models RNS and CMSSM, the dominant contribution to the weak scale can be extracted from the value of Δ_{EW}. Then the pocket universe value of m_Z^{PU} can be computed using Eq. 2.9 as

$$\frac{(m_Z^{PU})^2}{2}=\frac{(m_Z^{OU}\sqrt{\Delta_{EW}})^2}{2}-\mu_{PU}^2 \tag{4.1}$$

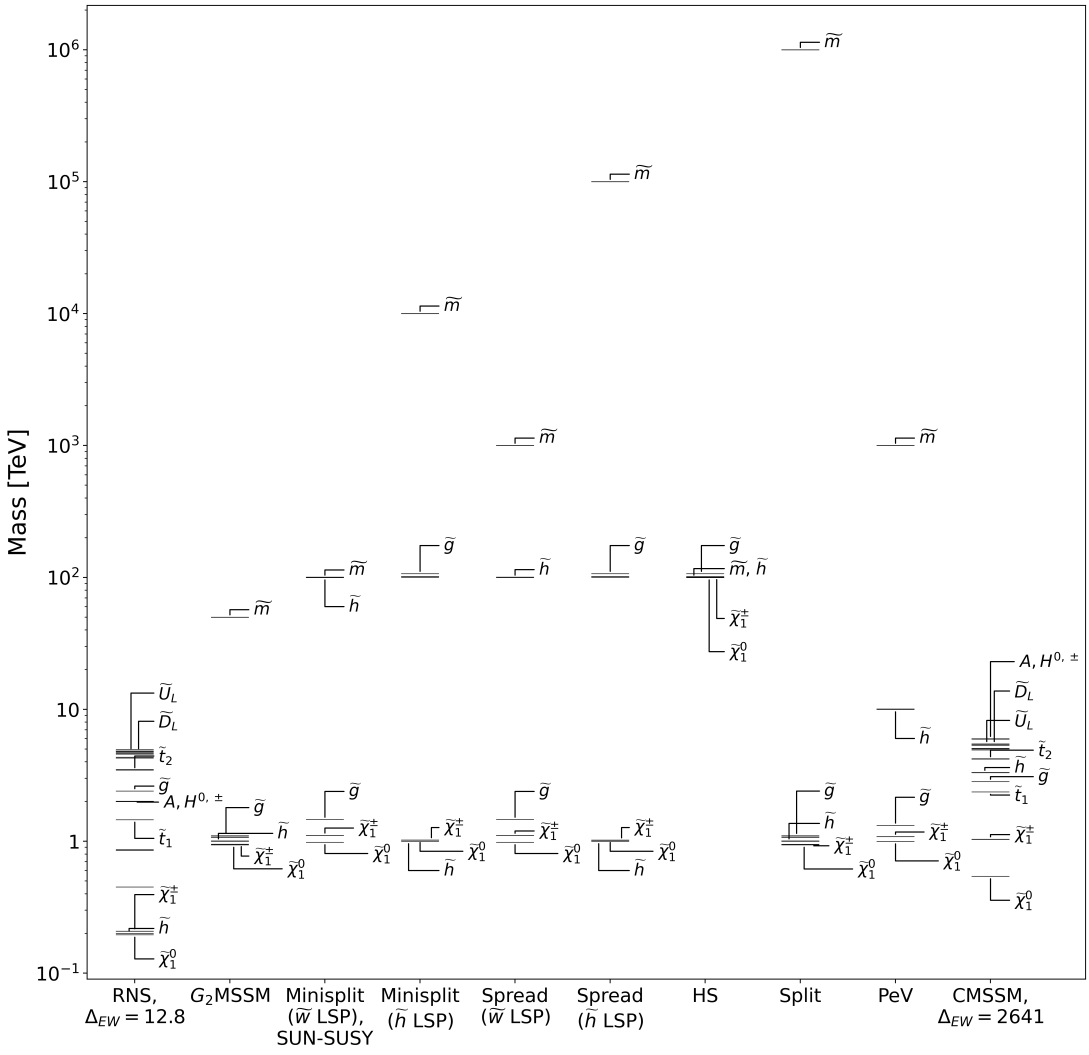

Figure 4.1: Mass spectra from various unnatural and natural SUSY models as depicted in Table 4.1.

(assuming the dominant contribution dominates all other contributions to $(m_Z^{PU})^2$, which is usually the case.) Here, $m_Z^{OU} = 91.2$ GeV, the value of m_Z in our universe (OU). In most SUSY spectrum calculations, the value of the μ parameter is finetuned to ensure that m_Z gains its measured value in our universe. However, in the multiverse, each pocket universe containing the MSSM as the LE-EFT will have a different value of μ_{PU} which will in general lead to a value for the weak scale which is very different from the one in our universe: $m_Z^{PU} \neq m_Z^{OU}$. In fact, frequently m_Z^{PU} may differ from m_Z^{OU} by many orders of magnitude. If it does, then one will have a pocket universe with m_{weak} outside the anthropic ABDS window, thus violating the atomic principle.

What is the likely distribution of SUSY μ_{PU} parameters in the multiverse? Here, we assume the μ parameter arises in the superpotential as in the Kim-Nilles (KN) solution to the SUSY μ problem[191],[6] where we expect $W \ni \lambda_\mu S^2 H_u H_d / m_P$. The PQ charged field S acquires a vev of order $f_a \sim 10^{11}$ GeV under PQ breaking so that a μ parameter arises:

$$\mu(KN) \sim \lambda_\mu f_a^2 / m_P \sim m_{weak}. \tag{4.2}$$

Thus, the KN μ parameter has the form of a (Planck-suppressed) Yukawa coupling, in accord with the other Yukawa couplings which occur in the superpotential. But the question is: what sort of distribution for μ would we expect on the landscape? For fixed λ_μ, this has been computed in a particular well-motivated KN solution

[6]For a recent review of twenty solutions to the SUSY μ problem, see Ref. [158].

based on an anomaly-free discrete R-symmetry $\mathbf{Z}_{24}^R$[192]. However, for non-fixed λ_μ, this may well be different. In fact, Donoghue, Dutta and Ross[193] make a convincing case that Yukawa couplings are distributed uniformly across the decades of possible values, which appears to match well with the measured fermion mass values. We will adopt the Donoghue *et al.* ansatz for the KN μ parameter as well: that no particular scale for the μ_{PU} value is favored over any other from the string landscape. This seems reasonable in that the only scale inherent in string theory is the string scale, and all other scales likely arise dynamically: *i.e.* there is no preferred scale for μ_{PU}. This corresponds to a landscape distribution $f_\mu \sim 1/\mu$ so that the integrated distribution is indeed scale invariant.

In Fig. 4.2, we show on the x-axis over 15 decades of possible values for μ_{PU}. For the RNS model, where the maximal contribution to the RHS of Eq. 2.9 is bounded to lie within a factor a few of our measured value of the weak scale, then there is a substantial range of μ_{PU} values leading to m_Z^{PU} lying within the (blue-shaded) ABDS window. We will take (quite arbitrarily) the lower limit of μ_{PU} to be ~ 10 GeV. Values of $\mu_{PU}(min)$ higher or lower by an order of magnitude from this value lead to differences in P_μ of a factor ~ 2 which is inconsequential for our purposes. The probability for a random value of μ_{PU} to give rise to m_Z^{PU} within the ABDS window is then

$$P_\mu \equiv \log_{10}(\mu_{PU}(max)/\mu_{PU}(min)) \tag{4.3}$$

i.e. the length of the interval of logarithmically distributed μ_{PU} values. Using

this interval, we find $P_\mu(RNS) \sim 1.4$.

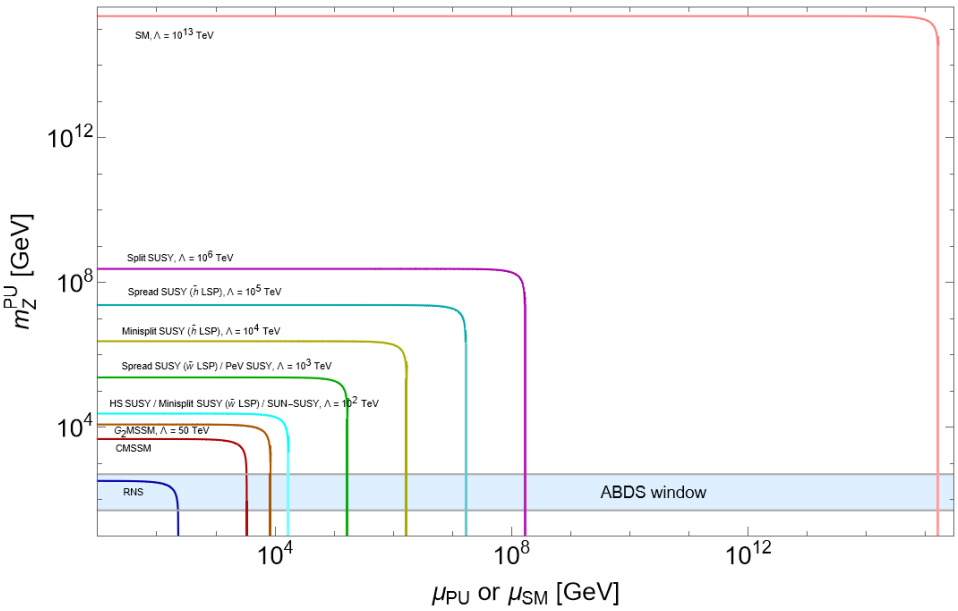

Figure 4.2: Values of m_Z^{PU} vs. μ_{PU} or μ_{SM} for various natural (RNS) and unnatural SUSY models and the SM. The ABDS window extends here from $m_Z^{PU} \sim 50 - 500$ GeV.

For the CMSSM benchmark model with $\Delta_{EW} = 2641$, then the maximal contribution to the RHS of Eq. 2.9 is well beyond the ABDS window. Thus, a finely-tuned value of μ_{PU} will be needed in order for m_Z^{PU} to lie within the ABDS window, in accord with the atomic principle. One will have to live in the nearly vertical portion of the red CMSSM curve, for which the interval length is $P_\mu(CMSSM) \sim 0.005$. While the absolute values of P_μ don't have a particular meaning (we don't know the overall normalization), the ratios of probabilities do. In this case, we would expect the RNS model to be $P_\mu(RNS)/P_\mu(CMSSM) \sim 260$ times more probable on the landscape than the CMSSM benchmark model. In this case, the "natural" value for the weak scale in the case of the CMSSM benchmark

model would be $m_{weak} \sim m_Z\sqrt{\Delta_{EW}} \sim 5$ TeV.

We can also calculate a value of P_μ for the SM, assuming the SM is valid all the way up to a scale $Q \sim m_{GUT}$ as is assumed in estimates of the SM vacuum stability[194]. Here, we will also assume that μ_{SM} has a scale invariant distribution so that the x-axis of Fig. 4.2 pertains to μ_{SM} of Eq. 2.19 as well as to μ_{PU}. Taking the value of $m_Z^{PU} \sim m_h^{PU}$, we can use Eq. 2.19 to plot the value of the weak scale in the SM. The plot is shown in Fig. 4.2 as the SM curve. Here, we see a value of $\mu_{SM} \sim 10^{15}$ GeV is needed for $m_Z^{PU}(SM)$ to lie within the ABDS window while the natural value of $m_Z^{PU}(SM)$ is $\sim 10^{15}$ GeV. This shows the extreme finetuning needed by the SM in order to ensure the weak scale lies within the ABDS window. We can compute $P_\mu(SM)$ and find it to be $\sim 7\cdot 10^{-27}$, that is the RNS model about 10^{26} times more likely than the SM to emerge from the landscape.

We can now also compute P_μ values for the various high-scale SUSY models listed in Table 4.1. The key point here is that quadratic divergences still cancel out at energy scales $Q > \tilde{m}$. But once Q drops below $\tilde{m}$, then we must integrate out the heavy sparticles in the LE-EFT and the quadratic divergences no longer cancel. Then we may use the uncanceled terms in Eq. 2.4 to compute corrections to the Higgs mass, again with $m_Z^{PU} \simeq m_h$. For most of these models, we take $\Lambda \sim \tilde{m} = m_0(3)$ to compute the curves of m_Z^{PU} vs. μ_{SM}, where now the Higgs potential is that of the SM for $Q < \tilde{m}$.[7]

The various curves are shown in Fig. 4.2 for the assorted high scale SUSY

[7]For the SM parameter values entering Eq. 2.4 in the case of high scale SUSY models with scale boundary $\tilde{m}$, we use FlexibleSUSY and FlexibleEFTHiggs to extract the appropriate values [195, 196, 197].

models of Table 4.1. We can then extract the values of P_μ for each case. As an example, Split SUSY with $m_0(3) \sim 10^6$ TeV gives $P_\mu \sim 7 \cdot 10^{-12}$ so that RNS is $\sim 10^{12}$ times more likely than Split SUSY to emerge from the landscape. Lest one be dismayed by the low relative probability for Split SUSY to emerge from the landscape, it is worth noting that the Split SUSY benchmark is $\sim 10^{15}$ times more likely to emerge from the landscape than the SM (when the SM is valid up to $Q = m_{GUT}$). Scaling $\tilde{m}$ to lower values in order to accommodate the measured value of m_h as in mini-split helps matters somewhat: in this case, mini-split with a wino LSP and $\tilde{m} \sim 10^2$ TeV has $P_\mu \sim 4 \cdot 10^{-4}$, so the RNS benchmark is more likely to emerge than the mini-split benchmark by a factor ~ 3000.

Chapter 5

Quantifying stringy naturalness from bottom to top

5.1 Stringy naturalness as a density measure in the landscape

Stringy naturalness may be viewed as a measure on the density and abundance of vacua satisfying some set of criteria, such as the ABDS condition. Additionally, we may require that an additional set of alternative criteria are satisfied, such as proper EWSB and absence of CCB minima (such as negative squared masses in squarks or sleptons). Here, stringy naturalness is defined as the following [198]:

Stringy naturalness: *The value of an observable $\mathcal{O}_2$ is more stringy natural than a value $\mathcal{O}_1$ if more phenomenologically viable vacua lead to $\mathcal{O}_2$ than to $\mathcal{O}_1$.*

In particular, choosing the mass of the Z boson and its relation to the ABDS window as a selection criterion for vacua satisfying the atomic principle, then we can say:

If more vacua lead to the ABDS window in scenario **A** than in scenario **B**, then scenario **A** is considered more *stringy natural* than scenario **B**.

In regards to "scenarios", one can compare different realizations of supersymmetry on the landscape, such as comparing high-scale SUSY against radiative

natural SUSY (RNS), or even against non-supersymmetric models like the Standard Model(albeit with different statistical distributions – see [17, 199]for detailed stringy constructions). While useful densities and distributions are given in these references, in practice this is a very broad and complex task in and of itself. In practice, a researcher may just have data on a single possible vacuum where m_Z is tuned to 91.1876 GeV, such as in an SLHA file for a supersymmetric spectrum generated by a spectrum generator. For this reason, it is necessary to create a stringy naturalness measure that can evaluate the density of ABDS-compliant (as well as EWSB-compliant and "no CCB"-compliant) vacua "surrounding" some initial vacuum in the landscape. These are the efforts presented here.

In [19], we determined an approximate relative vacuum density, P_μ, based on the Higgsino (or Higgs) mass parameter $\mu^{\rm PU}$ within some pocket universe of the landscape with variable m_Z. This effectively offered a comparison standard between scenarios, comparing the "width" of the ABDS window in these scenarios by evaluating m_Z^{PU} from the relevant weak-scale parameters and μ^{PU} with the Higgs minimization conditions (or weak-scale mass conditions in the Standard Model) in the following models:

- Radiative natural SUSY,
- mSUGRA/CMSSM,
- Split SUSY,
- Mini-split SUSY,

- Spread SUSY,
- High-scale SUSY,
- PeV SUSY,
- the Standard Model.

The evaluations to obtain this measure P_μ can be expressed as the following integral in Eq. (5.2). Let the lower edge of the ABDS window lie at ${}^{m_Z^{\rm OU}}/_2 = 45.6$ GeV, and the upper edge lie at $4m_Z^{\rm OU} = 364.8$ GeV. The $\mu^{\rm PU}$ term is distributed on the landscape in a fashion such that mu is uniformly distributed over the decades, i.e., the probability distribution of μ^{PU} is

$$f_\mu \sim \frac{1}{\log(10)\,|\mu^{\rm PU}|} \tag{5.1}$$

Then the density of vacua associated with vacua containing $\mu^{\rm PU}$ values leading to the ABDS window allow us to approximately compare different landscape vacuum scenarios as

$$\begin{aligned} P_\mu &= \int_{\mu^{\rm PU}({\rm min})}^{\mu^{\rm PU}({\rm max})} f_\mu \; d\mu^{\rm PU} \\ &= \log_{10}\left(\frac{\mu^{\rm PU}({\rm max})}{\mu^{\rm PU}({\rm min})}\right). \end{aligned} \tag{5.2}$$

Clearly, "wider" ABDS windows (as in RNS) will lead to many more vacua that are ABDS-compliant, relative to "narrower" ABDS windows (as in the Standard Model, up to $\sim 10^{26}$ times smaller of a density relative to RNS). Two primary "incompleteness" issues may arise here, however:

1. The density measure here is unnormalized and only can effectively compare different, pre-simulated scenarios. However, this may be a non-issue, as the current number of flux vacua in the string landscape with the MSSM or SM as its low-energy EFT is not a settled debate. Hence, this need not be addressed here, as the definition of stringy naturalness can easily be connected to the idea of the density of vacua in some neighborhood of the landscape.

2. There are other parameters potentially distributed on the landscape. For example, soft-SUSY-breaking (SSB) terms could be distributed on the landscape according to a power-law distribution, based on the number of F- and D-type SUSY breaking fields present in the theory [199]. A more complete vacuum density measure would incorporate the statistical contributions of these terms to the relative population of the ABDS window.

Given our understandings of the statistical distributions of soft terms on the landscape, when we couple the ABDS window criterion with other criteria such as proper EWSB and absence of CCB minima, we can address this second issue. An algorithm will be constructed below to permit a "point-by-point" evaluation of stringy naturalness.

While the overall SUSY breaking scale is distributed as a power-law, the different functional dependence[188, 189, 90] of the soft terms on the hidden sector SUSY breaking fields means that gaugino masses, the trilinear soft terms and the various scalar masses will effectively scan independently on the landscape[190].

Now it is an *advantage* that different scalar mass-squared terms scan independently (as expected in SUGRA) since the first/second generation scalars get pulled to much higher values than 3rd generation scalars, while the two Higgs soft masses are also non-universal and scan independently. This situation is borne out in Nilles *et al.* mini-landscape where different fields gain different soft masses due to their different geographical locations on the compactification manifold[200]. In terms of gravity mediation, then the so-called n-extra-parameter non-universal Higgs model (NUHMn) with parameters[13, 15]

$$m_0(i),\ m_{H_u},\ m_{H_d},\ m_{1/2}, A_0,\ \tan\beta \qquad (NUHM4) \tag{5.3}$$

provides the proper template. Since the matter scalars fill out a complete spinor rep of $SO(10)$, we assume each generation $i = 1 - 3$ is unified to $m_0(i)$. Also, for convenience one may ultimately trade m_{H_u} and m_{H_d} for the more convenient weak scale parameters m_A and μ. One may also build (and scan separately) the natural anomaly-mediated SUSY breaking model[182, 201] (nAMSB) and the natural generalized mirage mediation model[181] (nGMM).

5.1.1 The ABDS window

The anthropic selection on the landscape comes from the probability distribution f_{EWSB} to be discussed shortly. This involves a rather unheralded prediction of the MSSM: the value of the weak scale in terms of soft SUSY breaking parameters and μ, as displayed in Eq. (2.9). However, in the multiverse, here we rely on

the existence of a friendly neighborhood[22] wherein the LE-EFT contains the MSSM but where only dimensionful quantities such as Λ_{CC} and $v_u^2 + v_d^2$ scan, whilst dimensionless quantities like gauge and Yukawa couplings are determined by dynamics. This assumption leads to *predictivity* as we shall see.

Under these assumptions, then we ask what conditions lead to complex nuclei, atoms as we know them, and hence the ability to generate complex lifeforms in a pocket universe? For different values of soft terms, frequently one is pushed into a weak scale scalar potential with charge-or-color breaking minima (CCB) where one or more charged or colored scalar mass squared is driven tachyonic (i.e., $m^2 < 0$). Such CCB minima must be vetoed. Also, for too large of values of $m_{H_u}^2$, then its value is *not* driven to negative values and EW symmetry is not broken. These we label as "no EWSB" and veto them as well. In practice, we must check boundedness of the scalar potential from below in the vacuum stability conditions and that the origin of field space has been destabilized, at least at tree-level. Some leading loop-level contributions to these conditions have been presented in Appendix C.

At this point, we are left with (MS)SM vacua where EW symmetry is properly broken, but where $m_{weak} \sim m_{W,Z,h}$ is at a different value from what we see in our universe. Here, we rely on the prescient analysis of Agrawal, Barr, Donoghue and Seckel (ABDS)[80, 176]. If the derived value of the weak scale is bigger than ours by a factor $(2-5)$, then the light quark mass difference $m_d - m_u$ becomes so large that neutrons are no longer stable in the nucleus and nuclei with $Z \gg N$ are not bound; such pocket universes would have nuclei of single protons only,

and would be chemically inert. Likewise, if the PU value of the weak scale is a factor ~ 0.5 less than our measured value, then one obtains a universe with only neutrons – also chemically inert. The ABDS window of allowed values is that

$$0.5m_{weak}^{OU} < m_{weak}^{PU} \lesssim 4m_{weak}^{OU} \tag{5.4}$$

where we take the $(2-5)m_{weak}^{OU}$ to be $\sim 4m_{weak}^{OU}$ for definiteness, which is probably a conservative value. It is very central to our analysis and so is displayed in Fig. 5.1. Our anthropic condition f_{EWSB} is then that the scalar potential lead to minima with not only appropriate EWSB, but also that the derived value of the weak scale lie within the ABDS window. Vacua not fulfilling these conditions must be vetoed.[1] This lays the foundations for the requirements of a quantifiable

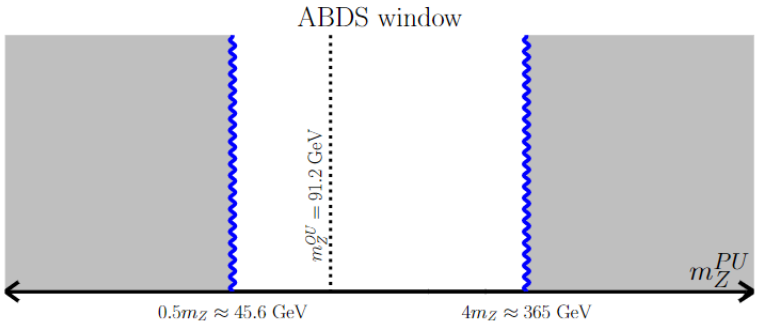

Figure 5.1: The ABDS-allowed window within the range of m_Z^{PU} values.

stringy naturalness measure, which will be elaborated upon in the next section.

[1]Early papers on this topic used instead a naturalness "penalty" of $f_{EWSB} \sim m_{weak}^2/m_{SUSY}^2$; this condition would allow for many of the vacua which are forbidden by our approach.

5.2 Requirements for a stringy naturalness measure

If one were to try and evaluate stringy naturalness in a reliable manner more rigorously than simply "counting dots" from a multiverse simulation [21], there are a few key details that *must* be included in the evaluation.

1. One must account for the probability distributions of terms (e.g., soft terms distributed as power law based on number of D and F SUSY-breaking fields) on the string landscape;

2. One must incorporate a method for establishing the density of the number of vacua leading to some observable, as given by the definition of stringy naturalness;

3. Since on the string landscape, m_Z is variable, one can use a set of selection criteria for "valid" vacua as:

   (a) The Z boson mass lies within the ABDS window, as determined by the weak-scale Higgs minimization conditions:

$$\frac{m_Z^2}{2} = \frac{m_{H_d}^2 + \Sigma_d - (m_{H_u}^2 + \Sigma_u)\tan^2(\beta)}{\tan^2(\beta) - 1} - \mu^2 \tag{5.5}$$

$$\sin(2\beta) = \frac{2b}{m_{H_u}^2 + \Sigma_u + m_{H_d}^2 + \Sigma_d + 2\mu^2}. \tag{5.6}$$

   $\Sigma_{u,d}$ are radiative loop corrections to these equations, which are listed in Appendix A. It is key that as the value of m_Z shifts in the landscape, *both* conditions Eqs. (5.5-5.6) must be satisfied to ensure criticality of

the scalar potential from the EFT viewpoint. Thus, a distribution of $\tan(\beta)$ is induced on the landscape through this requirement. Existence and stability of scalar potential extrema and subsequent minimization must also be ensured as in the points below.

(b) There are no CCB minima.

(c) The electroweak symmetry is satisfactorily broken, i.e., when the following weak-scale conditions are true:

$$2b < 2\mu^2 + m_{H_u}^2 + m_{H_d}^2, \tag{5.7}$$

$$b^2 > \left(\mu^2 + m_{H_u}^2\right)\left(\mu^2 + m_{H_d}^2\right). \tag{5.8}$$

There are potentially relevant loop corrections to these tree-level expressions. These corrections are listed in Appendix C.

(d) It will be otherwise assumed that the weak-scale structure and strong gauge couplings are assumed to be similar to their SM counterparts in our universe through stringy dynamics, ignoring contributions from the variable Higgs VEV. Gauge and Yukawa couplings can then be determined in the appropriate renormalization scheme from dynamics based on this construction. It must be noted that variations in $\tan(\beta)$ within the landscape to ensure minimization also will shift Yukawa couplings at tree-level.

Next, we construct an algorithm to accomplish these requirements and produce a

measure for evaluating stringy naturalness on a point-by-point basis.

5.3 Numerical precision and statistical considerations

Depending on the level of statistical rigor we would like to apply to this density measure, different approximations of the stringy naturalness value can be employed. The level of accuracy of these approximations are directly proportional to their levels of robustness for the corresponding statistical analyses of the landscape, and hence, the level of computational complexity. In brief, we present an approximate expression (à la P_μ) for computing the density of ABDS-compliant vacua emerging from the landscape around some initial vacuum. In the future, a more robust and specialized Monte-Carlo simulation algorithm for computing the density of ABDS-compliant vacua randomly emerging from the landscape can be produced. The landscape is assumed to be parameterized by the Minimally Supersymmetric Standard Model (MSSM) parameter space, in some local neighborhood surrounding one user-specified possible vacuum with the MSSM and Standard Model (SM) (with potentially different Higgs VEV and, by extension, Z boson mass) as its low-energy effective field theories (EFTs). The specific requirements are outlined in the previous section.

Many supersymmetric spectrum generators today (e.g., SoftSUSY, Isajet/Isasugra, SPheno, etc.) can provide predictions of the MSSM that are potentially testable at a collider. Often, the user is able to save their results to a standardized format, the SUSY Les Houches Accord (SLHA) [23, 24]. From this format, one

can compute various naturalness measures such as the electroweak naturalness measure Δ_{EW}, the high-scale naturalness measure Δ_{HS}, and the Barbieri-Giudice naturalness measure Δ_{BG} as described in the preceding Chapters. These can all be calculated from a user-submitted SLHA-format file, from the user's choice of spectrum generator, using the program natLHA, developed by D. Martinez [202]. In a similar sense, we have developed a program to compute a proposed stringy naturalness measure. In an approximate form, we can write this stringy naturalness measure as an analytic expression.

However, before introducing these expressions and algorithms, we must ensure we have a concrete method for determining the density of vacua. Included in this is the requirement of understanding the parameter space in which our parameters are distributed. For this reason, we parameterize some "friendly" neighborhood of the landscape surrounding an initial vacuum with the MSSM parameters as mentioned above. The MSSM in itself contains a vast parameter space, though, so we specifically restrict ourselves to the *real*-valued MSSM, but still maintain some generality by relaxing universality conditions, neglecting off-diagonal CP-violating effects. We also assume the relevant gauge-eigenstate mass matrices are diagonal. In our proposed parameter space here, we assume there are 30 fundamental soft supersymmetry-breaking (SSB) parameters (15 SSB squark/slepton masses, two SSB Higgs masses, nine SSB trilinear couplings, three SSB gaugino masses, and one SSB bilinear parameter) along with one SUSY-conserving parameter, μ, which is important for weak-scale physics. This full parameter space can then be written as the set:

$$\left\{ \begin{array}{c} m^2_{\widetilde{Q}_1}, m^2_{\widetilde{U}_1}, m^2_{\widetilde{D}_1}, m^2_{\widetilde{L}_1}, m^2_{\widetilde{E}_1}, m^2_{\widetilde{Q}_2}, m^2_{\widetilde{U}_2}, m^2_{\widetilde{D}_2}, m^2_{\widetilde{L}_2}, m^2_{\widetilde{E}_2}, \\ m^2_{\widetilde{Q}_3}, m^2_{\widetilde{U}_3}, m^2_{\widetilde{D}_3}, m^2_{\widetilde{L}_3}, m^2_{\widetilde{E}_3}, a_t, a_c, a_u, a_b, a_s, a_d, a_\tau, a_\mu, a_e, \\ m^2_{H_u}, m^2_{H_d}, M_1, M_2, M_3, B = b/\mu, \mu \end{array} \right\}.$$

An important note to consider here is that we are working in the regime of weak-scale physics and its minimization conditions, whereas these parameters are renormalization-scale dependent (see Appendix B). Thus, to approximately account for renormalization effects in a consistent manner, our parameterization of the landscape in terms of MSSM parameters is specifically through their weak-scale values. These weak-scale values will be coupled (within the regime of perturbativity) to GUT-scale parameters through the renormalization group flow, which then is assumed to be the consequence set by some stringy dynamics on the number and configuration of F- and D-type SUSY-breaking fields. No further assumptions are made in regards to the stringy aspects of the theory, as this is outside the regime of the EFT.

However, in regards to *practical naturalness*, we should compare contributions to the density of vacua that have ABDS-compliant weak scales. Thus, the stringy naturalness measure we construct will share more similarities with $\Delta_{\rm EW}$ in Eq. (2.10) than $\Delta_{\rm BG}$ or $\Delta_{\rm HS}$ in Eqs. (2.6-2.7)

Vacua in the landscape can be selected for analysis according to a well-defined set of selection criteria, which we will denote generally here as an indicator function

θ. θ is defined as

$$\theta = \theta(\text{conditions}) = \begin{cases} 1 & \text{if conditions are true,} \\ 0 & \text{otherwise.} \end{cases} \tag{5.9}$$

According to Douglas and others [199], these soft-supersymmetry breaking terms may be distributed in the string landscape according to the numbers n_F and n_D of F- and D-type SUSY breaking fields, where these fields may lie in some hidden sector or potentially within a more UV-complete theory that breaks down to the MSSM as an EFT somewhere below m_P, the reduced Planck scale. This can be expressed approximately as a density of vacua, scaled by the power law distribution provided by the number of SUSY-breaking fields on the soft supersymmetry breaking scale:

$$\begin{aligned} dN_{\text{vac, soft}} &\sim f_{\text{SUSY}}\left(m_{\text{soft}}\right) \cdot \theta \cdot dm_{\text{soft}} \\ &\sim m_{\text{soft}}^{2n_F+n_D-1} \cdot \theta \cdot dm_{\text{soft}}, \end{aligned} \tag{5.10}$$

m_{soft} here denotes the scale of the soft supersymmetry breaking terms and is typically expected $\sim 10^{11}$ GeV such that this scale is given by $m_{\text{soft}} \sim m_{\text{SUSY}}^2/m_P$ with $m_P \sim 2.4 \cdot 10^{18}$ GeV the reduced Planck mass. Douglas and others [199, 198] mention that the SUSY-breaking scale is on the order of the distance from the origin in SUSY-breaking field space, which is expressed in terms of the magnitudes

of the $F-$ and $D-$type SUSY breaking fields.

$$m_{\text{SUSY}}^4 = \sum_{n_F} |F_i|^2 + \frac{1}{2} \sum_{n_D} |D_j|^2$$

Since we are parameterizing this space in terms of the MSSM EFT parameters, we can construct a similar L_2 (Euclidean) norm measure computing the distance of a vacuum, parameterized by its parameter vector $\mathbf{p}$, from the origin of this parameter space. For this parameter vector $\mathbf{p}$, the L_2 norm takes the form

$$|\mathbf{p}|^2 = \sum_i |p_i|^2,$$

where a sum is taken over the magnitude squared of the components of $\mathbf{p}$.

In other words, m_{SUSY}^2 can be set using the L_2 norm (specifically $L_2(\mathbb{C})$) of mass-dimension 1 parameters in the soft SUSY-breaking sector. For mass-dimension 2 parameters, since we are just interested in the distance from the origin of parameter space, we only need the magnitude of a parameter $p_i = \sqrt{|p_i^2|}$. Note that μ is not a soft term and is not included in this measure, and so its effect on the $b = B\mu$ soft parameter must be carefully split into independent components B and μ, each of mass dimension 1. This leaves 30 soft SUSY breaking parameters with dimension-1 magnitude p_i in our parameter space. Hence,

$$\begin{aligned} m_{\text{soft}} &\sim \frac{m_{\text{SUSY}}^2}{m_p} \\ &\sim \frac{1}{m_p} \sum_{i=1}^{30} |p_i|^2 \end{aligned} \tag{5.11}$$

We then cast our density of vacua due to the soft parameters of the theory as

$$\begin{aligned} f_{\text{SUSY}} &\sim m_{\text{soft}}^{2n_F+n_D-1} \\ &\sim \frac{1}{m_p^n}\left(\sum_{i=1}^{30}|p_i|^2\right)^n \end{aligned} \tag{5.12}$$

where $n = 2n_F + n_D - 1$.

To turn this into a calculable expression that can be integrated, we convert the differential dm_{soft} to differentials dp_i in various directions of soft parameter space, based on the definitions above.

$$dm_{\text{soft}} \sim \frac{2}{m_p}\left[\sum_{i=1}^{30}|p_i|d|p_i|\right] \tag{5.13}$$

The full differential density of vacua in terms of the soft parameters in Eq. (5.10) may then be expanded and subsequently integrated to give the parametric dependence of the density as below.

$$dN_{\text{vac, soft}} \sim \frac{2}{m_p^{n+1}}\left(m_{\text{SUSY}}^2\right)^n\left[\sum_{i=1}^{30}|p_i|d|p_i|\right] \tag{5.14}$$

In integrating, consider the possibility that $m_{H_{u,d}}^2 < 0$, meaning $|m_{H_{u,d}}| = \sqrt{|m_{H_{u,d}}^2|}$. Squark and slepton squared masses should not run negative to avoid CCB minima, but the integration method in the $d|m_{H_{u,d}}|$ directions must be addressed. This is the reason for the $L_2(\mathbb{C})$ norm in our expressions for m_{SUSY}^2. Since we care about the "distance from the origin" of SUSY-breaking parameter space, and the solution will only depend on the magnitude of parameters $|p_i|$, then

if $p_i^2 < 0$, we may take $p_j = ib$ (where $i = \sqrt{-1}$) purely imaginary, with $b > 0$. The integration in this direction then proceeds along the positive imaginary axis $d|p_i| = db$, until the origin (or edge of the indicator θ) is encountered. If $p_i = 0$ is reached, the integration direction switches to run along the real axis, away from the origin – such that $p_i^2 > 0$ – until integration conditions are met according to the indicator function θ.

On the other hand, for parameters such that $p_i^2 = 0$, then integration with $|p_i|d|p_i|$ towards and away from the origin of parameter space can proceed along the real axis. Proceeding with this integration, we get the density of ABDS vacua below.

$$N_{\text{vac,soft}} \sim \left[c \sum_{j=1}^{30} \left(\left(m_{\text{SUSY}}^{2n+2} \right) \Big|_{p_{j,-}}^{p_{j,+}} \right) \right] \tag{5.15}$$

Here we adopt the general notation that $p_\pm$ denotes the left and right ends of the integration over dp, which in general depend on the satisfaction of the indicator function θ. The coefficients c are introduced here and serve to locally eliminate the mass dimension of the probability density within the available ABDS window. This follows from the idea that since

$$dN_{\text{vac}} \sim m_{\text{soft}}^n dm_{\text{soft}},$$

then after introducing a term c to account for the correct mass dimension, integrating both sides of this dependence shows that

$$N_{\text{vac}} \sim \frac{c}{n+1} m_{\text{soft}}^{n+1}.$$

Since N_{vac} accounts for a number of a vacua (a dimensionless quantity), this expression can be inverted to find the coefficient c parametrically as

$$c \sim \frac{n+1}{m_{\text{soft}}^{n+1}}.$$

Expanded in terms of m_{soft} in Eq. (5.11) and simplifying against factors of m_p gives the following calculable expression for c.

$$c = \frac{n+1}{(m_{\text{SUSY}}^2)^{n+1}} \tag{5.16}$$

Including this normalization factor is consistent with the idea of finding the vacuum density (relative to the SUSY scale) within ABDS-compliant parameter space near a user-supplied vacuum, within different directions of parameter space. In other words, we can compute on average within a model how the vacuum density shifts in the ABDS window relative to the distance scale of the user-supplied vacuum, serving as a representative point for the weak-scale model being tested. This provides a broader understanding of the shape of the ABDS-compliant landscape and incorporating values for models with an MSSM EFT while remaining consistent with the ideas motivating stringy naturalness.

To be consistent with the distribution of Standard Model fermion masses, then we suppose that the distribution of μ on the landscape can be expressed as a

$\log_{10}$-uniform distribution (simultaneously allowing for $\mu < 0$ solutions):

$$\begin{aligned} dN_{\text{vac},\,\mu} &\sim f_\mu(\mu) \cdot \theta \cdot \; d\mu \\ &\sim \frac{\theta}{\ln(10)|\mu|} \cdot d\mu. \end{aligned} \tag{5.17}$$

The factor of $\ln(10)$ serves to change the base of the logarithm obtained after integration to base 10, such that the probability associated with the μ parameter on the landscape is uniform across the decades. Note that integrating Eq. (5.17) then leads to the expression for P_μ in Eq. (5.2) (potentially with more appropriate integration bounds induced by θ). A similar idea, together with certain assumptions, allows us to come up with an explicit, but approximate evaluation of the desired ABDS density of vacua surrounding some initial point at which we can begin this integration process.

5.3.1 P_μ-esque expression

For deriving the approximate expression, we started with some assumptions on our statistical distributions. First, we assume each of the 30 specified soft terms and μ are all distributed independently of one another. Care must be taken particularly with the bilinear soft SUSY breaking term $b = B\mu$. The independent soft distribution must be assumed to be on the soft *linear* parameter B to ensure independence from the otherwise-distributed μ.

As a technical aside, varying the values of μ or B in turn affects the predicted value of $\tan(\beta)$, according to Eq. (5.6). In fact, variations in $m^2_{H_{u,d}}$ at tree-level

and the other soft terms at loop level alter this prediction as well, if we are indeed ensuring a minimized vacuum within the scalar potential and not a dangerous metastable or unstable state in the high-dimensional parameter space. Variations in this value of $\tan(\beta)$ then affects Yukawa couplings, which in turn affects the minimization conditions further. This is a glimpse "under the hood" into the dynamics governing the gauge and Yukawa couplings under our assumptions set forth here, though the effect on gauge couplings is lessened, as these effects would appear in the threshold corrections to the SM values, which are at loop level. The induced changes in these general directions of parameter space become strongly constrained by perturbativity bounds on $\tan(\beta)$. As a general rule of thumb, $\tan(\beta) \lesssim 2.5$ leads to a non-perturbative top Yukawa coupling, whereas $\tan(\beta) \gtrsim 60$ leads to a non-perturbative bottom and/or τ Yukawa coupling. In both cases, predictivity is lost, so vacua violating these bounds will be subject to one of our selection criteria, thus constraining these directions of parameter space further. This ties in closely with electroweak stability conditions, which are expanded upon in Appendix C.

For a given set of selection and integration criteria θ, the statistical independence assumption causes our selection criteria to select a hyperrectangular region in this 31-dimensional parameter space (30 dimensions of soft parameters, one dimension for the μ parameter, and within this space lies the original, user-supplied vacuum). In particular, the independence assumption specifies that the *boundaries* of the region defined by our indicator function θ are *rectangular*. In general, this is not the case. This is particularly important due to the high

dimensionality of this parameter space and the indicated region: it is a well known fact in geometry that in higher dimensional shapes and regions, the significant majority of the hypervolume of that shape lies near its boundary. In the context of the landscape, this would mean that the majority of vacua geometrically live near the boundaries of our selected region of parameter space. This distribution of vacua is then shifted further by the probability distributions of our parameters. Thus, an algorithm will follow that will attempt to maximize the ability to probe large regions of weak-scale parameter space surrounding an initial vacuum. This will provide a systematic probe on the string landscape "near" some user-supplied vacuum (USV) in addition to an "ABDS integrated density" near the USV.

Since we are counting vacua in the string landscape by parameterizing them in this high-dimensional parameter space, counting ABDS-compliant vacua is similar to finding a weighted hypervolume of the region of parameter space containing these ABDS-compliant vacua. Due to the high dimensionality, subtle variations in region boundaries can result in significant deviations in the evaluation of this weighted hypervolume, where the weights come from the known probability densities of each parameter. When the boundary of a statistically indicated region (such as the one indicated by θ) is nonrectangular, this implies that the boundary is inducing some correlations between the random variables at that boundary. So, despite the relative independence of statistical distributions in the bulk of the indicated region of parameter space, potentially important correlations are introduced at this region's boundaries, in direct contradiction with the assumption of (global) independence.

In other words, rectangular boundaries on our ABDS, CCB, and EWSB selection criteria, as imposed by the global assumption of statistical independence of randomly distributed variables, may provide an inaccurate vacuum density estimate due to boundary effects in our selection criteria. However, it can provide a rough, leading order idea of the magnitude of stringy naturalness for a vacuum.

Therefore, for some selection criteria represented as an indicator function $\theta(\text{criteria})$ and a joint probability density function $f(\vec{x})$ for a vector of random variables $\vec{x}$, a reasonable density measure can be expressed as

$$N \sim \int \theta(\text{ABDS, EWSB, no CCB}) f(\vec{x})\ d\vec{x}. \tag{5.18}$$

Then, in keeping with the tradition of smaller naturalness values corresponding to greater levels of "naturalness", a clear choice for the stringy naturalness measure is

$$\Delta_{\text{SN}} = \frac{1}{N}. \tag{5.19}$$

By scanning the parameter space in one direction at a time, starting at the user-supplied vacuum, one can find "endpoints" in each direction of the parameter space, akin to the "width" of the ABDS window computed in the P_μ measure. In general, this collection of endpoints on our parameters creates an approximately bounding hyperrectangle in the parameter space, approximately containing our subregion of interest. Consider the 2D example in Fig. 5.2 to illustrate this.

Fig. 5.2 demonstrates the idea that this method of computing independent probabilities is akin to computing the weighted area of the blue rectangle (weighted

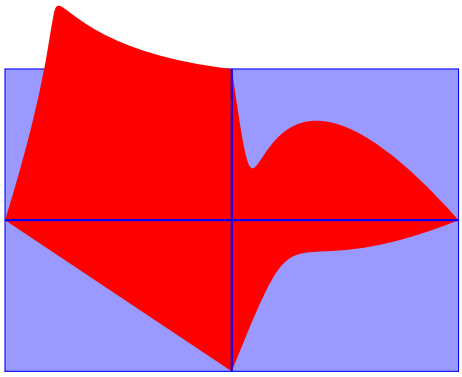

Figure 5.2: A 2D conceptual example showing the approximately bounding hyperrectangle (blue) mostly containing the desired subregion of the plane (red). The intersection of the vertical and horizontal dark blue lines represents the location of the user-submitted vacuum in this parameter space.

by the appropriate probability densities), whereas the "true" probability may be more like the weighted area of the red region. As such, since the blue region is usually at least as large as the red space, this could potentially overestimate the probability. The exception is when long "legs" of the red region leaving the blue bounding rectangle contribute significantly to the size of the red region as in Fig. 5.2, which may be less significant given an appropriate bounding rectangle or scanning regime. Moreover, the boundaries of the EWSB and no-CCB conditions are generally non-rectangular in this space. These approximation issues can be addressed with a more rigorous Monte-Carlo method, for example, but these differences will be considered sub-leading order.

Then, utilizing the probability density functions in Eqs. (5.10, 5.17) to count the relative abundance of ABDS-compliant vacua, we can write the following

approximate expression for Δ_{SN}. Here, we denote the number of soft terms in our parameter space by n_{soft} (in practice, we will use $n_{\text{soft}} = 30$). We will denote the probability density of a random variable x with $f_x(x)$. The bounds of integration obtained from the one-dimensional scans over points satisfying ABDS, EWSB and no-CCB conditions are generally denoted as $p_{i,\pm}$ and $\mu_{\pm}$.

$$\begin{aligned}\Delta_{\text{SN}} &= \frac{1}{N_{\text{vac, soft}} \cdot N_{\text{vac},\mu}} \\ &\approx \left\{ \left[\sum_{j=1}^{30} \left(c \left(m_{\text{SUSY}}^{2n+2} \right) \Big|_{p_{j,-}}^{p_{j,+}} \right) \right] \cdot \log_{10} \left(\left| \frac{\mu_+}{\mu_-} \right| \right) \right\}^{-1}\end{aligned} \tag{5.20}$$

Lastly, if one wished to just look at the differential vacuum density at the user-supplied vacuum point, the contribution to dN_{vac} will be as below, where one can construct a simpler measure $\delta_{\text{SN}} = 1/dN_{\text{vac}}$. The dimensional normalization gives units consistent with the previous results by normalizing relative to the SUSY scale at the USV point.

$$\begin{aligned}\delta_{\text{SN}} &= \log_{10} \left(\frac{1}{dN_{\text{vac}}} \right) \\ &= \log_{10} \left[\left(\frac{2(n+1)}{\log(10)|\mu| m_{\text{SUSY}}^2} \sum_{j=1}^{30} |p_j| \right)^{-1} \right]\end{aligned} \tag{5.21}$$

Thus, a change of ϵ in the measure δ_{SN} from

$$\delta_{\text{SN}} \to \delta_{\text{SN}} + \epsilon$$

approximately corresponds to a change in the differential vacuum density of

$$dN_{\rm vac} \to dN_{\rm vac} + 10^{-\delta_{\rm SN}} 10^{-\epsilon} \cdot (1 - 10^{\epsilon}).$$

The term in parentheses shows that if $\delta_{\rm SN}$ increases (less stringy natural), the differential vacuum density $dN_{\rm vac}$ decreases. On the other hand, if $\delta_{\rm SN}$ decreases (more stringy natural), then $dN_{\rm vac}$ increases.

Conceptually, $dN_{\rm vac}$ consists of the products of the joint probabilities from $d\mu$ and $dm_{\rm soft}$, which then connect to each dp_j. Here it is assumed that all differentials $d\mu, dp_j$ are of the same small order, and we seek to model the functional dependence of the coefficients for these differentials in its relationship to vacuum density on the landscape. Hence, in computing $dN_{\rm vac}$, the results are $\mathcal{O}(d\mu\ dp_j)$. The log for $\delta_{\rm SN}$ is used to tame the large numbers produced by dividing by a small $dN_{\rm vac}$.

5.3.2 Numerical method for Δ_{SN}

When implementing this result numerically, we need to know the stopping points of integration in each direction of parameter space. Here, we provide a conceptual approach to performing this task, though full numerical results are saved for a future work. If the user provides the program with an initial point potentially describing our universe, where EWSB conditions are satisfied at the weak scale, there are no CCB minima, and $m_Z = m_Z^{OU}$, then we can gradually vary away from this initial point through small increments in m_Z and solve for the corresponding changes in the scanned soft parameter p_i and ratio of Higgs vev's $\tan(\beta)$. After

each small increment in m_Z, the scalar potential is re-minimized at loop-level through a Newton-Raphson method iterator, producing an updated tuple of parameters $(m'_Z, p'_i, \tan(\beta'), p_{i\neq j})$ that (hopefully) satisfy the indicator conditions in θ and the minimization conditions. More robustly, since $\tan(\beta)$ and m_Z both arise from the Higgs VEVs $v_{u,d}$, one could vary the parameter p_i from the initial point and determine its effect on $v_{u,d}$ through a similar iterative solver. In doing so, we are making a more direct connection with minimization of the scalar potential via the non-zero Higgs VEVs, and then extracting information on m_Z and $\tan(\beta)$ as a result.

Newton's method may be sensitive to the initial guesses provided to the system. This is accounted for on an as-needed basis through linearization of the system due to a small shift of $p_i \to p_i + \delta$, where $\delta \in \mathbb{R}$ is small. The minimization conditions are then assumed to be satisfied at a close point $(v_u + dv_u, v_d + dv_d)$ for "small" (a subjective term here) dv_u, dv_d. Other sub-leading terms in this linearization will be $\mathcal{O}(dv_{u,d}^2)$ and will be neglected in this approximation.

However, hypersensitivity (or even insensitivity) of these Higgs VEVs on specific parameters p_i may prove to have a convergence basin in Newton's method with width much smaller than floating-point precision can allow, or the minimization conditions can even prove too sensitive to extremely tuned parameters, again due to float-point precision. Both of these have been addressed by using the C++ library Boost's MPFR multiprecision backend to use extended precision floating point variables to 50 decimal places.

Recall that the large dimension of this problem, such as in the MSSM parameter

space, greatly exacerbates boundary effects seen in the bounds of the integrals above. Therefore, a more sophisticated method for efficiently approximating the integrals in Δ_{SN} while obeying the correct bounds may use a Monte Carlo integrator with a Monte Carlo semi-stratified importance sampler to select points for the integration. The idea is outlined in the bullet points below:

- We know one point within the region of desired integration: the user-submitted vacuum specified by an SLHA file.

- Akin to the hyperrectangle formulation of Eq. (5.20), we can find one-dimensional boundaries to our integration region, relative to our initial point. We save these one-dimensional bounds for future use.

- We partition the 31-dimensional parameter space into two-dimensional slices containing the "origin" (the original SLHA-supplied vacuum). There are $\binom{31}{2} = 465$ such slices, and each of these slices are bounded in each perpendicular direction by the respective one-dimensional bounds of that slice, obtained previously. We then sample from the appropriate distributions within these slices or within the whole parameter space to refine the Monte Carlo integration estimate of Δ_{SN}.

  - In practice, for some points of the Monte Carlo integration routine, we can start by randomly sampling two integers uniformly between 1 and 31, including these endpoints. These will index two of the 31 parameters in our space, allowing us to select a random two-dimensional slice of our large parameter space. From this random slice, a planar region

exists that is roughly bounded by the individual one-dimensional limits obtained from the user-submitted file and contains the user-supplied vacuum. This two-dimensional region then can be sampled uniformly to find a new vacuum to test for inclusion in the Monte Carlo integrator. If the relevant conditions are satisfied (EWSB, CCB, and ABDS), then the value is added into the Monte Carlo integrator – otherwise, the Monte Carlo integrator effectively adapts the integration region, refining it according to this conditional sampled failure.

  - The sampled region contains the original vacuum by construction and approximately contains the desired region of integration within the random slice.

- This process is iterated until some specified level of convergence in the integral between successive iterations is reached.

We perform this integration with a Monte Carlo integration technique using a "semi-stratified" importance sampling mechanism, where semi-stratified refers to an alternation between sampling the entire parameter space and sampling slices, as described above. In practice, this means we sample points from each of the slices of our parameter space according to the probability densities of the points in these planes, which are easily computable since the parameters are independently distributed with known densities. Since the sampling distribution matches the integrand we are approximating the integral of, this is an example of ideal importance sampling, or self-normalized importance sampling. The integral

approximation for a scalar-valued vector function $f_S(\vec{x})$ over a region S contained in a larger region R involves N sample points $\vec{x}_1, \ldots, \vec{x}_N$, each drawn from R with the selection distribution $f(\vec{x})$. But the target probability density $f_S(\vec{x})$ simply consists of a probability density function very similar to $f(\vec{x})$ convolved with a binary indicator function θ indicating the region S within R. With this nearly optimal choice in selection distribution, the integral is approximated as

$$\begin{aligned} I = \int_S f_S(\vec{x})\, d\vec{x} &\approx \frac{1}{N}\sum_{i=1}^{N} \frac{f_S(\vec{x}_i)}{f(\vec{x}_i)} \\ &\approx \frac{1}{N}\sum_{i=1}^{N} \left(\begin{cases} 1 & \text{if } \vec{x}_i \in S \\ 0 & \text{otherwise} \end{cases} \right) \\ &= \frac{n_S}{N}. \end{aligned} \tag{5.22}$$

In other words, with this choice of Monte Carlo integrator, we can approximate the integrals of the densities in Δ_{SN} as a the number of vacua n_S satisfying the conditions of θ, divided by the total number of vacua, N, scanned in the scanning region. This is in alignment with the definition of stringy naturalness we began with, so this lends credence to this selection of a Monte Carlo integrator while simultaneously approximately minimizing the variance of our approximation.

Thus, using this careful Monte Carlo simulation and integrator, we approximate Δ_{SN} more rigorously than in Eq. (5.20) as

$$\begin{aligned} \Delta_{\text{SN}} &\approx \frac{n_{\theta,A}}{N_A} \\ &= \frac{n_{\theta,\text{tot}} N_A}{n_{\theta,A} N_{\text{tot}}}, \end{aligned} \tag{5.23}$$

where $N_{\rm A}$ is the total number of vacua scanned in a hyperrectangle approximately bounding the ABDS region, and $n_{\theta,A}$ is the number of vacua scanned in $N_{\rm A}$ satisfying EWSB, no-CCB, and ABDS conditions.

To assist with stability of the Monte Carlo integrator's convergence on a solution, as well as protecting its sensitivity to outliers in the limit of large N, a smooth relative error cutoff may be used involving a simple moving average of the integral approximation across the iterations $\{N-k, N-k+1, \ldots, N-1, N\}$, where this moving average is represented by the function $M(I_{N-k}, \ldots, I_N, k)$:

$$\epsilon > \frac{|M(I_{N-k}, \ldots, I_{N-1}, I_N, k) - I_N|}{I_N}. \tag{5.24}$$

This condition determines the convergence and termination of the iterative approximation. Good choices for ϵ may be $\epsilon = 10^{-3}$ or $\epsilon = 10^{-6}$, though exact analyses with these are left for a future work. Smaller values of epsilon would require a (potentially significantly) greater number of sample points N for an accurate evaluation. In practice, we take $k = 100$ to ensure adequate smoothing of data based on empirical observation obtained during the simulation.

5.3.3 Yukawa and gauge couplings

Note that so far, little has been mentioned regarding Yukawa and gauge couplings in our systematic landscape scans. One might naïvely think that the Yukawas and gauge couplings could be held invariant between different vacua. However, since the MSSM parameter B is considered fundamental in regards to the soft

parameter distributions, $b = B\mu$ is no longer a free parameter to be solved for from the second Higgs minimization condition, Eq. (5.6). Instead b(weak) is fixed by its GUT scale value and corresponding RGE running, meaning $\tan(\beta)$ must no longer be fixed for consistency, but instead must be solved for on a point-by-point basis along with m_Z. Thus, part of the routine in checking the conditions in θ entails finding a simultaneous solution (m_Z, β) to Eqs. (5.5, 5.6). Special care will be taken in a future version of the natLHA software to account for this continual minimization of the scalar potential while we gradually search for the integral bounds appearing in $\Delta_{\rm SN}$.

5.4 An algorithm for stringy naturalness from SLHA outputs

Below is a series of flowcharts demonstrating the algorithm, code-named DSN4SLHA, presented here. For formatting purposes, the algorithm has been split into three flowcharts below. The full flowchart may be seen in the README file at https://github.com/Dmartinez-96/DSN4SLHA.

Though we leave these evaluations of the full integrated $\Delta_{\rm SN}$ measure to a future work and instead just present the mathematical ideas here, in the next chapter we will demonstrate these ideas through the *differential* stringy naturalness measure $\delta_{\rm SN}$.

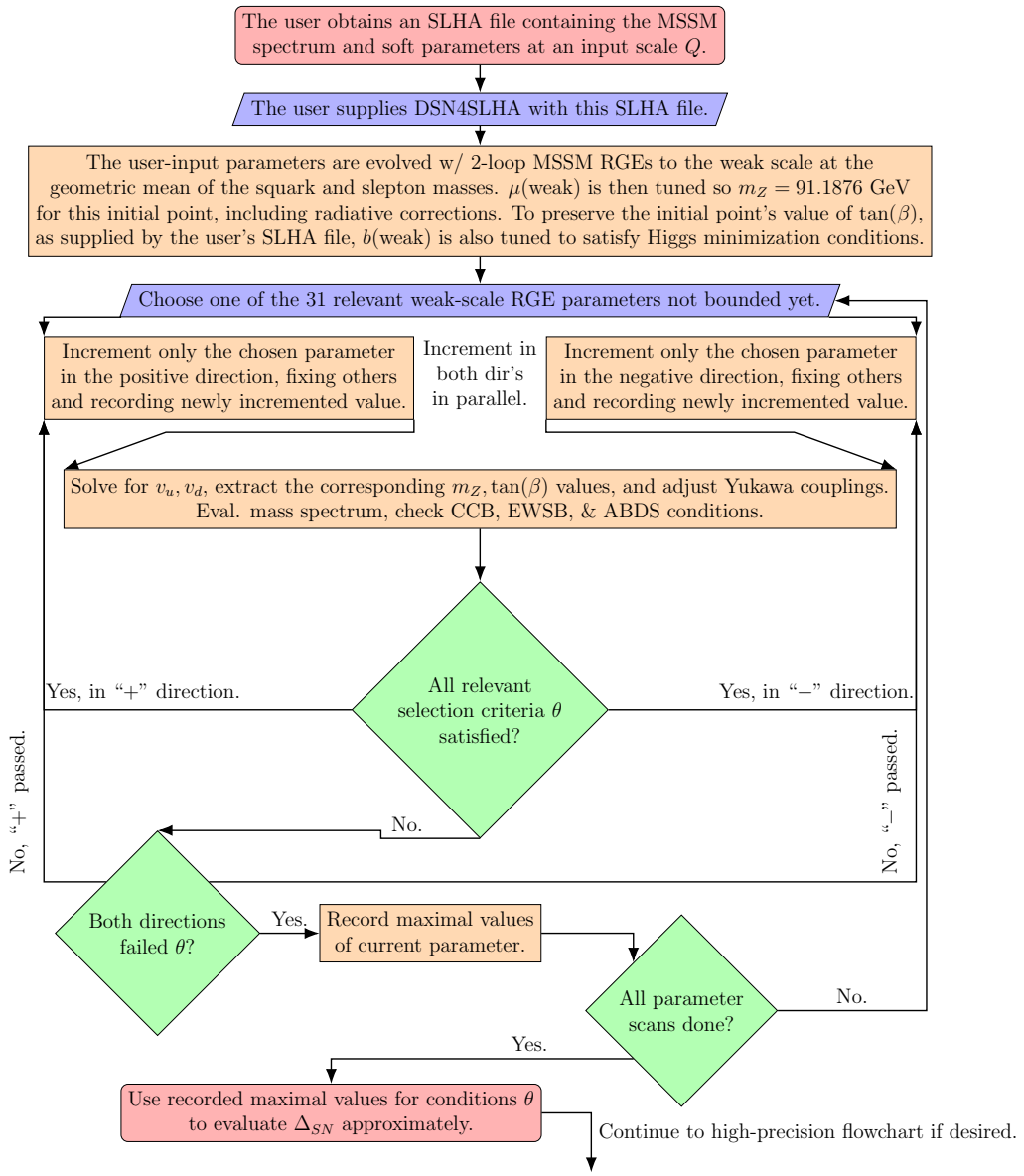

Figure 5.3: A flowchart describing the approximate, P_μ-esque derivation of Δ_{SN} as in Eq. (5.20).

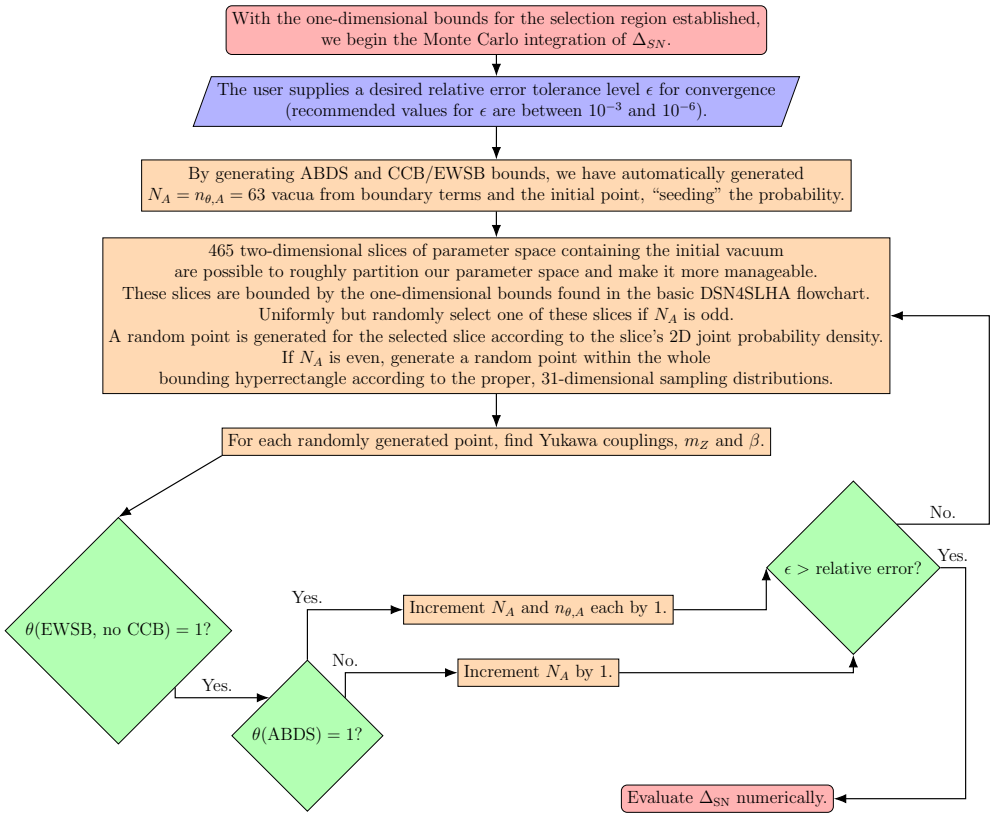

Figure 5.4: A flowchart describing the Monte Carlo integration with stratified importance sampling to approximate Δ_{SN} as Eq. (5.23). This method is amenable to parallelization, adding the results for the n's and N's from independent Monte Carlo integrators running in parallel to speed up computations. A combination of stratified importance sampling from the 2D slices with full-space importance sampling helps adequately cover this high-dimensional space.

Chapter 6

Results and discussion

6.1 Surveying $\delta_{\rm SN}$ for SUSY models on the landscape

Below we survey some SUSY models on the string landscape and their respective $\delta_{\rm SN}$ values, as determined by Eq. (5.21). The results are presented for an example BM point of each model, as generated by SoftSUSY v4.1.17 [119, 203, 204, 205].

Model	$\Delta_{\rm EW}$	$\delta_{\rm SN}$	$dN_{\rm vac}/dN_{\rm vac}(RNS)$
CMSSM	2367.4	7.2174	$6.912 \cdot 10^{-2}$
G_2-MSSM	17045	8.3578	$5.003 \cdot 10^{-3}$
Mini-Split ($\tilde{w}$LSP)	$2.4210 \cdot 10^{6}$	10.056	$1.002 \cdot 10^{-4}$
PeV SUSY	$6.1433 \cdot 10^{6}$	10.920	$1.371 \cdot 10^{-5}$
Spread ($\tilde{w}$LSP)	$3.5753 \cdot 10^{6}$	11.140	$8.260 \cdot 10^{-6}$
Mini-Split ($\tilde{h}$LSP)	$5.9054 \cdot 10^{8}$	12.727	$2.138 \cdot 10^{-7}$
Spread ($\tilde{h}$LSP)	$5.2311 \cdot 10^{10}$	14.889	$1.472 \cdot 10^{-9}$
HS-SUSY	$2.42100 \cdot 10^{6}$	10.058	$9.977 \cdot 10^{-9}$
Split SUSY	$4.6581 \cdot 10^{12}$	16.866	1.552×10^{-11}
RNS	15.761	6.057	1

Table 6.1: A survey of some unnatural and natural SUSY models along with some examples of the stringy naturalness measure $\Delta_{\rm SN}$ and electroweak naturalness measure $\Delta_{\rm EW}$ from an example BM point in the model. The stringy naturalness measures are calculated using Eq. (5.20). It is assumed in this calculation of $\Delta_{\rm SN}$ that there is a single F-type SUSY-breaking field, leading to a total linear power-law draw on the soft terms. As predicted by our P_μ hypothesis, it is clear that RNS models provide the most stringy natural model amongst our selection of SUSY models.

A robust method for computing the *integrated* vacuum density, which contributes to what we have termed $\Delta_{\rm SN}$, is currently under development. The final version will be released in a future version of natLHA.

However, from just looking at the differential vacuum density contributions

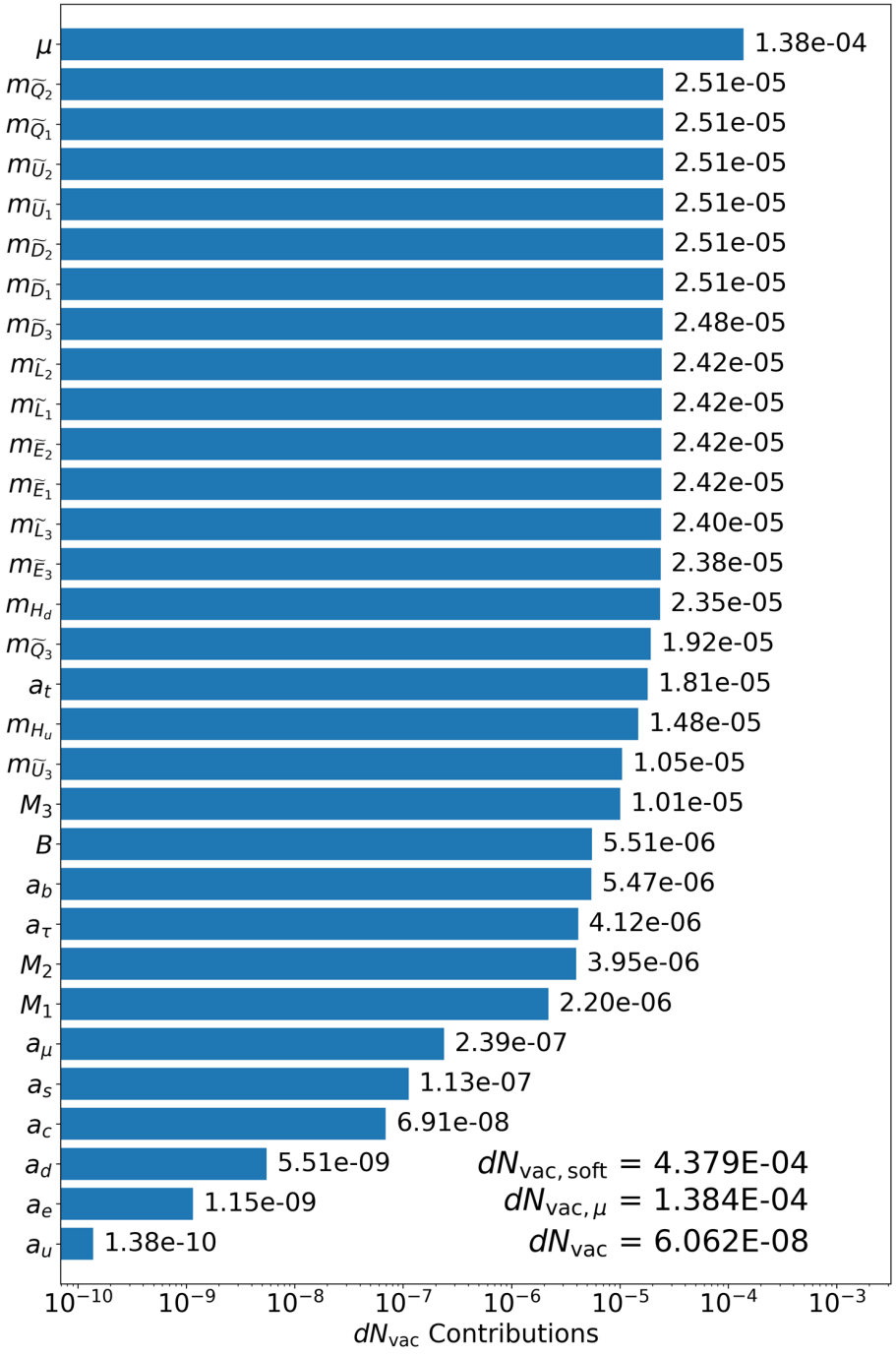

Figure 6.1: Bar chart of Δ_{SN} contributions for the CMSSM model BM point in Table 6.1 with $m_0 = 5$ TeV, $m_{1/2} = 1$ TeV, $A_0 = -8$ TeV, and $\tan(\beta) = 10$ at the input GUT scale of $M_G \simeq 1.4 \cdot 10^{16}$ GeV.

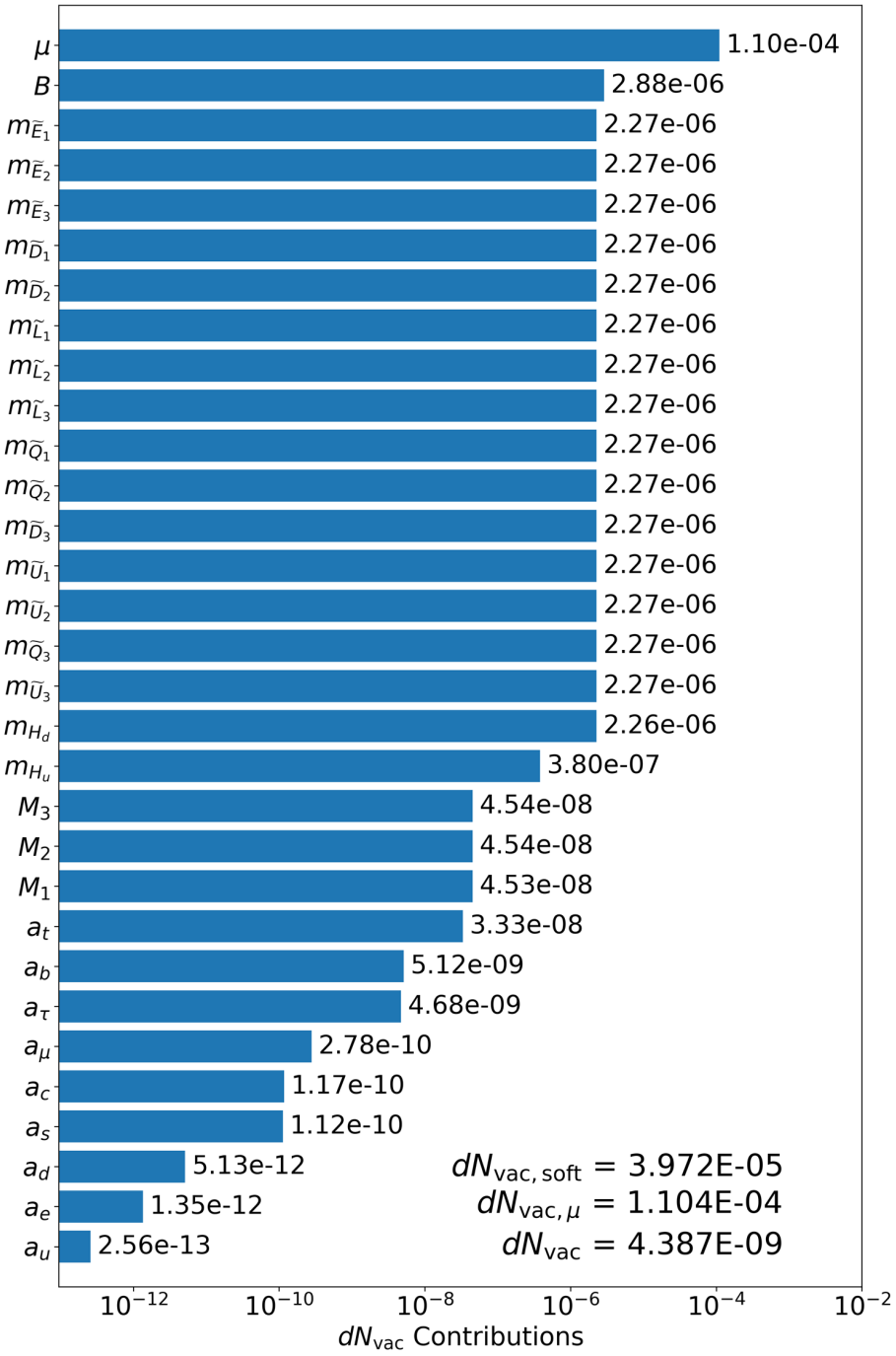

Figure 6.2: Bar chart of Δ_{SN} contributions for the G_2-MSSM model BM point in Table 6.1 with $m_0 = 50$ TeV, $m_{1/2} = 1$ TeV, $A_0 = 0$ TeV, $\mu = 1$ TeV, $m_A(\text{pole}) = 50$ TeV, and $\tan(\beta) = 10$ at the input GUT scale of $M_G \simeq 1.5 \cdot 10^{16}$ GeV.

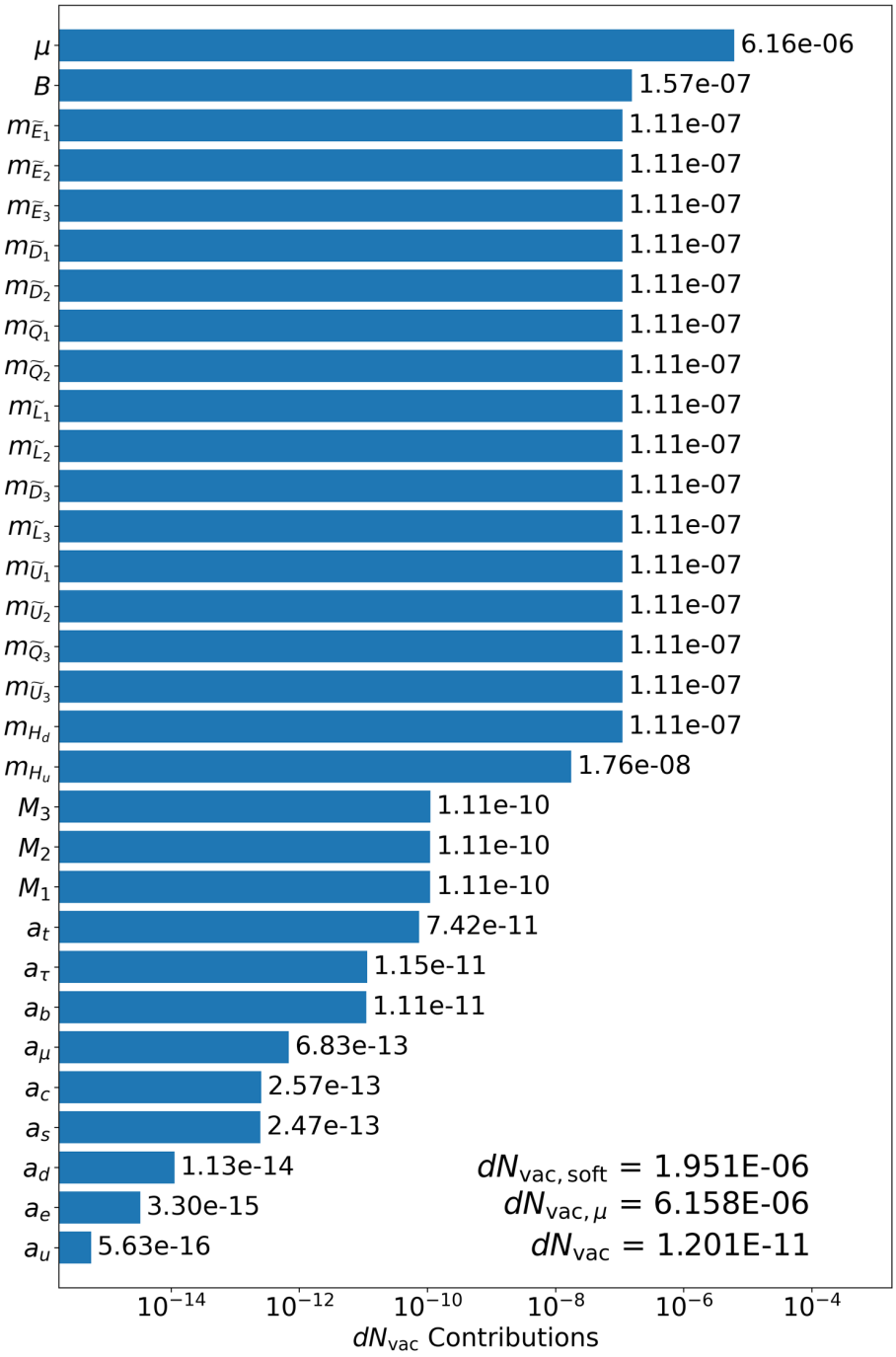

Figure 6.3: Bar chart of Δ_{SN} contributions for the PeV-SUSY model BM point in Table 6.1 with $m_0 = 1$ PeV, $m_{1/2} = 1$ TeV, $A_0 = 0$ TeV, $\mu = 1$ TeV, $m_A(\text{pole}) = 1$ PeV, and $\tan(\beta) = 10$ at the input SUSY scale of $M_s = 1$ PeV.

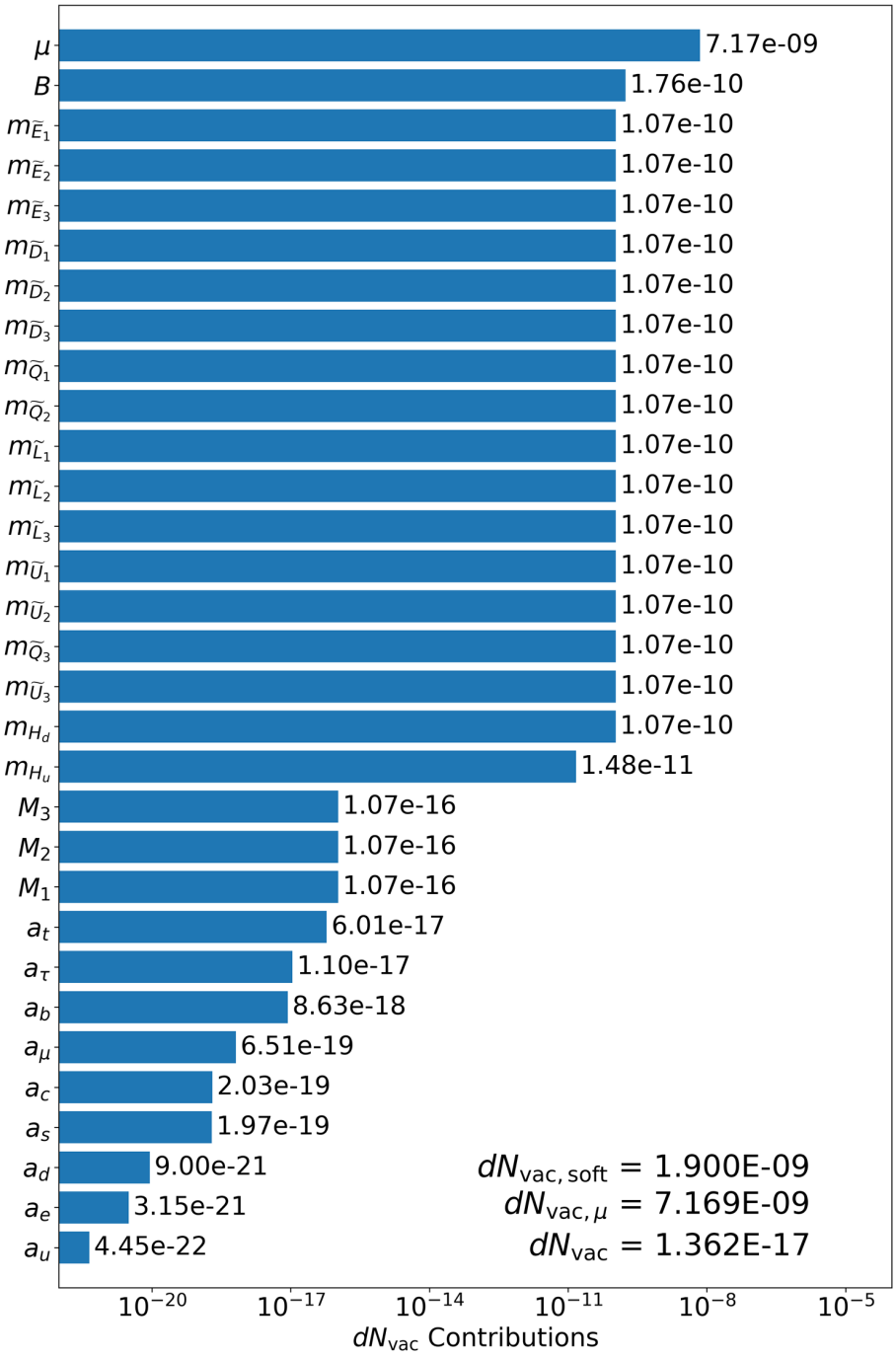

Figure 6.4: Bar chart of Δ_{SN} contributions for the Split SUSY model BM point in Table 6.1 with $m_0 = 100$ PeV, $m_{1/2} = 1$ TeV, $A_0 = 0$ TeV, $\mu = 1$ TeV, $m_A(\text{pole}) = 100$ PeV, and $\tan(\beta) = 10$ at the input SUSY scale of $M_s = 100$ PeV.

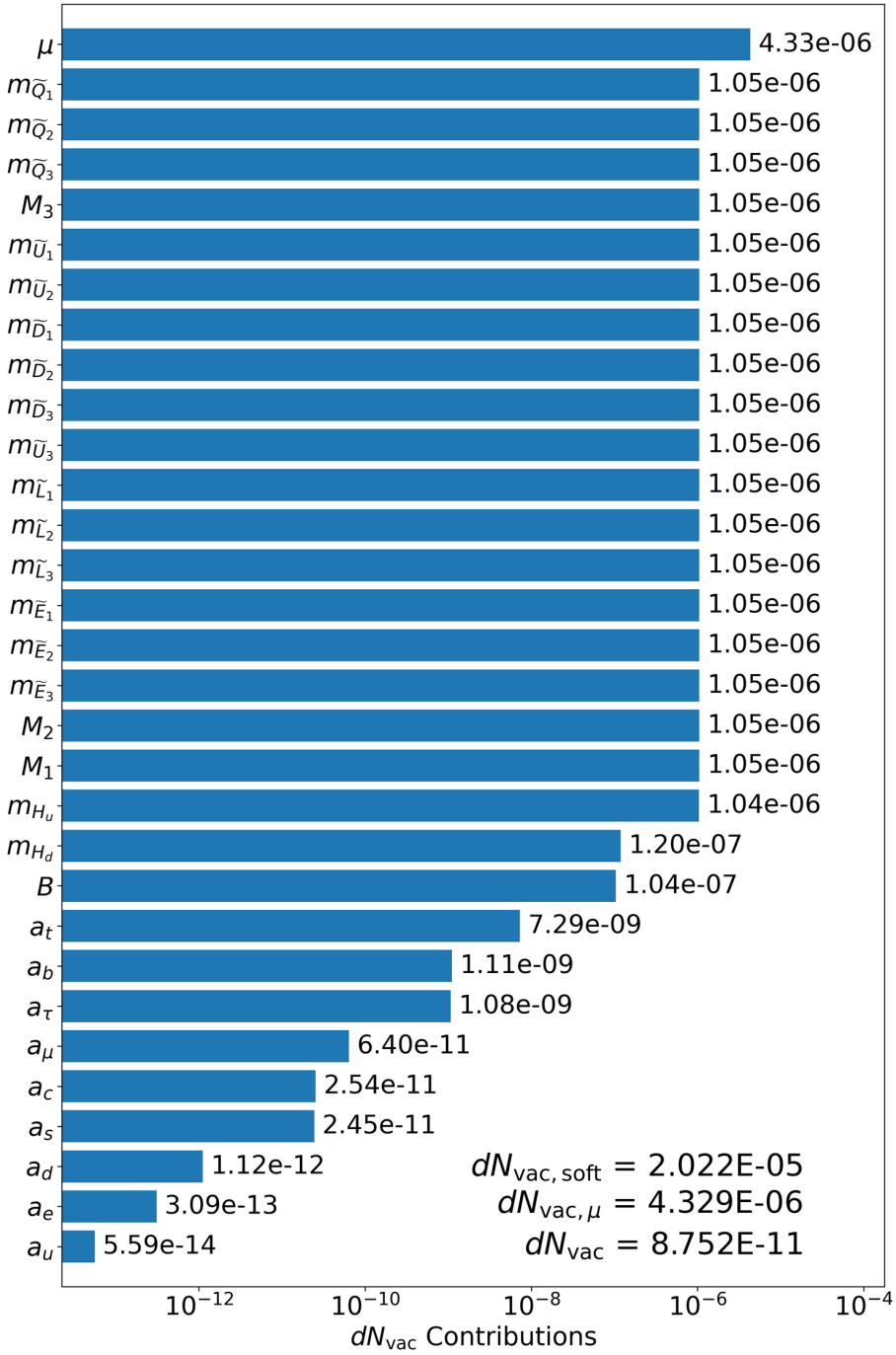

Figure 6.5: Bar chart of Δ_{SN} contributions for the HS-SUSY model BM point in Table 6.1 with $m_0 = 100$ TeV, $m_{1/2} = 100$ TeV, $A_0 = 0$ TeV, $\mu = 100$ TeV, $m_A(\text{pole}) = 100$ TeV, and $\tan(\beta) = 10$ at the input GUT scale of $M_G \simeq 4.1 \cdot 10^{17}$ GeV.

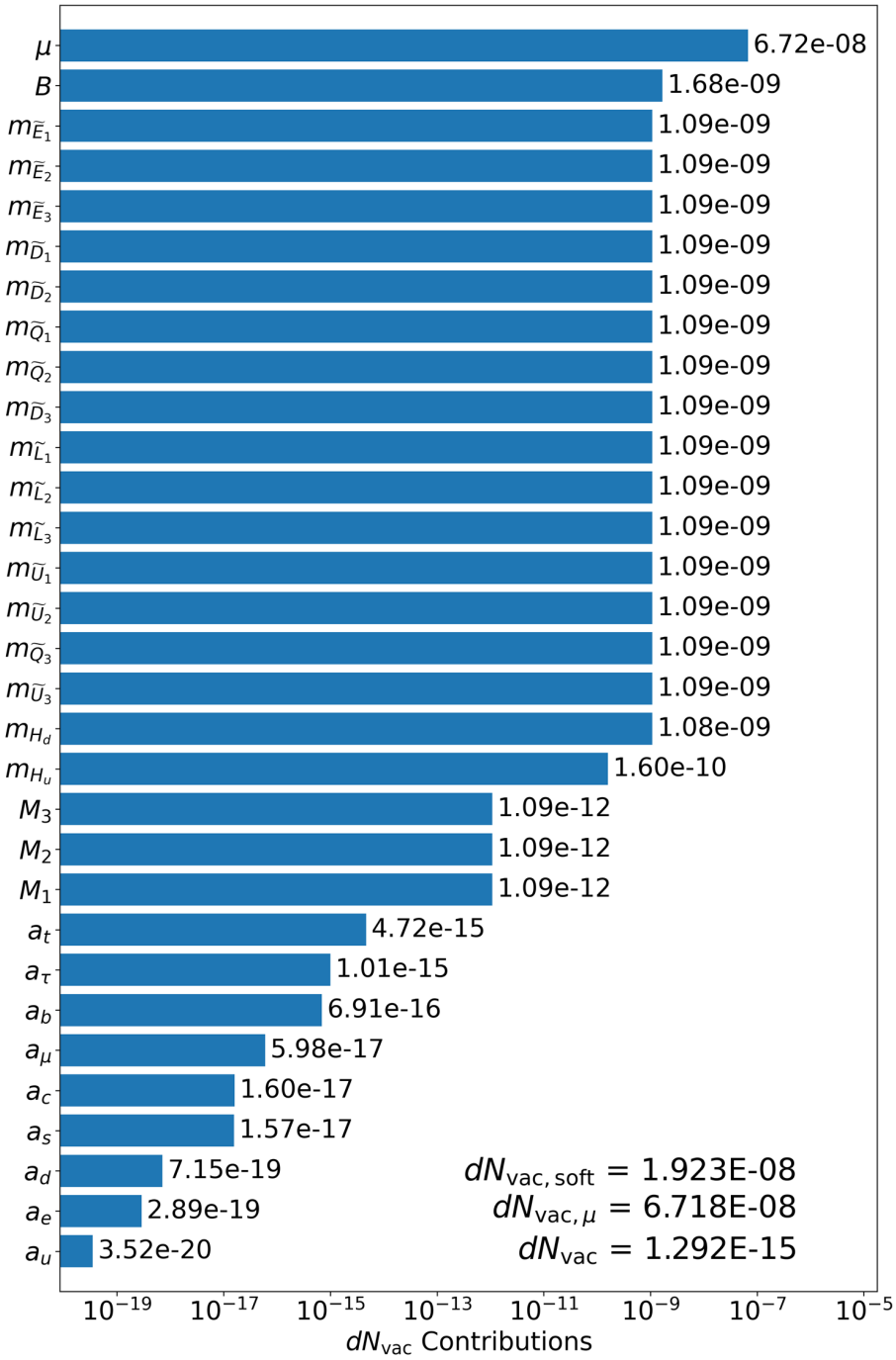

Figure 6.6: Bar chart of Δ_{SN} contributions for the Spread SUSY model with higgsino LSP BM point in Table 6.1 with $m_0 = 100$ PeV, $m_{1/2} = 100$ TeV, $A_0 = 0$ TeV, $\mu = 100$ TeV, $m_A(\text{pole}) = 100$ PeV, and $\tan(\beta) = 10$ at the input SUSY scale of $M_s = 100$ PeV.

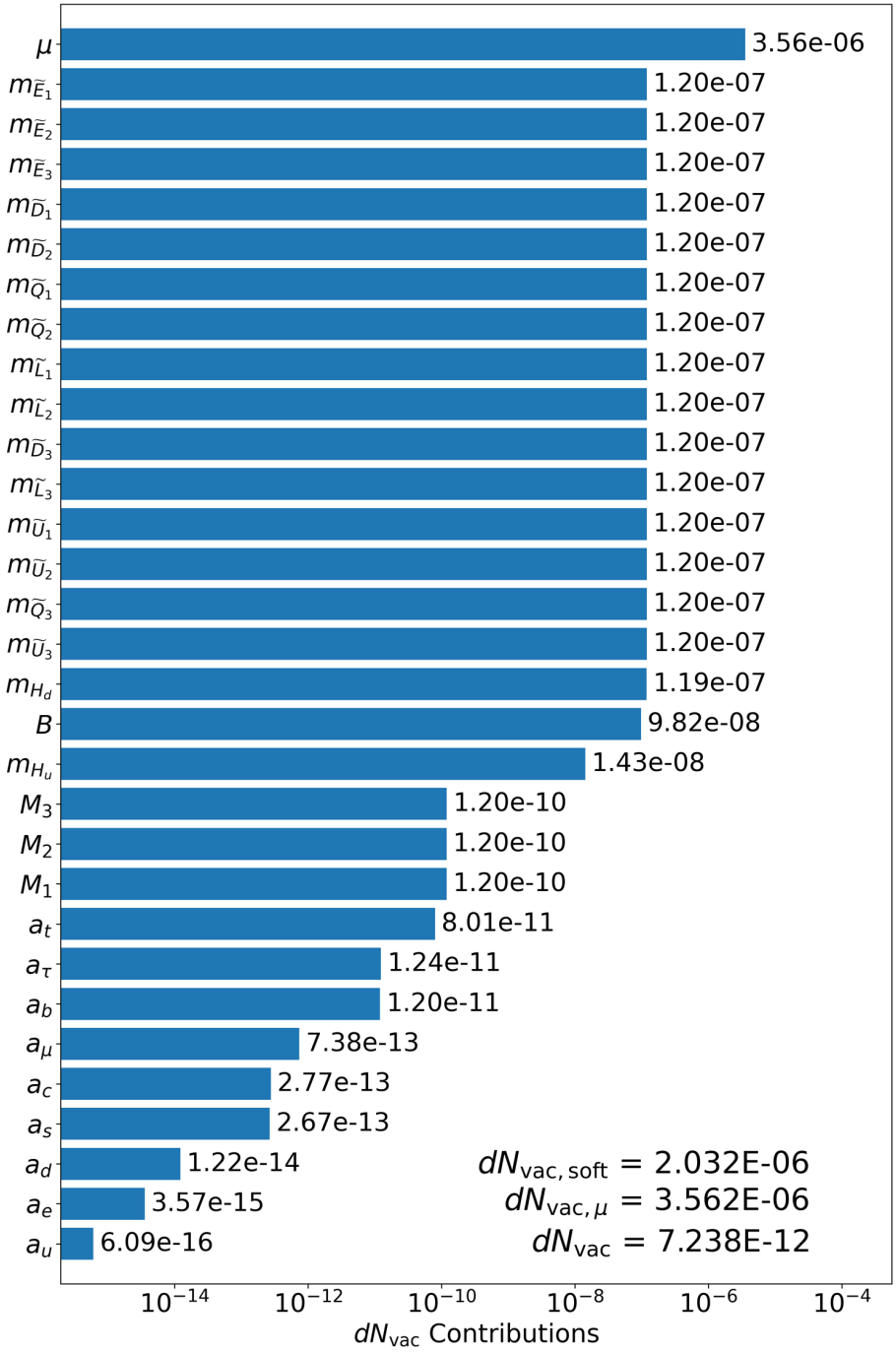

Figure 6.7: Bar chart of Δ_{SN} contributions for the Spread SUSY model with wino LSP BM point in Table 6.1 with $m_0 = 1$ PeV, $m_{1/2} = 1$ TeV, $A_0 = 0$ TeV, $\mu = 100$ TeV, $m_A(\text{pole}) = 1$ PeV, and $\tan(\beta) = 10$ at the input SUSY scale of $M_s = 1$ PeV.

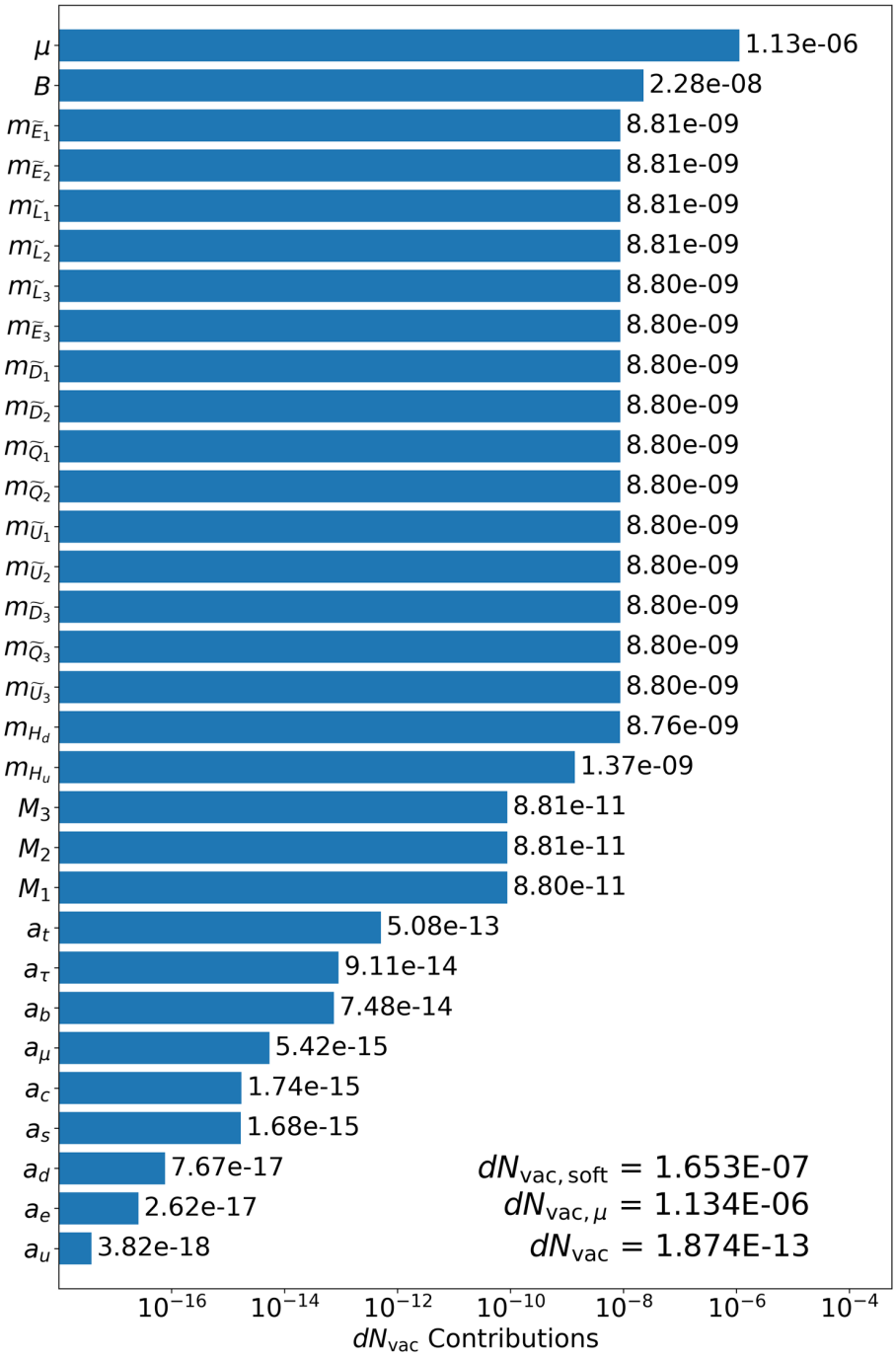

Figure 6.8: Bar chart of Δ_{SN} contributions for the Mini-Split SUSY model with higgsino LSP BM point in Table 6.1 with $m_0 = 100$ TeV, $m_{1/2} = 10$ TeV, $A_0 = 0$ TeV, $\mu = 1$ TeV, $m_A(\text{pole}) = 100$ TeV, and $\tan(\beta) = 10$ at the input GUT scale of $M_G \simeq 4.4 \cdot 10^{17}$ GeV.

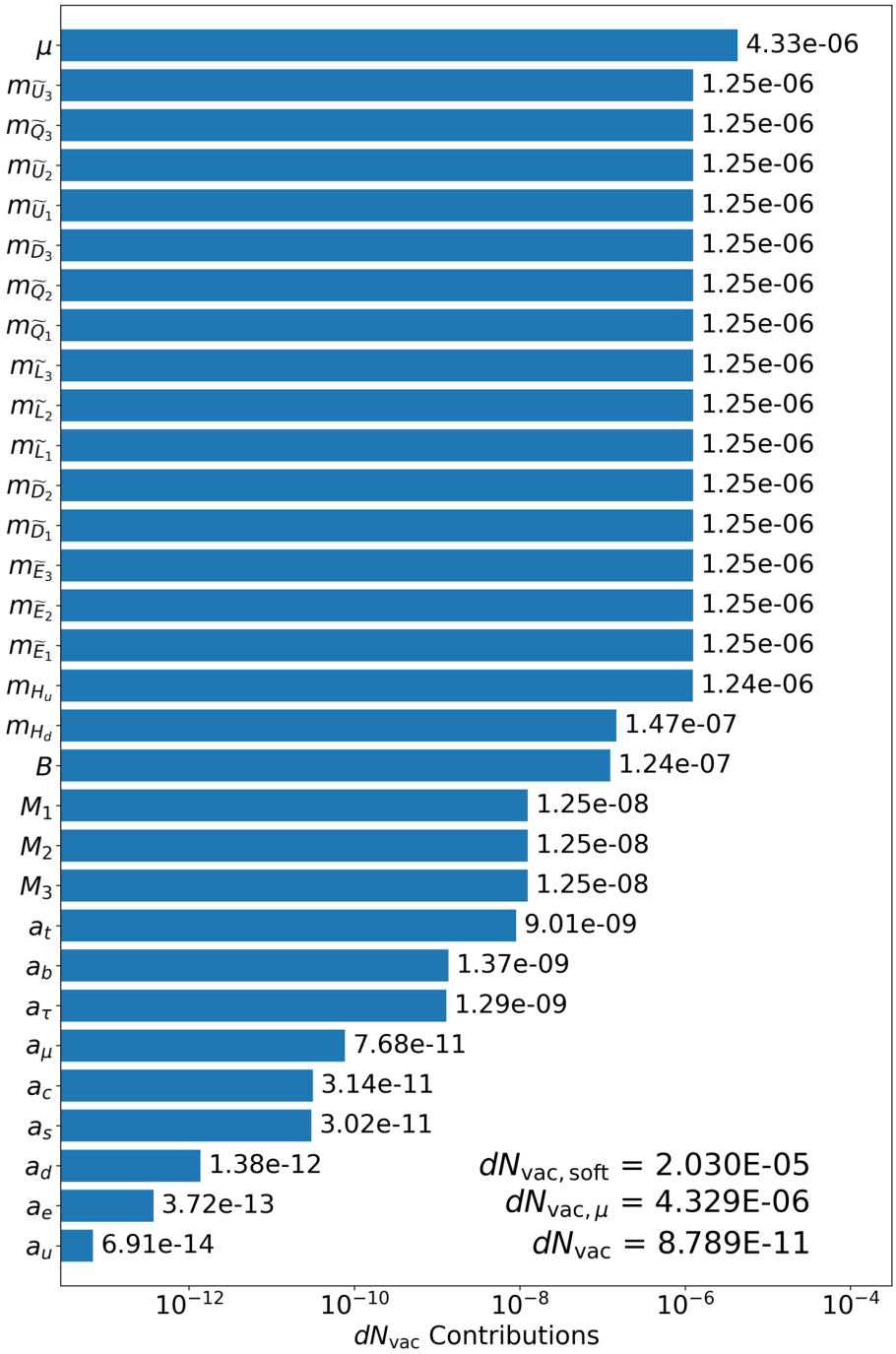

Figure 6.9: Bar chart of Δ_{SN} contributions for the Mini-Split SUSY model with wino LSP BM point in Table 6.1 with $m_0 = 100$ TeV, $m_{1/2} = 1$ TeV, $A_0 = 0$ TeV, $\mu = 100$ TeV, $m_A(\text{pole}) = 100$ TeV, and $\tan(\beta) = 10$ at the input GUT scale of $M_G \simeq 3.0 \cdot 10^{17}$ GeV.

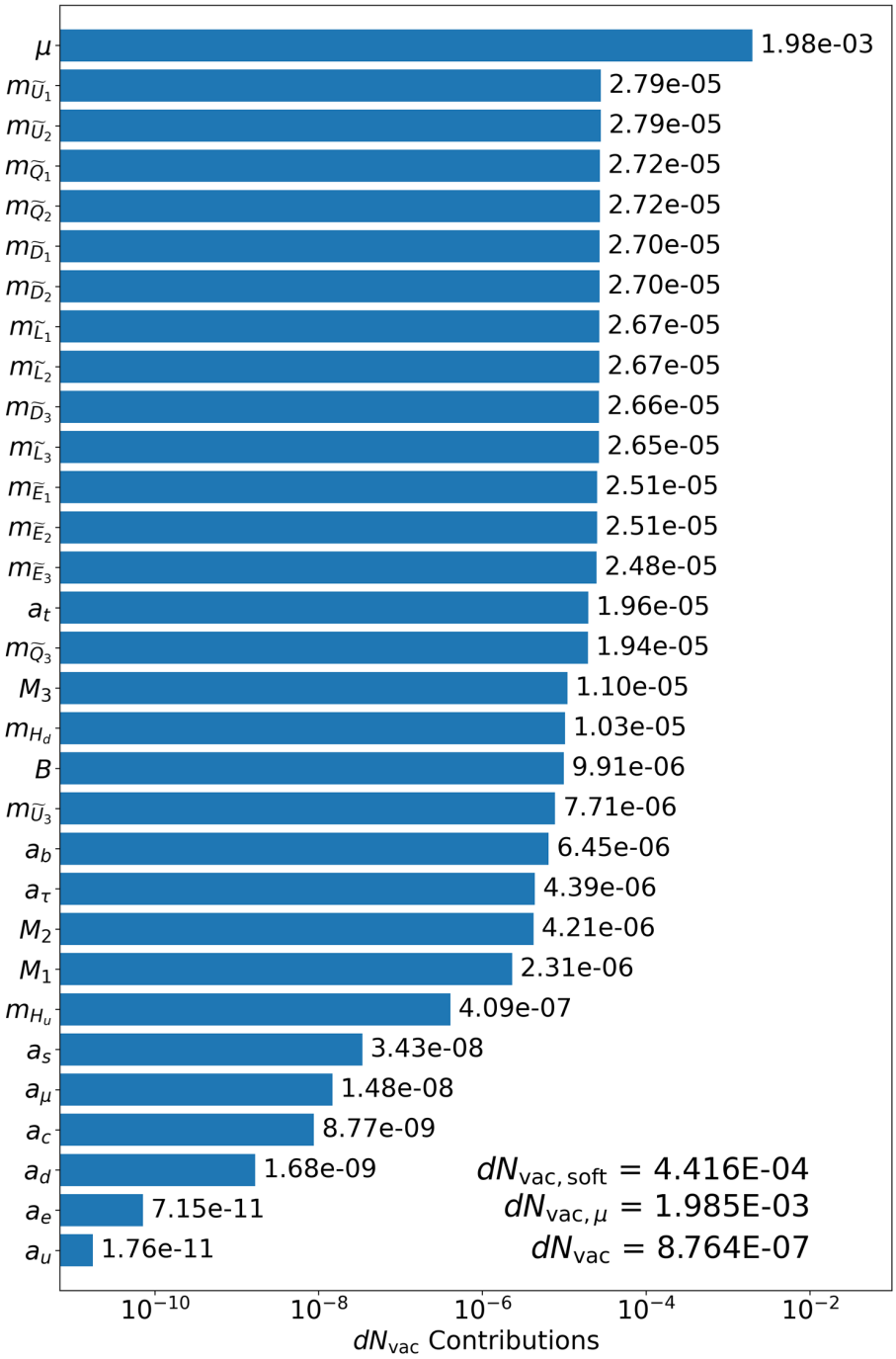

Figure 6.10: Bar chart of Δ_{SN} contributions for the RNS (NUHM2) model BM point in Table 6.1 with $m_0 = 5$ TeV, $m_{1/2} = 1$ TeV, $A_0 = -8$ TeV, $\mu = 200$ GeV, $m_A(\text{pole}) = 2$ TeV, and $\tan(\beta) = 10$ at the input GUT scale of $M_G \simeq 1.7 \cdot 10^{16}$ GeV.

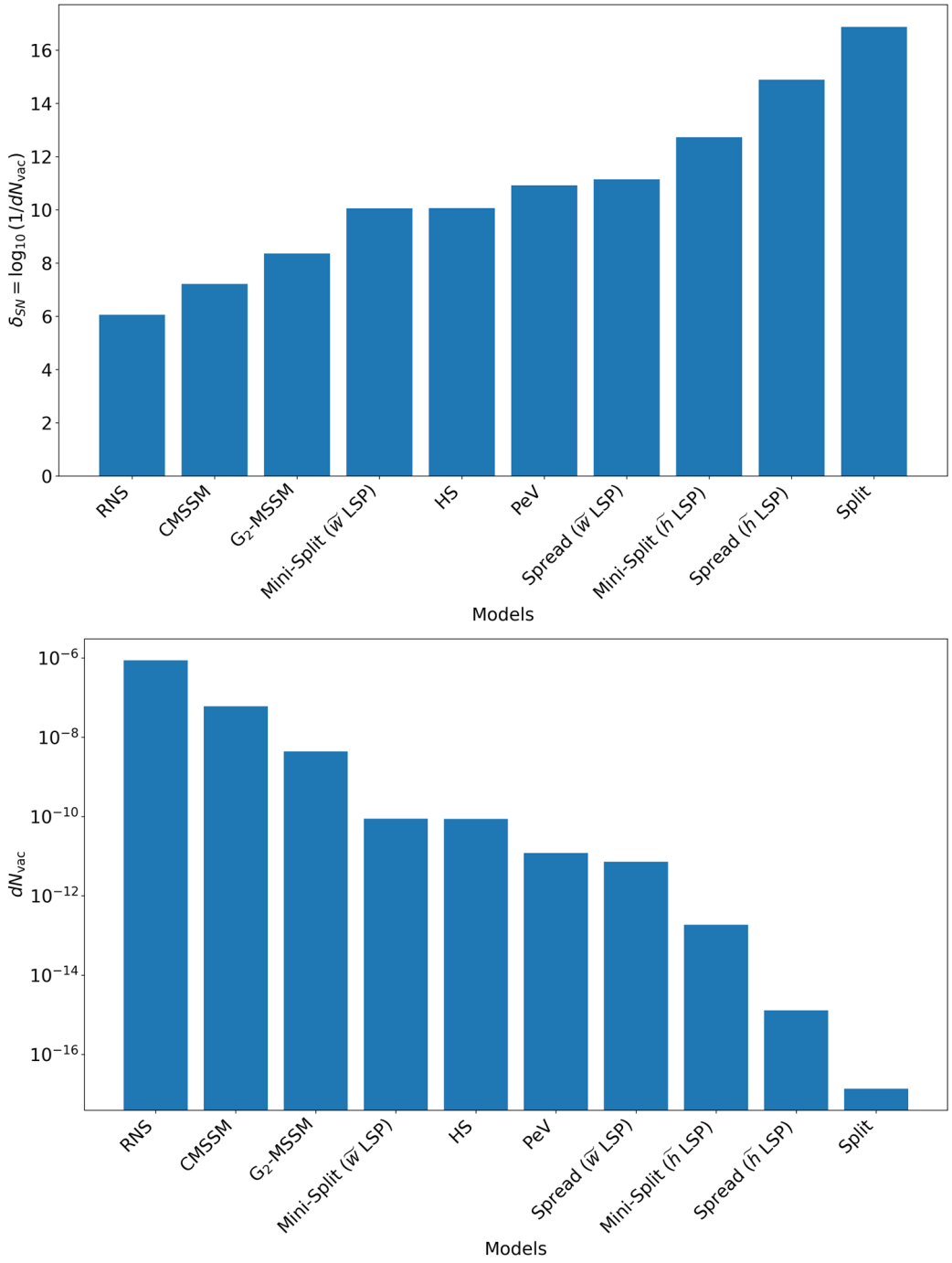

Figure 6.11: Bar charts summarizing the contributions to (a) the differential stringy naturalness measure $\delta_{\rm SN}$ and (b) the differential vacuum density measure $dN_{\rm vac}$, exemplified in Figs. (6.1 - 6.10).

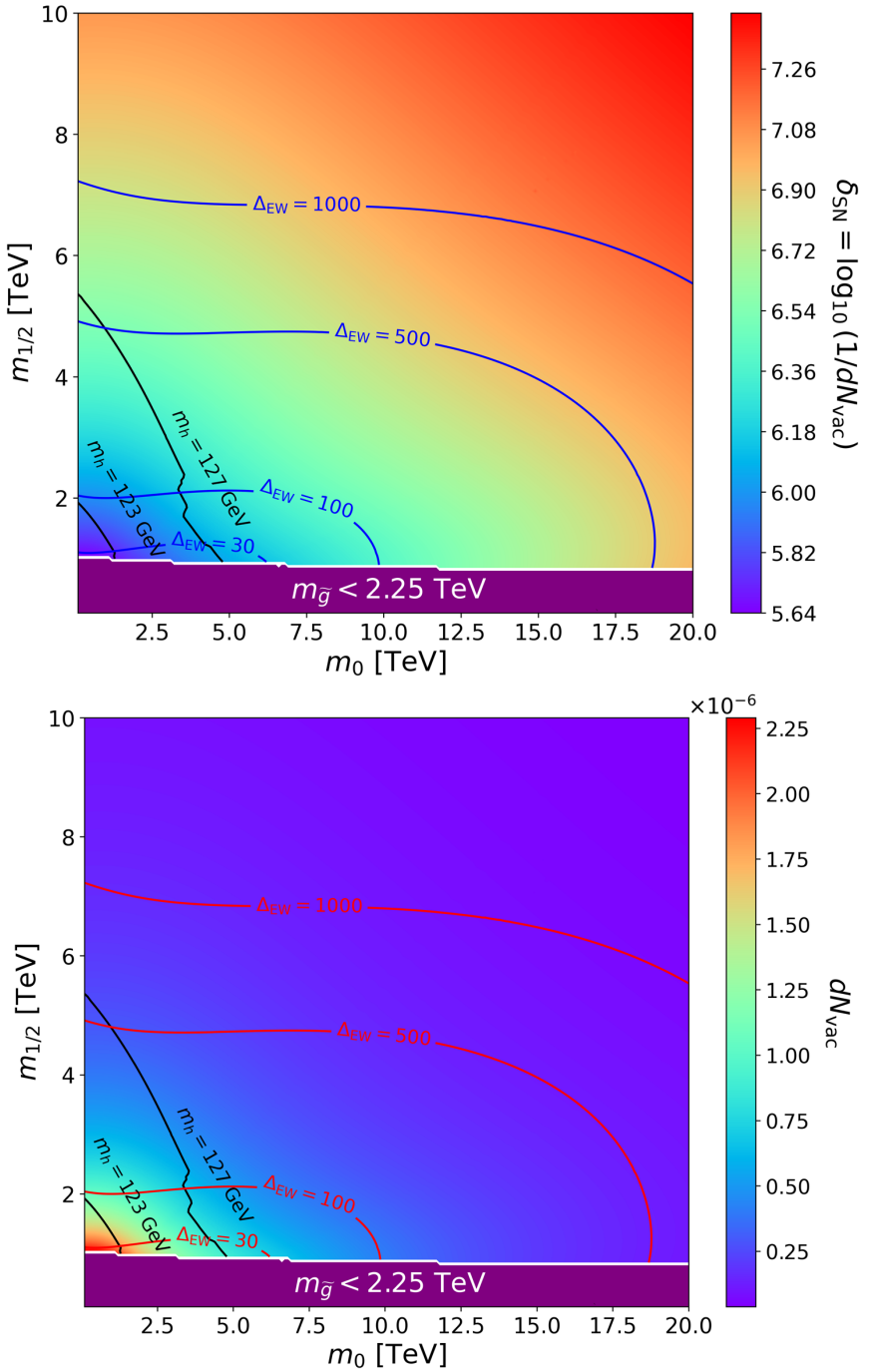

Figure 6.12: Stringy naturalness plane scans from $m_0 = 100$ GeV to 20 TeV and $m_{1/2} = 100$ GeV to 10 TeV for the NUHM2 parameter space, where $\mu = 200$ GeV, $m_A(\text{pole}) = 2$ TeV, $A_0 = -1.6m_0$, and $\tan(\beta) = 10$. In subfigure *a*), the differential stringy naturalness measure δ_{SN} (Eq. (5.21)) is plotted. In subfigure *b*), the differential vacuum density dN_{vac} (Eqs. (5.14,5.17)) is plotted. Note the significantly larger densities (lower δ_{SN}) when compared to an unnatural model, like the CMSSM, in Fig. 6.13 or Table 6.1.

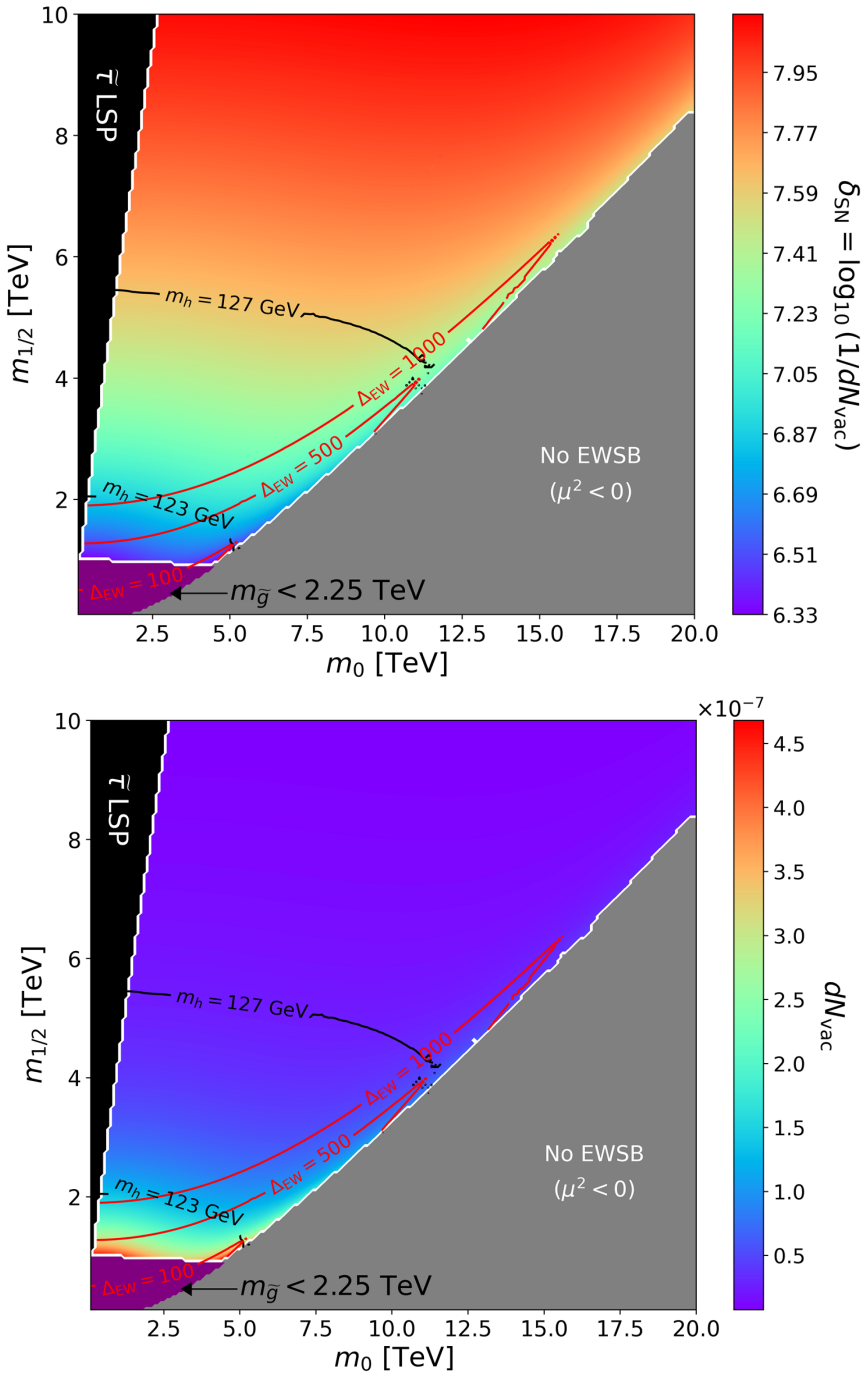

Figure 6.13: Stringy naturalness plane scans from $m_0 = 100$ GeV to 20 TeV and $m_{1/2} = 100$ GeV to 10 TeV for the CMSSM parameter space, where $A_0 = 0$ and $\tan(\beta) = 10$. In subfigure *a*), the differential stringy naturalness measure $\delta_{\rm SN}$ (Eq. (5.21)) is plotted. In subfigure *b*), the differential vacuum density $dN_{\rm vac}$ (Eqs. (5.14, 5.17)) is plotted.

above, our hypothesis of RNS stringy naturalness is strongly supported. First, consider the μ contributions to these measures. With our P_μ analysis, we noted that due to the intense fine-tuning of μ against $m_Z^{\rm PU}$ within the ABDS window, then larger values of μ result in smaller values of P_μ. Similarly, here we see that *smaller* values of μ give a *larger* contribution to the differential vacuum density measure. Conversely, *larger* values of μ *suppress* the differential vacuum density measure. So, combined with our knowledge that finetuning constrains the volume of our μ parameter space in order to produce vacua in the ABDS window, it is immediately clear that for finetuned models, integrating the differential vacuum density will produce *smaller* density measures than in the case of RNS, where finetuning is low. This comes from two factors:

- In integrating a given point within the domain of integration, the size of the individual contribution ($\delta_{\rm SN}(\mu)$) from that point is *inversely proportional* to the finetuning of the μ parameter.

- The "width" of the domain of integration is *also inversely proportional* to this level of finetuning.

Hence, adding up tiny numbers over a tiny interval (as in finetuned models) results in a lower integration value compared to adding up larger numbers over a larger interval (as in RNS).

Similarly, as the scale of SUSY parameters (and thus the scale of SUSY breaking) rises, the same idea arises. If a given soft parameter p has high finetuning at the weak scale, then it does not afford much "wiggle room" in

parameter space to accomodate ABDS vacua. Additionally, since

$$dN_{\text{vac, soft}} \sim \frac{2(n+1)}{m_{\text{SUSY}}^2}\left[\sum_{i=1}^{30}|p_i|d|p_i|\right],$$

then clearly larger values of m_{SUSY}^2 also suppress the differential density. Thus, the same logic applies in this sector: in finetuned models, we are adding up tiny numbers over a tiny interval, giving a tiny result (few vacua). In RNS, we are adding up larger numbers over a larger interval, giving a larger result (more vacua). Thus, these results seem consistent with our hypothesis on stringy naturalness and RNS.

Chapter 7

Conclusions

To conclude this dissertation, we offer some summarizing remarks from the preceding chapters. As bounds for supersymmetric masses increase from LHC findings (or lack thereof), the Little Hierarchy Problem describing the burgeoning gap between the known weak scale and the unknown SUSY scale has become a thorny issue in the side of the particle physics frontier community. It is a commonly held belief that if supersymmetry exists, then it must be extremely finetuned to accommodate these experimental bounds.

Here, we have presented many arguments on why this is truly not an issue, and how radiative natural supersymmetry with practical naturalness is not only consistent with our current understanding of experimental data, but also predicts supersymmetry to lie just beyond the reach of current colliders. Many alternative hypotheses have been proposed in the literature to attempt to address this Little Hierarchy Problem in alternative ways, as in Chapter 3. However, these often require mathematical gymnastics to remain consistent with current experimental data, and each come with their own slew of issues that remain to be explained, such as charged LSPs, difficulty accommodating the correct Higgs mass, or vacuum instability.

If we forego the concept of practical naturalness, then there are still many different realizable but highly finetuned versions of supersymmetry are still experimentally viable, as were outlined in Chapter 2. Even the Standard Model alone

may still be a sufficient EFT model, if we permit an extreme degree of finetuning. However, when put into the context of the string landscape, we demonstrated in the preceding section and in Chapters 4, 5 that this is *extremely* unlikely to be the case, and in fact, that RNS is exponentially more probable to emerge from the string landscape and describe a universe with chemistry such as our own, compared to these finetuned supersymmetric or SM theories.

Some tasks for future work are listed below:

- For stringy naturalness, the differential vacuum density measures provided in Chapter 5 should be integrated carefully. This entails constructing a numerical routine that dynamically searches for the bounds of integration in each parameter p while ensuring proper vacuum minimization at loop-level.

- The integration region will generally be non-rectangular, introducing nonlinear correlations between variables at the boundaries of the EWSB-compliant, no CCB, and ABDS-compliant regions of parameter space. This should be addressed for accuracy in the future. For example, after rectangular bounds are obtained as in the previous point, one may perform a Monte-Carlo simulation and sampling on the hyperrectangle of parameter space selected to obtain a more accurate measure of the integrated vacuum density.

- In each step of integrating the differential vacuum density, threshold corrections may shift gauge and Yukawa coupling values. The threshold corrections involve the evaluation of various Passarino-Veltman functions that depend on the soft SUSY breaking parameters, as well as the value of m_Z and

m_W, which are shifting from vacuum to vacuum in our scans here. These effects should be incorporated, but are in general higher-order effects that, within the regime of perturbativity, should be smalller than the leading-order analyses presented here. This enhancement should be carefully balanced against the idea of "predictivity" to ensure the results are mathematically sound but also physically viable.

- Further efforts can be made to reduce the effect of the renormalization scale (not a physical observable, but rather a parameter introduced to handle infinities arising from loop calculations) on the predicted values of m_Z^{PU}.

- Higher order stabilization conditions – particularly 1-loop conditions for CCB and 2-loop conditions for EWSB – are still lacking from natLHA and may provide some additional "width" to the ABDS windows tested.

- The analyses provided above should be performed on other realizations of supersymmetry, such as GMSB and nAMSB.

- In the SM, we provided an approximate evaluation of the P_μ measure. It may be possible to incorporate other parameters of the SM theory (such as quark and lepton masses) and our ABDS analysis to provide a more thorough evaluation of the relative abundance of SM vacua on the string landscape. This can then be compared to the values obtained from SUSY vacua.

- Connections between our Euclidean interpretation of the SUSY scale and the

original Euclidean interpretation relating to the number of F- and D-type SUSY-breaking fields within a larger theory should be expanded upon.

The next several decades of experimental data will prove to be invaluable in the discovery or elimination of supersymmetry as a viable theory. The arguments presented here are favorable towards its discovery within the context of RNS.

Appendix A

Radiative corrections in the MSSM

A.1 The Higgs scalar potential: an EFT approach

In the effective field theory approach, one may minimize the Higgs field VEV-dependent scalar potential to get constraints and requirements on electroweak symmetry breaking in the MSSM. This effective scalar potential can be subject to loop corrections above its tree-level expression, and generally is written as follows.

$$V(v_u, v_d) = V_{\text{tree}}(v_u, v_d) + \Delta V(v_u, v_d) \tag{A.1}$$

In the minimized vacuum, the tree-level potential V_{tree} can be written in terms of the neutral Higgs fields $h^0_{u,d}$ that obtain non-zero VEVs $v_{u,d}$, soft SUSY-breaking parameters $m^2_{H_{u,d}}$ and b, the superpotential parameter μ, and the SU(2) and U(1) gauge couplings g and g'.

$$\begin{aligned} V_{\text{tree}} = &\left(m^2_{H_u} + \mu^2\right)\left|h^0_u\right|^2 + \left(m^2_{H_d} + \mu^2\right)\left|h^0_d\right|^2 \\ &- b(h^0_u h^0_d + \text{c.c.}) + \frac{g'^2 + g^2}{8}\left(\left|h^0_u\right|^2 - \left|h^0_d\right|^2\right)^2 \end{aligned} \tag{A.2}$$

In the remainder of these appendices, we work in the $\overline{\text{DR}}$' renormalization scheme.

At tree-level, the Higgs minimization conditions correspond to when the derivatives of V_{tree} are equal to zero, together with appropriate stability conditions from Appendix C. At the minimum where these conditions are satisfied appropriately,

the values of the fields h_u^0 and $|h_d^0|$ determine the values of the Higgs VEVs. Through definitions of mass parameters, angles, and with algebraic manipulation, one arrives at the following tree-level minimization conditions.

$$2b = \sin(2\beta)\left(m_{H_u}^2 + m_{H_d}^2 + 2\mu^2\right) \tag{A.3}$$

$$m_Z^2 = \frac{(m_{H_u}^2 - m_{H_d}^2)}{\cos(2\beta)} - (m_{H_u}^2 + m_{H_d}^2 + 2\mu^2) \tag{A.4}$$

Often in the literature, one may see Eq. (A.4) instead expressed in terms of the ratio of the Higgs VEVs, $\tan(\beta) = \frac{v_u}{v_d}$:

$$\frac{m_Z^2}{2} = \frac{m_{H_d}^2 - m_{H_u}^2 \tan^2(\beta)}{\tan^2(\beta) - 1} - \mu^2. \tag{A.5}$$

Alternatively, one can solve for $\tan(\beta) > 0$ in terms of SSB and superpotential parameters as in Eq. (A.6) below.

$$\tan(\beta) = \frac{m_{H_u}^2 + m_{H_d}^2 + 2\mu^2 + \sqrt{(m_{H_u}^2 + m_{H_d}^2 + 2\mu^2)^2 - 4b^2}}{2b} \tag{A.6}$$

A.2 One-loop corrections to the scalar potential

Radiative corrections to the Higgs potential may be particularly important in regards to practical naturalness and proper electroweak symmetry breaking, especially those arising from the stop sector in the MSSM. The tree-level VEV-dependent scalar potential is given in Eq. (A.2). The total, loop-corrected effective

potential may then be expressed as

$$V_{\text{eff}} = V_{\text{tree}} + \Delta V,$$

with ΔV containing loop corrections to the tree-level potential. These loop corrections come from the VEV-dependent masses of the MSSM spectrum at tree-level, in the one-loop case. Higher order corrections typically involve more complicated expressions.

The one-loop correction to the effective potential is given as

$$\begin{aligned}\Delta V_{\text{1-loop}}(v_u, v_d) = \frac{1}{64\pi^2} \sum_i \Bigg[& q_i C_i m_i^4(v_u, v_d)(-1)^{2s_i} \\ & \times (2s_i + 1) \left(\log \left(\frac{m_i^2(v_u, v_d)}{Q^2} \right) - \frac{3}{2} \right) \Bigg],\end{aligned} \tag{A.7}$$

where the sum runs over all SUSY and SM particles whose (tree-level) squared masses $m_i^2(v_u, v_d)$ are a function of the Higgs VEVs v_u and v_d. The scalar potential is evaluated at the renormalization scale Q, as are many of the terms in the expressions in the entirety of the Appendices. Each particle contributes an electric charge factor $q_i = 1$ for uncharged species i and $q_i = 2$ for charged species i. Similarly, each particle contributes a color charge factor $C_i = 1$ for uncolored particles and $C_i = 3$ for colored particles. The spin of particle i is represented by s_i. In the literature, the sum over the spins and masses is called a "supertrace", denoted as

$$\text{STr}(\mathcal{M}^n) = \sum_i (-1)^{2s_i}(2s_i + 1) m_i^n. \tag{A.8}$$

Corrections to the Higgs minimization conditions are calculated from derivatives of the loop-corrected Higgs scalar potential. In practice, this amounts to the following replacements in Eqs. (A.3 - A.6):

$$m_{H_u}^2 \to m_{H_u}^2 + \frac{1}{2v_u}\frac{\partial \Delta V}{\partial v_u}, \qquad m_{H_d}^2 \to m_{H_d}^2 + \frac{1}{2v_d}\frac{\partial \Delta V}{\partial v_d}. \tag{A.9}$$

We denote the correction derivative terms as $\frac{1}{2v_i}\frac{\partial \Delta V}{\partial v_i} \equiv \Sigma_i$ for $i = u, d$. Note that in some instances of the literature, the radiative corrections are instead expressed as $\Sigma_{u,d}^{u,d}$, which exploit the $SU(2)$ symmetry for the derivatives and are defined as

$$\Sigma_{u,d}^{u,d} = \frac{\partial \Delta V}{\partial v_{u,d}^2}.$$

These can be obtained from the expressions presented below through reorganization via the chain rule in calculus. However, it must be noted that for the loop corrections to the second Higgs minimization condition presented in Eq. (A.3), then there exist other corrections of the form

$$\Sigma_u^d = \frac{\partial \Delta V}{\partial v_u \partial v_d}.$$

These must be included to obtain the correct loop-level expressions in this minimization condition, and thus minimize the Higgs potential with the correct value of $\tan(\beta)$. This is not an issue if instead the derivatives are computed with the *linear* Higgs VEVs, as in our definition of the $\Sigma_{u,d}$ terms.

Differentiating Eq. (A.7) yields the expression

$$\Sigma_{u,d} = \frac{1}{32\pi^2} \sum_i \Bigg[q_i C_i (-1)^{2s_i} (2s_i + 1) \times m_i^2 \left(\frac{1}{2v_{u,d}} \frac{\partial m_i^2}{\partial v_{u,d}} \right) \left(\log \left(\frac{m_i^2}{Q^2} \right) - 1 \right) \Bigg] \tag{A.10}$$

The individual contributions

$$\delta_{u,d}(i) \equiv \frac{1}{2v_{u,d}} \frac{\partial m_i^2}{\partial v_{u,d}} \tag{A.11}$$

are listed in the following subsections. The full radiative corrections are then obtained by substituting in the appropriate derivatives to Eq. (A.10) above.

A.2.1 Obtaining the tree-level mass (squared) spectrum

The tree-level mass matrices in the MSSM can be determined using the MSSM Lagrangian, in particular, the soft SUSY breaking sector of the Lagrangian. The parameters herein are numerically determined mostly through the use of the Renormalization Group Equation parameters listed in Appendix B, at a scale where higher order logarithmic corrections may be reduced or minimized. In practice, we often find ourselves obtaining the eigenvalues of a 2×2 matrix $\mathcal{M}^\dagger \mathcal{M} \equiv \mathcal{M}^2$. For each particle in the SM and MSSM spectra, we assume the entries in these mass squared matrices are *real*. For a general 2×2 square matrix of the form

$$\mathcal{M}^2 = \begin{bmatrix} a & b \\ c & d \end{bmatrix},$$

then $\mathcal{M}^2$ will have eigenvalues of the form

$$m^2_{1,2} = \frac{1}{2}\left(a + d \pm \sqrt{(a-d)^2 + 4bc}\right). \tag{A.12}$$

In the remainder of this Appendix, we will denote the lighter mass eigenvalue (the "$-$" expression above) with the subscript index "1", as in m^2_1, whereas the heavier mass eigenvalue (the "$+$" expression above) will be denoted by the subscript index "2", as in m^2_2.

A.2.2 SM particles

Gauge bosons

In the Standard Model sector, we can write the electroweak gauge boson squared masses $m^2_{Z,W}$ in terms of the Higgs VEVs $v_{u,d}$. The Z boson squared mass is given at tree-level as

$$m^2_Z = \frac{(g^2 + g'^2)\, v^2}{2} \tag{A.13}$$

and the tree-level W boson squared mass is

$$m^2_W = \frac{g^2 v^2}{2}. \tag{A.14}$$

The derivatives of these masses entering into Eq. (A.10) are listed below.

$$\delta_u(Z) = \delta_d(Z) = \frac{g^2 + g'^2}{2} \tag{A.15}$$

$$\delta_u(W) = \delta_d(W) = \frac{g^2}{2} \tag{A.16}$$

Quarks and leptons

At tree-level, the quarks and leptons depend on Yukawa couplings and the Higgs VEVs $v_{u,d}$. For up-type quarks, denoted here as U_g where $g = 1, 2, 3$ indexes the generation of the quark, the tree-level squared mass is given by

$$m_{U_g}^2 = y_{U_g}^2 v_u^2. \tag{A.17}$$

For example, $m_{U_3}^2$ corresponds to the tree-level squared mass of the top quark. For down-type quarks, denoted here as D_g with generation index g, the tree-level squared mass is given by

$$m_{D_g}^2 = y_{D_g}^2 v_d^2. \tag{A.18}$$

Lastly, for Standard Model charged leptons, denoted here as E_g with generation index g, the tree-level squared mass is

$$m_{E_g}^2 = y_{E_g}^2 v_d^2. \tag{A.19}$$

The derivatives of the Standard Model quark and lepton sector in Eq. (A.10) are listed below.

$$\delta_u(U_g) = y_{U_g}^2 \tag{A.20}$$

$$\delta_d(U_g) = 0 \tag{A.21}$$

$$\delta_u(D_g) = 0 \tag{A.22}$$

$$\delta_d(D_g) = y_{D_g}^2 \tag{A.23}$$

$$\delta_u(E_g) = 0 \tag{A.24}$$

$$\delta_d(E_g) = y_{E_g}^2 \tag{A.25}$$

A.2.3 SUSY particles

Higgs bosons

The Higgs masses can be obtained by expressing the gauge-eigenstate Higgs fields (h_u^0, h_d^0) and (h_u^+, h_d^{-*}) in terms of the fields (h^0, H^0, G^0, A^0) and $(G^\pm, H^\pm)$ as well as the Higgs VEVs (v_u, v_d). These fields form the Higgs mass eigenstate basis. By minimizing the tree-level potential, one obtains

$$m_{A^0}^2 = m_{H_u}^2 + m_{H_d}^2 + 2\mu^2, \tag{A.26}$$

$$m_{h^0,H^0}^2 = \frac{1}{2}\left(m_{A^0}^2 + m_Z^2 \mp \sqrt{(m_{A^0}^2 - m_Z^2)^2 + 4m_Z^2 m_{A^0}^2 \sin^2(2\beta)}\right), \tag{A.27}$$

and

$$m^2_{H^\pm} = m^2_{A^0} + m^2_W. \tag{A.28}$$

The Nambu-Goldstone bosons $G^{0,\pm}$ are shown to be massless after minimization of the tree-level potential. In Eq. (A.27), we use the convention that the h^0 state is the lighter neutral Higgs mass eigenstate.

The derivatives in Eq. (A.10) are listed below.

$$\delta_u(H^\pm) = \delta_d(H^\pm) = \frac{g^2}{2} \tag{A.29}$$

$$\delta_u(h^0, H^0) = \frac{g^2 + g'^2}{4}\left(1 \mp \frac{\left[m^2_Z + m^2_{A^0}\left(2 + 4\cos(2\beta) + \cos(4\beta)\right)\right]}{m^2_{H^0} - m^2_{h^0}}\right) \tag{A.30}$$

$$\delta_d(h^0, H^0) = \frac{g^2 + g'^2}{4}\left(1 \mp \frac{\left[m^2_Z + m^2_{A^0}\left(2 - 4\cos(2\beta) + \cos(4\beta)\right)\right]}{m^2_{H^0} - m^2_{h^0}}\right) \tag{A.31}$$

The "-" ("+") terms correspond to the derivatives of $m^2_{h^0(H^0)}$.

Neutralinos

The term in the MSSM Lagrangian leading to the neutralino masses is given in terms of the gauge-eigenstate fields ψ^0 by

$$\mathcal{L}_{\widetilde{Z}^0} \ni -\frac{1}{2}\left[\left(\psi^0\right)^T \mathcal{M}_{\widetilde{Z}^0}\psi^0 + \text{ c.c.}\right] \tag{A.32}$$

The *unsquared* neutralino mass matrix is given by

$$\mathcal{M}_{\widetilde{Z}^0} = \begin{bmatrix} M_1 & 0 & -g'v_d/\sqrt{2} & g'v_u/\sqrt{2} \\ 0 & M_2 & gv_d/\sqrt{2} & -gv_u/\sqrt{2} \\ -g'v_d/\sqrt{2} & gv_d/\sqrt{2} & 0 & -\mu \\ g'v_u/\sqrt{2} & -gv_u/\sqrt{2} & -\mu & 0 \end{bmatrix} \tag{A.33}$$

One may diagonalize this matrix to obtain the mass eigenvalues, which are the square roots of the squared mass eigenvalues. Explicit expressions are attainable here, though it involves solving quartic polynomials, leading to unintuitive and unwieldy solutions. Hence, the expressions for the neutralino squared masses will not be reproduced here, though it is simple to solve for them on a modern computer. The complexity lies in then taking the derivatives of these unwieldy expressions. This complexity can be reduced using features of basic calculus and linear algebra.

Since the neutralino squared masses come from the eigenvalues of the square of Eq. (A.33), we can obtain derivatives of these squared masses through derivatives on the characteristic polynomial of the *unsquared* mass matrix. Denoting an eigenvalue of the squared mass matrix as λ, the characteristic polynomial reads

$$p(\lambda) = 0 = \lambda^4 + a\lambda^3 + b\lambda^2 + c\lambda + d. \tag{A.34}$$

The coefficients a, b, c, d are all functions of the Higgs VEVs v_u, v_d, and so are the

eigenvalues $\lambda(v_u, v_d)$. Then, by a careful application of the chain rule, one obtains

$$\begin{aligned}\delta_{u,d}(\widetilde{Z}_i^0) &= \frac{1}{2v_{u,d}}\frac{\partial m^2_{\widetilde{Z}^0,i}}{\partial v_{u,d}} \\ &= \left[-\left(\frac{\lambda}{v_{u,d}}\right)\frac{\frac{\partial a}{\partial v_{u,d}}\lambda^3 + \frac{\partial b}{\partial v_{u,d}}\lambda^2 + \frac{\partial c}{\partial v_{u,d}}\lambda + \frac{\partial d}{\partial v_{u,d}}}{4\lambda^3 + 3a\lambda^2 + 2b\lambda + c}\right]_{\lambda = m_{\widetilde{Z}^0,i}}\end{aligned} \tag{A.35}$$

with $i = 1, 2, 3, 4$. The characteristic polynomial for the neutralino mass matrix gives terms we list below.

$$a = -\left(M_1 + M_2\right) \tag{A.36}$$

$$b = M_1 M_2 - m_Z^2 - \mu^2 \tag{A.37}$$

$$c = \frac{v^2}{2}\left(g^2 M_1 + g'^2 M_2\right) + \left(M_1 + M_2\right)\mu^2 - m_Z^2 \mu \sin(2\beta) \tag{A.38}$$

$$d = \frac{v^2}{2}\left(g^2 M_1 + g'^2 M_2\right)\mu \sin(2\beta) - M_1 M_2 \mu^2 \tag{A.39}$$

Differentiating these expressions gives the following terms, which then allow us to compute radiative corrections from the neutralino sector.

$$\frac{\partial a}{\partial v_u} = \frac{\partial a}{\partial v_d} = 0 \tag{A.40}$$

$$\frac{\partial b}{\partial v_u} = -(g^2 + g'^2)v_u \tag{A.41}$$

$$\frac{\partial b}{\partial v_d} = -(g^2 + g'^2)v_d \tag{A.42}$$

$$\frac{\partial c}{\partial v_u} = \left(g^2 M_1 + g'^2 M_2\right)v_u - \left(g^2 + g'^2\right)\mu v_d \tag{A.43}$$

$$\frac{\partial c}{\partial v_d} = \left(g^2 M_1 + g'^2 M_2\right)v_d - \left(g^2 + g'^2\right)\mu v_u \tag{A.44}$$

$$\frac{\partial d}{\partial v_u} = \left(g^2 M_1 + g'^2 M_2\right) \mu v_d \tag{A.45}$$

$$\frac{\partial d}{\partial v_d} = \left(g^2 M_1 + g'^2 M_2\right) \mu v_u \tag{A.46}$$

Charginos

The term in the MSSM Lagrangian leading to the chargino masses is given in terms of the gauge-eigenstate fields $\psi^{\pm}$ by

$$\mathcal{L}_{\widetilde{C}^{\pm}} \ni -\frac{1}{2}\left[\left(\psi^{\pm}\right)^T \mathcal{M}_{\widetilde{C}^{\pm}} \psi^{\pm} + \text{ c.c.}\right] \tag{A.47}$$

The chargino *unsquared* mass matrix $\mathcal{M}_{\widetilde{C}^{\pm}}$ takes the form

$$\begin{aligned} \mathcal{M}_{\widetilde{C}^{\pm}} &= \begin{bmatrix} \mathbf{0} & \mathcal{X}^T \\ \mathcal{X} & \mathbf{0} \end{bmatrix} \\ &= \begin{bmatrix} 0 & 0 & M_2 & g v_d \\ 0 & 0 & g v_u & \mu \\ M_2 & g v_u & 0 & 0 \\ g v_d & \mu & 0 & 0 \end{bmatrix} \end{aligned} \tag{A.48}$$

The two distinct eigenvalues of the *squared* mass matrix $\mathcal{M}^{\dagger}_{\widetilde{C}^{\pm}} \mathcal{M}_{\widetilde{C}^{\pm}}$, each with degeneracy of two are given as

$$\begin{aligned} m^2_{\widetilde{C}^{\pm}_{1,2}} = \frac{1}{2}\Bigg(& M_2^2 + \mu^2 + 2m_W^2 \\ & \pm \sqrt{\left(M_2^2 + \mu^2 + 2m_W^2\right)^2 - 4\left(\mu M_2 - m_W^2 \sin(2\beta)\right)^2} \Bigg). \end{aligned} \tag{A.49}$$

This leads to derivatives in the radiative corrections in Eq. (A.10) of the form

$$\delta_u(\widetilde{C}^{\pm}_{1,2}) = \frac{g^2}{2}\left(1 \pm \frac{[M_2^2 + \mu^2 - g^2 v^2 \cos(2\beta) + 2M_2\mu\cot(\beta)]}{m^2_{\widetilde{C}^{\pm}_2} - m^2_{\widetilde{C}^{\pm}_1}}\right) \tag{A.50}$$

and

$$\delta_d(\widetilde{C}^{\pm}_{1,2}) = \frac{g^2}{2}\left(1 \pm \frac{[M_2^2 + \mu^2 + g^2 v^2 \cos(2\beta) + 2M_2\mu\tan(\beta)]}{m^2_{\widetilde{C}^{\pm}_2} - m^2_{\widetilde{C}^{\pm}_1}}\right), \tag{A.51}$$

where the "-" ("+") terms correspond to the derivatives of $m^2_{\widetilde{C}^{\pm}_{1(2)}}$.

Squarks

The squarks and sleptons have masses that depend on gauge-eigenstate contributions, as well as hyperfine splitting contributions coming from the particle's isospin, hypercharge, the gauge couplings g and g', and the Higgs VEVs. These hyperfine splitting contributions arise from D-term quartic interactions in the MSSM Lagrangian. For a squark or slepton field $\widetilde{f}$, the splitting function takes the form

$$\Delta_{\widetilde{f}} = \frac{(v_u^2 - v_d^2)}{2}\left(Y_{\widetilde{f}} g'^2 - I_{3\widetilde{f}} g^2\right) \tag{A.52}$$

where $I_{3\widetilde{f}}$ is the third component of the weak isospin of field $\widetilde{f}$, and $Y_{\widetilde{f}}$ is its hypercharge. The squark hyperfine splitting functions are listed in Table A.1 below.

The squarks obtain masses from the following form of terms in the Lagrangian

$\widetilde{f}$	$\Delta_{\widetilde{f}}$
$\widetilde{U}_L$	$(v_u^2 - v_d^2)\left(\frac{g'^2}{6} - \frac{g^2}{4}\right)$
$\widetilde{U}_R$	$-(v_u^2 - v_d^2)\left(\frac{4g'^2}{3}\right)$
$\widetilde{D}_L$	$(v_u^2 - v_d^2)\left(\frac{g^2}{4} + \frac{g'^2}{6}\right)$
$\widetilde{D}_R$	$(v_u^2 - v_d^2)\frac{g'^2}{3}$

Table A.1: Hyperfine splitting functions as in Eq. (A.52) of left- and right-handed squark fields. Up-type squark fields are denoted as $\widetilde{U}$ and down-type squark fields are denoted as $\widetilde{D}$. These contributions are generation-independent.

$$\mathcal{L}_{\widetilde{q}_g} \ni -\begin{bmatrix} \widetilde{q}^*_{g,L} & \widetilde{q}^*_{g,R} \end{bmatrix} \mathcal{M}^2_{\widetilde{q}_g} \begin{bmatrix} \widetilde{q}_{g,L} \\ \\ \widetilde{q}_{g,R} \end{bmatrix}. \tag{A.53}$$

The fields $\widetilde{q}_g$ denote up-type squarks $\widetilde{U}_g$ or down-type squarks $\widetilde{D}_g$ generation $g = 1, 2, 3$. For example,

$$\widetilde{U}_3 = \begin{bmatrix} \widetilde{t}_L \\ \\ \widetilde{t}_R \end{bmatrix}$$

corresponds to the stop gauge-eigenstate fields. The squared mass matrix of the up-type squarks then will be written for each generation g in terms of the left- and right-handed running squark masses $m^2_{\widetilde{Q}_g}$ and $m^2_{\widetilde{U}_g}$ (determined via RGE running, described in Appendix B), the Standard Model quark squared masses $m^2_{U_g}$ (found in Eq. (A.17)), the up-type soft trilinear couplings a_{U_g}, the superpotential parameter μ, the hyperfine splitting functions above in Table A.1,

and the Higgs VEVs.

$$\mathcal{M}^2_{\widetilde{U}_g} = \begin{bmatrix} m^2_{\widetilde{Q}_g} + m^2_{U_g} + \Delta_{\widetilde{U}_L} & a_{U_g} v_u - \mu y_{U_g} v_d \\ a_{U_g} v_u - \mu y_{U_g} v_d & m^2_{\widetilde{\overline{U}}_g} + m^2_{U_g} + \Delta_{\widetilde{U}_R} \end{bmatrix} \tag{A.54}$$

This leads to the mass eigenvalues listed below.

$$\begin{aligned} m^2_{\widetilde{U}_{g,1,2}} = \frac{1}{2}\Bigg(& m^2_{\widetilde{Q}_g} + m^2_{\widetilde{\overline{U}}_g} + 2m^2_{U_g} + \Delta_{\widetilde{U}_L} + \Delta_{\widetilde{U}_R} \\ & \pm \sqrt{(m^2_{\widetilde{Q}_g} + \Delta_{\widetilde{U}_L} - m^2_{\widetilde{\overline{U}}_g} - \Delta_{\widetilde{U}_R})^2 + 4(a_{U_g} v_u - \mu y_{U_g} v_d)^2} \Bigg) \end{aligned} \tag{A.55}$$

The lighter (heavier) mass eigenvalue $m^2_{\widetilde{U}_g,1(2)}$ corresponds to the "-" ("+") term above.

Differentiating with respect to the Higgs VEVs gives the following contributions in Eq. (A.10).

$$\begin{aligned} \delta_u(\widetilde{U}_{g,1,2}) = y^2_{U_g} & - \frac{(g^2 + 2g'^2)}{8} \\ & \pm \frac{1}{m^2_{\widetilde{U}_{g,2}} - m^2_{\widetilde{U}_{g,1}}} \Bigg(a^2_{U_g} - \frac{1}{24}(3g^2 - 10g'^2)(m^2_{\widetilde{Q}_g} - m^2_{\widetilde{\overline{U}}_g}) \\ & \qquad - \frac{1}{288}(3g^2 - 10g'^2)^2 v^2 \cos(2\beta) \\ & \qquad - a_{U_g} y_{U_g} \mu \cot(\beta) \Bigg) \end{aligned} \tag{A.56}$$

$$\delta_d(\widetilde{U}_{g,1,2}) = \frac{(g^2+2g'^2)}{8} \pm \frac{1}{m^2_{\widetilde{U}_{g,2}} - m^2_{\widetilde{U}_{g,1}}} \Bigg(y^2_{U_g}\mu^2 + \frac{1}{24}(3g^2-10g'^2)(m^2_{\widetilde{Q}_g} - m^2_{\widetilde{\overline{U}}_g}) + \frac{1}{288}(3g^2-10g'^2)^2 v^2 \cos(2\beta) - a_{U_g} y_{U_g} \mu \tan(\beta) \Bigg) \tag{A.57}$$

Again, the derivative of the lighter (heavier) mass eigenvalue $m^2_{\widetilde{U}_g,1(2)}$ corresponds to the "-" ("+") term above.

Analysis of the down-type squarks and their tree-level masses proceeds in a very similar manner. The squared mass matrix of down-type squarks of generation g takes the form below.

$$\mathcal{M}^2_{\widetilde{D}_g} = \begin{bmatrix} m^2_{\widetilde{Q}_g} + m^2_{D_g} + \Delta_{\widetilde{D}_L} & a_{D_g} v_d - \mu y_{D_g} v_u \\ a_{D_g} v_d - \mu y_{D_g} v_u & m^2_{\widetilde{\overline{D}}_g} + m^2_{D_g} + \Delta_{\widetilde{D}_R} \end{bmatrix} \tag{A.58}$$

The mass eigenvalues are listed here.

$$m^2_{\widetilde{D}_{g,1,2}} = \frac{1}{2}\Bigg(m^2_{\widetilde{Q}_g} + m^2_{\widetilde{\overline{D}}_g} + 2m^2_{D_g} + \Delta_{\widetilde{D}_L} + \Delta_{\widetilde{D}_R} \pm \sqrt{(m^2_{\widetilde{Q}_g} + \Delta_{\widetilde{D}_L} - m^2_{\widetilde{\overline{D}}_g} - \Delta_{\widetilde{D}_R})^2 + 4(a_{D_g} v_d - \mu y_{D_g} v_u)^2} \Bigg) \tag{A.59}$$

The lighter (heavier) mass eigenvalue $m^2_{\widetilde{D}_g,1(2)}$ corresponds to the "-" ("+") term.

Differentiating with respect to the Higgs VEVs gives the following contributions

in Eq. (A.10).

$$\begin{aligned}\delta_u(\widetilde{D}_{g,1,2}) = \frac{(g^2+2g'^2)}{8} \\ \pm \frac{1}{m^2_{\widetilde{D}_{g,2}} - m^2_{\widetilde{D}_{g,1}}} \Bigg(y^2_{D_g}\mu^2 + \frac{1}{24}(3g^2-2g'^2)(m^2_{\widetilde{Q}_g} - m^2_{\widetilde{\overline{D}}_g}) \\ - \frac{1}{288}(3g^2-2g'^2)^2 v^2 \cos(2\beta) \\ - a_{D_g} y_{D_g} \mu \cot(\beta) \Bigg)\end{aligned} \tag{A.60}$$

$$\begin{aligned}\delta_d(\widetilde{D}_{g,1,2}) = y^2_{D_g} - \frac{(g^2+2g'^2)}{8} \\ \pm \frac{1}{m^2_{\widetilde{D}_{g,2}} - m^2_{\widetilde{D}_{g,1}}} \Bigg(a^2_{D_g} - \frac{1}{24}(3g^2-2g'^2)(m^2_{\widetilde{Q}_g} - m^2_{\widetilde{\overline{D}}_g}) \\ + \frac{1}{288}(3g^2-2g'^2)^2 v^2 \cos(2\beta) \\ - a_{D_g} y_{D_g} \mu \tan(\beta) \Bigg)\end{aligned} \tag{A.61}$$

The derivative of the lighter (heavier) mass eigenvalue $m^2_{\widetilde{D}_{g,1(2)}}$ corresponds to the "-" ("+") term above.

Sleptons

The charged sleptons in the MSSM obtain masses at tree level by the same analysis as the down-type squarks, with some substitutions. The charged sleptons obtain masses from the following form of terms in the Lagrangian

$$\mathcal{L}_{\widetilde{\ell}_g} \ni -\begin{bmatrix} \widetilde{\ell}^*_{g,L} & \widetilde{\ell}^*_{g,R} \end{bmatrix} \mathcal{M}^2_{\widetilde{\ell}_g} \begin{bmatrix} \widetilde{\ell}_{g,L} \\ \widetilde{\ell}_{g,R} \end{bmatrix}. \tag{A.62}$$

The squared mass matrix of the charged slepton of generation g takes the form below.

$$\mathcal{M}^2_{\widetilde{\ell}_g} = \begin{bmatrix} m^2_{\widetilde{L}_g} + m^2_{E_g} + \Delta_{\widetilde{E}_L} & a_{E_g} v_d - \mu y_{E_g} v_u \\ a_{E_g} v_d - \mu y_{E_g} v_u & m^2_{\widetilde{\overline{E}}_g} + m^2_{E_g} + \Delta_{\widetilde{E}_R} \end{bmatrix} \tag{A.63}$$

The hyperfine splitting functions of the charged sleptons are listed here in Table A.2.

$\widetilde{\ell}$	$\Delta_{\widetilde{f}}$
$\widetilde{E}_L$	$(v_u^2 - v_d^2)\left(\frac{g^2}{4} - \frac{g'^2}{2}\right)$
$\widetilde{E}_R$	$(v_u^2 - v_d^2) g'^2$

Table A.2: Hyperfine splitting functions as in Eq. (A.52) of left- and right-handed charged slepton fields. These contributions are generation-independent.

The mass eigenvalues are listed here.

$$\begin{aligned} m^2_{\widetilde{E}_{g,1,2}} = \frac{1}{2}\Bigg(& m^2_{\widetilde{L}_g} + m^2_{\widetilde{\overline{E}}_g} + 2m^2_{E_g} + \Delta_{\widetilde{E}_L} + \Delta_{\widetilde{E}_R} \\ & \pm \sqrt{(m^2_{\widetilde{L}_g} + \Delta_{\widetilde{E}_L} - m^2_{\widetilde{\overline{E}}_g} - \Delta_{\widetilde{E}_R})^2 + 4(a_{E_g} v_d - \mu y_{E_g} v_u)^2} \Bigg) \end{aligned} \tag{A.64}$$

The lighter (heavier) mass eigenvalue $m^2_{\widetilde{E}_g,1(2)}$ corresponds to the "-" ("+") term.

Differentiating with respect to the Higgs VEVs gives the following contributions

in Eq. (A.10).

$$\begin{aligned}\delta_u(\widetilde{E}_{g,1,2}) = \frac{(g^2+2g'^2)}{8} \\ \pm \frac{1}{m^2_{\widetilde{E}_{g,2}} - m^2_{\widetilde{E}_{g,1}}}\Bigg(y^2_{E_g}\mu^2 + \frac{1}{8}(g^2-6g'^2)(m^2_{\widetilde{L}_g} - m^2_{\widetilde{\overline{E}}_g}) \\ - \frac{1}{32}(g^2-6g'^2)^2 v^2\cos(2\beta) \\ - a_{E_g} y_{E_g}\mu\cot(\beta)\Bigg)\end{aligned} \tag{A.65}$$

$$\begin{aligned}\delta_d(\widetilde{E}_{g,1,2}) = y^2_{E_g} - \frac{(g^2+2g'^2)}{8} \\ \pm \frac{1}{m^2_{\widetilde{E}_{g,2}} - m^2_{\widetilde{E}_{g,1}}}\Bigg(a^2_{E_g} - \frac{1}{8}(g^2-6g'^2)(m^2_{\widetilde{L}_g} - m^2_{\widetilde{\overline{E}}_g}) \\ + \frac{1}{32}(g^2-6g'^2)^2 v^2\cos(2\beta) \\ - a_{E_g} y_{E_g}\mu\tan(\beta)\Bigg)\end{aligned} \tag{A.66}$$

The derivative of the lighter (heavier) mass eigenvalue $m^2_{\widetilde{E}_{g,1(2)}}$ corresponds to the "-" ("+") term above.

Lastly, the neutral sleptons (sneutrinos) have tree-level masses

$$m^2_{\widetilde{\nu}_g} = m^2_{\widetilde{L}_g} + \frac{(g'^2+g^2)}{4}(v_d^2 - v_u^2), \tag{A.67}$$

where g indexes the generation as before, which lead to the simple derivatives

$$\delta_{u,d}(\widetilde{\nu}_g) = \mp\frac{(g^2+g'^2)}{4} \tag{A.68}$$

The "-" ("+") derivative corresponds to $\delta_{u(d)}$.

A.3 Two-loop corrections to the scalar potential

Higher order corrections than those seen in Section A.2 can also be relevant to radiative electroweak symmetry breaking and in addressing the finetuning issues seen in the Little Hierarchy Problem and naturalness. For example, the tree-level gluino mass $m_{\tilde{g}} = M_3$ is just expressed in terms of the soft SUSY breaking parameter M_3 and does not depend on the Higgs VEVs. However, higher order effects can exist within the scalar potential, particularly dominant effects of $\mathcal{O}(\alpha_s\alpha_t + \alpha_t^2)$. We focus here on terms of $\mathcal{O}(\alpha_s\alpha_t)$, as the effects of heavy gluinos can contribute potentially significant corrections to the minimization conditions through these terms.

The renormalized two-loop effective potential consists of two parts: a finite part with the renormalization prescription as in CITE HERE, and a part coming from derivatives of the ϵ-suppressed terms in the unrenormalized one-loop effective potential with respect to bare parameters p_i. ϵ is the regulator of the spacetime dimension against UV divergences.

$$\Delta V_{\text{2-loop}} = V_{\text{2-loop}}^{(\text{finite})} + \frac{\partial V_{\text{1-loop}}^{(\epsilon)}}{\partial p_i}\delta p_i \tag{A.69}$$

δp_i denotes the coefficient of the $\frac{1}{\epsilon}$ term in the one-loop part of the counterterm for the bare parameter p_i. $V_{\text{1-loop}}^{(\epsilon)}$ is the epsilon-suppressed term of the unrenormalized

one-loop effective potential mentioned above and is reproduced from CITE HERE.

$$V_{\text{1-loop}}^{(\epsilon)} = \frac{-1}{64\pi^2}\text{STr}\left(\mathcal{M}^4\right)\left[\frac{\pi^2}{12} + \frac{7}{4} - \frac{3}{2}\log\left(\frac{\mathcal{M}^2}{Q^2}\right) + \frac{1}{2}\log^2\left(\frac{\mathcal{M}^2}{Q^2}\right)\right] \tag{A.70}$$

For the purposes of radiative corrections to the Higgs potential minimization conditions Eq. (A.3,A.4), we only need expressions for the derivatives of the two-loop part of this potential. By considering the "gaugeless limit" of the potential as in CITE HERE, wherein the strong gauge coupling is the only non-vanishing gauge coupling, and the top Yukawa is the only non-vanishing Yukawa coupling, we can construct approximate but analytical formulae for the $\mathcal{O}(\alpha_t\alpha_s)$ contributions to the Higgs minimization condition loop corrections.

We denote the angle $\theta_{\tilde{t}}$ that diagonalizes the squared stop mass matrix in Eq. (A.54) by the tree-level relation

$$\sin(2\theta_{\tilde{t}}) = \frac{2v_u}{m_{\tilde{t}_1^2} - m_{\tilde{t}_2^2}}\left(a_t + \mu y_t \cot(\beta)\right). \tag{A.71}$$

In our gaugeless limit, the derivatives of the field-dependent parts of the two-loop renormalized effective potential can be written in terms of this angle in Eq. (A.71), the stop squared masses in Eq. (A.55) and the top quark mass.

$$\Sigma_{d,\text{2-loop}} = \frac{y_t}{v_d}\mu\sin(2\theta_{\tilde{t}})F_{\text{2-loop}} \tag{A.72}$$

$$\Sigma_{u,\text{2-loop}} = \frac{a_t}{v_u}\mu\sin(2\theta_{\tilde{t}})F_{\text{2-loop}} + 2y_t^2 G_{\text{2-loop}} \tag{A.73}$$

The formulae for the 2-loop functions $F_{\text{2-loop}}, G_{\text{2-loop}}$ are computed in the $\overline{\text{DR}}$ scheme in terms of the gluino mass, the stop masses, the top quark mass, and the gaugeless limit couplings. The expressions may be found in Appendix B of CITE HERE and need not be reproduced here.

Appendix B

Renormalization group equations in the MSSM

The renormalization group equations in the MSSM are listed below. The Yukawa couplings $\mathcal{Y}_f$ are 3×3 real, diagonal matrices in generation space, indexed by the generation g. In Appendix A, we denoted the diagonal elements of these matrices as follows: the g-th generation up-type Yukawa couplings by y_{U_g}, down-type Yukawa couplings by y_{D_g}, and lepton-type Yukawa coupligns by y_{E_g}. It is also assumed that the soft trilinear couplings $\mathbf{a}_f = \mathcal{Y}_f \mathcal{A}_f$ are 3×3 real, diagonal matrices in generation space. The superpotential parameter μ is taken to be real (though μ may be negative), as is the Higgs soft bilinear parameter $b = B\mu$. All soft SUSY breaking (SSB) squared masses are required to be real and positive (the latter being required to avoid charge- and/or color-breaking minima that may occur in the vacuum with tachyonic squark or sleptons), except the Higgs parameters $m^2_{H_{u,d}}$ which may run negative. Table B.1 describes the renormalized parameters entering the equations in the proceeding sections.

The general form of the two-loop RGEs for a parameter p will be presented in terms of the one-loop part $\beta_p^{(1\ell)}$ and the two-loop part $\beta_p^{(2\ell)}$ as in Eq. (B.1), where Q_0 is a reference scale unit and Q is the renormalization scale. Summation of repeated indices will be ignored here in Appendix B.

Renormalized parameter	Description
g_i	Gauge coupling for SM gauge group i
$\mathcal{Y}_f$	Yukawa coupling matrix for f-type fermions
$\mathbf{a}_f$	SSB trilinear coupling matrix for f-type fermions
M_i	SSB gaugino mass for SM gauge group i
μ	SUSY-preserving superpotential parameter μ
b	SSB Higgs bilinear parameter
$m^2_{H_u}$	Up-type SSB Higgs mass^2
$m^2_{H_d}$	Down-type SSB Higgs mass^2
$m^2_{\widetilde{Q}_g}$	Left SSB squark mass^2 of gen. g
$m^2_{\widetilde{U}_g}$	Right up-type SSB squark mass^2 of gen. g
$m^2_{\widetilde{D}_g}$	Right down-type SSB squark mass^2 of gen. g
$m^2_{\widetilde{L}_g}$	Left SSB slepton mass^2 of gen. g
$m^2_{\widetilde{E}_g}$	Right SSB slepton mass^2 of gen. g

Table B.1: Renormalized parameters and corresponding descriptions of these parameters. Standard Model gauge groups are indexed according to $i = 1 \leftrightarrow U(1)$, $i = 2, 3 \leftrightarrow SU(2, 3)$. Generation indices g run from $g = 1 - 3$, where generation $g = 1$ contains the up and down quarks and the electron in the SM content. Fermions in $\mathcal{Y}_f$ and $\mathbf{a}_f$ can be up-type, down-type, or lepton-type.

$$\begin{aligned}\beta_p &\equiv \frac{dp}{d\log\left(Q/Q_0\right)} \\ &= \frac{\beta_p^{(1\ell)}}{16\pi^2} + \frac{\beta_p^{(2\ell)}}{(16\pi^2)^2}\end{aligned} \tag{B.1}$$

In numerically solving the two-loop RGEs β_p below, we obtain $p(Q)$, or the parameter p evaluated at the renormalization Q. In practice, this involves evolving p from some initial scale Λ where the boundary condition for p is defined – such as the gauge unification (GUT) scale where g_1 and g_2 unify – to the target scale Q. Table B.2 lists some typical scales where the different renormalized quantities discussed here have their boundary conditions and definitions, as well as typical sources of these boundary values.

For matrix equations below as in the Yukawa and soft trilinear couplings, traces of a matrix $\mathcal{X}$ are denoted $\mathrm{Tr}(\mathcal{X})$. Through an abuse of notation, we use the notation that, in matrix equations, $\mathrm{Tr}(\mathcal{X})$ implies that the scalar $\mathrm{Tr}(\mathcal{X})$ is multiplied on the appropriate size of identity matrix, usually 3×3. Similarly, if a scalar is being added to a matrix, this should be interpreted as the scaled identity matrix adding to the second summand matrix.

B.1 One-loop

B.1.1 Gauge couplings and superpotential parameters

Gauge couplings

The one-loop RGEs for the gauge couplings are listed below. i indexes the Standard Model gauge group as described in Table B.1. GUT-normalized coefficients are

Parameter	Typical BC scale	Typical MSSM source
g_i	Q_{weak}	Exp. data + thresholds
$\mathcal{Y}_f$	Q_{weak}	Exp. data + thresholds
$\mathbf{a}_f$	Q_{GUT}	SSB
M_i	Q_{GUT}	SSB
μ	Q_{SUSY}	Higgs minimization
b	Q_{SUSY}	Higgs minimization
$m^2_{H_u}$	Q_{GUT} or Q_{int}	SSB
$m^2_{H_d}$	Q_{GUT} or Q_{int}	SSB
$m^2_{\widetilde{Q}_g}$	Q_{GUT} or Q_{int}	SSB
$m^2_{\widetilde{U}_g}$	Q_{GUT} or Q_{int}	SSB
$m^2_{\widetilde{D}_g}$	Q_{GUT} or Q_{int}	SSB
$m^2_{\widetilde{L}_g}$	Q_{GUT} or Q_{int}	SSB
$m^2_{\widetilde{E}_g}$	Q_{GUT} or Q_{int}	SSB

Table B.2: Typical scales at which RGE boundary conditions are defined and where those boundary conditions typically come from in the MSSM theory. In the MSSM, gauge unification often occurs around the GUT scale $Q_{\text{GUT}} \sim 2 \times 10^{16}$ GeV. Intermediate scales Q_{int} lie between the weak scale ($Q_{\text{weak}} \sim 100$ GeV) and a high scale such as the GUT scale. The SUSY scale is the scale where logarithmic corrections from Appendix A are minimized. In the MSSM, this is typically of the order $Q_{\text{SUSY}} \sim \sqrt{m_{\widetilde{t}_1} m_{\widetilde{t}_2}}$.

given here with columns and rows labeled according to the indices.

$$b_i = \begin{bmatrix} \frac{33}{5} & i=1 \\ 1 & i=2 \\ -3 & i=3 \end{bmatrix} \tag{B.2}$$

$$\beta_{g_i}^{(1\ell)} = b_i g_i^3 \tag{B.3}$$

Yukawa couplings

The one-loop Yukawa coupling RGEs are listed below, without ignoring the Yukawas of the first two generations, but assuming the Yukawas are diagonalized in generation space. In this generation space, the Yukawa couplings may be written in the following matrix form.

$$\beta_{\mathcal{Y}_U}^{(1\ell)} = \mathcal{Y}_U \left[3\mathrm{Tr}\left(\mathcal{Y}_U^2\right) + 3\mathcal{Y}_U^2 + \mathcal{Y}_D^2 - \frac{13g_1^2}{15} - 3g_2^2 - \frac{16g_3^2}{3} \right] \tag{B.4}$$

$$\beta_{\mathcal{Y}_D}^{(1\ell)} = \mathcal{Y}_D \left[\mathrm{Tr}\left(3\mathcal{Y}_D^2 + \mathcal{Y}_L^2\right) + 3\mathcal{Y}_D^2 + \mathcal{Y}_U^2 - \frac{7g_1^2}{15} - 3g_2^2 - \frac{16g_3^2}{3} \right] \tag{B.5}$$

$$\beta_{\mathcal{Y}_L}^{(1\ell)} = \mathcal{Y}_L \left[\mathrm{Tr}\left(3\mathcal{Y}_D^2 + \mathcal{Y}_L^2\right) + 3\mathcal{Y}_L^2 - \frac{9g_1^2}{5} - 3g_2^2 \right] \tag{B.6}$$

Superpotential parameter μ

The superpotential parameter μ has the one-loop RGE below.

$$\beta_\mu^{(1\ell)} = \mu\left[\mathrm{Tr}\left(3(\mathcal{Y}_U^2+\mathcal{Y}_D^2)+\mathcal{Y}_L^2\right)-3\left(\frac{1}{5}g_1^2+g_2^2\right)\right] \tag{B.7}$$

B.1.2 Soft parameters

Soft trilinear couplings

The one-loop soft trilinear coupling RGEs are listed below. These 3×3 matrices in generation space are sometimes referred to as "reduced" trilinear couplings and are factored as $\mathbf{a}_f = \mathcal{Y}_f\mathcal{A}_f$. Here we will use these reduced matrices $\mathbf{a}_f$, and the RGEs will be presented in the diagonal, 3×3 matrix form.

$$\begin{aligned}\beta_{\mathbf{a}_U}^{(1\ell)} = \mathbf{a}_U&\left[3\mathrm{Tr}\left(\mathcal{Y}_U^2\right)+5\mathcal{Y}_U^2+\mathcal{Y}_D^2-\frac{13g_1^2}{15}-3g_2^2-\frac{16}{3}g_3^2\right]\\ &+\mathcal{Y}_U\Bigg[6\mathrm{Tr}\left(\mathcal{Y}_U\mathbf{a}_U\right)+4\mathcal{Y}_U\mathbf{a}_U+2\mathcal{Y}_D\mathbf{a}_D\\ &\qquad+\frac{26}{15}M_1g_1^2+6M_2g_2^2+\frac{32}{3}M_3g_3^2\Bigg]\end{aligned} \tag{B.8}$$

$$\begin{aligned}\beta_{\mathbf{a}_D}^{(1\ell)} = \mathbf{a}_D&\left[\mathrm{Tr}\left(3\mathcal{Y}_D^2+\mathcal{Y}_L^2\right)+5\mathcal{Y}_D^2+\mathcal{Y}_U^2-\frac{7g_1^2}{15}-3g_2^2-\frac{16}{3}g_3^2\right]\\ &+\mathcal{Y}_D\Bigg[\mathrm{Tr}\left(6\mathcal{Y}_D\mathbf{a}_D+2\mathcal{Y}_L\mathbf{a}_L\right)+4\mathcal{Y}_D\mathbf{a}_D+2\mathcal{Y}_U\mathbf{a}_U\\ &\qquad+\frac{14}{15}M_1g_1^2+6M_2g_2^2+\frac{32}{3}M_3g_3^2\Bigg]\end{aligned} \tag{B.9}$$

$$\begin{aligned}\beta^{(1\ell)}_{\mathbf{a}_L} = \mathbf{a}_L &\left[\mathrm{Tr}\left(3\mathcal{Y}_D^2 + \mathcal{Y}_L^2\right) + 5\mathcal{Y}_L^2 - \frac{9g_1^2}{5} - 3g_2^2\right] \\ &+ \mathcal{Y}_L\left[\mathrm{Tr}\left(6\mathcal{Y}_D\mathbf{a}_D + 2\mathcal{Y}_L\mathbf{a}_L\right) + 4\mathcal{Y}_L\mathbf{a}_L\right. \\ &\left.+ \frac{18}{5}M_1 g_1^2 + 6M_2 g_2^2\right]\end{aligned} \tag{B.10}$$

Higgs bilinear parameter

The soft Higgs bilinear parameter $b = B\mu$ has the one-loop RGE below.

$$\begin{aligned}\beta_b^{(1\ell)} = &\frac{b}{\mu}\beta_\mu^{(1\ell)} \\ &+ \mu\left[\mathrm{Tr}\left(6(\mathbf{a}_U\mathcal{Y}_U + \mathbf{a}_D\mathcal{Y}_D) + 2\mathbf{a}_L\mathcal{Y}_L\right) + 6\left(\frac{1}{5}g_1^2M_1 + g_2^2M_2\right)\right]\end{aligned} \tag{B.11}$$

B.1.3 Soft masses

Gaugino masses

The one-loop SSB gaugino mass RGEs are listed below. i indexes the Standard Model gauge group as described in Table B.1. The coefficients b_i are given in Eq. (B.2).

$$\beta^{(1\ell)}_{M_i} = 2b_i g_i^2 M_i \tag{B.12}$$

Scalar masses

For the SSB scalar squared mass one-loop RGEs, we utilize the shorthand notation

$$\widetilde{S} = m_{H_u}^2 - m_{H_d}^2 + \mathrm{Tr}\left(\mathcal{M}_{\widetilde{Q}}^2 - \mathcal{M}_{\widetilde{L}}^2 - 2\mathcal{M}_{\widetilde{\overline{U}}}^2 + \mathcal{M}_{\widetilde{\overline{D}}}^2 + \mathcal{M}_{\widetilde{\overline{E}}}^2\right) \tag{B.13}$$

with the diagonalized matrices of the squarks and sleptons of the form below in generation space.

$$\mathcal{M}^2_{\widetilde{f}} = \begin{bmatrix} m^2_{\widetilde{f}_1} & 0 & 0 \\ 0 & m^2_{\widetilde{f}_2} & 0 \\ 0 & 0 & m^2_{\widetilde{f}_3} \end{bmatrix}$$

Below we list the Higgs and scalar squared mass RGEs at one-loop order.

Higgs masses

$$\beta^{(1\ell)}_{m^2_{H_u}} = 6\mathrm{Tr}\left[(m^2_{H_u} + \mathcal{M}^2_{\widetilde{Q}} + \mathcal{M}^2_{\widetilde{U}})\mathcal{Y}^2_U + \mathbf{a}^2_U\right] - \frac{3}{5}g_1^2\left(2M_1^2 - \widetilde{S}\right) - 6g_2^2M_2^2 \quad \text{(B.14)}$$

$$\begin{aligned}\beta^{(1\ell)}_{m^2_{H_d}} &= 6\mathrm{Tr}\left[(m^2_{H_d} + \mathcal{M}^2_{\widetilde{Q}} + \mathcal{M}^2_{\widetilde{D}})\mathcal{Y}^2_D + \mathbf{a}^2_D\right] \\ &\quad + 2\mathrm{Tr}\left[(m^2_{H_d} + \mathcal{M}^2_{\widetilde{L}} + \mathcal{M}^2_{\widetilde{E}})\mathcal{Y}^2_L + \mathbf{a}^2_L\right] - \frac{3}{5}g_1^2\left(2M_1^2 + \widetilde{S}\right) \\ &\quad - 6g_2^2M_2^2\end{aligned} \quad \text{(B.15)}$$

Squark masses

The one-loop soft squark squared mass RGEs are listed below. The RGEs are presented in the real, diagonal 3×3 matrix form.

$$\begin{aligned}\beta^{(1\ell)}_{\mathcal{M}^2_{\widetilde{Q}}} &= 2\left[(\mathcal{M}^2_{\widetilde{Q}} + \mathcal{M}^2_{\widetilde{U}} + m^2_{H_u})\mathcal{Y}^2_U + (\mathcal{M}^2_{\widetilde{Q}} + \mathcal{M}^2_{\widetilde{D}} + m^2_{H_d})\mathcal{Y}^2_D + \mathbf{a}^2_U + \mathbf{a}^2_D\right] \\ &\quad - \frac{g_1^2}{5}\left(M_1^2 - \frac{2}{3}\widetilde{S}\right) - 6g_2^2M_2^2 - \frac{32}{3}g_3^2M_3^2\end{aligned} \quad \text{(B.16)}$$

$$\beta^{(1\ell)}_{\mathcal{M}^2_{\widetilde{U}}} = 4\left[(\mathcal{M}^2_{\widetilde{Q}} + \mathcal{M}^2_{\widetilde{U}} + m^2_{H_u})\mathcal{Y}^2_U + \mathbf{a}^2_U\right] - \frac{4}{15}g_1^2\left(8M_1^2 + 3\widetilde{S}\right) - \frac{32}{3}g_3^2 M_3^2 \tag{B.17}$$

$$\beta^{(1\ell)}_{\mathcal{M}^2_{\widetilde{D}}} = 4\left[(\mathcal{M}^2_{\widetilde{Q}} + \mathcal{M}^2_{\widetilde{D}} + m^2_{H_d})\mathcal{Y}^2_D + \mathbf{a}^2_D\right] - \frac{2}{5}g_1^2\left(\frac{4}{3}M_1^2 - \widetilde{S}\right) - \frac{32}{3}g_3^2 M_3^2 \tag{B.18}$$

Slepton masses

The one-loop soft slepton squared mass RGEs are listed below. The RGEs are presented in the real, diagonal 3×3 matrix form.

$$\beta^{(1\ell)}_{\mathcal{M}^2_{\widetilde{L}}} = 2\left[(\mathcal{M}^2_{\widetilde{L}} + \mathcal{M}^2_{\widetilde{E}} + m^2_{H_d})\mathcal{Y}^2_L + \mathbf{a}^2_L\right] - \frac{3}{5}g_1^2\left(2M_1^2 + \widetilde{S}\right) - 6g_2^2 M_2^2 \tag{B.19}$$

$$\beta^{(1\ell)}_{\mathcal{M}^2_{\widetilde{E}}} = 4\left[(\mathcal{M}^2_{\widetilde{L}} + \mathcal{M}^2_{\widetilde{E}} + m^2_{H_d})\mathcal{Y}^2_L + \mathbf{a}^2_L\right] - \frac{6}{5}g_1^2\left(4M_1^2 - \widetilde{S}\right) \tag{B.20}$$

B.2 Two-loop

B.2.1 Gauge couplings and superpotential parameters

Gauge couplings

The two-loop RGEs for the gauge couplings are listed below. i and j index the Standard Model gauge group as described in Table B.1. f indexes the fermion type (up-type, down-type, or lepton-type) being summed over. The GUT-normalized coefficients are given here with columns and rows labeled according to the indices.

$$b_i^j = \begin{array}{c} \begin{matrix} j=1 & j=2 & j=3 \end{matrix} \\ \begin{bmatrix} \frac{199}{25} & \frac{27}{5} & \frac{88}{5} \\ \frac{9}{5} & 25 & 24 \\ \frac{11}{5} & 9 & 14 \end{bmatrix} \end{array} \begin{matrix} \\ i=1 \\ i=2 \\ i=3 \end{matrix} \tag{B.21}$$

$$C_i^f = \begin{array}{c} \begin{matrix} f=U & f=D & f=L \end{matrix} \\ \begin{bmatrix} \frac{26}{5} & \frac{14}{5} & \frac{18}{5} \\ 6 & 6 & 2 \\ 4 & 4 & 0 \end{bmatrix} \end{array} \begin{matrix} \\ i=1 \\ i=2 \\ i=3 \end{matrix} \tag{B.22}$$

$$\beta_{g_i}^{(2\ell)} = g_i^3 \left[\sum_{j=1}^{3} b_i^j g_j^2 - \sum_{f=U,D,L} C_i^f \mathrm{Tr}\left(\mathcal{Y}_f^2\right) \right] \tag{B.23}$$

Yukawa couplings

The two-loop Yukawa coupling RGEs are listed below. These equations are expressed as real, diagonal 3×3 matrices.

$$\begin{aligned}\beta_{\mathcal{Y}_U}^{(2\ell)} = \mathcal{Y}_U \Bigg[& \left(\frac{4}{5}g_1^2 + 16g_3^2 - 9\mathcal{Y}_U^2\right) \mathrm{Tr}\left(\mathcal{Y}_U^2\right) + 2\left(\frac{1}{5}g_1^2 + 3g_2^2 - 2\mathcal{Y}_U^2\right)\mathcal{Y}_U^2 \\ & + \left(\frac{2}{5}g_1^2 - 2\mathcal{Y}_U^2 - 2\mathcal{Y}_D^2 - \mathrm{Tr}\left(3\mathcal{Y}_D^2 + \mathcal{Y}_L^2\right)\right)\mathcal{Y}_D^2 \\ & - 3\mathrm{Tr}\left(3\mathcal{Y}_U^4 + \mathcal{Y}_U^2\mathcal{Y}_D^2\right) + g_1^2\left(\frac{2743}{450}g_1^2 + g_2^2 + \frac{136}{45}g_3^2\right) \\ & + g_2^2\left(\frac{15}{2}g_2^2 + 8g_3^2\right) - \frac{16}{9}g_3^4\Bigg]\end{aligned} \tag{B.24}$$

$$\begin{aligned}\beta_{\mathcal{Y}_D}^{(2\ell)} = \mathcal{Y}_D \Bigg[& \left(\frac{4}{5}g_1^2 - 2\mathcal{Y}_U^2 - 3\mathrm{Tr}\left(\mathcal{Y}_U^2\right)\right)\mathcal{Y}_U^2 + \frac{6}{5}g_1^2\mathrm{Tr}\left(\mathcal{Y}_L^2\right) \\ & + \left(\frac{4}{5}g_1^2 + 6g_2^2 - 2\mathcal{Y}_U^2 - 4\mathcal{Y}_D^2 - 3\mathrm{Tr}\left(3\mathcal{Y}_D^2 + \mathcal{Y}_L^2\right)\right)\mathcal{Y}_D^2 \\ & - 2\left(\frac{1}{5}g_1^2 - 8g_3^2\right)\mathrm{Tr}\left(\mathcal{Y}_D^2\right) - 3\mathrm{Tr}\left(3\mathcal{Y}_D^4 + \mathcal{Y}_U^2\mathcal{Y}_D^2 + \mathcal{Y}_L^4\right) \\ & + g_1^2\left(\frac{287}{90}g_1^2 + g_2^2 + \frac{8}{9}g_3^2\right) + g_2^2\left(\frac{15}{2}g_2^2 + 8g_3^2\right) - \frac{16}{9}g_3^4\Bigg]\end{aligned} \tag{B.25}$$

$$\begin{aligned}\beta_{\mathcal{Y}_L}^{(2\ell)} = \mathcal{Y}_L \Bigg[& \left(-\frac{2}{5}g_1^2 + 16g_3^2\right)\mathrm{Tr}\left(\mathcal{Y}_D^2\right) - 3\mathrm{Tr}\left(3\mathcal{Y}_D^4 + \mathcal{Y}_U^2\mathcal{Y}_D^2 + \mathcal{Y}_L^4\right) \\ & - \left(4\mathcal{Y}_L^2 - 6g_2^2 + 3\mathrm{Tr}\left(3\mathcal{Y}_D^2 + \mathcal{Y}_L^2\right)\right)\mathcal{Y}_L^2 \\ & + g_1^2\left(\frac{6}{5}\mathrm{Tr}\left(\mathcal{Y}_L^2\right) + \frac{9}{5}g_2^2 + \frac{27}{2}g_1^2\right) + \frac{15}{2}g_2^2\Bigg]\end{aligned} \tag{B.26}$$

Superpotential parameter μ

The superpotential parameter μ has the two-loop RGE below.

$$\begin{aligned}\beta_\mu^{(2\ell)} = \mu\Bigg[& 4\left(\frac{1}{5}g_1^2 + 4g_3^2\right)\mathrm{Tr}\left(\mathcal{Y}_U^2\right) - 2\left(\frac{1}{5}g_1^2 - 8g_3^2\right)\mathrm{Tr}\left(\mathcal{Y}_D^2\right) \\ & + \frac{6}{5}g_1^2\mathrm{Tr}\left(\mathcal{Y}_L^2\right) \\ & - 3\mathrm{Tr}\left(3(\mathcal{Y}_U^4 + \mathcal{Y}_D^4) + \mathcal{Y}_L^4 + 2\mathcal{Y}_U^2\mathcal{Y}_D^2\right) \\ & + 9g_1^2\left(\frac{23}{50}g_1^2 + \frac{1}{5}g_2^2\right) + \frac{15}{2}g_2^4\Bigg]\end{aligned} \tag{B.27}$$

B.2.2 Soft parameters

Soft trilinear couplings

The two-loop soft trilinear coupling RGEs are listed below. These equations are expressed as real, diagonal 3×3 matrices.

$$
\begin{aligned}
\beta^{(2\ell)}_{\mathbf{a}_U} = \mathbf{a}_U \Bigg[& \left(12g_2^2 - 4\mathcal{Y}_D^2 - 6\mathcal{Y}_U^2 - 15\mathrm{Tr}\left(\mathcal{Y}_U^2\right)\right)\mathcal{Y}_U^2 \\
& + \left(\frac{2}{5}g_1^2 - 2\mathcal{Y}_D^2 - \mathrm{Tr}\left(3\mathcal{Y}_D^2 + \mathcal{Y}_L^2\right)\right)\mathcal{Y}_D^2 \\
& - 3\mathrm{Tr}\left(3\mathcal{Y}_U^4 + \mathcal{Y}_U^2\mathcal{Y}_D^2\right) + \left(\frac{4}{5}g_1^2 + 16g_3^2\right)\mathrm{Tr}\left(\mathcal{Y}_U^2\right) \\
& + g_1^2\left(\frac{2743}{450}g_1^2 + g_2^2 + \frac{136}{45}g_3^2\right) + g_2^2\left(\frac{15}{2}g_2^2 + 8g_3^2\right) - \frac{16}{9}g_3^4\Bigg] \\
+ \mathcal{Y}_U \Bigg[& -2\Bigg(9\mathrm{Tr}(\mathbf{a}_U\mathcal{Y}_U) + 7\mathbf{a}_U\mathcal{Y}_U + 2\mathbf{a}_D\mathcal{Y}_D \\
& \qquad + \frac{2}{5}g_1^2M_1 + 6g_2^2M_2\Bigg)\mathcal{Y}_U^2 \\
& - \left(\mathrm{Tr}\left(6\mathbf{a}_D\mathcal{Y}_D + 2\mathbf{a}_L\mathcal{Y}_L\right) + 8\mathbf{a}_D\mathcal{Y}_D + 2\mathbf{a}_U\mathcal{Y}_U + \frac{4}{5}g_1^2M_1\right)\mathcal{Y}_D^2 \\
& + 6\left(\frac{1}{5}g_1^2 + g_2^2 - 2\mathrm{Tr}\left(\mathcal{Y}_U^2\right)\right)\mathbf{a}_U\mathcal{Y}_U \\
& + \left(\frac{4}{5}g_1^2 - \mathrm{Tr}\left(6\mathcal{Y}_D^2 + 2\mathcal{Y}_L^2\right)\right)\mathbf{a}_D\mathcal{Y}_D \\
& + 8\left(\frac{1}{5}g_1^2 + 4g_3^2\right)\mathrm{Tr}\left(\mathbf{a}_U\mathcal{Y}_U\right) - 8\left(\frac{1}{5}g_1^2M_1 + 4g_3^2M_3\right)\mathrm{Tr}\left(\mathcal{Y}_U^2\right) \\
& - 6\mathrm{Tr}\left(6\mathcal{Y}_U^3\mathbf{a}_U + \mathcal{Y}_U\mathcal{Y}_D^2\mathbf{a}_U + \mathcal{Y}_D\mathcal{Y}_U^2\mathbf{a}_D\right) \\
& - 2g_1^2\left(\frac{2743}{225}g_1^2M_1 + g_2^2(M_1+M_2) + \frac{136}{45}g_3^2(M_1+M_3)\right) \\
& - 2g_2^2\left(15g_2^2M_2 - 8g_3^2(M_2+M_3)\right) + \frac{64}{9}g_3^4M_3\Bigg]
\end{aligned}
\tag{B.28}
$$

$$
\begin{aligned}
\beta^{(2\ell)}_{\mathbf{a}_D} = \mathbf{a}_D \Bigg[& \left(\frac{4}{5}g_1^2 - 3\mathrm{Tr}\left(\mathcal{Y}_U^2\right) - 2\mathcal{Y}_U^2 - 4\mathcal{Y}_D^2\right)\mathcal{Y}_U^2 \\
& + \left(\frac{6}{5}g_1^2 + 12g_2^2 - 6\mathcal{Y}_D^2 - 5\mathrm{Tr}\left(3\mathcal{Y}_D^2 + \mathcal{Y}_L^2\right)\right)\mathcal{Y}_D^2 \\
& - \left(\frac{2}{5}g_1^2 - 16g_3^2\right)\mathrm{Tr}\left(\mathcal{Y}_D^2\right) + \frac{6}{5}g_1^2\mathrm{Tr}(\mathcal{Y}_L^2) \\
& - 3\mathrm{Tr}\left(3\mathcal{Y}_D^4 + \mathcal{Y}_U^2\mathcal{Y}_D^2 + \mathcal{Y}_L^2\right) + g_1^2\left(\frac{287}{90}g_1^2 + g_2^2 + \frac{8}{9}g_3^2\right) \\
& + g_2^2\left(\frac{15}{2}g_2^2 + 8g_3^2\right) - \frac{16}{9}g_3^4\Bigg] \\
+ \mathcal{Y}_D \Bigg[& -2\left(\frac{4}{5}g_1^2M_1 + \mathbf{a}_D\mathcal{Y}_D + 4\mathbf{a}_U\mathcal{Y}_U + 3\mathrm{Tr}(\mathbf{a}_U\mathcal{Y}_U)\right)\mathcal{Y}_U^2 \\
& - 2\Bigg(\frac{4}{5}g_1^2M_1 + 6g_2^2M_2 - 2\mathbf{a}_U\mathcal{Y}_U - 7\mathbf{a}_D\mathcal{Y}_D \\
& \qquad - 3\mathrm{Tr}\left(3\mathbf{a}_D\mathcal{Y}_D + \mathbf{a}_L\mathcal{Y}_L\right)\Bigg)\mathcal{Y}_D^2 \\
& + 2\left(\frac{4}{5}g_1^2 - 3\mathrm{Tr}\left(\mathcal{Y}_U^2\right)\right)\mathbf{a}_U\mathcal{Y}_U \\
& + 2\left(\frac{3}{5}g_1^2 + 3g_2^2 - 2\mathrm{Tr}\left(3\mathcal{Y}_D^2 + \mathcal{Y}_L^2\right)\right)\mathbf{a}_D\mathcal{Y}_D \\
& - 6\mathrm{Tr}\left(6\mathbf{a}_D\mathcal{Y}_D^3 + \mathbf{a}_U\mathcal{Y}_U\mathcal{Y}_D^2 + \mathbf{a}_D\mathcal{Y}_D\mathcal{Y}_U^2 + 2\mathbf{a}_L\mathcal{Y}_L^3\right) \\
& - 4\left(\frac{1}{5}g_1^2 - 8g_3^2\right)\mathrm{Tr}\left(\mathbf{a}_D\mathcal{Y}_D\right) + \frac{12}{5}g_1^2\mathrm{Tr}\left(\mathbf{a}_L\mathcal{Y}_L\right) \\
& + 4\left(\frac{1}{5}g_1^2M_1 - 8g_3^2M_3\right)\mathrm{Tr}\left(\mathcal{Y}_D^2\right) - \frac{12}{5}g_1^2M_1\mathrm{Tr}\left(\mathcal{Y}_L^2\right) \\
& - 2\left(\frac{287}{45}g_1^2M_1 + g_2^2(M_1+M_2) + \frac{16}{9}g_3^2(M_1+M_3)\right) \\
& - 2g_2^2\left(15g_2^2M_2 + 8g_3^2(M_2+M_3)\right) + \frac{64}{9}g_3^4M_3\Bigg]
\end{aligned}
\tag{B.29}
$$

$$
\begin{aligned}
\beta^{(2\ell)}_{\mathbf{a}_L} = \mathbf{a}_L \Bigg[& \left(-2\left(\frac{3}{5}g_1^2 - 6g_2^2\right) - 6\mathcal{Y}_L^2 - 5\mathrm{Tr}\left(3\mathcal{Y}_D^2 + \mathcal{Y}_L^2\right)\right)\mathcal{Y}_L^2 \\
& + \frac{6}{5}g_1^2\mathrm{Tr}\left(\mathcal{Y}_L^2\right) - 2\left(\frac{1}{5}g_1^2 - 8g_3^2\right)\mathrm{Tr}\left(\mathcal{Y}_D^2\right) \\
& - 3\mathrm{Tr}\left(3\mathcal{Y}_D^4 + \mathcal{Y}_L^4 + \mathcal{Y}_U^2\mathcal{Y}_D^2\right) + 3g_1^2\left(\frac{9}{2}g_1^2 + \frac{3}{5}g_2^2\right) + \frac{15}{2}g_2^4\Bigg] \\
+ \mathcal{Y}_L \Bigg[& -2\left(6g_2^2 M_2 + 7\mathbf{a}_L\mathcal{Y}_L + 3\mathrm{Tr}\left(3\mathbf{a}_D\mathcal{Y}_D + \mathbf{a}_L\mathcal{Y}_L\right)\right)\mathcal{Y}_L^2 \\
& + 2\left(\frac{3}{5}g_1^2 + 3g_2^2 - 2\mathrm{Tr}\left(3\mathcal{Y}_D^2 + \mathcal{Y}_L^2\right)\right)\mathbf{a}_L\mathcal{Y}_L \\
& - 6\mathrm{Tr}\left(6\mathbf{a}_D\mathcal{Y}_D^3 + 2\mathbf{a}_L\mathcal{Y}_L^3 + \mathbf{a}_U\mathcal{Y}_U\mathcal{Y}_D^2 + \mathbf{a}_D\mathcal{Y}_D\mathcal{Y}_U^2\right) \\
& - \frac{12}{5}g_1^2 M_1\mathrm{Tr}\left(\mathcal{Y}_L^2\right) + \frac{12}{5}g_1^2\mathrm{Tr}\left(\mathbf{a}_L\mathcal{Y}_L\right) \\
& - 4\left(\frac{1}{5}g_1^2 - 8g_3^2\right)\mathrm{Tr}\left(\mathbf{a}_D\mathcal{Y}_D\right) \\
& + 4\left(\frac{1}{5}g_1^2 M_1 - 8g_3^2 M_3\right)\mathrm{Tr}\left(\mathcal{Y}_D^2\right) \\
& - 18\left(3g_1^2 M_1 + \frac{1}{5}g_2^2\left(M_1 + M_2\right)\right) - 30g_2^4 M_2\Bigg]
\end{aligned}
\tag{B.30}
$$

Higgs bilinear parameter

The soft Higgs bilinear parameter $b = B\mu$ has the two-loop RGE below.

$$\begin{aligned}\beta_b^{(2\ell)} = & \frac{b}{\mu}\beta_\mu^{(2\ell)} \\ & + \mu\Bigg[8\left(\frac{1}{5}g_1^2 + 4g_3^2\right)\mathrm{Tr}\left(\mathbf{a}_U\mathcal{Y}_U\right) - 4\left(\frac{1}{5}g_1^2 - 8g_3^2\right)\mathrm{Tr}(\mathbf{a}_D\mathcal{Y}_D) \\ & \quad + \frac{12}{5}g_1^2\mathrm{Tr}\left(\mathbf{a}_L\mathcal{Y}_L\right) - 8\left(\frac{1}{5}g_1^2M_1 + 4g_3^2M_3\right)\mathrm{Tr}\left(\mathcal{Y}_U^2\right) \\ & \quad + 4\left(\frac{1}{5}g_1^2M_1 - 8g_3^2M_3\right)\mathrm{Tr}\left(\mathcal{Y}_D^2\right) - \frac{12}{5}g_1^2M_1\mathrm{Tr}\left(\mathcal{Y}_L^2\right) \\ & \quad - 12\mathrm{Tr}\left(3(\mathbf{a}_U\mathcal{Y}_U^3 + \mathbf{a}_D\mathcal{Y}_D^3) + \mathbf{a}_U\mathcal{Y}_U\mathcal{Y}_D^2 + \mathbf{a}_D\mathcal{Y}_D\mathcal{Y}_U^2 + \mathbf{a}_L\mathcal{Y}_L^3\right) \\ & \quad - \frac{18}{5}g_1^2\left(\frac{23}{5}g_1^2M_1 + g_2^2(M_1+M_2)\right) - 30g_2^4M_2\Bigg]\end{aligned} \tag{B.31}$$

B.2.3 Soft masses

Gaugino masses

The two-loop SSB gaugino mass RGEs are listed below. i and j index the Standard Model gauge group as described in Table B.1. The coefficients b_i^j and C_i^f are given in Eqs. (B.21,B.22).

$$\begin{aligned}\beta_{M_i}^{(2\ell)} = 2g_i^2\Bigg\{\sum_{j=1}^{3} b_i^j g_j^2\left(M_i + M_j\right) + \sum_{f=U,D,L} C_i^f\Big[\mathrm{Tr}\left(\mathcal{Y}_f\mathbf{a}_f\right) \\ - M_i\mathrm{Tr}\left(\mathcal{Y}_f^2\right)\Big]\Bigg\}\end{aligned} \tag{B.32}$$

Scalar masses

For the SSB scalar squared mass two-loop RGEs, we utilize the shorthand notation in Eq. (B.13) and the following.

$$\begin{aligned}
\widetilde{S}' = & \operatorname{Tr}\left[(4\mathcal{M}^2_{\widetilde{\overline{U}}} - \mathcal{M}^2_{\widetilde{Q}} - 3m^2_{H_u})\mathcal{Y}^2_U\right] \\
& - \operatorname{Tr}\left[\left(\mathcal{M}^2_{\widetilde{Q}} + 2\mathcal{M}^2_{\widetilde{\overline{U}}} - 3m^2_{H_d}\right)\mathcal{Y}^2_D\right] \\
& + \operatorname{Tr}\left[\left(\mathcal{M}^2_{\widetilde{L}} - 2\mathcal{M}^2_{\widetilde{\overline{E}}} + m^2_{H_d}\right)\mathcal{Y}^2_L\right] \\
& + \left[\frac{1}{30}g_1^2 + \frac{3}{2}g_2^2 + \frac{8}{3}g_3^2\right]\operatorname{Tr}(\mathcal{M}^2_{\widetilde{Q}}) - \frac{16}{3}\left(\frac{1}{5}g_1^2 + g_3^2\right)\operatorname{Tr}\left(\mathcal{M}^2_{\widetilde{\overline{U}}}\right) \\
& + \frac{2}{3}\left(\frac{1}{5}g_1^2 + 4g_3^2\right)\operatorname{Tr}\left(\mathcal{M}^2_{\widetilde{\overline{D}}}\right) \\
& + 3\left(\frac{1}{10}g_1^2 + \frac{1}{2}g_2^2\right)\left[m^2_{H_u} - m^2_{H_d} - \operatorname{Tr}\left(\mathcal{M}^2_{\widetilde{L}}\right)\right] + \frac{6}{5}g_1^2\operatorname{Tr}\left(\mathcal{M}^2_{\widetilde{\overline{E}}}\right)
\end{aligned} \tag{B.33}$$

$$\sigma_1 = \frac{g_1^2}{5}\left[3(m^2_{H_u} + m^2_{H_d}) + \operatorname{Tr}\left(\mathcal{M}^2_{\widetilde{Q}} + 8\mathcal{M}^2_{\widetilde{\overline{U}}} + 2\mathcal{M}^2_{\widetilde{\overline{D}}} + 3\mathcal{M}^2_{\widetilde{L}} + 6\mathcal{M}^2_{\widetilde{\overline{E}}}\right)\right] \tag{B.34}$$

$$\sigma_2 = g_2^2\left[m^2_{H_u} + m^2_{H_d} + \operatorname{Tr}\left(3\mathcal{M}^2_{\widetilde{Q}} + \mathcal{M}^2_{\widetilde{L}}\right)\right] \tag{B.35}$$

$$\sigma_3 = g_3^2\operatorname{Tr}\left(2\mathcal{M}^2_{\widetilde{Q}} + \mathcal{M}^2_{\widetilde{\overline{U}}} + \mathcal{M}^2_{\widetilde{\overline{D}}}\right) \tag{B.36}$$

with the squared mass matrices of the squarks and sleptons real and diagonalized in generation space. Below we list the Higgs and scalar squared mass RGEs at one-loop order.

Higgs masses

$$
\begin{aligned}
\beta^{(2\ell)}_{m^2_{H_u}} =& -36\mathrm{Tr}\left[(\mathcal{M}^2_{\widetilde{Q}}+\mathcal{M}^2_{\widetilde{\overline{U}}}+m^2_{H_u})\mathcal{Y}^4_U\right] \\
&-6\mathrm{Tr}\left[(2\mathcal{M}^2_{\widetilde{Q}}+\mathcal{M}^2_{\widetilde{\overline{U}}}+\mathcal{M}^2_{\widetilde{\overline{D}}}+m^2_{H_u}+m^2_{H_d})\mathcal{Y}^2_U\mathcal{Y}^2_D\right] \\
&-6\mathrm{Tr}\left[\left(12\mathbf{a}^2_U+\mathbf{a}^2_D\right)\mathcal{Y}^2_U+\mathbf{a}^2_U\mathcal{Y}^2_D+2\mathbf{a}_U\mathbf{a}_D\mathcal{Y}_U\mathcal{Y}_D\right] \\
&+8\left(\frac{1}{5}g_1^2+4g_3^2\right)\mathrm{Tr}\left[\left(\mathcal{M}^2_{\widetilde{Q}}+\mathcal{M}^2_{\widetilde{\overline{U}}}+m^2_{H_u}\right)\mathcal{Y}^2_U+\mathbf{a}^2_U\right] \\
&+\frac{16}{5}g_1^2\left[M_1^2\mathrm{Tr}\left(\mathcal{Y}^2_U\right)-M_1\mathrm{Tr}\left(\mathbf{a}_U\mathcal{Y}_U\right)\right] \\
&+64g_3^2\left[M_3^2\mathrm{Tr}\left(\mathcal{Y}^2_U\right)-M_3\mathrm{Tr}\left(\mathbf{a}_U\mathcal{Y}_U\right)\right] \\
&+\frac{3}{5}g_1^2\left[\frac{207}{5}g_1^2M_1^2+6g_2^2(M_1^2+M_2^2+M_1M_2)+2\widetilde{S}'+\sigma_1\right] \\
&+3g_2^2\left(11g_2^2M_2^2+\sigma_2\right)
\end{aligned}
\tag{B.37}
$$

$$
\begin{aligned}
\beta^{(2\ell)}_{m^2_{H_d}} =& -36\mathrm{Tr}\left[(\mathcal{M}^2_{\widetilde{Q}} + \mathcal{M}^2_{\widetilde{\overline{D}}} + m^2_{H_d})\mathcal{Y}^4_D\right] \\
& - 6\mathrm{Tr}\left[(2\mathcal{M}^2_{\widetilde{Q}} + \mathcal{M}^2_{\widetilde{\overline{U}}} + \mathcal{M}^2_{\widetilde{\overline{D}}} + m^2_{H_u} + m^2_{H_d})\mathcal{Y}^2_U\mathcal{Y}^2_D\right] \\
& - 12\mathrm{Tr}\left[\left(\mathcal{M}^2_{\widetilde{L}} + \mathcal{M}^2_{\widetilde{\overline{E}}} + m^2_{H_d}\right)\mathcal{Y}^4_L\right] \\
& - 6\mathrm{Tr}\left[\left(12\mathbf{a}^2_D + \mathbf{a}^2_U\right)\mathcal{Y}^2_D + \mathbf{a}^2_D\mathcal{Y}^2_U + 2(\mathbf{a}_U\mathbf{a}_D\mathcal{Y}_U\mathcal{Y}_D + \mathbf{a}^2_L\mathcal{Y}^2_L)\right] \\
& - 4\left(\frac{1}{5}g_1^2 + 8g_3^2\right)\mathrm{Tr}\left[\left(\mathcal{M}^2_{\widetilde{Q}} + \mathcal{M}^2_{\widetilde{\overline{D}}} + m^2_{H_d}\right)\mathcal{Y}^2_D + \mathbf{a}^2_D\right] \\
& - \frac{8}{5}g_1^2\left[M_1^2\mathrm{Tr}\left(\mathcal{Y}^2_D\right) - M_1\mathrm{Tr}\left(\mathbf{a}_D\mathcal{Y}_D\right)\right] \\
& + 64g_3^2\left[M_3^2\mathrm{Tr}\left(\mathcal{Y}^2_D\right) - M_3\mathrm{Tr}\left(\mathbf{a}_D\mathcal{Y}_D\right)\right] \\
& + \frac{12}{5}g_1^2\Bigg(\mathrm{Tr}\left[(\mathcal{M}^2_{\widetilde{L}} + \mathcal{M}^2_{\widetilde{\overline{E}}} + m^2_{H_d})\mathcal{Y}^2_L\right] \\
& \qquad + 2(M_1^2\mathrm{Tr}(\mathcal{Y}^2_L) - M_1\mathrm{Tr}(\mathbf{a}_L\mathcal{Y}_L))\Bigg) \\
& + \frac{3}{5}g_1^2\left[\frac{207}{5}g_1^2M_1^2 + 6g_2^2(M_1^2 + M_2^2 + M_1M_2) - 2\widetilde{S}' + \sigma_1\right] \\
& + 3g_2^2\left(11g_2^2M_2^2 + \sigma_2\right)
\end{aligned}
\tag{B.38}
$$

Squark masses

The two-loop soft squark squared mass RGEs are listed below. The RGEs are presented in the real, diagonal 3×3 matrix form.

$$
\begin{aligned}
\beta^{(2\ell)}_{\mathcal{M}^2_{\widetilde{Q}}} = 2\mathcal{Y}_U^2 \Bigg[& \frac{4}{5} g_1^2 \left(\mathcal{M}^2_{\widetilde{Q}} + \mathcal{M}^2_{\widetilde{\overline{U}}} + m^2_{H_u} + 2M_1^2 \right) \\
& - 4(\mathcal{M}^2_{\widetilde{Q}} + \mathcal{M}^2_{\widetilde{\overline{U}}} + m^2_{H_u}) \mathcal{Y}_U^2 \\
& - 3(\mathcal{M}^2_{\widetilde{Q}} + \mathcal{M}^2_{\widetilde{\overline{U}}} + 2m^2_{H_u}) \mathrm{Tr}(\mathcal{Y}_U^2) - 3\mathrm{Tr}(\mathbf{a}_U^2) \\
& - 3\mathrm{Tr}\left((\mathcal{M}^2_{\widetilde{Q}} + \mathcal{M}^2_{\widetilde{\overline{U}}}) \mathcal{Y}_U^2 \right) - 8\mathbf{a}_U^2 \Bigg] \\
+ 2\mathcal{Y}_D^2 \Bigg[& \frac{2}{5} g_1^2 \left(\mathcal{M}^2_{\widetilde{Q}} + \mathcal{M}^2_{\widetilde{\overline{D}}} + m^2_{H_d} + 2M_1^2 \right) \\
& - 4(\mathcal{M}^2_{\widetilde{Q}} + \mathcal{M}^2_{\widetilde{\overline{D}}} + m^2_{H_d}) \mathcal{Y}_D^2 - \mathrm{Tr}(3\mathbf{a}_D^2 + \mathbf{a}_L^2) \\
& - \left(\mathcal{M}^2_{\widetilde{Q}} + \mathcal{M}^2_{\widetilde{\overline{D}}} + 2m^2_{H_d} \right) \mathrm{Tr}(3\mathcal{Y}_D^2 + \mathcal{Y}_L^2) \\
& - \mathrm{Tr}\left(3(\mathcal{M}^2_{\widetilde{Q}} + \mathcal{M}^2_{\widetilde{\overline{D}}}) \mathcal{Y}_D^2 + (\mathcal{M}^2_{\widetilde{L}} + \mathcal{M}^2_{\widetilde{\overline{E}}}) \mathcal{Y}_L^2 \right) - 8\mathbf{a}_D^2 \Bigg] \\
- 4\mathbf{a}_U \mathcal{Y}_U & \left[3\mathrm{Tr}(\mathbf{a}_U \mathcal{Y}_U) + \frac{4}{5} g_1^2 M_1 \right] \\
- 4\mathbf{a}_D \mathcal{Y}_D & \left[\mathrm{Tr}(3\mathbf{a}_D \mathcal{Y}_D + \mathbf{a}_L \mathcal{Y}_L) + \frac{2}{5} g_1^2 M_1 \right] \\
+ 2\mathbf{a}_U^2 & \left(\frac{4}{5} g_1^2 - 3\mathrm{Tr}(\mathcal{Y}_U^2) \right) + 2\mathbf{a}_D^2 \left(\frac{2}{5} g_1^2 - \mathrm{Tr}(3\mathcal{Y}_D^2 + \mathcal{Y}_L^2) \right) \\
+ \frac{1}{5} g_1^2 \Bigg[& \frac{199}{15} g_1^2 M_1^2 + 2g_2^2 (M_1^2 + M_2^2 + M_1 M_2) \\
& + \frac{32}{9} g_3^2 (M_1^2 + M_3^2 + M_1 M_3) + 2\widetilde{S}' + \frac{1}{3}\sigma_1 \Bigg] \\
+ g_2^2 & \left[33 g_2^2 M_2 + 32 g_3^2 (M_2^2 + M_3^2 + M_2 M_3) + 3\sigma_2 \right] \\
- \frac{16}{3} g_3^2 & \left[8 g_3^2 M_3^2 + \sigma_3 \right]
\end{aligned}
\tag{B.39}
$$

$$
\begin{aligned}
\beta^{(2\ell)}_{\mathcal{M}^2_{\widetilde{\overline{U}}}} = 4\mathcal{Y}_U^2 \Bigg[& 6g_2^2 M_2^2 - \frac{2}{5} g_1^2 M_1^2 \\
& - 2(\mathcal{M}^2_{\widetilde{Q}} + \mathcal{M}^2_{\widetilde{\overline{U}}} + m^2_{H_u})\mathcal{Y}_U^2 - 3\mathrm{Tr}\left[(\mathcal{M}^2_{\widetilde{Q}} + \mathcal{M}^2_{\widetilde{\overline{U}}})\mathcal{Y}_U^2\right] \\
& - \left(2\mathcal{M}^2_{\widetilde{Q}} + \mathcal{M}^2_{\widetilde{\overline{U}}} + \mathcal{M}^2_{\widetilde{\overline{D}}} + m^2_{H_d}\right)\mathcal{Y}_D^2 - 3\mathrm{Tr}\left(\mathbf{a}_U^2\right) \\
& - 3(\mathcal{M}^2_{\widetilde{Q}} + \mathcal{M}^2_{\widetilde{\overline{U}}} + 2m^2_{H_u})\mathrm{Tr}(\mathcal{Y}_U^2) - 4\mathbf{a}_U^2 - \mathbf{a}_D^2 \\
& - \left(\frac{1}{5}g_1^2 - 3g_2^2\right)\left(\mathcal{M}^2_{\widetilde{Q}} + \mathcal{M}^2_{\widetilde{\overline{U}}} + m^2_{H_u}\right) \Bigg] \\
& - 8\mathbf{a}_U\mathcal{Y}_U\left[\mathbf{a}_D\mathcal{Y}_d + 3\mathrm{Tr}(\mathbf{a}_U\mathcal{Y}_U) - \frac{1}{5}g_1^2 M_1 + 3g_2^2 M_2\right] \\
& - 4\mathbf{a}_U^2\left[\frac{1}{5}g_1^2 - 3g_2^2 + 3\mathrm{Tr}(\mathcal{Y}_U^2) + \mathcal{Y}_D^2\right] \\
& + \frac{8}{5}g_1^2\left[\frac{428}{15}g_1^2 M_1^2 + \frac{64}{9}g_3^2(M_1^2 + M_3^2 + M_1 M_3) + \frac{2}{3}\sigma_1 - \widetilde{S}'\right] \\
& - \frac{16}{3}g_3^2\left[8g_3^2 M_3^2 - \sigma_3\right]
\end{aligned}
\tag{B.40}
$$

$$
\begin{aligned}
\beta^{(2\ell)}_{\mathcal{M}^2_{\widetilde{D}}} = & -4\mathcal{Y}_U^2\left[\left(2\mathcal{M}^2_{\widetilde{Q}}+\mathcal{M}^2_{\widetilde{U}}+\mathcal{M}^2_{\widetilde{D}}+m^2_{H_d}\right)\mathcal{Y}_D^2+\mathbf{a}_D^2\right] \\
& +4\mathcal{Y}_D^2\left[\frac{2}{5}g_1^2M_1^2+6g_2^2M_2^2-2\left(\mathcal{M}^2_{\widetilde{Q}}+\mathcal{M}^2_{\widetilde{D}}+m^2_{H_d}\right)\mathcal{Y}_D^2\right. \\
& \quad -\left(\mathcal{M}^2_{\widetilde{Q}}+\mathcal{M}^2_{\widetilde{D}}+2m^2_{H_d}\right)\mathrm{Tr}\left(3\mathcal{Y}_D^2+\mathcal{Y}_L^2\right) \\
& \quad -\mathrm{Tr}\left(3(\mathcal{M}^2_{\widetilde{Q}}+\mathcal{M}^2_{\widetilde{U}})\mathcal{Y}_D^2+(\mathcal{M}^2_{\widetilde{L}}+\mathcal{M}^2_{\widetilde{E}})\mathcal{Y}_L^2\right) \\
& \quad -\mathrm{Tr}(3\mathbf{a}_D^2+\mathbf{a}_L^2)-16\mathbf{a}_D^2-4\mathbf{a}_U^2 \\
& \quad \left.+\left(\frac{1}{5}g_1^2+3g_2^2\right)\left(\mathcal{M}^2_{\widetilde{Q}}+\mathcal{M}^2_{\widetilde{D}}+m^2_{H_d}\right)\right] \\
& -8\mathbf{a}_D\mathcal{Y}_D\left[\mathbf{a}_U\mathcal{Y}_U+\mathrm{Tr}\left(3\mathbf{a}_D\mathcal{Y}_D+\mathbf{a}_L\mathcal{Y}_L\right)+\frac{1}{5}g_1^2M_1+3g_2^2M_2\right] \\
& +4\mathbf{a}_D^2\left[\frac{1}{5}g_1^2+3g_2^2-\mathrm{Tr}\left(3\mathcal{Y}_D^2+\mathcal{Y}_L^2\right)\right] \\
& +\frac{4}{5}g_1^2\left[\frac{202}{15}g_1^2M_1^2+\frac{32}{9}g_3^2(M_1^2+M_3^2+M_1M_3)+\widetilde{S}'+\frac{1}{3}\sigma_1\right] \\
& -\frac{16}{3}g_3^2\left[8g_3^2M_3^2-\sigma_3\right]
\end{aligned}
\tag{B.41}
$$

Slepton masses

The two-loop soft slepton squared mass RGEs are listed below. The RGEs are presented in the real, diagonal 3×3 matrix form.

$$
\begin{aligned}
\beta^{(2\ell)}_{\mathcal{M}^2_{\widetilde{L}}} = & -2\mathcal{Y}_L^2\Bigg[4\left(\mathcal{M}^2_{\widetilde{L}}+\mathcal{M}^2_{\widetilde{\overline{E}}}+m^2_{H_d}\right)\mathcal{Y}_L^2 \\
& \qquad +\left(\mathcal{M}^2_{\widetilde{L}}+\mathcal{M}^2_{\widetilde{\overline{E}}}+2m^2_{H_d}\right)\mathrm{Tr}(3\mathcal{Y}_D^2+\mathcal{Y}_L^2) \\
& \qquad +\mathrm{Tr}\left(3(\mathcal{M}^2_{\widetilde{Q}}+\mathcal{M}^2_{\widetilde{\overline{D}}})\mathcal{Y}_D^2+(\mathcal{M}^2_{\widetilde{L}}+\mathcal{M}^2_{\widetilde{\overline{E}}})\mathcal{Y}_L^2\right) \\
& \qquad +8\mathbf{a}_L^2+\mathrm{Tr}(3\mathbf{a}_D^2+\mathbf{a}_L^2) \\
& \qquad -\frac{6}{5}g_1^2\left(\mathcal{M}^2_{\widetilde{L}}+\mathcal{M}^2_{\widetilde{\overline{E}}}+m^2_{H_d}+2M_1^2\right)\Bigg] \\
& -4\mathbf{a}_L\mathbf{Y}_L\left[\frac{6}{5}g_1^2M_1+\mathrm{Tr}(3\mathbf{a}_U\mathcal{Y}_U+\mathbf{a}_L\mathcal{Y}_L)\right] \\
& +2\mathbf{a}_L^2\left[\frac{6}{5}g_1^2-\mathrm{Tr}(3\mathcal{Y}_D^2+\mathcal{Y}_L^2)\right] \\
& +\frac{3}{5}g_1^2\left[\frac{207}{5}g_1^2M_1^2+6g_2^2\left(M_1^2+M_2^2+M_1M_2\right)-2\widetilde{S}'+\sigma_1\right] \\
& +3g_2^2\left(11g_2^2M_2^2+\sigma_2\right)
\end{aligned}
\tag{B.42}
$$

$$
\begin{aligned}
\beta^{(2\ell)}_{\mathcal{M}^2_{\widetilde{E}}} = & -2\mathcal{Y}_L^2\Bigg[4\left(\mathcal{M}^2_{\widetilde{L}}+\mathcal{M}^2_{\widetilde{\overline{E}}}+m^2_{H_d}\right)\mathcal{Y}_L^2+8\mathbf{a}_L^2 \\
& \qquad +2\left(\mathcal{M}^2_{\widetilde{L}}+\mathcal{M}^2_{\widetilde{\overline{E}}}+2m^2_{H_d}\right)\mathrm{Tr}\left(3\mathcal{Y}_D^2+\mathcal{Y}_L^2\right) \\
& \qquad +2\mathrm{Tr}\left(3(\mathcal{M}^2_{\widetilde{Q}}+\mathcal{M}^2_{\widetilde{\overline{D}}})\mathcal{Y}_D^2+(\mathcal{M}^2_{\widetilde{L}}+\mathcal{M}^2_{\widetilde{\overline{E}}})\mathcal{Y}_L^2\right) \\
& \qquad +2\mathrm{Tr}\left(3\mathbf{a}_D^2+\mathbf{a}_L^2\right)+\frac{12}{5}g_1^2M_1^2-12g_2^2M_2^2 \\
& \qquad +6\left(\frac{1}{5}g_1^2+g_2^2\right)\left(\mathcal{M}^2_{\widetilde{L}}+\mathcal{M}^2_{\widetilde{\overline{E}}}+m^2_{H_d}\right)\Bigg] \\
& -8\mathbf{a}_L\mathcal{Y}_L\left[\mathrm{Tr}\left(3\mathbf{a}_D\mathcal{Y}_D+\mathbf{a}_L\mathcal{Y}_L\right)-\frac{3}{5}g_1^2M_1+3g_2^2M_2\right] \\
& -4\mathbf{a}_L^2\left[3\left(\frac{1}{5}g_1^2+g_2^2\right)+\mathrm{Tr}(3\mathcal{Y}_D^2+\mathcal{Y}_L^2)\right] \\
& +\frac{12}{5}g_1^2\left[\frac{234}{5}g_1^2M_1^2+\widetilde{S}'+\sigma_1\right]
\end{aligned}
\tag{B.43}
$$

Appendix C

Stability conditions for proper EWSB

The conditions for proper electroweak symmetry breaking (EWSB) can provide strong constraints on the parameter space of the MSSM, especially in the context of the string landscape and in comparing models of physically realizable supersymmetry. In this Appendix, we review and formalize the conditions required to ensure proper electroweak symmetry breaking, based on the nature of critical points in the field space of the scalar potential Eq. (A.1).

The well-known tree-level conditions and the less well-known loop-level conditions for proper EWSB in the MSSM are listed below, with elaboration on the notion of vacuum stability, as the literature tends to misrepresent classifications of vacuum stability with regards to EWSB. Minimization of the scalar potential occurs as in Appendix A, where the scalar potential $V(h_u^0, h_d^0)$ is a function of the neutral Higgs fields, and at some point(s) in field space, critical points occur:

$$\frac{\partial V}{\partial h_u^0} = \frac{\partial V}{\partial h_d^0} = 0.$$

Such a point will satisfy the equations Eq. (A.3-A.5) at tree-level, and then at loop level with the inclusion of the corrections in Eq. (A.9-A.10).

C.1 Destabilizing the origin of field space

C.1.1 Tree level

We begin with the tree-level scalar potential Eq. (A.2). Two conditions exist to guarantee the stability of the vacuum and that EWSB occurs properly. The first is to check whether the scalar potential fails to develop a minimum at the origin of neutral scalar field space, where $h_u^0 = 0 = h_d^0$. If not, then the Higgs scalars will fail to develop non-zero VEVs, and EWSB will fail to occur as expected. Two possibilities arise for an unstable origin of field space, which is naturally a critical point of the scalar potential: either the origin is a saddle point of field space, or it is a maximum. In order to accurately classify the stability of these critical points, we must construct the matrix of derivatives of the tree-level scalar potential V_{tree}, called the *Hessian*. The form of the Hessian is listed below for a general (real) point (h_u^0, h_d^0) of field space.

$$\mathbb{H}\left[V_{\text{tree}}(h_u^0, h_d^0)\right] = \begin{bmatrix} \frac{\partial^2 V_{\text{tree}}}{(\partial h_u^0)^2} & \frac{\partial^2 V_{\text{tree}}}{\partial h_u^0 \partial h_d^0} \\ \frac{\partial^2 V_{\text{tree}}}{\partial h_u^0 \partial h_d^0} & \frac{\partial^2 V_{\text{tree}}}{(\partial h_d^0)^2} \end{bmatrix} \tag{C.1}$$

At a critical point of field space, one can perform the multivariable second derivative test with this Hessian. If a critical point has a Hessian whose eigenvalues are *opposite sign*, then the critical point is a saddle point. Since the determinant is equal to the product of the eigenvalues, then this condition amounts to checking whether the *determinant* of the Hessian Eq. (C.1) is negative.

However, if the determinant is instead *positive*, we must check one more

condition to test whether the point of field space is a minimum or maximum, as the determinant alone here is insufficient for proper analysis. The determinant being positive implies that both of the Hessian's eigenvalues are the same sign, which can occur if both values are negative, or if both are positive. Thus, one must check the signs of one of the diagonal entries of the Hessian here to determine the nature of the critical point. For example, if at a critical point whose Hessian has positive determinant, and

$$\frac{\partial^2 V}{(\partial h_u^0)^2} < \ (>)\ 0,$$

then that critical point will be a maximum (minimum) by this second derivative test.

At tree level and at the origin of field space, the Hessian takes the form below.

$$\mathbb{H}\left[V(0,0)\right] = \begin{bmatrix} m_{H_u}^2 + \mu^2 & -b \\ -b & m_{H_d}^2 + \mu^2 \end{bmatrix} \tag{C.2}$$

If the origin is a saddle point of field space, then this would mean that

$$\begin{gathered} \det(\mathbb{H}\left[V(0,0)\right]) < 0 \implies \\ (m_{H_u}^2 + \mu^2)(m_{H_d}^2 + \mu^2) < b^2 \end{gathered} \tag{C.3}$$

If instead the inequality sign is flipped in Eq. (C.3), but $\mathrm{Tr}\left(\mathbb{H}\left[V(0,0)\right]\right) < (>)\ 0$, then the origin will be a maximum (minimum), and the origin will succeed (fail) in destabilization. The qualitative effects of these results are summarized in Table C.1. In the case where the origin is a maximum, extra care must be taken to

ensure that the CP-odd pseudoscalar Higgs mass remains positive at loop level, as the tree-level expression here implies that $m_A^2 < 0$.

Stability type	Hessian determinant sign	Hessian diagonal sign
Saddle point	$-$	Not needed
Minimum	$+$	$+$
Maximum	$+$	$-$

Table C.1: Summary of the requirements on the scalar potential's Hessian for classifying the stability of critical points of field space for EWSB. Highlighted rows are potentially phenomenologically allowed cases at the origin of field space, so that this origin is destabilized and EWSB can occur as expected.

C.1.2 Loop level

At loop level, it is possible that destabilization of a tree-level stable vacuum field space's origin can occur. To examine the effects of this, one must consider the loop-corrected effective potential in Eq. (A.1) and adjust the Hessian in Eq. (C.2) accordingly. This loop-corrected Hessian is listed below.

$$\mathbb{H}\left[V\left(0,0\right)\right] = \begin{bmatrix} m_{H_u}^2 + \mu^2 + \frac{\partial^2 \Delta V}{(\partial h_u^0)^2}\Big|_{h_u^0 = h_d^0 = 0} & -b + \frac{\partial^2 \Delta V}{\partial h_u^0 \partial h_d^0}\Big|_{h_u^0 = h_d^0 = 0} \\ -b + \frac{\partial^2 \Delta V}{\partial h_u^0 \partial h_d^0}\Big|_{h_u^0 = h_d^0 = 0} & m_{H_d}^2 + \mu^2 + \frac{\partial^2 \Delta V}{(\partial h_d^0)^2}\Big|_{h_u^0 = h_d^0 = 0} \end{bmatrix} \tag{C.4}$$

By taking the determinant of this matrix and utilizing Table C.1, one can determine the stability of the origin of field space for EWSB at loop level. The second derivatives in Eq. (C.4) may be computed via derivatives of the expressions in Appendix A, then limiting $v_u \to 0, v_d \to 0$, while leaving their ratio $v_u/v_d = \tan(\beta)$

fixed, since the field-dependent masses by extension depend somewhat on the specific value of β. These expressions are listed below.

Second derivatives on the diagonal of the Hessian of the form

$$\frac{\partial^2 \Delta V}{\left(\partial h^0_{u,d}\right)^2} \equiv \Sigma^{(2)}_{uu,dd}$$

can be expressed as follows.

$$\begin{aligned}\Sigma^{(2)}_{uu,dd} = \sum_i \Bigg\{ & \frac{1}{32\pi^2} q_i C_i (-1)^{2s_i} (2s_i+1) \\ & \times \Bigg[\left(\frac{\partial m_i^2}{\partial v_{u,d}}\right)^2 \log\left(\frac{m_i^2}{Q^2}\right) \\ & \quad + m_i^2 \left(\frac{\partial^2 m_i^2}{(\partial v_{u,d})^2}\right) \left(\log\left(\frac{m_i^2}{Q^2}\right) - 1\right) \Bigg] \Bigg\} \Bigg|_{v_u = v_d = 0}\end{aligned} \tag{C.5}$$

Second derivatives on the off-diagonal of the Hessian of the form

$$\frac{\partial^2 \Delta V}{\partial h^0_u \partial h^0_d} = \frac{\partial^2 \Delta V}{\partial h^0_d \partial h^0_u} \equiv \Sigma^{(2)}_{ud}$$

can be expressed as follows.

$$\begin{aligned}\Sigma^{(2)}_{ud} = \sum_i \Bigg\{ & \frac{1}{32\pi^2} q_i C_i (-1)^{2s_i} (2s_i+1) \\ & \times \Bigg[\frac{\partial m_i^2}{\partial v_u} \frac{\partial m_i^2}{\partial v_d} \log\left(\frac{m_i^2}{Q^2}\right) \\ & \quad + m_i^2 \left(\frac{\partial^2 m_i^2}{\partial v_u \partial v_d}\right) \left(\log\left(\frac{m_i^2}{Q^2}\right) - 1\right) \Bigg] \Bigg\} \Bigg|_{v_u = v_d = 0}\end{aligned} \tag{C.6}$$

The individual contributions $\Sigma^{(2)}_{uu,dd,ud}$ are listed in the following subsections, having

taken $v_{u,d} \to 0$ in such a way that we maintain their ratio $v_u/v_d = \tan(\beta)$. This limiting towards the origin of field space is performed *after* the derivatives with respect to the appropriate fields are taken.

SM particles

The one-loop contributions to the vacuum stability condition for Standard Model particles are listed below.

Gauge bosons

The radiative corrections to the vacuum stability conditions vanish upon taking the limit $v \to 0$ for the W and Z SM gauge bosons.

$$\Sigma^{(2)}_{uu}(Z) = \Sigma^{(2)}_{dd}(Z) = \Sigma^{(2)}_{ud}(Z) = 0 \tag{C.7}$$

Quarks and leptons

Similar to the gauge bosons, the radiative corrections to the vacuum stability conditions vanish upon taking the limit $v \to 0$ for the SM fermions $f_{\rm SM}$ (quarks and leptons).

$$\Sigma^{(2)}_{uu}(f_{\rm SM}) = \Sigma^{(2)}_{dd}(f_{\rm SM}) = \Sigma^{(2)}_{ud}(f_{\rm SM}) = 0 \tag{C.8}$$

SUSY particles

The one-loop contributions to the vacuum stability condition for SUSY particles are listed below.

Higgs bosons

For the neutral Higgs bosons, the diagonal terms of the Hessian are given below.

$$\Sigma_{uu}^{(2)}(h^0) = \Sigma_{dd}^{(2)}(h^0) = 0 \tag{C.9}$$

$$\Sigma_{uu}^{(2)}(H^0) = \frac{(g^2+g'^2)}{8\pi^2}\left[m_{A^0}^2\cos^4(\beta)\,(2\cos(2\beta)-1)\left(\log\left(\frac{m_{A^0}^2}{Q^2}\right)-1\right)\right] \tag{C.10}$$

$$\Sigma_{dd}^{(2)}(H^0) = \frac{-(g^2+g'^2)}{8\pi^2}\left[m_{A^0}^2\sin^4(\beta)\,(2\cos(2\beta)+1)\left(\log\left(\frac{m_{A^0}^2}{Q^2}\right)-1\right)\right] \tag{C.11}$$

The off-diagonal second derivatives take the forms below.

$$\Sigma_{ud}^{(2)}(h^0) = 0 \tag{C.12}$$

$$\Sigma_{ud}^{(2)}(H^0) = \frac{(g^2+g'^2)}{16\pi^2}\left[m_{A^0}^2\sin^3(2\beta)\left(\log\left(\frac{m_{A^0}^2}{Q^2}\right)-1\right)\right] \tag{C.13}$$

For the charged Higgs bosons, the diagonal terms of the Hessian are given below.

$$\Sigma_{uu}^{(2)}(H^\pm) = \Sigma_{dd}^{(2)}(H^\pm) = \frac{g^2}{16\pi^2}m_{A^0}^2\left[\log\left(\frac{m_{A^0}^2}{Q^2}\right)-1\right] \tag{C.14}$$

The off-diagonal second derivatives vanish.

$$\Sigma^{(2)}_{ud}(H^{\pm}) = 0 \tag{C.15}$$

Neutralinos

The neutralino terms are more computationally challenging to obtain due to the fact that the neutralino mass squared eigenvalues arise from solutions to the fourth degree characteristic polynomial of the mass matrix squared. Alternatively, as in Appendix A, we can compute derivatives of the eigenvalues of the *unsquared* mass matrix through the chain rule on its characteristic polynomial. A straightforward application of the chain rule reveals the general form of the second derivative we desire below.

$$\frac{\partial^2 m^2_{\widetilde{Z}^0,i}}{\partial y \partial x} = 2\left[\frac{\partial m_{\widetilde{Z}^0,i}}{\partial y}\frac{\partial m_{\widetilde{Z}^0,i}}{\partial x} + m_{\widetilde{Z}^0,i}\frac{\partial^2 m_{\widetilde{Z}^0}}{\partial x \partial y}\right] \tag{C.16}$$

Letting x, y be v_u and/or v_d then permits us to compute the eigenvalues with the following formula, obtained via the chain rule from the characteristic polynomial of the *unsquared* mass matrix, whose coefficients are given in Eqs. (A.36 - A.39). First derivatives take the form here. Simplifications have been made, considering that $\partial a/\partial v_{u,d} = 0$, as seen in Eq. (A.36).

$$\frac{\partial m_{\widetilde{Z}^0,i}}{\partial v_{u,d}} = -\left[\frac{\frac{\partial b}{\partial v_{u,d}}\lambda^2 + \frac{\partial c}{\partial v_{u,d}}\lambda + \frac{\partial d}{\partial v_{u,d}}}{4\lambda^3 + 3a\lambda^2 + 2b\lambda + c}\right]_{\lambda = m_{\widetilde{Z}^0,i}} \tag{C.17}$$

The second derivatives then follow, where x or y can be v_u and/or v_d, depending on the derivative in question. We denote the i'th eigenvalue of the neutralino

mass matrix as $\lambda = m_{\widetilde{Z}^0,i}$, where $i = 1-4$.

$$\frac{\partial^2\lambda}{\partial y\partial x} = \left\{ \frac{\left(12\lambda^2+6a\lambda+2b\right)\frac{\partial\lambda}{\partial y}+2\lambda\frac{\partial b}{\partial y}+\frac{\partial c}{\partial y}}{\left(4\lambda^3+3a\lambda^2+2b\lambda+c\right)^2} - \frac{\left[\left(2\lambda\frac{\partial b}{\partial x}+\frac{\partial c}{\partial x}\right)\frac{\partial\lambda}{\partial y}+\left(\frac{\partial^2 b}{\partial y\partial x}\lambda^2\right)+\left(\frac{\partial^2 c}{\partial y\partial x}\lambda\right)+\left(\frac{\partial^2 d}{\partial y\partial x}\right)\right]}{4\lambda^3+3a\lambda^2+2b\lambda+c} \right\} \tag{C.18}$$

The explicit expressions obtained are long and unwieldy. However, after taking the limit of $v_{u,d} \to 0$, the result simplifies well. Algebraically, it can be shown that terms of the form $\frac{\partial\lambda}{\partial v_{u,d}}$ vanish when we take $v_{u,d} = 0$ (after the derivative), where $\lambda = m_{\widetilde{Z}^0,i}$ and $i = 1-4$. The first derivatives of the characteristic polynomial coefficients also vanish at the origin of field space. However, some of the second derivatives of the characteristic polynomial coefficients survive and are listed below – all others vanish.

$$\left.\frac{\partial^2 b}{\left(\partial v_u\right)^2}\right|_{v_u=v_d=0} = \left.\frac{\partial^2 b}{\left(\partial v_d\right)^2}\right|_{v_u=v_d=0} = -\left(g^2+g'^2\right) \tag{C.19}$$

$$\left.\frac{\partial^2 c}{\left(\partial v_u\right)^2}\right|_{v_u=v_d=0} = \left.\frac{\partial^2 b}{\left(\partial v_d\right)^2}\right|_{v_u=v_d=0} = M_1 g^2 + M_2 g'^2 \tag{C.20}$$

$$\left.\frac{\partial^2 c}{\partial v_u \partial v_d}\right|_{v_u=v_d=0} = -\left(g^2+g'^2\right)\mu \tag{C.21}$$

$$\left.\frac{\partial^2 d}{\partial v_u \partial v_d}\right|_{v_u=v_d=0} = \left(M_1 g^2 + M_2 g'^2\right)\mu \tag{C.22}$$

With these evaluations complete, the full form of the second derivatives is listed below. We denote a neutralino mass $m_{\widetilde{Z}^0,i}$ evaluated at the origin of field space by $\widetilde{\lambda}$. The expressions for the neutralino masses simplify tremendously at

the origin of field space. Evaluating the eigenvalues of the neutralino mass matrix at the origin of field space simply reveals the following eigenvalues.

$$\widetilde{\lambda} \in \{\mu, -\mu, M_1, M_2\} \tag{C.23}$$

The second derivatives of the neutralino eigenvalues at the origin of field space are below.

$$\left.\frac{\partial^2 \lambda}{\left(\partial v_{u,d}\right)^2}\right|_{v_u=v_d=0}^{\lambda=m_{\widetilde{Z}^0,i}} = \frac{(g^2+g'^2)\widetilde{\lambda}^2 - (M_1 g^2 + M_2 g'^2)\widetilde{\lambda}}{4\widetilde{\lambda}^3 - 3(M_1+M_2)\widetilde{\lambda}^2 + (2(M_1 M_2 - \mu^2))\widetilde{\lambda} - M_1 M_2 \mu^2} \tag{C.24}$$

$$\left.\frac{\partial^2 \lambda}{\partial v_u \partial v_d}\right|_{v_u=v_d=0}^{\lambda=m_{\widetilde{Z}^0,i}} = \frac{(g^2+g'^2)\mu\widetilde{\lambda} - (M_1 g^2 + M_2 g'^2)\mu}{4\widetilde{\lambda}^3 - 3(M_1+M_2)\widetilde{\lambda}^2 + (2(M_1 M_2 - \mu^2))\widetilde{\lambda} - M_1 M_2 \mu^2} \tag{C.25}$$

Finally, the one-loop neutralino contributions to the scalar potential's Hessian then take the following forms.

$$\Sigma_{uu}^{(2)}\left(\widetilde{Z}_i^0\right) = \Sigma_{dd}^{(2)}\left(\widetilde{Z}_i^0\right) = -\frac{\widetilde{\lambda}^3}{8\pi^2}\left[\log\left(\frac{\widetilde{\lambda}^2}{Q^2}\right) - 1\right]\left[\left.\frac{\partial^2 \lambda}{\left(\partial v_{u,d}\right)^2}\right|_{v_u=v_d=0}^{\lambda=m_{\widetilde{Z}^0,i}}\right] \tag{C.26}$$

$$\Sigma_{ud}^{(2)}\left(\widetilde{Z}_i^0\right) = -\frac{\widetilde{\lambda}^3}{8\pi^2}\left[\log\left(\frac{\widetilde{\lambda}^2}{Q^2}\right) - 1\right]\left[\left.\frac{\partial^2 \lambda}{\partial v_u \partial v_d}\right|_{v_u=v_d=0}^{\lambda=m_{\widetilde{Z}^0,i}}\right] \tag{C.27}$$

Charginos

The one-loop chargino contributions to the scalar potential's Hessian are listed below. The lighter eigenstate (index 1) corresponds to the upper signs, and the

heavier eigenstate (index 2) corresponds to the lower signs.

$$\begin{aligned}\Sigma_{uu}^{(2)}\left(\widetilde{C}_{1,2}^{\pm}\right) &= \Sigma_{dd}^{(2)}\left(\widetilde{C}_{1,2}^{\pm}\right) \\ &= \frac{\mp g^2}{16\pi^2}\frac{\left(M_2^2+\mu^2\mp|M_2^2-\mu^2|\right)^2}{|M_2^2-\mu^2|} \\ &\quad\times\left[\log\left(\frac{M_2^2+\mu^2\mp|M_2^2-\mu^2|}{2Q^2}\right)-1\right]\end{aligned} \tag{C.28}$$

$$\begin{aligned}\Sigma_{ud}^{(2)}\left(\widetilde{C}_{1,2}^{\pm}\right) &= \frac{\pm g^2 M_2\mu}{16\pi^2}\frac{\left(M_2^2+\mu^2\mp|M_2^2-\mu^2|\right)}{|M_2^2-\mu^2|} \\ &\quad\times\left[\log\left(\frac{M_2^2+\mu^2\mp|M_2^2-\mu^2|}{2Q^2}\right)-1\right]\end{aligned} \tag{C.29}$$

Squarks

The one-loop up-type squark $\widetilde{U}_g$ of generation g contributions to the scalar potential's Hessian are listed below. Here, $m^2_{\widetilde{U}_g}$ denotes the mass of the right-handed SSB up-type gauge eigenstate squark running squared mass of generation g. $\Sigma_{uu}^{(2)}\left(\widetilde{U}_{g,i}\right)$ with $i=1,2$ denotes the one-loop Hessian contribution from the i'th up-squark mass eigenstate of generation g ($i=1$ for the lighter state or 2 for the heavier state as usual). The top sign corresponds to the lighter eigenstate,

and the bottom sign corresponds to the heavier eigenstate.

$$\begin{aligned}\Sigma_{uu}^{(2)}\left(\widetilde{U}_{g,1,2}\right) = & \frac{\pm\left(m_{\widetilde{Q}_g}^2 + m_{\widetilde{U}_g}^2 \mp \left|m_{\widetilde{Q}_g}^2 - m_{\widetilde{U}_g}^2\right|\right)}{128\pi^2\left|m_{\widetilde{Q}_g}^2 - m_{\widetilde{U}_g}^2\right|} \\ & \times \left[\log\left(\frac{m_{\widetilde{Q}_g}^2 + m_{\widetilde{U}_g}^2 \mp \left|m_{\widetilde{Q}_g}^2 - m_{\widetilde{U}_g}^2\right|}{2Q^2}\right) - 1\right] \\ & \times \Bigg[\left(3g^2 - 10g'^2\right)\left(m_{\widetilde{Q}_g}^2 - m_{\widetilde{U}_g}^2\right) - 24a_{U_g}^2 \\ & \qquad \mp 3\left(g^2 + 2g'^2 - 8y_{U_g}^2\right)\left|m_{\widetilde{Q}_g}^2 - m_{\widetilde{U}_g}^2\right|\Bigg]\end{aligned} \tag{C.30}$$

$$\begin{aligned}\Sigma_{dd}^{(2)}\left(\widetilde{U}_{g,1,2}\right) = & \frac{\mp\left(m_{\widetilde{Q}_g}^2 + m_{\widetilde{U}_g}^2 \mp \left|m_{\widetilde{Q}_g}^2 - m_{\widetilde{U}_g}^2\right|\right)}{128\pi^2\left|m_{\widetilde{Q}_g}^2 - m_{\widetilde{U}_g}^2\right|} \\ & \times \left[\log\left(\frac{m_{\widetilde{Q}_g}^2 + m_{\widetilde{U}_g}^2 \mp \left|m_{\widetilde{Q}_g}^2 - m_{\widetilde{U}_g}^2\right|}{2Q^2}\right) - 1\right] \\ & \times \Bigg[\left(3g^2 - 10g'^2\right)\left(m_{\widetilde{Q}_g}^2 - m_{\widetilde{U}_g}^2\right) + 24y_{U_g}^2\mu^2 \\ & \qquad \mp 3\left(g^2 + 2g'^2\right)\left|m_{\widetilde{Q}_g}^2 - m_{\widetilde{U}_g}^2\right|\Bigg]\end{aligned} \tag{C.31}$$

$$\begin{aligned}\Sigma_{ud}^{(2)}\left(\widetilde{U}_{g,1,2}\right) = & \frac{\pm 3a_{U_g}y_{U_g}\mu}{16\pi^2\left|m_{\widetilde{Q}_g}^2 - m_{\widetilde{U}_g}^2\right|} \\ & \times \left[\log\left(\frac{m_{\widetilde{Q}_g}^2 + m_{\widetilde{U}_g}^2 \mp \left|m_{\widetilde{Q}_g}^2 - m_{\widetilde{U}_g}^2\right|}{2Q^2}\right) - 1\right] \\ & \times \left(m_{\widetilde{Q}_g}^2 + m_{\widetilde{U}_g}^2 \mp \left|m_{\widetilde{Q}_g}^2 - m_{\widetilde{U}_g}^2\right|\right)\end{aligned} \tag{C.32}$$

The one-loop down-type squark $\widetilde{D}_g$ of generation g contributions to the scalar potential's Hessian are listed below. Here, $m_{\widetilde{D}_g}^2$ denotes the mass of the right-handed SSB down-type gauge eigenstate squark running squared mass of genera-

tion g. $\Sigma_{uu}^{(2)}\left(\widetilde{D}_{g,i}\right)$ with $i = 1, 2$ denotes the one-loop Hessian contribution from the i'th down-squark mass eigenstate of generation g (again, $i = 1$ for the lighter state or 2 for the heavier state as usual). Once more, the top sign corresponds to the lighter eigenstate, and the bottom sign corresponds to the heavier eigenstate.

$$\begin{aligned}\Sigma_{uu}^{(2)}\left(\widetilde{D}_{g,1,2}\right) = & \frac{\mp\left(m_{\widetilde{Q}_g}^2 + m_{\widetilde{D}_g}^2 \mp \left|m_{\widetilde{Q}_g}^2 - m_{\widetilde{D}_g}^2\right|\right)}{128\pi^2\left|m_{\widetilde{Q}_g}^2 - m_{\widetilde{D}_g}^2\right|} \\ & \times \left[\log\left(\frac{m_{\widetilde{Q}_g}^2 + m_{\widetilde{D}_g}^2 \mp \left|m_{\widetilde{Q}_g}^2 - m_{\widetilde{D}_g}^2\right|}{2Q^2}\right) - 1\right] \\ & \times \Bigg[\left(3g^2 - 2g'^2\right)\left(m_{\widetilde{Q}_g}^2 - m_{\widetilde{D}_g}^2\right) + 24y_{D_g}^2\mu^2 \\ & \qquad \mp 3\left(g^2 + 2g'^2\right)\left|m_{\widetilde{Q}_g}^2 - m_{\widetilde{D}_g}^2\right|\Bigg]\end{aligned} \tag{C.33}$$

$$\begin{aligned}\Sigma_{dd}^{(2)}\left(\widetilde{D}_{g,1,2}\right) = & \frac{\pm\left(m_{\widetilde{Q}_g}^2 + m_{\widetilde{D}_g}^2 \mp \left|m_{\widetilde{Q}_g}^2 - m_{\widetilde{D}_g}^2\right|\right)}{128\pi^2\left|m_{\widetilde{Q}_g}^2 - m_{\widetilde{D}_g}^2\right|} \\ & \times \left[\log\left(\frac{m_{\widetilde{Q}_g}^2 + m_{\widetilde{D}_g}^2 \mp \left|m_{\widetilde{Q}_g}^2 - m_{\widetilde{D}_g}^2\right|}{2Q^2}\right) - 1\right] \\ & \times \Bigg[\left(3g^2 - 2g'^2\right)\left(m_{\widetilde{Q}_g}^2 - m_{\widetilde{D}_g}^2\right) - 24a_{D_g}^2 \\ & \qquad \mp 3\left(g^2 + 2g'^2 - 8y_{D_g}^2\right)\left|m_{\widetilde{Q}_g}^2 - m_{\widetilde{D}_g}^2\right|\Bigg]\end{aligned} \tag{C.34}$$

$$\begin{aligned}\Sigma_{ud}^{(2)}\left(\widetilde{D}_{g,1,2}\right) = & \frac{\pm 3a_{D_g}y_{D_g}\mu}{16\pi^2\left|m_{\widetilde{Q}_g}^2 - m_{\widetilde{D}_g}^2\right|} \\ & \times \left[\log\left(\frac{m_{\widetilde{Q}_g}^2 + m_{\widetilde{D}_g}^2 \mp \left|m_{\widetilde{Q}_g}^2 - m_{\widetilde{D}_g}^2\right|}{2Q^2}\right) - 1\right] \\ & \times \left(m_{\widetilde{Q}_g}^2 + m_{\widetilde{D}_g}^2 \mp \left|m_{\widetilde{Q}_g}^2 - m_{\widetilde{D}_g}^2\right|\right)\end{aligned} \tag{C.35}$$

Sleptons

The one-loop charged slepton $\widetilde{E}_g$ of generation g contributions to the scalar potential's Hessian are listed below. Here, $m^2_{\widetilde{E}_g}$ denotes the mass of the right-handed SSB gauge eigenstate charged slepton running squared mass of generation g. $\Sigma^{(2)}_{uu}\left(\widetilde{E}_{g,i}\right)$ with $i = 1, 2$ denotes the one-loop Hessian contribution from the i'th charged slepton mass eigenstate of generation g (again, $i = 1$ for the lighter state or 2 for the heavier state as usual). Once more, the top sign corresponds to the lighter eigenstate, and the bottom sign corresponds to the heavier eigenstate.

$$\begin{aligned}\Sigma^{(2)}_{uu}\left(\widetilde{E}_{g,1,2}\right) = &\frac{\mp\left(m^2_{\widetilde{L}_g} + m^2_{\widetilde{E}_g} \mp \left|m^2_{\widetilde{L}_g} - m^2_{\widetilde{E}_g}\right|\right)}{128\pi^2\left|m^2_{\widetilde{L}_g} - m^2_{\widetilde{E}_g}\right|} \\ &\times\left[\log\left(\frac{m^2_{\widetilde{L}_g} + m^2_{\widetilde{E}_g} \mp \left|m^2_{\widetilde{L}_g} - m^2_{\widetilde{E}_g}\right|}{2Q^2}\right) - 1\right] \\ &\times\left[\left(g^2 - 6g'^2\right)\left(m^2_{\widetilde{L}_g} - m^2_{\widetilde{E}_g}\right) + 8y^2_{E_g}\mu^2\right. \\ &\qquad\left.\mp\left(g^2 + 2g'^2\right)\left|m^2_{\widetilde{L}_g} - m^2_{\widetilde{E}_g}\right|\right]\end{aligned} \tag{C.36}$$

$$\begin{aligned}\Sigma^{(2)}_{dd}\left(\widetilde{E}_{g,1,2}\right) = &\frac{\pm\left(m^2_{\widetilde{L}_g} + m^2_{\widetilde{E}_g} \mp \left|m^2_{\widetilde{L}_g} - m^2_{\widetilde{E}_g}\right|\right)}{128\pi^2\left|m^2_{\widetilde{L}_g} - m^2_{\widetilde{E}_g}\right|} \\ &\times\left[\log\left(\frac{m^2_{\widetilde{L}_g} + m^2_{\widetilde{E}_g} \mp \left|m^2_{\widetilde{L}_g} - m^2_{\widetilde{E}_g}\right|}{2Q^2}\right) - 1\right] \\ &\times\left[\left(g^2 - 6g'^2\right)\left(m^2_{\widetilde{L}_g} - m^2_{\widetilde{E}_g}\right) - 8a^2_{E_g}\right. \\ &\qquad\left.\mp\left(g^2 + 2g'^2 - 8y^2_{E_g}\right)\left|m^2_{\widetilde{L}_g} - m^2_{\widetilde{E}_g}\right|\right]\end{aligned} \tag{C.37}$$

$$\Sigma_{ud}^{(2)}\left(\widetilde{E}_{g,1,2}\right) = \frac{\pm a_{E_g} y_{E_g} \mu}{16\pi^2 \left| m_{\widetilde{L}_g}^2 - m_{\widetilde{E}_g}^2 \right|} \times \left[\log\left(\frac{m_{\widetilde{L}_g}^2 + m_{\widetilde{E}_g}^2 \mp \left| m_{\widetilde{L}_g}^2 - m_{\widetilde{E}_g}^2 \right|}{2Q^2} \right) - 1 \right] \times \left(m_{\widetilde{L}_g}^2 + m_{\widetilde{E}_g}^2 \mp \left| m_{\widetilde{L}_g}^2 - m_{\widetilde{E}_g}^2 \right| \right) \tag{C.38}$$

Finally, the one-loop neutral slepton (sneutrino) $\widetilde{\nu}_g$ of generation g contributions to the scalar potential's Hessian are listed below.

$$\Sigma_{uu}^{(2)}\left(\widetilde{\nu}_g\right) = \frac{-\left(g^2 + g'^2\right)}{64\pi^2} m_{\widetilde{L}_g}^2 \left[\log\left(\frac{m_{\widetilde{L}_g}^2}{Q^2} \right) - 1 \right] \tag{C.39}$$

$$\Sigma_{dd}^{(2)}\left(\widetilde{\nu}_g\right) = \frac{\left(g^2 + g'^2\right)}{64\pi^2} m_{\widetilde{L}_g}^2 \left[\log\left(\frac{m_{\widetilde{L}_g}^2}{Q^2} \right) - 1 \right] \tag{C.40}$$

$$\Sigma_{ud}^{(2)}\left(\widetilde{\nu}_g\right) = 0 \tag{C.41}$$

C.2 Bounding the scalar potential from below

C.2.1 Tree level

In addition to requiring that the origin of field space be destabilized, it is also important for vacuum stability that the Higgs scalar potential remains bounded from below and does not precipitously run off to unbounded, large, negative values for arbitrarily large values of the Higgs fields $h_{u,d}^0$. Due to the form of the scalar potential at tree level, Eq. (A.2), the risk of being unbounded from below mainly arises from directions of field space termed D-flat directions, i.e., where $|h_u^0| = |h_d^0|$. In such directions, the quartic term of Eq. (A.2) will cancel. Then requiring that

the scalar potential in this direction is positive for arbitary D-flat field values amounts to the second EWSB condition below.

$$2b < (m_{H_u}^2 + m_{H_d}^2 + 2\mu^2) \tag{C.42}$$

Should Eq. (C.42) fail to hold, then issues arise at the very least with the minimization process, as we can no longer find a real mixing angle β in the half-open interval $[\pi/4, \pi/2)$ that satisfies the tree-level minimization condition Eq. (A.3). It is possible that this is rectified at loop level, but bodes as a very bad sign for proper EWSB and a stable vacuum to occur.

C.2.2 Loop level

Similar to in Appendix C.1.2, one may obtain a loop-corrected version of Eq. (C.42) by adding the loop corrections in Eq. (A.1) to the analysis in Appendix C.2.1. Then, for any arbitrary D-flat value of the Higgs fields $|h_u^0| = |h_d^0| = \gamma$ – which also implies $\tan(\beta) \to 1$ – one may try to naïvely update Eq. (C.42) to the expression below.

$$\begin{aligned} 2b &< m_{H_u}^2 + m_{H_d}^2 + 2\mu^2 + \frac{1}{\gamma^2}\Delta V\Big|_{D\text{-flat}} \\ &\sim m_{H_u}^2 + m_{H_d}^2 + 2\mu^2 + \frac{1}{\gamma^2}\Delta V\Big|_{\tan(\beta)\to 1, v_u\to\gamma, v_d\to\gamma} \end{aligned} \tag{C.43}$$

This may seem correct, especially since for very large values of $|h_u^0| = |h_d^0| = \gamma$, the loop contributions ΔV are suppressed by γ^{-2}. However, care must still be taken in ensuring the expected behavior for large field values.

In the D-flat directions of field space, at tree level, the dominant terms for large Higgs field values γ in the scalar potential are $\mathcal{O}(\gamma^2)$. At the one-loop level, however, the dominant terms in the scalar potential actually are $\mathcal{O}(\gamma^2 \log(\gamma))$, which grows faster for large field values than the tree-level expression. This asymptotic nature of the scalar potential is summarized in Table C.2.

Tree level	One-loop level
$\mathcal{O}(\gamma^2)$	$\mathcal{O}(\gamma^2 \log(\gamma))$

Table C.2: Order of the dominant terms in the Higgs scalar potential for arbitrary large Higgs field values γ in the D-flat direction, $|h_u^0| = |h_d^0| = \gamma$.

Thus, at the one-loop level, to check boundedness from below of the scalar potential, it suffices to check whether $\Delta V \to \pm\infty$ as $\gamma \to \infty$ since either case will dominate the asymptotic behavior of V_{tree}. By analyzing the coefficients of the dominant terms from Table C.2, it turns out that the coefficient is positive definite, as shown in Eq. (C.44).

$$\Delta V_{\text{1-loop, dom.}} \sim g^4 \gamma^2 \log(\gamma) \tag{C.44}$$

For this reason, the D-flat direction of $\tan(\beta) = 1$ can never be a minimum for arbitrarily large field values at the one-loop level. As such, in this D-flat direction, then the one-loop level is automatically bounded from below.

At the one-loop level, one must be careful of non-D-flat directions in the neutral Higgs field space. By keeping ourselves constrained to the standard parameter space where $\tan(\beta) > 1$, such directions will be dominated by terms of

$\mathcal{O}(\gamma_{u,d}^4 \log(\gamma_{u,d}))$ for large Higgs field values $|h_u^0| = \gamma_u$ and $|h_d^0| = \gamma_d$. This differs from (and dominates) the dominant tree-level terms of $\mathcal{O}(\gamma_{u,d}^4)$, as summarized in Table C.3. By analyzing the sign of the coefficients of these dominant terms,

Tree level	One-loop level
$\mathcal{O}(\gamma_{u,d}^4), \mathcal{O}(\gamma_u^2\gamma_d^2)$	$\mathcal{O}(\gamma_{u,d}^4 \log(\gamma_{u,d})), \mathcal{O}(\gamma_u^2\gamma_d^2 \log(\gamma_{u,d}))$

Table C.3: Order of the dominant terms in the Higgs scalar potential for arbitrary large Higgs field values $\gamma_{u,d} = |h_{u,d}^0|$ in a generic direction of field space, with $\tan(\beta) = \frac{\gamma_u}{\gamma_d} > 1$.

one may arrive at the following condition to ensure that the scalar potential is bounded below in the generic field space direction $\tan(\beta) > 1$, presented in Eq. (C.45). This condition should be coupled with the condition in Eq. (C.46), coming from the loop-corrected version of Eq. (A.6), for numerical stability and to ensure a real value of $\tan(\beta)$:

$$\Xi_L > \cos(2\beta)\Xi_R, \tag{C.45}$$

where

$$\Xi_L = 8(g^2 + 2g'^2)\left[3\mathrm{Tr}\left(\mathcal{Y}_D^2 - \mathcal{Y}_U^2\right) + \mathrm{Tr}\left(\mathcal{Y}_L^2\right)\right]$$

and

$$\Xi_R = 13g^4 + 299g'^4 - 8\left(2g'^2 + g^2\right)\left[3\mathrm{Tr}\left(\mathcal{Y}_U^2 + \mathcal{Y}_D^2\right) + \mathrm{Tr}\left(\mathcal{Y}_L^2\right)\right]$$
$$- 18g^2g'^2$$

A real value of $\tan(\beta)$ at loop level is achieved so long as the condition below holds.

$$2b < m_{H_u}^2 + \Sigma_u + m_{H_d}^2 + \Sigma_d + 2\mu^2 \tag{C.46}$$

References

[1] B. Allanach, Computer Physics Communications **143**, 305–331 (2002).

[2] A. Buckley, (2015).

[3] H. Baer and X. Tata, *Weak scale supersymmetry: From superfields to scattering events* (Cambridge University Press, ADDRESS, 2006).

[4] E. Witten, Nucl. Phys. B **188**, 513 (1981).

[5] R. K. Kaul, Phys. Lett. B **109**, 19 (1982).

[6] M. T. Grisaru, W. Siegel, and M. Roček, Nucl. Phys. B **159**, 429 (1979).

[7] G. L. Kane, C. F. Kolda, L. Roszkowski, and J. D. Wells, Phys. Rev. D **49**, 6173 (1994).

[8] A. H. Chamseddine, R. L. Arnowitt, and P. Nath, Nucl. Phys. B Proc. Suppl. **101**, 145 (2001).

[9] A. H. Chamseddine, R. Arnowitt, and P. Nath, Phys. Rev. Lett. **49**, 970 (1982).

[10] R. Barbieri, S. Ferrara, and C. Savoy, Phys. Lett. B **119**, 343 (1982).

[11] L. J. Hall, J. D. Lykken, and S. Weinberg, Phys. Rev. D **27**, 2359 (1983).

[12] D. Matalliotakis and H. P. Nilles, Phys. Lett. B **144**, 419 (1994).

[13] J. R. Ellis, T. Falk, K. A. Olive, and Y. Santoso, Nucl. Phys. B **652**, 259 (2003).

[14] J. R. Ellis, K. A. Olive, and Y. Santoso, Phys. Lett. B **539**, 107 (2002).

[15] H. Baer, A. Mustafayev, S. Profumo, A. Belyaev, and X. Tata, JHEP **07**, 065 (2005).

[16] H. Baer, J. Ferrandis, S. Kraml, and W. Porod, Phys. Rev. D **73**, 015010 (2006).

[17] M. R. Douglas, Journal of High Energy Physics **2003**, 046–046 (2003).

[18] S. Weinberg, Phys. Rev. Lett. **59**, 2607 (1987).

[19] H. Baer, V. Barger, D. Martinez, and S. Salam, Journal of High Energy Physics **2022**, (2022).

[20] A. H. GUTH, Annals of the New York Academy of Sciences **950**, 66–82 (2001).

[21] H. Baer, V. Barger, S. Salam, and D. Sengupta, (2022).

[22] N. Arkani-Hamed, S. Dimopoulos, and S. Kachru, (2005).

[23] P. Skands, B. Allanach, H. Baer, C. Balazs, G. Belanger, F. Boudjema, A. Djouadi, R. Godbole, J. Guasch, S. Heinemeyer, W. Kilian, J.-L. Kneur, S. Kraml, F. Moortgat, S. Moretti, M. Muhlleitner, W. Porod, A. Pukhov, P. Richardson, S. Schumann, P. Slavich, M. Spira, and G. Weiglein, Journal of High Energy Physics **2004**, 036 (2004).

[24] B. Allanach, C. Balázs, G. Bélanger, M. Bernhardt, F. Boudjema, D. Choudhury, K. Desch, U. Ellwanger, P. Gambino, R. Godbole, T. Goto, J. Guasch, M. Guchait, T. Hahn, S. Heinemeyer, C. Hugonie, T. Hurth, S. Kraml, S. Kreiss, J. Lykken, F. Moortgat, S. Moretti, S. Peñaranda, T. Plehn, W. Porod, A. Pukhov, P. Richardson, M. Schumacher, L. Silvestrini, P. Skands, P. Slavich, M. Spira, G. Weiglein, and P. Wienemann, Computer Physics Communications **180**, 8 (2009).

[25] S. Dimopoulos, S. Raby, and F. Wilczek, Phys. Rev. D **24**, 1681 (1981).

[26] U. Amaldi, W. de Boer, and H. Furstenau, Phys. Lett. B **260**, 447 (1991).

[27] J. Ellis, S. Kelley, and D. Nanopoulos, Physics Letters B **260**, 131 (1991).

[28] P. Langacker and M. Luo, Phys. Rev. D **44**, 817 (1991).

[29] P. Slavich *et al.*, Eur. Phys. J. C **81**, 450 (2021).

[30] L. E. Ibanez and G. G. Ross, Phys. Lett. B **110**, 215 (1982).

[31] L. Alvarez-Gaumé, J. Polchinski, and M. B. Wise, Nuclear Physics B **221**, 495 (1983).

[32] S. Heinemeyer, W. Hollik, G. Weiglein, and L. Zeune, Journal of High Energy Physics **2013**, (2013).

[33] M. B. Green, J. H. Schwarz, and E. Witten, *SUPERSTRING THEORY. VOL. 1: INTRODUCTION*, *Cambridge Monographs on Mathematical Physics* (PUBLISHER, ADDRESS, 1988).

[34] M. B. Green, J. H. Schwarz, and E. Witten, *SUPERSTRING THEORY. VOL. 2: LOOP AMPLITUDES, ANOMALIES AND PHENOMENOLOGY* (PUBLISHER, ADDRESS, 1988).

[35] J. Polchinski, *String theory. Vol. 1: An introduction to the bosonic string*, *Cambridge Monographs on Mathematical Physics* (Cambridge University Press, ADDRESS, 2007).

[36] J. Polchinski, *String theory. Vol. 2: Superstring theory and beyond*, *Cambridge Monographs on Mathematical Physics* (Cambridge University Press, ADDRESS, 2007).

[37] A. Hebecker, *Naturalness, String Landscape and Multiverse: A Modern Introduction with Exercises*, Vol. 979 of *Lecture Notes in Physics* (PUBLISHER, ADDRESS, 2021).

[38] P. Candelas, G. T. Horowitz, A. Strominger, and E. Witten, Nucl. Phys. B **258**, 46 (1985).

[39] R. Bousso and J. Polchinski, JHEP **06**, 006 (2000).

[40] S. Ashok and M. R. Douglas, JHEP **01**, 060 (2004).

[41] L. Susskind, 247 (2003).

[42] N. Craig *et al.*, (2022).

[43] M. Narain *et al.*, (2022).

[44] J. R. Ellis, K. Enqvist, D. V. Nanopoulos, and F. Zwirner, Mod. Phys. Lett. A **1**, 57 (1986).

[45] R. Barbieri and G. F. Giudice, Nucl. Phys. B **306**, 63 (1988).

[46] B. de Carlos and J. A. Casas, Phys. Lett. B **309**, 320 (1993).

[47] G. W. Anderson and D. J. Castano, Phys. Rev. D **52**, 1693 (1995).

[48] S. Dimopoulos and G. F. Giudice, Phys. Lett. B **357**, 573 (1995).

[49] P. H. Chankowski, J. R. Ellis, and S. Pokorski, Phys. Lett. B **423**, 327 (1998).

[50] P. H. Chankowski, J. R. Ellis, M. Olechowski, and S. Pokorski, Nucl. Phys. B **544**, 39 (1999).

[51] M. Bastero-Gil, G. L. Kane, and S. F. King, Phys. Lett. B **474**, 103 (2000).

[52] H. Abe, T. Kobayashi, and Y. Omura, Phys. Rev. D **76**, 015002 (2007).

[53] R. K. Ellis *et al.*, (2019).

[54] J. N. Butler *et al.*, (2023).

[55] G. 't Hooft, NATO Sci. Ser. B **59**, 135 (1980).

[56] R. Barbieri and A. Strumia, in *4th Rencontres du Vietnam: Physics at Extreme Energies (Particle Physics and Astrophysics)* (PUBLISHER, ADDRESS, 2000).

[57] A. Birkedal, Z. Chacko, and M. K. Gaillard, JHEP **10**, 036 (2004).

[58] A. Canepa, Rev. Phys. **4**, 100033 (2019).

[59] H. Baer, V. Barger, and M. Savoy, Phys. Rev. D **93**, 035016 (2016).

[60] M. J. G. Veltman, Acta Phys. Polon. B **12**, 437 (1981).

[61] L. Susskind, Phys. Rev. D **20**, 2619 (1979).

[62] M. K. Gaillard and B. W. Lee, Phys. Rev. D **10**, 897 (1974).

[63] G. F. Giudice, 155 (2008).

[64] J. L. Feng, K. T. Matchev, and T. Moroi, Phys. Rev. Lett. **84**, 2322 (2000).

[65] J. L. Feng, K. T. Matchev, and T. Moroi, Phys. Rev. D **61**, 075005 (2000).

[66] R. L. Arnowitt and P. Nath, in *6th Summer School Jorge Andre Swieca on Nuclear Physics* (PUBLISHER, ADDRESS, 1993).

[67] H. Baer, V. Barger, and D. Mickelson, Phys. Rev. D **88**, 095013 (2013).

[68] H. Baer, V. Barger, D. Mickelson, and M. Padeffke-Kirkland, Phys. Rev. D **89**, 115019 (2014).

[69] H. Murayama, in *ICTP Summer School in Particle Physics* (PUBLISHER, ADDRESS, 2000), pp. 296–335.

[70] R. Harnik, G. D. Kribs, D. T. Larson, and H. Murayama, Phys. Rev. D **70**, 015002 (2004).

[71] Z. Chacko, Y. Nomura, and D. Tucker-Smith, Nucl. Phys. B **725**, 207 (2005).

[72] R. Kitano and Y. Nomura, Phys. Lett. B **631**, 58 (2005).

[73] R. Kitano and Y. Nomura, Phys. Rev. D **73**, 095004 (2006).

[74] M. Papucci, J. T. Ruderman, and A. Weiler, JHEP **09**, 035 (2012).

[75] C. Brust, A. Katz, S. Lawrence, and R. Sundrum, JHEP **03**, 103 (2012).

[76] H. Baer, V. Barger, P. Huang, A. Mustafayev, and X. Tata, Phys. Rev. Lett. **109**, 161802 (2012).

[77] H. Baer, V. Barger, and D. Martinez, Eur. Phys. J. C **82**, 172 (2022).

[78] K. L. Chan, U. Chattopadhyay, and P. Nath, Phys. Rev. D **58**, 096004 (1998).

[79] M. R. Douglas, Comptes Rendus Physique **5**, 965 (2004).

[80] V. Agrawal, S. M. Barr, J. F. Donoghue, and D. Seckel, Phys. Rev. D **57**, 5480 (1998).

[81] H. Baer, V. Barger, and S. Salam, Phys. Rev. Research. **1**, 023001 (2019).

[82] P. Z. Skands *et al.*, JHEP **07**, 036 (2004).

[83] R. L. Workman *et al.*, PTEP **2022**, 083C01 (2022).

[84] J. L. Feng, Ann. Rev. Nucl. Part. Sci. **63**, 351 (2013).

[85] L. E. Ibanez, C. Lopez, and C. Munoz, Nucl. Phys. B **256**, 218 (1985).

[86] A. Lleyda and C. Munoz, Phys. Lett. B **317**, 82 (1993).

[87] S. P. Martin, Phys. Rev. D **75**, 115005 (2007).

[88] S. P. Martin and M. T. Vaughn, Phys. Rev. D **50**, 2282 (1994), [Erratum: Phys.Rev.D 78, 039903 (2008)].

[89] B. C. Allanach, J. P. J. Hetherington, M. A. Parker, and B. R. Webber, JHEP **08**, 017 (2000).

[90] A. Brignole, L. E. Ibanez, and C. Munoz, Nucl. Phys. B **422**, 125 (1994), [Erratum: Nucl.Phys.B 436, 747–748 (1995)].

[91] K. J. Bae, H. Baer, N. Nagata, and H. Serce, Phys. Rev. D **92**, 035006 (2015).

[92] H. Baer, V. Barger, P. Huang, D. Mickelson, A. Mustafayev, and X. Tata, Phys. Rev. D **87**, 035017 (2013).

[93] H. Baer, V. Barger, and M. Savoy, Phys. Scripta **90**, 068003 (2015).

[94] L. Alvarez-Gaume, J. Polchinski, and M. B. Wise, Nucl. Phys. B **221**, 495 (1983).

[95] H. Baer, V. Barger, M. Savoy, and H. Serce, Phys. Lett. B **758**, 113 (2016).

[96] H. Baer, V. Barger, P. Huang, D. Mickelson, A. Mustafayev, and X. Tata, Phys. Rev. D **87**, 115028 (2013).

[97] H. Baer, V. Barger, and D. Sengupta, Phys. Rev. Res. **1**, 033179 (2019).

[98] A. Dedes and P. Slavich, Nucl. Phys. B **657**, 333 (2003).

[99] H. Baer, V. Barger, J. S. Gainer, H. Serce, and X. Tata, Phys. Rev. D **96**, 115008 (2017).

[100] H. Baer, V. Barger, S. Salam, and H. Serce, Phys. Rev. D **104**, 115025 (2021).

[101] M. R. Douglas, (2004).

[102] H. Baer, V. Barger, H. Serce, and K. Sinha, JHEP **03**, 002 (2018).

[103] H. Baer, V. Barger, D. Martinez, and S. Salam, Physical Review D **108**, (2023).

[104] G. Aad *et al.*, JHEP **02**, 143 (2021).

[105] T. C. Collaboration *et al.*, JHEP **10**, 244 (2019).

[106] J. Lykken and M. Spiropulu, Sci. Am. **310N5**, 36 (2014).

[107] M. Dine, Ann. Rev. Nucl. Part. Sci. **65**, 43 (2015).

[108] N. Craig, in *Beyond the Standard Model after the first run of the LHC* (PUBLISHER, ADDRESS, 2013).

[109] A. Mustafayev and X. Tata, Indian J. Phys. **88**, 991 (2014).

[110] H. Baer, C. Balazs, P. Mercadante, X. Tata, and Y. Wang, Phys. Rev. D **63**, 015011 (2001).

[111] H. Baer, V. Barger, S. Salam, D. Sengupta, and K. Sinha, Eur. Phys. J. ST **229**, 3085 (2020).

[112] H. Baer, V. Barger, and P. Huang, JHEP **11**, 031 (2011).

[113] H. Baer, A. Mustafayev, and X. Tata, Phys. Rev. D **90**, 115007 (2014).

[114] H. Baer, V. Barger, D. Sengupta, and X. Tata, Phys. Rev. D **105**, 095017 (2022).

[115] H. Baer, A. Lessa, S. Rajagopalan, and W. Sreethawong, JCAP **06**, 031 (2011).

[116] F. E. Paige, S. D. Protopopescu, H. Baer, and X. Tata, (2003).

[117] H. Baer, C.-H. Chen, R. B. Munroe, F. E. Paige, and X. Tata, Phys. Rev. D **51**, 1046 (1995).

[118] A. Djouadi, J.-L. Kneur, and G. Moultaka, Comput. Phys. Commun. **176**, 426 (2007).

[119] B. C. Allanach, Comput. Phys. Commun. **143**, 305 (2002).

[120] W. Porod, Comput. Phys. Commun. **153**, 275 (2003).

[121] H. Bahl, T. Hahn, S. Heinemeyer, W. Hollik, S. Paßehr, H. Rzehak, and G. Weiglein, Comput. Phys. Commun. **249**, 107099 (2020).

[122] J. Pardo Vega and G. Villadoro, JHEP **07**, 159 (2015).

[123] D. M. Pierce, J. A. Bagger, K. T. Matchev, and R.-j. Zhang, Nucl. Phys. B **491**, 3 (1997).

[124] S. Cassel, D. M. Ghilencea, and G. G. Ross, Phys. Lett. B **687**, 214 (2010).

[125] H. Baer, K.-Y. Choi, J. E. Kim, and L. Roszkowski, Phys. Rept. **555**, 1 (2015).

[126] J. D. Wells, in *11th International Conference on Supersymmetry and the Unification of Fundamental Interactions* (PUBLISHER, ADDRESS, 2003).

[127] J. D. Wells, Phys. Rev. D **71**, 015013 (2005).

[128] M. Dine, A. Kagan, and S. Samuel, Phys. Lett. B **243**, 250 (1990).

[129] G. F. Giudice and A. Romanino, Nucl. Phys. B **699**, 65 (2004), [Erratum: Nucl.Phys.B 706, 487–487 (2005)].

[130] N. Arkani-Hamed and S. Dimopoulos, JHEP **06**, 073 (2005).

[131] N. Arkani-Hamed, S. Dimopoulos, G. F. Giudice, and A. Romanino, Nucl. Phys. B **709**, 3 (2005).

[132] G. F. Giudice and A. Strumia, Nucl. Phys. B **858**, 63 (2012).

[133] V. Barger, J. Jiang, P. Langacker, and T. Li, Nucl. Phys. B **726**, 149 (2005).

[134] V. Barger, N. G. Deshpande, J. Jiang, P. Langacker, and T. Li, Nucl. Phys. B **793**, 307 (2008).

[135] S. A. R. Ellis and J. D. Wells, Phys. Rev. D **96**, 055024 (2017).

[136] E. Bagnaschi, G. F. Giudice, P. Slavich, and A. Strumia, JHEP **09**, 092 (2014).

[137] A. Arvanitaki, N. Craig, S. Dimopoulos, and G. Villadoro, JHEP **02**, 126 (2013).

[138] N. Arkani-Hamed, A. Gupta, D. E. Kaplan, N. Weiner, and T. Zorawski, (2012).

[139] L. J. Hall and Y. Nomura, JHEP **01**, 082 (2012).

[140] M. Tegmark, A. Aguirre, M. Rees, and F. Wilczek, Phys. Rev. D **73**, 023505 (2006).

[141] B. S. Acharya, K. Bobkov, G. Kane, P. Kumar, and D. Vaman, Phys. Rev. Lett. **97**, 191601 (2006).

[142] B. S. Acharya, K. Bobkov, G. L. Kane, J. Shao, and P. Kumar, Phys. Rev. D **78**, 065038 (2008).

[143] B. S. Acharya, P. Kumar, K. Bobkov, G. Kane, J. Shao, and S. Watson, JHEP **06**, 064 (2008).

[144] B. S. Acharya, S. A. R. Ellis, G. L. Kane, B. D. Nelson, and M. J. Perry, Phys. Rev. Lett. **117**, 181802 (2016).

[145] H. Murayama, Y. Nomura, and D. Poland, Phys. Rev. D **77**, 015005 (2008).

[146] G. Perez, T. S. Roy, and M. Schmaltz, Phys. Rev. D **79**, 095016 (2009).

[147] H. D. Kim and J.-H. Kim, JHEP **05**, 040 (2009).

[148] S. P. Martin, Phys. Rev. D **97**, 035006 (2018).

[149] M. Luty and R. Sundrum, Phys. Rev. D **67**, 045007 (2000).

[150] L. Randall and R. Sundrum, Nucl. Phys. B **557**, 79 (1999).

[151] G. F. Giudice, M. A. Luty, H. Murayama, and R. Rattazzi, JHEP **12**, 027 (1998).

[152] A. Anisimov, M. Dine, M. Graesser, and S. D. Thomas, Phys. Rev. D **65**, 105011 (2002).

[153] M. Dine, P. J. Fox, E. Gorbatov, Y. Shadmi, Y. Shirman, and S. D. Thomas, Phys. Rev. D **70**, 045023 (2004).

[154] N. J. Craig and D. Green, JHEP **09**, 113 (2009).

[155] G. F. Giudice and R. Rattazzi, Phys. Rept. **322**, 419 (1999).

[156] T. S. Roy and M. Schmaltz, Phys. Rev. D **77**, 095008 (2008).

[157] G. F. Giudice and A. Masiero, Phys. Lett. B **206**, 480 (1988).

[158] K. J. Bae, H. Baer, V. Barger, and D. Sengupta, Phys. Rev. D **99**, 115027 (2019).

[159] V. D. Barger, G. F. Giudice, and T. Han, Phys. Rev. D **40**, 2987 (1989).

[160] H. K. Dreiner, Adv. Ser. Direct. High Energy Phys. **21**, 565 (2010).

[161] K.-Y. Choi, L. Covi, J. E. Kim, and L. Roszkowski, JHEP **04**, 106 (2012).

[162] M. Carena and H. E. Haber, Prog. Part. Nucl. Phys. **50**, 63 (2003).

[163] M. Srednicki, K. A. Olive, and J. Silk, Nucl. Phys. B **279**, 804 (1987).

[164] J. Aalbers *et al.*, Phys. Rev. Lett. **131**, 041002 (2023).

[165] D. Poland, D. Simmons-Duffin, and A. Vichi, JHEP **05**, 110 (2012).

[166] D. Poland and A. Stergiou, JHEP **12**, 121 (2015).

[167] D. Green and D. Shih, JHEP **09**, 026 (2012).

[168] T. Hahn, S. Heinemeyer, W. Hollik, H. Rzehak, and G. Weiglein, Comput. Phys. Commun. **180**, 1426 (2009).

[169] B. S. Acharya and E. Witten, (2001).

[170] B. S. Acharya, JHEP **08**, 128 (2020).

[171] I. n. García Etxebarria, M. Montero, K. Sousa, and I. Valenzuela, JHEP **12**, 032 (2020).

[172] S. Dimopoulos, S. Raby, and F. Wilczek, Phys. Rev. D **24**, 1681 (1981).

[173] S. Dimopoulos and H. Georgi, Nucl. Phys. B **193**, 150 (1981).

[174] M. R. Douglas and S. Kachru, Rev. Mod. Phys. **79**, 733 (2007).

[175] A. Linde, Rept. Prog. Phys. **80**, 022001 (2017).

[176] V. Agrawal, S. M. Barr, J. F. Donoghue, and D. Seckel, Phys. Rev. Lett. **80**, 1822 (1998).

[177] A. G. Cohen, D. B. Kaplan, and A. E. Nelson, Phys. Lett. B **388**, 588 (1996).

[178] J. A. Bagger, J. L. Feng, N. Polonsky, and R.-J. Zhang, Phys. Lett. B **473**, 264 (2000).

[179] K. J. Bae, H. Baer, V. Barger, and R. W. Deal, JHEP **02**, 138 (2022).

[180] L. Susskind, in *From Fields to Strings: Circumnavigating Theoretical Physics: A Conference in Tribute to Ian Kogan* (PUBLISHER, ADDRESS, 2004), pp. 1745–1749.

[181] H. Baer, V. Barger, H. Serce, and X. Tata, Phys. Rev. D **94**, 115017 (2016).

[182] H. Baer, V. Barger, and D. Sengupta, Phys. Rev. D **98**, 015039 (2018).

[183] I. Broeckel, M. Cicoli, A. Maharana, K. Singh, and K. Sinha, JHEP **10**, 015 (2020).

[184] S. Kachru, R. Kallosh, A. D. Linde, and S. P. Trivedi, Phys. Rev. D **68**, 046005 (2003).

[185] H. Baer, V. Barger, and A. Mustafayev, Phys. Rev. D **85**, 075010 (2012).

[186] H. Baer, V. Barger, D. Martinez, and S. Salam, JHEP **03**, 186 (2022).

[187] E. Cremmer, S. Ferrara, L. Girardello, and A. Van Proeyen, Nucl. Phys. B **212**, 413 (1983).

[188] S. K. Soni and H. A. Weldon, Phys. Lett. B **126**, 215 (1983).

[189] V. S. Kaplunovsky and J. Louis, Phys. Lett. B **306**, 269 (1993).

[190] H. Baer, V. Barger, S. Salam, and D. Sengupta, Phys. Rev. D **102**, 075012 (2020).

[191] J. E. Kim and H. P. Nilles, Phys. Lett. B **138**, 150 (1984).

[192] H. Baer, V. Barger, D. Sengupta, and R. W. Deal, Phys. Rev. D **104**, 015037 (2021).

[193] J. F. Donoghue, K. Dutta, and A. Ross, Phys. Rev. D **73**, 113002 (2006).

[194] G. Degrassi, S. Di Vita, J. Elias-Miro, J. R. Espinosa, G. F. Giudice, G. Isidori, and A. Strumia, JHEP **08**, 098 (2012).

[195] P. Athron, J.-h. Park, D. Stöckinger, and A. Voigt, Comput. Phys. Commun. **190**, 139 (2015).

[196] P. Athron, J.-h. Park, T. Steudtner, D. Stöckinger, and A. Voigt, JHEP **01**, 079 (2017).

[197] P. Athron, M. Bach, D. Harries, T. Kwasnitza, J.-h. Park, D. Stöckinger, A. Voigt, and J. Ziebell, Comput. Phys. Commun. **230**, 145 (2018).

[198] H. Baer, V. Barger, and S. Salam, Physical Review Research **1**, (2019).

[199] M. R. Douglas, (2004).

[200] H. P. Nilles and P. K. S. Vaudrevange, Mod. Phys. Lett. A **30**, 1530008 (2015).

[201] H. Baer, V. Barger, J. Bolich, J. Dutta, and D. Sengupta, Phys. Rev. D **109**, 035011 (2024).

[202] H. Baer, V. Barger, and D. Martinez, The European Physical Journal C **82**, (2022).

[203] B. C. Allanach, C. H. Kom, and M. Hanussek, Comput. Phys. Commun. **183**, 785 (2012).

[204] B. C. Allanach, A. Bednyakov, and R. Ruiz de Austri, Comput. Phys. Commun. **189**, 192 (2015).

[205] B. C. Allanach, S. P. Martin, D. G. Robertson, and R. R. de Austri, (2016).

[206] E. Witten, Nuclear Physics B **188**, 513 (1981).

[207] C. Han, D. Kim, S. Munir, and M. Park, JHEP **04**, 132 (2015).

[208] A. Tumasyan *et al.*, JHEP **04**, 091 (2022).

[209] Z. Han, G. D. Kribs, A. Martin, and A. Menon, Phys. Rev. D **89**, 075007 (2014).

[210] G. Aad *et al.*, Eur. Phys. J. C **81**, 600 (2021), [Erratum: Eur.Phys.J.C 81, 956 (2021)].

[211] G. Aad *et al.*, Phys. Rev. D **101**, 052005 (2020).

[212] D. Agin, B. Fuks, M. D. Goodsell, and T. Murphy, (2023).

[213] D. Buttazzo, G. Degrassi, P. P. Giardino, G. F. Giudice, F. Sala, A. Salvio, and A. Strumia, JHEP **12**, 089 (2013).

[214] F. Vissani, Phys. Rev. D **57**, 7027 (1998).

[215] H. Baer, V. Barger, D. Martinez, and S. Salam, Phys. Rev. D **108**, 035050 (2023).

[216] H. Baer, V. Barger, D. Martinez, and S. Salam, JHEP **09**, 125 (2022).

[217] H. Baer, V. Barger, S. Salam, and D. Sengupta, in *Snowmass 2021* (PUBLISHER, ADDRESS, 2022).

[218] M. Dine, G. Festuccia, A. Morisse, and K. van den Broek, JHEP **06**, 014 (2008).

[219] M. Dine and J. D. Mason, Rept. Prog. Phys. **74**, 056201 (2011).

[220] M. Dine, G. Festuccia, and A. Morisse, JHEP **09**, 013 (2009).

[221] S. Heinemeyer, W. Hollik, D. Stockinger, A. M. Weber, and G. Weiglein, JHEP **08**, 052 (2006).

[222] H. Baer, V. Barger, and D. Martinez, The European Physical Journal C **82**, (2022).

[223] L. Susskind, (2004).

[224] H. Baer, V. Barger, D. Martinez, and S. Salam, Entropy **26**, 275 (2024).

[225] H. Baer, A. Mustafayev, S. Profumo, A. Belyaev, and X. Tata, Journal of High Energy Physics **2005**, 065–065 (2005).

[226] M. van Beekveld, S. Caron, and R. Ruiz de Austri, JHEP **01**, 147 (2020).

[227] M. van Beekveld, W. Beenakker, S. Caron, R. Peeters, and R. Ruiz de Austri, Phys. Rev. D **96**, 035015 (2017).

[228] G. Belanger, S. Kraml, and A. Pukhov, Phys. Rev. D **72**, 015003 (2005).

[229] S. P. Martin, Phys. Rev. D **65**, 116003 (2002).

[230] T. Ibrahim and P. Nath, Phys. Rev. D **66**, 015005 (2002).

[231] S. P. Martin, Adv. Ser. Direct. High Energy Phys. **18**, 1 (1998).

[232] B. Allanach, S. Kraml, and W. Porod, in *10th International Conference on Supersymmetry and Unification of Fundamental Interactions (SUSY02)* (PUBLISHER, ADDRESS, 2002), pp. 904–910.

[233] L. E. Ibanez and C. Lopez, Phys. Lett. B **126**, 54 (1983).

[234] G. F. Giudice and R. Rattazzi, Nucl. Phys. B **757**, 19 (2006).

[235] F. Gabbiani, E. Gabrielli, A. Masiero, and L. Silvestrini, Nucl. Phys. B **477**, 321 (1996).

[236] C. K. M. Klein, Master's thesis, Heidelberg, Max Planck Inst., 2019.

[237] J. R. Ellis and D. Ross, Phys. Lett. B **506**, 331 (2001).

[238] H. Baer, A. Mustafayev, E.-K. Park, and X. Tata, JCAP **01**, 017 (2007).

[239] S. Profumo, T. Stefaniak, and L. Stephenson Haskins, Phys. Rev. D **96**, 055018 (2017).

[240] M. Badziak, M. Olechowski, and P. Szczerbiak, Phys. Lett. B **770**, 226 (2017).

[241] N. Arkani-Hamed, A. Delgado, and G. F. Giudice, Nucl. Phys. B **741**, 108 (2006).

[242] T. Cohen, M. Lisanti, A. Pierce, and T. R. Slatyer, JCAP **10**, 061 (2013).

[243] J. Fan and M. Reece, JHEP **10**, 124 (2013).

[244] A. Pomarol and D. Tommasini, Nucl. Phys. B **466**, 3 (1996).

[245] J. R. Ellis, S. Kelley, and D. V. Nanopoulos, Phys. Lett. B **260**, 131 (1991).

[246] H. M. Lee, S. Raby, M. Ratz, G. G. Ross, R. Schieren, K. Schmidt-Hoberg, and P. K. S. Vaudrevange, Nucl. Phys. B **850**, 1 (2011).

[247] P. Langacker and M.-x. Luo, Phys. Rev. D **44**, 817 (1991).

[248] J. Aalbers *et al.*, (2022).

[249] H. Baer, V. Barger, and A. Mustafayev, JHEP **05**, 091 (2012).

[250] A. Arbey, M. Battaglia, A. Djouadi, F. Mahmoudi, and J. Quevillon, Phys. Lett. B **708**, 162 (2012).

[251] E. Aprile *et al.*, Phys. Rev. Lett. **121**, 111302 (2018).

[252] H. Baer, V. Barger, and H. Serce, Phys. Rev. D **94**, 115019 (2016).

[253] S. Heinemeyer, W. Hollik, G. Weiglein, and L. Zeune, JHEP **12**, 084 (2013).

[254] H. P. Nilles, PoS **CORFU2016**, 017 (2017).

[255] H. Baer, V. Barger, and D. Sengupta, Phys. Rev. Res. **2**, 013346 (2020).

[256] A. Falkowski, O. Lebedev, and Y. Mambrini, JHEP **11**, 034 (2005).

[257] K. Choi, K. S. Jeong, T. Kobayashi, and K.-i. Okumura, Phys. Rev. D **75**, 095012 (2007).

[258] K. Choi, A. Falkowski, H. P. Nilles, and M. Olechowski, Nucl. Phys. B **718**, 113 (2005).

[259] H. Baer, A. Mustafayev, S. Profumo, A. Belyaev, and X. Tata, Phys. Rev. D **71**, 095008 (2005).

[260] W. Buchmuller, K. Hamaguchi, O. Lebedev, and M. Ratz, in *GUSTAVOFEST: Symposium in Honor of Gustavo C. Branco: CP Violation and the Flavor Puzzle* (PUBLISHER, ADDRESS, 2005), pp. 143–156.

[261] H. P. Nilles, S. Ramos-Sanchez, and P. K. S. Vaudrevange, AIP Conf. Proc. **1200**, 226 (2010).

[262] M. Farina, D. Pappadopulo, and A. Strumia, JHEP **08**, 022 (2013).

[263] H. Baer, V. Barger, and D. Sengupta, Phys. Lett. B **790**, 58 (2019).

[264] M. Demirtas, N. Gendler, C. Long, L. McAllister, and J. Moritz, (2021).

[265] P. N. Bhattiprolu and S. P. Martin, Phys. Rev. D **104**, 055014 (2021).

[266] M. Dine and A. Kusenko, Rev. Mod. Phys. **76**, 1 (2003).

[267] K. J. Bae, H. Baer, H. Serce, and Y.-F. Zhang, JCAP **01**, 012 (2016).

[268] H. K. Dreiner, H. E. Haber, and S. P. Martin, *From Spinors to Supersymmetry* (Cambridge University Press, Cambridge, UK, 2023).

[269] H. Baer, V. Barger, S. Salam, D. Sengupta, and X. Tata, Phys. Lett. B **810**, 135777 (2020).

[270] B. C. Allanach and T. Cridge, (2017).

[271] B. C. Allanach, P. Athron, L. C. Tunstall, A. Voigt, and A. G. Williams, Comput. Phys. Commun. **185**, 2322 (2014).

[272] B. C. Allanach and M. A. Bernhardt, Comput. Phys. Commun. **181**, 232 (2010).